Geographia Technica

Geographia Technica

Technical Geography

an International Journal for the Progress of Scientific Geography

2019 – No. 2

Cluj University Press

C o n t e n t s

Geographia Technica

DO RIVERS UPSTREAM WEIRS HAVE LOTICS OR LENTICS CHARACTERISTICS?

Francesco DONATI[1], Laurent TOUCHART[2], Pascal BARTOUT[3]

ABSTRACT:

In France the multitude of weirs that exist in rivers could affect the quality of aquatic ecosystems. The current context of recovery of the good state of watercourses, dictated by the European Water Framework Directive, requires understanding of their impact, in order to address operations of river restoration. One of the risks connected to this kind of structure is the loss of lotics characteristics of streams, in favour of lentics characteristics. In fact, they cause a reduction in speed flow, favouring the formation of zones with lentic flow. Through the study of thermal stratification, the major discriminant between running and stagnant waters, the aim of this study is to understand the nature of rivers situated upstream weirs, using four study sites. Results show that the presence of a weir is not synonymous of substitution of the lotic characteristics of a watercourse. Lentic behavior of waters has only been observed when certain environmental and hydrological conditions have been met in the reach.

Key-words: *Weirs, Thermal stratification, River ecosystem, Water Framework Directive.*

1. INTRODUCTION

In Europe, the context of improvement and preservation of water quality dictated by the Water Framework Directive requires the identification of the causes of alteration of aquatic environment, to guide renaturation efforts (Roche, et al., 2005). The profuse of hydraulic structures that characterize fluvial landscapes of Europe are one of the possible causes of the degradation of river quality (e.g. Tricart et al., 1991). Therefore, it is crucial for water resources administrators to determine the impact of this type of infrastructures.

The rivers of metropolitan France are potentially exposed to degradation caused by hydraulic structures, because of their diffusion on the country's rivers. Among these structures there are weirs, omnipresent within the French hydrographic network. In a watercourse, the presence of a weir causes a modification of its hydraulic conditions, whose most remarkable effect is the formation of a zone of slow flow velocity upstream (Csiki & Rhoads, 2010). This speed reduction could be such as to provoke a sort of dam effect, favouring the formation of zones of lentic flow (Malavoi & Salgues, 2011) and the substitution of lotic features of the watercourse by lentic characteristics (Souchon & Nicolas, 2011), but studies to confirm or invalidate it are missing for French contexts.

Are watercourses upstream weirs converted into stagnant water bodies or do they retain their current water characteristics? Through French case studies, using the water temperature parameter, which is the main cause of water density stratification, the objective of this study is to try and answer to this question to give a better understanding of the effects of weirs on aquatic environments.

[1,2,3] *Université d'Orléans, Département de Géographie, 45065 Orléans, France, francesco.donati@univ-orleans.fr, laurent.touchart@univ-orleans.fr, pascal.bartout@univ-orleans.fr.*

2. STUDY AREA

To provide an answer to the issue, two study areas were equipped, chosen in climatic contexts typical of metropolitan France, to consider two types of hydro-climatic situations. The first site is in the Mauves river, a tributary of the Loire river that flows for 45 km in the department of Loiret, in the west of the Orleans agglomeration. The geology of its watershed is mainly characterised by Beauce limestone and sediments of different types from the Cenozoic period (Ausilio, 1984). Overall, the forest cover of this territory is weak, but throughout the banks of the Mauves grows a dense riparian forest, which in some places assumes the features of a veritable alluvial forest, as in correspondence of the Departmental Natural Park of "Courtils des Mauves», located in the village of Meung sur Loire. A degraded oceanic climate characterises this area (Escourrou, 1982): the nearest weather station (that one of Bricy), over the period 1981-2010, measured an average temperature of 11.2°C and average rainfall of 642 mm (infoclimat.fr data). The average flow of the Mauves is 1.075 m3/s (BanqueHydro data). This study area consists of three distinct water mill reaches: the most upstream is the Nivelle mill one, the central is the Marais mill one and the further downstream is the St. Hilaire mill one. Respectively, they measure about 900, 400 and 500 meters. The first and second reaches are consecutive to each other, the last is separated from the others by the short reach of another mill. The three mills are equipped with a weir, whose height is between 0.5 and 1 meter (ROE data), with valve.

The second site is in the North Zinsel river, a tributary of the Moder river which flows for 43 km between the departments of Moselle (57) and Bas-Rhin (67), in the North-East of France. From a geological point of view, it is in the Vosges du Nord massif and the watershed, whose outlet is the study area, is entirely characterized by Vosgian sandstone of lower Trias and Buntsandstein. 94% of the land cover of this territory is characterized by forest. The oceanic climate influence is even more degraded, and it is exacerbated by altitude (Escourrou, 1982, op.cit): the closest weather station (that of Mouterhouse), over the period 1981-2010, measured a temperature average of 9.5°C and an average rainfall of 989.8 mm (infoclimat.fr data). In correspondence of the study area, the average flow of the Zinsel du Nord is 0.596 m^3/s (Parc Naturel Régional des Vosges du Nord data). This study area consists of a reach of about 200 meters, circumstantiated downstream by a weir 1.50 meters high, located in the downtown of the village of Baerenthal. In the upstream part of the reach the stream hasn't got any riparian vegetation, unlike the central and final parts, where several trees shade the stream.

3. METHODOLOGY

3.1. The techniques and instruments used to differentiate the lotic and lentic operation of rivers upstream weirs

To understand if rivers upstream weirs retain their lotic features or they have lentic characteristics, the methodology deployed is based on the study of the thermal properties of the water. Indeed, the major discriminant between running and stagnant waters is the thermal stratification of the water column (Wilhem, 1960; Touchart, 2002). Although it has moments of uniformity, the normality of a stagnant water is its stratification according to a vertical temperature-density gradient, whereas the normality of a running water is the physicochemical homogeneity of the water column, because turbulence prevents the distinction of water layers and their superposition (Touchart, 2007, a). Therefore, the

portions of watercourses upstream weir were studied as if they were lentic ecosystems, with techniques that are commonly used in limnology.

The temperature of the water column was measured using chains of thermometers. This device is widely used for the thermal study of lakes or ponds and it allows to measure the temperature of the water at different depths and see if there are thermal gradients between the surface and the bottom (Touchart, 2001; Touchart 2002, *op cit*; Choffel et al., 2017). Although it is a typical instrument for limnological works, this tool has already been used in fluvial areas and upstream of weirs (eg Bormans et al., 1997; Webster et al., 1997). The chains used for this research consist of an 8mm-diameter mesh, one end of which was attached to a buoy with a circumference of 25 cm. Although the chain was already considerably heavy, the other end was attached to a large concrete block, in order to anchor the device securely to the stream bed. Two recording thermometers (HOBO *Water Temperature Pro v2 Data Logger - U22-001*, with an accuracy of ± 0.21°C and a resolution of 0.02°C at 25°C) were attached to the chain and programmed to measure the temperature of the water with a time step of 60 minutes.

In the Mauves a thermometer was attached 10 cm below the surface of the water, and the second at a depth of 50 cm; in the North Zinsel, too, a thermometer was attached 10 cm below the water surface, but the second was placed at a 70 cm depth. In both cases a piece of chain was left between the deepest thermometer and the stream bed, so that the device followed the fluctuations of the water level and the probe never touched the bottom. The thermometers were set up on 02/02/2018 in the Zinsel of the North and on 24/02/2018 in the Mauves and they worked until 31/12/2018, collecting a total of 35,529 water temperature data. At the Nivelle water mill, the data relating to the period from the end of September to the beginning of December were lost.

3.2. Choice of instruments location

In the four study areas, the chains of thermometers were positioned where the flow was slowest to collect the data where the conditions were as lentic as possible. To determine the location of the instruments a preliminary study of the velocities in the reaches was carried out. Four equally spaced transects were established and on these the flow velocity was measured using a current meter (Flowtracker 2 with an accuracy of ± 1% for a measured speed of +0.0025 m/s and a resolution of 0.0001 m/s).

The methodology used is the same for the measurement of discharge through the exploration of velocity field described in Le Coz, et al. (2011): each transect was divided into a n number of verticals, on which velocities were sampled in several points. The number and the depth of each point were established following the indications of the current meter. Then the average speed was calculated for each transect and the thermometers were installed in the area where the velocity values were the lowest.

3.3. Data analysis

In order to understand if the water column has thermal stratifications and determine their intensity, the hourly delta Δ between surface temperature and depth was calculated. The temporality of thermal stratifications was studied through the daily Δ_{min}, the minimum thermal difference between the surface and the bottom of the water column during a day: when Δ_{min} is equal to 0 the thermal stratification lasts less than 24 hours. Any value within the error range of thermometers has been recorded as $\Delta = 0$.
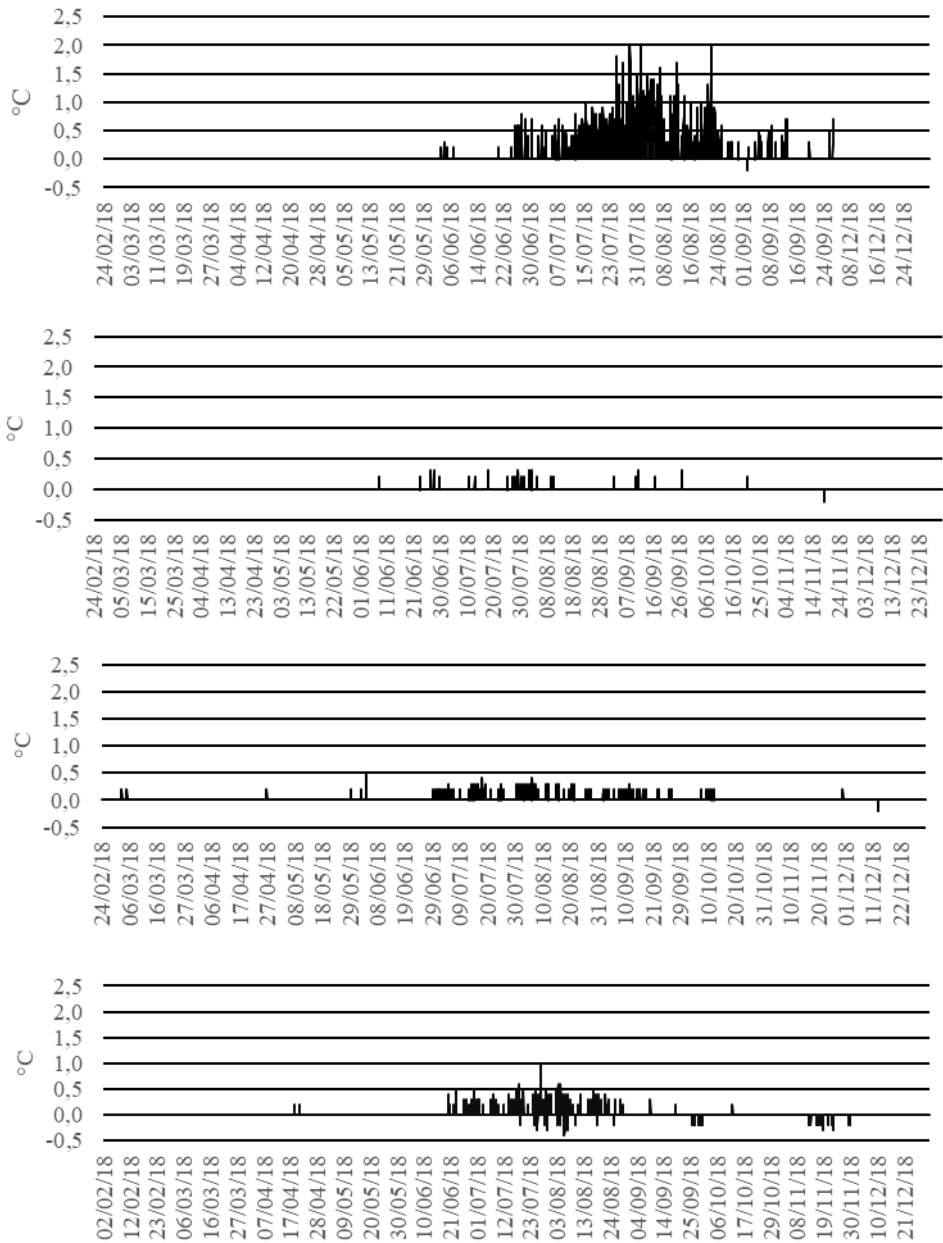
Fig. 1. The evolution of delta in the water column of study areas. From the top to the bottom: Nivelle Water mill, Marais water mill, St. Hilaire water mill, Baerenthal reach.
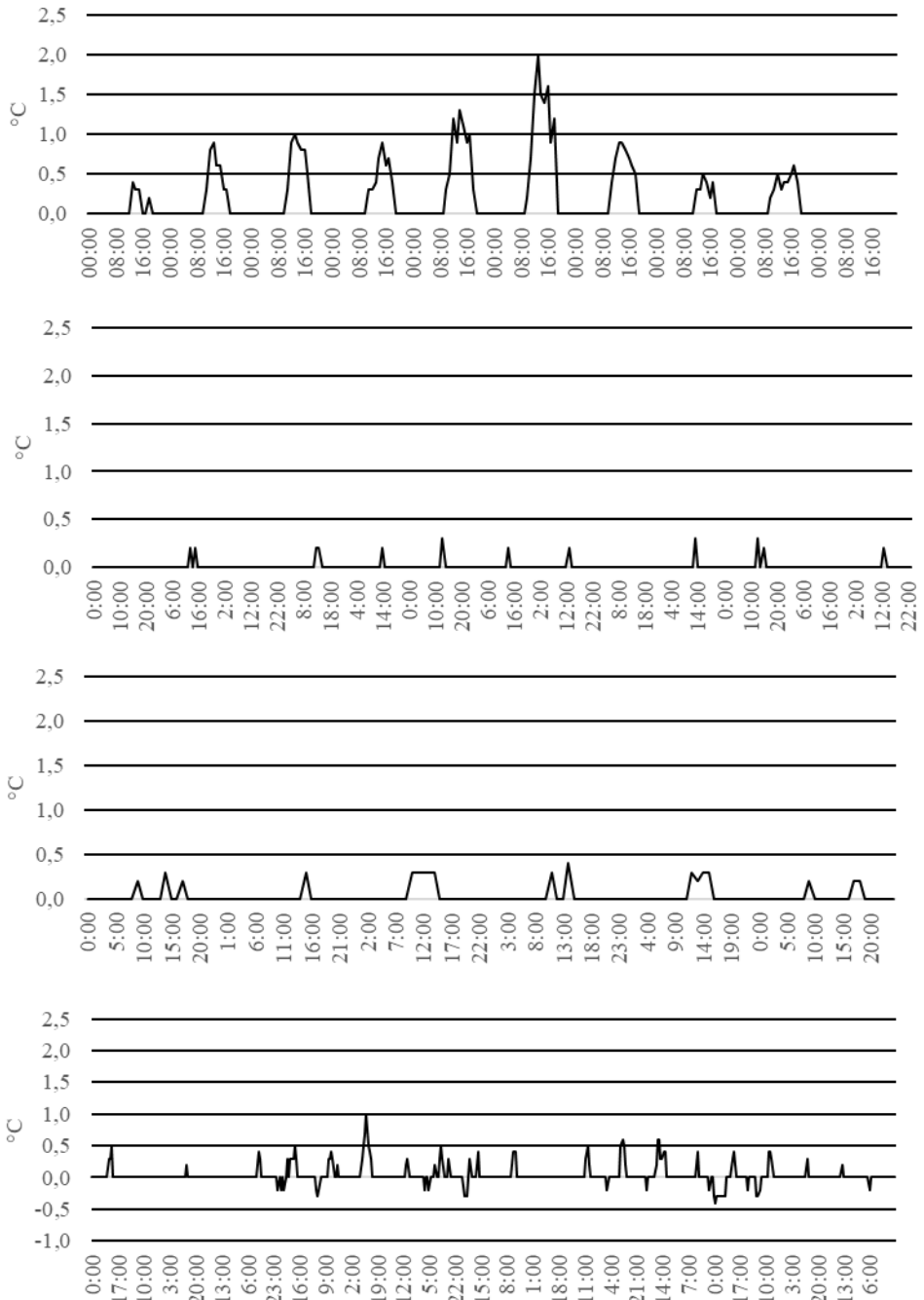
Fig. 2. The evolution of delta in the water column of study areas, during the longer periods of thermal stratification. From the top to the bottom: Nivelle Water mill (17/08-26-08), Marais water mill (25/07-05/08), St. Hilaire water mill (03/08-09/08), Baerenthal's reach (20/07-10/08).

4. RESULTS AND DISCUSSIONS

Graphs in **Fig. 1** show the evolution of the thermal delta between the two extremes of the water column of the four reaches under study. Overall, it is possible to single out two moments: one during which the values of Δ fall within the margin of error of thermometers, during Winter, Spring and Autumn, and another during which Δ is greater than this interval, during the Summer. From 21/06 to 23/09, the Nivelle water mill reach is the one with the most marked thermal heterogeneity of the water column: on average, Δ was 0.6°C, with peaks of 2°C. In the other reaches on the Mauves Δ values are less important, averaging 0.2°C in the two study areas, with peaks of 0.3°C at the Marais water mill and 0.4°C that of St. Hilaire. Baerenthal Δ has mean values of 0.3°C and peaks of 1°C; here Δ also reached negative values, when the water at surface was colder than water at depth, whose maximum value was -0.4 °C. We suppose that these moments of negative delta, which occurred almost always during the night, are due to the convective cooling of the water which determines a heat loss of the layers close to the surface (Lemmin, 1995).

From a temporal point of view, also the Nivelle water mill is the one which presents the more important values, with a total of 545 hours of heterothermia (supposing that during the period during which the data were lost $\Delta = 0$, this number corresponds to 7% of the study period and 19% of the summer period). At the Marais and St. Hilaire water mills, this value is respectively 32 and 143 hours (the, 0.4% and 1.9% of the study period and 1% and 4% of the summer period) and in Baerenthal 204 hours (the 2% of the study period and 5% of the summer period). The moments of $\Delta \neq 0$ never last for long periods, but they are rather episodic, lasting only some hours within a day. Averaging, at the Nivelle water mill the moment of heterothermia lasted 6 hours (maximum duration 15 hours on 12/08), in the water mills of Marais and St. Hilaire 1 hour (maximum duration respectively of 3 hours on 27/09 and 5 hours the 05/08) and in Baerenthal 2 hours (maximum duration 12 hours on 06/08). In each field of study, the daily Δ_{min} was always 0, which means that at least one moment of the day the water column was homothermal. If we deepen the temporality of the episodes of $\Delta \neq 0$ we realize that most take place between the end of the morning and the first hours of the afternoon, between 12:00pm and 3:00pm, as we can see from the graph in **Fig. 3**.
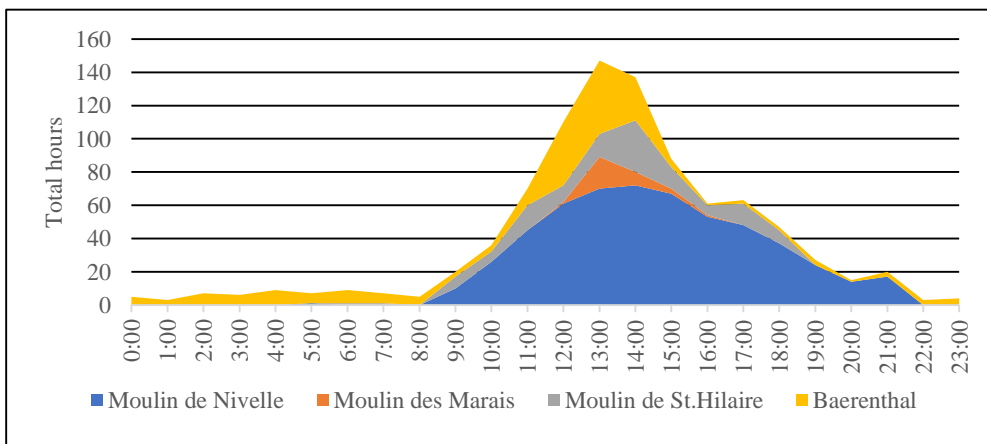
Fig. 3. The moments of the days during which the heterothermia of the water column was present.

With an even finer temporal analysis it is possible to understand how temperatures evolve at different depths within a day. As an example, see above the evolution of temperatures at Nivelle mill at the surface and at depth during one of the days of maximum thermal heterogeneity of the water column. In the morning, the surface waters are warmer than the deep waters, warming is greatest between the end of the morning and the beginning of the afternoon. The warming of the surface waters stopped during the afternoon and it is the deep waters which warm up most of the time. In the evening the deep waters stop warming up, while the surface gets colder; during the night it is the whole column of water that cools down. Such an evolution has been observed in all the fields of study.

Table 1.

The evolution of temperature at the top ant at the bottom of water column at Neville water mill, the 29/07.

m	8:00-10:00	10:00-13:00	13:00-18:00	18:00-22:00	22:00-00:00	00:00-05:00
-0,1	+0,7 °C	+1,8 °C	0 °C	-0,5 °C	-0,3°C	-0,7°C
-0,5	+0,3 °C	+0,2 °C	+1,2 °C	0 °C	-0,2°C	-0,7°C

In order to understand if the upstream of weirs retains its lotic features or if the presence of this structure has induced the formation of lentic characteristics, it is necessary to consider the temporality of thermal stratification episodes, rather than their intensity. In fact, in streams too it is possible to observe thermal stratifications (Torgersen et al., 2001, Handcock et al., 2012, Wawrzyniak, 2012), but the difference with those of the water bodies is principally temporal and concerned its duration, frequency and stability (Touchart, 2007, op.cit.). The graphs in **Fig. 3** show the evolution of the thermal delta in the different study areas during longer periods of heterogeneity. In Marais and St. Hilaire water mills and in the reach of Baerenthal, micro-stratification episodes occur mainly in the early afternoon and last for an average of one to two hours. Their duration during the summer is so low that we cannot speak of lotic behaviours, but it is more appropriate to speak of an exception to the normal physicochemical homogeneity that characterises the watercourse. Different is the case of Nivelle water mill. Here, the periods of thermal heterogeneity of the water column are not only more intense, but they exceed the first hours of the afternoon and in some cases, they last for a large part of the day. Although their total duration during the hot season is still much lower compared to the moments of homogeneity, during certain periods of the Summer it is possible to speak of an obvious lentic behaviour. For example, between the beginning of July and the end of August the thermal stratification moments amount to 31% of the total time. During this period the thermal evolution of the water column is clearly polymictic continuous, with thermal stratifications lasting only some hours in the day (Anctil, 2017). This type of evolution is the same that characterises some water bodies, such as the pellicular ponds of some decimetre depth of the Center-West of France (Touchart, 2007 b) or marshes (Oertli & Frossard, 2013).

How to explain these differences from one study areas to another? The thermal stratification and its degree of intensity are controlled by the work of a stratifying thermal energy and a destructive energy, which in a watercourse are respectively solar energy and the water flow on the bed surface or the wind blowing (Bormans et al., 1997, *op.cit.*). If in correspondence of the reaches there is a factor that disturbs or accentuates the action of its elements, the thermal evolution of the water column could change much. One of these factors is the vegetation that grows around the channel of the river. Indeed, a number of

studies has shown that the riparian forest has a great influence on the temperature of rivers, favouring or preventing sunshine (Webb et al., 2008). As we said, throughout the Nivelle water mill reach a fairly dense riparian forest grows, except for clearings that are formed in some places; in this site the thermometers are in correspondence of one of these sectors where the riparian forest is less dense and where the river is exposed to a more intense sunshine. The reach of the Marais water mill too is also sunny throughout its course, as the vegetation is present only on the right bank. Upstream of the St. Hilaire water mill, the river is in a similar situation to that found upstream of the Nivelle water mill, with stream areas that are sunnier than others, but here the sensors were placed in a shady place. These details could explain the low values of delta Δ in this last field of study and the more marked values observed in the reach of Nivelle water mill, but why was the same thermal operation not observed in the Marais water mill reach that is also exposed to the sun?

Mitrovic et al. (2005) state that a velocity greater than or equal to 0.05 m/s is enough to prevent the formation of thermal stratifications. The speed measurements collected throughout the study period in the different study areas show that only at the Nivelle water mill the flow repeatedly had a speed below this threshold. Therefore, upstream of the Nivelle mill all the favourable conditions for the development of a thermal stratification would be brought together.

4. CONCLUSIONS

For the first time for French rivers, the collected data provide an insight into the internal thermal operation of water upstream of the river weirs, which makes it possible to distinguish the type of operation that characterises them. Results shows that the presence of a weir is not synonymous of substitution of the lotic characteristics of a watercourse. Indeed, only in one of the study areas among the four studied, that of the Nivelle water mill, a thermal operation similar to that of certain bodies of water was observe, and even then exclusively during the central months of the Summer. During the warmer part of the year, in the other study areas also the physical homogeneity of the water column was "disturbed", but the episodic nature of these moments of heterogeneity consents to classify them as normal thermal stratification observable in watercourses. The appearance of lentic features does not seem to depend on climatic factors, but rather on local factors. Indeed, they have only been observed when certain environmental conditions have been met in the reach, including good exposure to sunshine and a particularly slow flow.

R E F E R E N C E S

Ausilio, É. (1984). *Étude générale de la qualité des Mauves à Meung sur Loire.* Assocition des Riverains et des amis des Mauves - Ministère de l'Agriculture - Service d'Aménagement des Eaux de la Region Centre.

Bormans, M., Maier, H., Burch, M., & Baker, P. (1997, Volume 48). Temperature stratification in the lower River murray, Australia: implication for cyanobacterial bloom development. *Marine and Freshwater Research (CSIRO publishing)*, pp. 647-654.

Choffel, Q., Touchart, L., Bartout, P., & Al Domany, M. (2017). Temporal and spatial variations in heat content of french pond . *Geographia Technica*, pp. 9-22.

Csiki, S., & Rhoads, B. L. (2010). Hydraulic and geomorphological effects of run-of-river dams. *Progress in Physical Geography*, pp. 755-780.

Escourrou, G. (1982). *Le climat de la France.* Paris: Presses Universitaires de France.

Handcock, R. N., Torgersen, C. E., Cherkauer, K. A., Gillespie, A. R., Tockner, K., Faux, N. R., & Tan, J. (2012). Thermal Infrared Remote Sensing of Water Temperature in Riverine Landscapes. Dans P. E. Carbonneau, & H. Piégay, *Management, Fluvial Remote Sensing for Science and.* Chichester: Wiley-Blackwell.

Le Coz, J., Camenen, B., Dramais , G., Ribot-Bruno, J., Ferry, M., & Rosique, J.-L. (2011). *Contrôle des débits réglementaires. Application de l'article L.214-18 du Code de l'environnement.* ONEMA.

Lemmin, U. (1995). Limnologie physique. Dans R. Pourriot, & M. Meybeck, *Limnologie générale* (pp. 61-106). Paris: Masson.

Malavoi, J.-R., & Salgues, D. (2011, Février). Arasement et dérasement de seuils. Aide à la définition de Cahier des Charges pour les études de faisabilité Compartiments hydromorphologie et hydroécologie. ONEMA - CEMAGREF.

Mitrovic, M. S., Oliver, R. L., Rees, C., Bowling, L. C., & Buckney, R. T. (2003). Critical flow velocities for growth and dominance aof Anabaena circinalis in some turbid freshwater rivers. *Freshwater Biology*, pp. 164-174.

Oertli, B., & Frossard, P.-a. (2013). *Mares et étangs. Écologie, gestion, amenagement et valorisation.* Lausanne: Presses polytechniques et universitaires romandes.

Roche, P.-A., Billen, G., Bravard , J.-P., Décamps, H., Pennequin, D., Vindimian, E., & Wasson, J.-G. (2005, 02). Les enjeux de recherche liés à la directive-cadre européenne sur l'eau. *Comptes Rendus Geosciences*, pp. 1-25.

Souchon, Y., & Nicolas, V. (2011, Novembre). Barrages et seuils : principaux impacts environnementaux. ONEMA, CEMAGREF.

Torgersen, C. E., Faux, N. R., McIntosh, B. A., Poage, J. N., & Norton, J. D. (2001). Airborne thermal remote sensing for water temperature assessment in rivers and streams. *Remote Sensing Of Envionnement* , pp. 386-398.

Touchart, L. (2001). De la température de l'eau à la géographie des lacs. Université de Limoges, Thèse d'HDR en géographie, 480 p.

Touchart, L. (2002). *Limnologie physique et dynamique.* Paris: L'Harmattan.

Touchart, L. (2007 a). La définition de l'étang en géographie limnologique. Dans A. Angéliaume-Descamps, F. Ardillier-Carras, D. Banas, P. Bartout, C. Bernard, C. G.Genest, . . . L. Touchart, *Géographie de l'étang. Des theories globales aux pratiques locales.* (pp. 14-53). Paris: L'Harmattan.

Touchart, L. (2007 b). L'étang et la temperature de l'eau : un ensemble d'impacts géographiques. Dans A. Angéliaume-Descamps, F. Ardillier-Carras, D. Banas, P. Bartout, C. Bernard, C. G.Genest, . . . L. Touchart, *Géographie de l'étang. Des theories globales aux pratiques locales.* (pp. 119-156). Paris: L'harmattan.

Tricart, J., & Bravard , J.-P. (1991). L'aménagement des trois plus grands fleuves européens : Rhin, Rhône et Danube. Problèmes et méfaits. *Annales de Géographie*, pp. 668-713.

Wawrzyniak, V. (2012, 12 12). Etude multi-échelle de la température de surface des cours d'eau par imagerie infrarouge thermique : exemples dans le bassin du Rhône . Thèse de doctorat en Géographie et d'Aménagement soutenue à l'Université Jean Moulin Lyon 3.

Webb, B. W., Hannah, M. D., Moore, D. R., Brown, L. E., & Nobilis, F. (2008, 02 26). Recent advances in stream and river temperature research. *Hydrological Processes*, pp. 902-918.

Webster, I. T., Jones, G. J., Oliver, R. L., Bormans, M., & Sherman, B. S. (1997). *Control strategies for cyanobacterial blooms in weir pools.* Murray Darling Basin Commission: National Resource Management Strategy.

Wilhem, F. (1960). Die Seen als geographisches Forschungsobjekt. *Berichte zur deutschen Landeskunde*, pp. 305-321.

DISPERSION MODEL PROSPECTIVE OF AIR POLLUTION IN TIRANA

Medjon HYSENAJ [1]

ABSTRACT:
Outdoor air pollution is the most hazard challenge of many governments. Strictly policies followed by continue alert thresholds are being followed. Environmental issue canalized in air quality in the capital of Albania is the prior thematic analyzed in this paper. We figured to create a filter which gradually puzzles out the leading cause to exceed the limits settled by the WHO guidelines and the EU's AAQ directives. The paper tries to create potential scenario from the replacement of the passenger's vehicle fleet from the current Euro 3 to Euro 4 and over. The opportunity to structure evaluation maps for air assessment based on the outcome creates a clear overview of the current situation. Digital maps are a potential source of solution for many environmental issues. Spatial technology is fast and reliable to estimate population exposure to outdoor pollution. Geostatistical data offer reliable solution to perceive dispersion model issues. In this paper we concentrate on air pollution data (PM10).

Key-words: *geostatistic, dispersion model, spatial technology, digital map, PM10, air quality index.*

1. INTRODUCTION

Transportation is one of the vital components in modern human daily life; however, it has both productive effects on human development and detrimental effects on public health (Al Koas, 2010). The global concern for the environment is motivated by the role that the environment has on human society (Seferkolli, 2010). The paper aims to embrace environmental challenges we are facing nowadays. Almost every government policies are running toward reducing harmful elements derived from water, earth or air pollution. The last one will turn to be primary concern in this study as it overcomes EU's AAQ directives also WHO guidelines not only in daily values but also in annual terms.

The effect of air pollution on public health, vegetation, and more generally, on the human society and the ecosystem has been a burning issue in recent years (Deb and Tsay, 2018). Air quality models are designed to create a better perspective for further decision-making and establishment of strong and healthy policies. To create predictive scenarios helps maintain the right balance through all enrolled actors. Also maximizes the chances to find the right solution to the problem. Spatiotemporal modeling methods offer expanding opportunities to environmental research because they allow a user to display and model the spatial relationships and patterns between causes and effect when geographic distribution is part of the problem (Wang, 2008). We think that actual air data retrieved from monitor stations are caused by one main factor; deteriorated use of the passenger's vehicle fleet in circulation which mainly belongs to standard Euro 3. The paper goal is to predict the air pollution trend in case of upgrading the standard of the vehicle fleet.

Air quality management includes monitoring and analysis of pollutant concentration, spatial distribution of pollutant concentration, and assessment of no. of environmental factors affected by air pollutants, health risk map (Pandey et al, 2013). Currently 27% of the urban population lives in Tirana (Our World in Data, 2017) where the world average

[1]*University of Shkodër, Department of Geography, Shkodër, Albania, medjon.hysenaj@unishk.edu.al.*

indicator is 16%. Also many developed European countries such as Italy or Germany these values are even lower respectively 9.8% and 5.8%. The impact of urban air pollution on the environments and human health has drawn increasing concerns from researchers, policymakers and citizens (Xie, 2017). Commonly used indicators describing PM that are relevant to health refer to the mass concentration of particles with a diameter of less than 10 μm (PM10) and of particles with a diameter of less than 2.5 μm (PM2.5) (WHO, 2013). According to statistics absolute deaths from ambient PM10 air pollution is followed by concerning values.

PM causes a variety of human health and economic impacts each year (e.g., mortality, morbidity, DALYs, lost income from work absences, costs of health care (USAID, 2012). The number of premature deaths caused by air pollution (due to negative impact of PM2.5) in Albania is 16.9% compared to more developed European countries most of whom rely on values below 3%. There is a large spatial variability associated with air pollution; therefore even in a small area air pollution varies widely from place to place (Wijeratne, 2003). The amount of available data is limited and subject of short term measurements. The lacks of coordination, reduced government budget, misleading enhanced policies are ranked through the major causes of the current situation.

2. METHODS AND ANALYSES

The paper emphasis the fact that we need to split the problem into several steps (**Fig. 1**) until we understand the primary cause and the future policy to follow. Through all the harmful matters regarding air pollution we decided to concentrate our study on the particulate matter also known as (PM) rather than other matters such as Nitrogen oxides (NOx), Carbon monoxide (CO), Hydrocarbons (HC), due to its high risk impact it has revealed in many similar researches. Also statistics from the Ministry of Environment confirm that the average presence of particular matter in the air compared to AAQ directives is apparently higher than other elements.

Define Strategy (Predictive Scenario)	5
Alert Threshold Excedeed	4
Integrate gathered data into visual tabloid	3
Identify responsible category (tools or logistic)	2
Calculate primary phenomenon related to air pollution	1
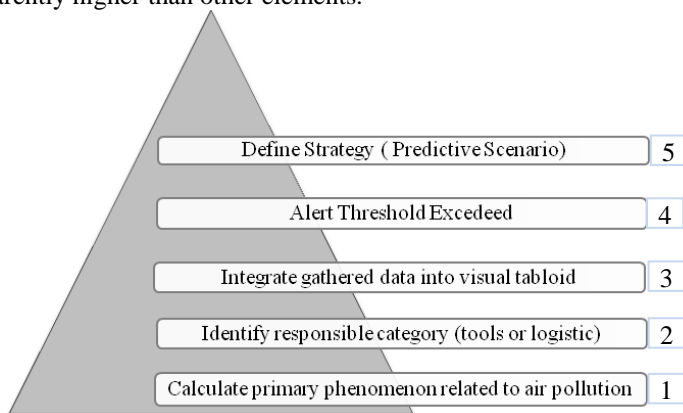
Fig. 1. Hierarchical steps for air pollution management.

PM10 originates from both natural and anthropogenic sources (Netherland Court of Audit, 2019). According to statistics the principal source of airborne PM10 matter in European cities is anthropogenic due to road traffic emissions, particularly from diesel vehicles (Air Quality in Europe, 2018). Data retrieved from IFBZ (**Tab. 1**) confirm the results follow the same trend for Tirana.

Primary sources of air pollution in Tirana.

	Primary sources of air pollution	Elements/Components	Impact (%)
1	Sea Air Masses	Cl	0.8
2	Soil dust including air masses from the Sahara	Ti, Mn, Fe, Sr	3.3
3	Transformation of S oxides into sulfate / burning of mazut	S, BC, V, Cr, Ni, Zn, Pb	1.1
4	Emissions from the construction industry / cement factories	Ca, Zn, BC	18.8
5	Natural source contaminated by traffic re-circulation	Ca, K, Fe, Mn, Sr, S	**42.8**
6	Traffic emissions / waste incineration or industries	V, Cr, Mn, Ni, Br, Pb, BC	13.3
7	Wood heating emissions	K, Fe, Cu, BC	19.8

Source: IFBZ (Institute of Applied Nuclear Physic)
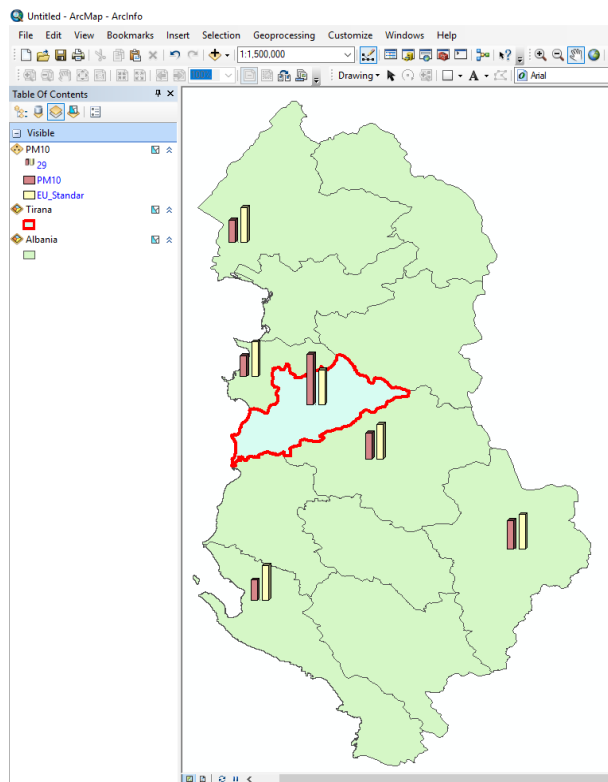
Fig. 2. Air pollution, PM10 index, Albania administrative territory (Sw; ArcMap 10.6)
Source: INSTAT; Comparative level EU Standard.

The monitor process has significant time and reliability limits. Many geographic areas still lack constant data and above all continuous control. Monitoring equipments need to be calibrated and verified. Understanding pollutants` spatial distribution and monitoring the air quality by applying geospatial approaches is challenging and topical in data quality research field (Enkhtur, 2013). At a large scale investigation (**Fig. 2**) spatial dispersion of

PM10 matters identify the capital as the most polluted zone in the country. Meanwhile other districts rely on sustainable values close or below the limits settled by AAQs directives. Due to increasing air pollution in Tirana we insist that immediate measures need to be taken by responsible actors cause every day citizens suffer first from the current situation, second from the lack of awareness. From **Fig. 3** we understand that PM10 average data from the last five years are above the limit (40 μg/m^3) daily. Not only, is the future trend to reach higher values.
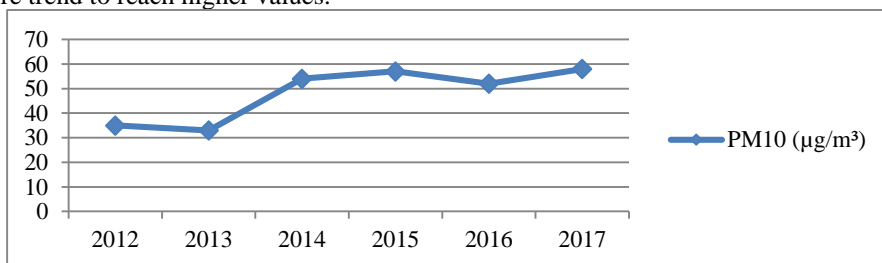
Fig. 3. Average PM10 index in Tirana; Source: INSTAT.

An important indicator of the current situation is that compared to other districts Tirana ranks at first place with 233 vehicles per 1000 inhabitants, which is far lower from the average of EU countries offered by EUROSTAT 505 vehicles per 1000 inhabitants. Meaning, emissions issues exist as a matter of fact not from large number of vehicles than the year of production and maintenance condition. We must create a better view of which category shares the largest fleet. Categorized by fuel type (**Fig. 4**) 72 % of them are diesel vehicles. We notice that passenger vehicles shares 79% of the entire fleet and that 69% of this category (**Fig. 5**) are 11-20 years old. If we compare outcome values to those in **Table 2** we notice that Euro 3 standard prevails.
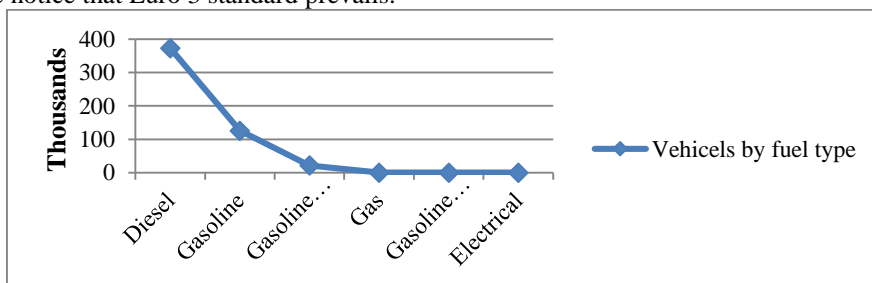
Fig. 4. Source: Ministry of Transport and Infrastructure.
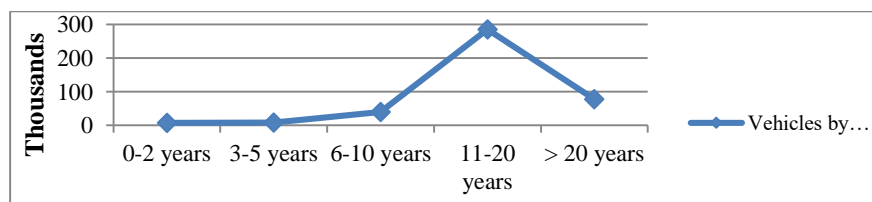
Fig. 5. Source: Ministry of Transport and Infrastructure.

Emissions standard - New type approvals.

Emissions standard	Applied to new passenger car approvals from:	Applied to most new registrations from:
Euro 1	1 July 1992	31 December 1992
Euro 2	1 January 1996	1 January 1997
Euro 3	1 January 2000	1 January 2001
Euro 4	1 January 2005	1 January 2006
Euro 5	1 September 2009	1 January 2011
Euro 6	1 September 2014	1 September 2015

Source: RAC, UK

After the calculation of the primary phenomenon related to air pollution (step 1) and identify responsible category (step 2) we are ready to step 3; integration of data retrieved from monitor stations into dispersion models. Our zone of study is located at latitude: $41.33°$ and longitude: $19.82°$ with an elevation: 103 m. We exploit data retrieved from five monitor stations. They are geographically distributed in areas with consistent vehicle traffic. They cover an area of 1630 km2 and 5420 m perimeter. Geographical data rely on a scale of 1: 200 m with a transverse Mercator projection; Projected coordinate system: UTM Zone 34 N. The Spatial Information Sciences (SIS) provides mature solutions for data and policy integration, since the nature of problem is specific to geo-spatial distribution [Sertel et al, 2012]. We notice four stations evidently exceed EU limit. Station 1 and 2 reveal values far behind the limit respectively by 119% and 79% (**Fig. 6**). The World Health Organization (WHO) implies air quality guidelines that are even stricter than the AAQ directives. If we compare the pollution trend focused on the city main streets and center location through a period of five years we notice that the situation has not improved or evolved at all (**Fig. 7**).
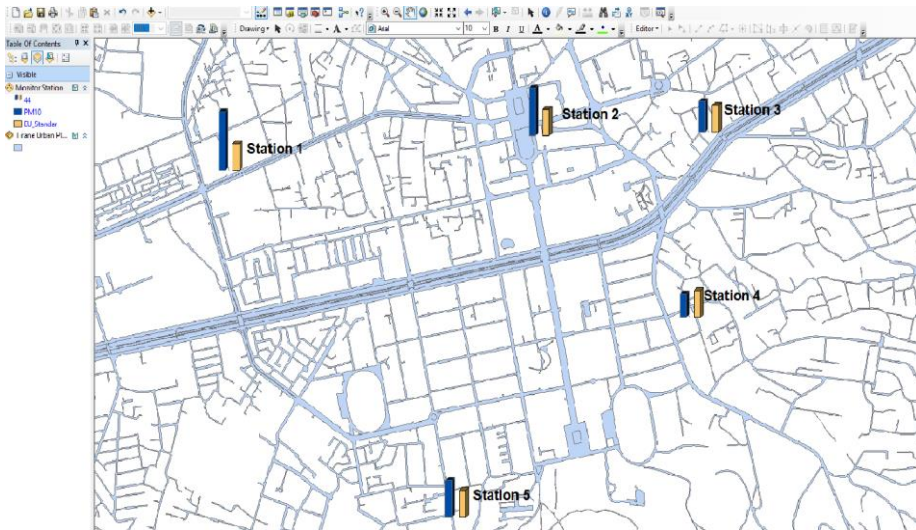
Fig. 6. Air pollution, PM10 index, city center; Data source: Ministry of Environment, 2018

Comparative level; EU Standard 40 microgram/m^3.
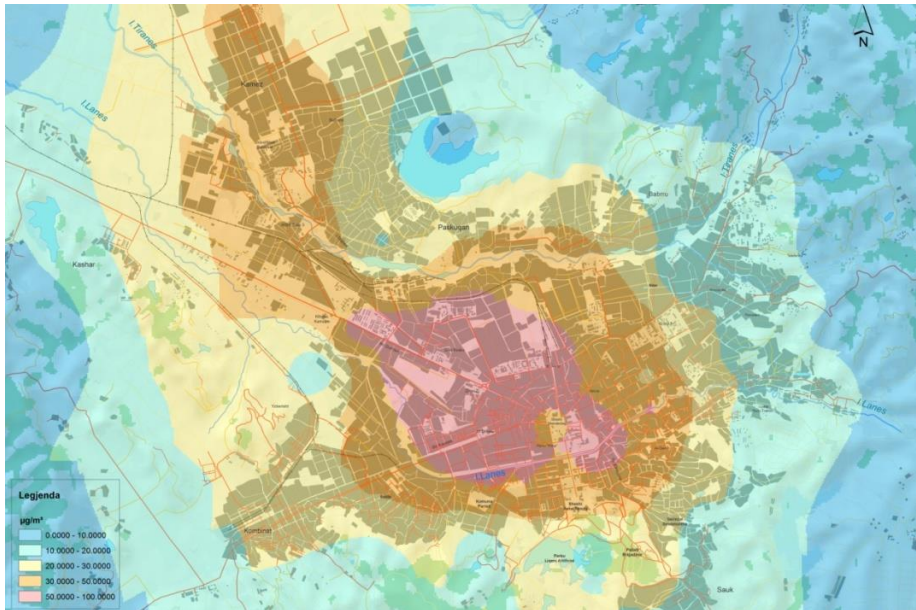
Fig. 7. PM10 dispersion; Data source: National Environment Agency, 2014.

On the other hand long terms measurements to calculate daily limit values per year could not succeed due to lack of budget and coordination between actors and policies, thought we can deduce from partially measurement retrieved from station 3 and 5 (**Fig. 8**).
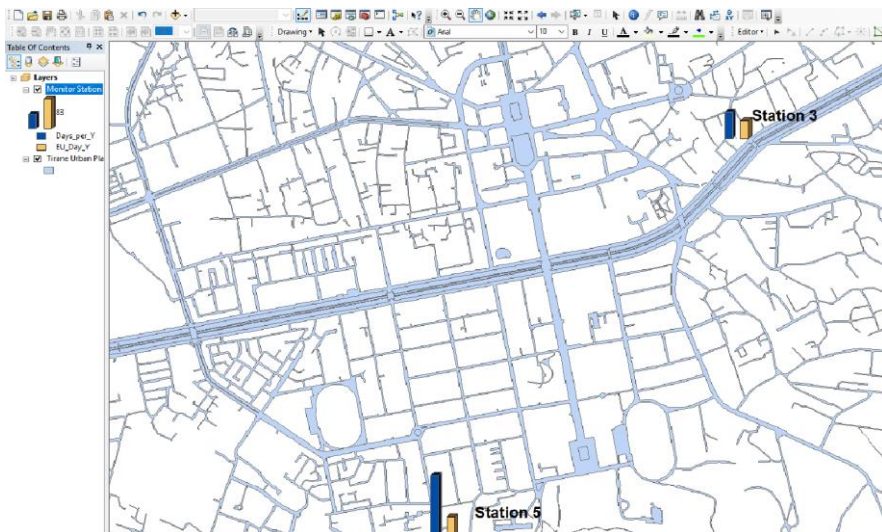
Fig. 8. Air pollution, PM10 index, Data source: Ministry of Environment
Comparative level; EU Standard 50 microgram/m3 - Permitted exceeds per year 35 days.

We have 21 days exceed from 28% time coverage at station 3 and 76 days exceed from 45% time coverage at station 5. Though a full year analytic process could lead us to an alarming situation leading approximately to 166 and 73 days of exceed from 35 days limit per year according to AAQ directives. This scenario could be even more pessimistic if we could have the possibility to apply long term measurement to station 1 and 2 which as above mentioned both denote much more polluted areas.

3. RESULTS AND DISCUSSIONS

We highlight the current environment position in the capital; also define main factors that influence its persistent deterioration. The goal is to create a clear picture for the right measures. If we consider current data, what with happen in case we decide to massively replace most of the vehicle fleet basically through long term policies supported by government and NGO actors? We deduce potential values from a possible fleet category transition. Euro 3 emissions for passenger cars is 0.05 g/km compared to Euro 4 (0.025 g/km) or Euro 5b and further (Euro 6b, c, d) which is 0.0045 g/km (**Fig. 9**). From Euro 3 to Euro 6 we notice a consistent decrease of the particular matter (PM10) emission respectively by 50 % and 91%. We exploit the outcome indicators to calculate a potential transition of fleet replacement.

Based on the emission index we settle a proportionally report between (euro 3-euro 4 reduce emission by 50%) and (euro 3-euro 5 reduce emission by 91%). If we apply this index to values retrieved from the five monitor stations we retrieve more optimistic results of air pollution (**Tab. 3**).
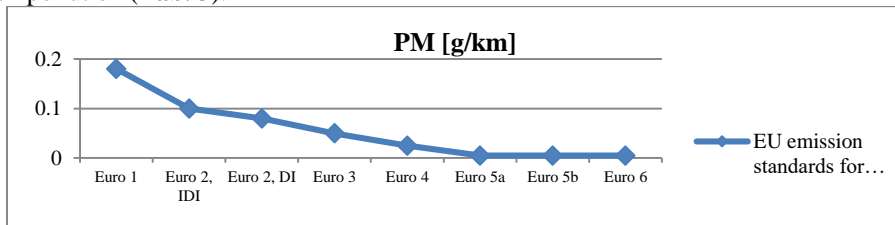
Fig. 9. Source: Ecopoint, EU emission standards for passenger cars.

Table 3.

Vehicle fleet Replacement - Potential Scenario

PM10 Scenario (Predictive data for each monitor station based on Euro vehicle emissions)					
Monitor Stations		**Euro 3**	**Euro 4**	**Euro 5b >**	
"21 Dhjetori" Street	Station 1	87.78	43.89	8	EU limit 40 microgram/m3
Municipality of Tirana	Station 2	71.85	35.9	6.4	
Ministry of Environment	Station 3	46	23	4.1	
Public Health Directorate	Station 4	34.4	17.2	3	
National Agency of Environment	Station 5	55.2	27.6	4.9	

50%

91%

(Input-Data under column Euro 3 represent current measured values; Output- Predicted Data under column Euro 4, 5; Values express microgram/m^3).

If we convert vehicles to Euro 4 all values fall approximate to settled limit or below the assigned EU threshold standard. Meanwhile Euro 5 vehicles and over not only accomplish all EU requirements but also reveal quite an optimistic panoramic situation of air quality definitely bypassing all pollution issue. We presume that the current values corresponding to the EU daily limits per year will also follow the new trend. **Figure 10**, **11** expose a future air index dispersion model based on calculated data (**Tab. 3**). Values below column (Euro 3) correspond to current measured values.
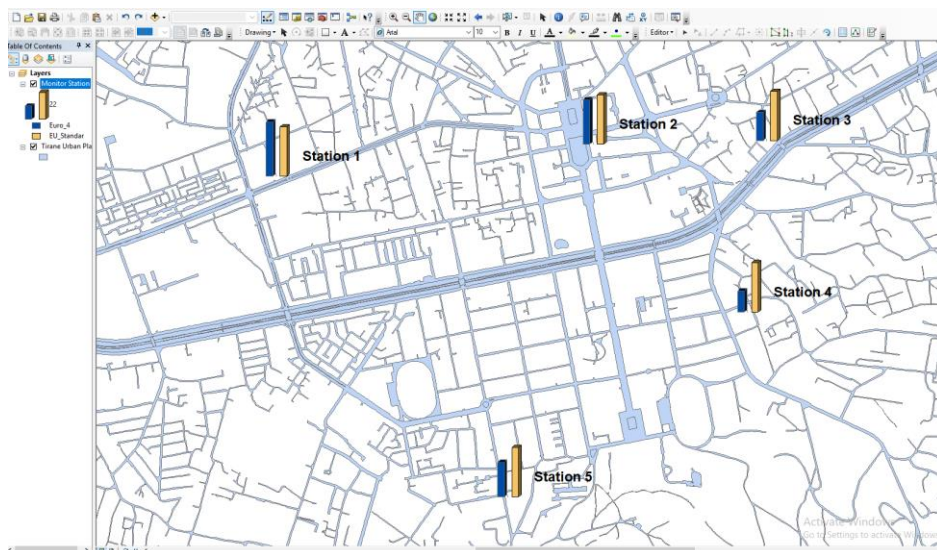
Fig. 10. Air pollution, PM10 index; Comparative level; EU Standard 40 microgram/m^3. Vehicles fleet replacement scenario to Euro 4.
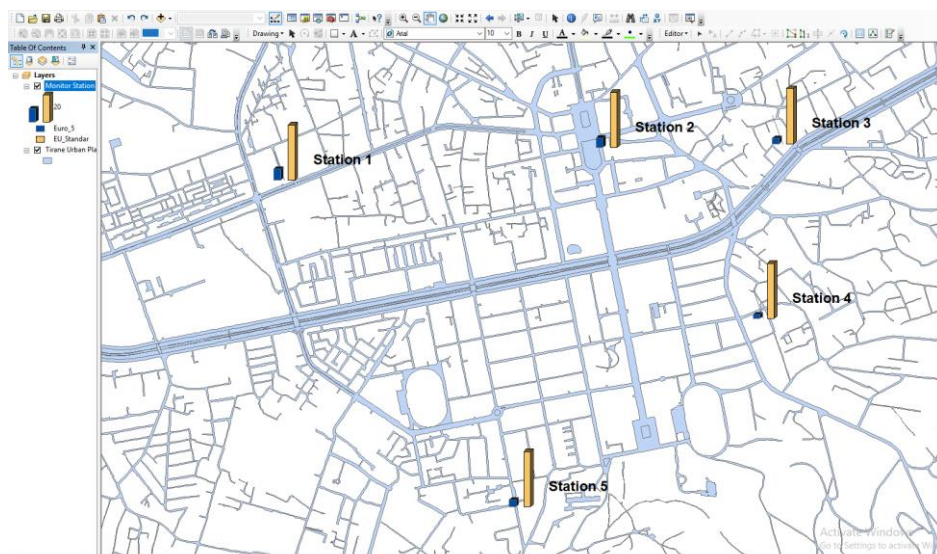
Fig. 11. Air pollution, PM10 index; Comparative level; EU Standard 40 microgram/m^3. Vehicles fleet replacement scenario to Euro 5.

5. CONCLUSIONS

The large scale development spatial tools have recognized recent years create a new exploitation perspective toward the management of environmental issues. Population perception toward air pollution must change. The ability to manage several layers contemporary intertwined with the possibility to reflect continues data results turns mapping process of primary importance to the current situation.

We believe that spatial technology creates a closer approach to the solution of managing air quality. It works as a bridge to connect all participating actors. As an issue that is strictly connected to geographical conception and spatial perspective air pollution must and should rely on spatial technology. We tried to create a filter to analyze air concern moving from the bottom to the top of the pyramid. The successive steps of the pyramid help us identify areas that crossed the red line also the principal causes.

Measured elements such as Ca, K, Fe, Mn, Sr, S address traffic re-circulation as the primary source of traffic pollution to reach a value of 43% of the total amount of elements. Approximately 70 % of the entire vehicle fleet belongs to Euro 3. Based on the emission index we settle a proportionally report between (euro 3-euro 4 reduce emission by 50%) and (euro 3-euro 5 reduce emission by 91%). If we apply this index to values retrieved from the five monitor stations we retrieve more optimistic results of air pollution.

From the held analysis we deduce that the replacement of the passenger's vehicle fleet from Euro 3 to Euro 4 will normalize the air risk probability into appropriate value close to AAQ directives but still higher than WHO guidelines. Meanwhile a possible leap into Euro 5 definitely accomplishes both requirements. Performed calculations reveal that the current situation in Tirana has a potential solution but it requires immediate enrolment of government entities through strict policies toward environment protection.

R E F E R E N C E S

Air Quality in Europe. (2018) https://www.airqualitynow.eu/pollution_home.php

Al Koas K A. (2010) GIS based Mapping and Statistical Analysis of Air Pollution and Mortality in Brisbane, Faculty of Build Environment and Engineering, Queensland University of Technology, Australia

Deb S., Tsay R. S. (2018) Spatio-temporal models with space-time interaction and their applications to air pollution data, University of Chicago, 1−32

Ecopoint Inc. (2019) https://www.dieselnet.com/standards/eu/ld.php

Enkhtur B. (2013) Geostatistical modeling and mapping of air pollution, Faculty of Geo-Information and Earth Observation, University of Twente, The Netherlands.

INSTAT. (2017) Albanian Institute of Statistics, www.instat.gov.al

Ministry of Environment. (2017) https://mjedisi.gov.al/.

Ministry of Transport and Infrastructure. (2017) www.infrastruktura.gov.al

National Environment Agency. (2014) http://www.akm.gov.al/cil%c3%absia-e-mjedisit.html#monitorime

Netherland Court of Audit. (2019) Supreme Audit Office of Poland Joint Report on Air Quality

Our World in Data. (2017) Population in the largest city (% of urban population), https://ourworldindata.org/grapher/population-in-the-largest-city?tab=chart&time=1960..2017&country=ALB

Pandey M., Singh V., Vaishya R .C, Shukla A K. (2013) Analysis & Application of GIS Based Air Quality Monitoring- State of Art, *International Journal of Engineering Research & Technology*, 3788–3789

Royal Automobile Club (RAC). (2018) www.rac.co.uk/drive/advice/emissions/euro-emissions-standards

Seferkolli L. (2009) An Environmental Atlas of Albania, Institute for Geoinformatics, University of Muenster

Sertel E., Demirel H., Kaya S. (2012) Predictive mapping of air pollutants: a spatial approach, Faculty of Civil Engineering, Maslak Istanbul, 5–10

USAID, CCAD. (2012) Overview of Particle Air Pollution (PM2.5 and PM10) Air Quality Communication WorkshopSan Salvador, El Salvador

Wang X. Y. (2008) Spatial analyses of long-term exposure to air pollution and cardio respiratory mortality in Brisbane, Australia, Institute of Health and Biomedical Innovation, Queensland University of Technology

Wijeratne I. (2003) Mapping of dispersion of Urban Air Pollution using Remote Sensing Techniques and ground station data, 125–130

World Health Organization. (2013) Health Effects of Particular Matter,

http://www.euro.who.int/__data/assets/pdf_file/0006/189051/Health-effects-of-particulate-matter-final-Eng.pdf

Xie X., Semanjski I., Gautama S., Tsiligianni E., Deligiannis N., Rajan R. T., Pasveer .F, Philips W. (2017) Review of Urban Air Pollution Monitoring and Exposure Assessment Methods, *International Journal of GeoInformation*, 389–410

EVALUATION OF BURNED AREAS WITH SENTINEL-2 USING SNAP: THE CASE OF KINETA AND MATI, GREECE, JULY 2018[1]

Kamill Daniel KOVÁCS[2]

ABSTRACT:
The aim of this paper is to compare the two largest forest fires that occurred in Greece in July 2018 using metrics for burned area and burn severity mapping, derived only from free satellite data. Sentinel-2 satellite images of the European Space Agency (ESA) within the Copernicus program provide a spatial resolution of 10 m, which facilitates more accurate monitoring of environmental phenomena such as forest fires. The processing of the satellite images and the calculation of the metrics was performed using SNAP software, which is an open-source software developed by ESA. The mapping of the obtained results was performed in the QGIS software, which is also an open-source software. The delimitation of the burned area and the classification of the severity of both wildfires was performed using the Relativized Burn Ratio (RBR) satellite index. These results were contrasted with the Copernicus Emergency Management Service (EMS) maps related to these two events. Our results obtained in relation to the size of the burned area show smaller affected areas than the Copernicus Emergency Management Service maps. This is explained by the different methods used in the delimitation of the burned areas. In the case of Mati's wildfire the EMS has created the thematic layer by means of visual interpretation using post-event satellite image and in the case of Kineta's wildfire was applied a semi-automatic approach. Moreover, in this study is proposed and evaluated a new burn severity metric, the burned vegetation index (BVI) which shows where the most significant changes in healthy vegetation occurred. This new index was compared with RBR, dNDVI and dNBR using statistical correlation. The results indicate that BVI shows better the burned vegetation and its statistical correlation with RBR is significant ($R^2 = 0.92$).

Key words: burned area mapping, burn severity, RBR, BVI.

1. INTRODUCTION

Fires are a common phenomenon in Mediterranean forest ecosystems, with regime change in the Mediterranean Basin mainly due to changes in land use and climate change (Pausas, 1999). According to Spanish statistics (MAPAMA, 2016) recorded from 1970 to 2010, the total number of forest fires in Spain showed a trend of decline. However, in the Euro-Mediterranean area, in recent decades, there has been a growing trend in the percentage of burned areas by large forest fires (>500 ha) compared to the total burned area per year (San-Miguel-Ayanz & Camia, 2009; Spano et al., 2014).

Following Keeley (2009), the concept of *fire severity* refers to the loss of organic matter both "on" and "under-soil" caused by the passage of fire, and should be differentiated from *burn severity*, which by including the response of the ecosystem (González-De Vega et al., 2015; Regueira et al., 2015; Fontúrbel et al., 2015) is more

---

[1] This work was presented at the "George Vâlsan" National Conference for Students held at the Babeş-Bolyai University, Faculty of Geography, 5-7 April 2019, Cluj-Napoca.
[2] *Babeş-Bolyai University, 400006 Cluj-Napoca, Romania, kovcsdniel962@gmail.com*

complex to assess and involves prior knowledge of the existing community before the fire and its response to fire (Moya et al., 2009). In general, to estimate fire severity from satellite images, standardized methods based on spectral indices are used, such as the normalized difference vegetation index (NDVI) and the normalized burn ratio (NBR) (Chuvieco, 1999). The effect of fire on the ecosystem is closely linked to the burn severity (Vallejo et al., 2012; González et al., 2016), being greater the damage produced in vulnerable areas with low site quality, such as arid and semi-arid areas of Mediterranean climate (Hedo et al., 2014). This damage linked to the high burn severity can even affect instant energy flows (Sánchez et al., 2009) and their resilience (Paula et al., 2009; Tessler et al., 2014). Ecosystem resilience, understood as *engineering resilience*, is the rate of natural recovery to pre-disruption balance (Cantarello et al., 2017) and it is necessary to understand how certain transient states move from the transition to final stages (Doblas-Miranda et al., 2017). Knowing this problem is necessary for the correct sustainable management of the landscape, especially in areas sensitive to desertification, where the damage of recurrent and severe forest fires could lead the ecosystem to irreversible stages, causing the loss of ecosystem services (Doblas-Miranda et al., 2015), such as carbon storage capacity (Moya et al., 2014). Therefore, correct post-fire management must be based on knowledge of the relationships between ecosystem resilience, fire severity and ecosystem recovery (Díaz-Delgado & Pons, 1999).

Numerous severity indices have been developed, highlighting the standardized NBR difference (dNBR), the standardized difference of NDVI (dNDVI) and the relative version of dNBR (RdNBR); all of them used as independent variables used to deduce the field indices of severity at the pixel level. There is a wide range of studies that demonstrate their sensitivity to changes in severity classes (Chu & Guo, 2014). Both NDVI and NBR are widely validated for severity assessment, although the best results seem to be obtained from NBR-based indices (Escuin et al., 2008) as it combines two infrared bands (NIR and SWIR) that respond better to fire detection (Vlassova et al., 2014). However, the results are discussed given the low reliability in the zoning of soil severity with these methods versus those of vegetation (Vega et al., 2013) and the influence of several factors that determine the calculation, such as the local conditions, characteristics and conditions of pre- and post-fire vegetation and the time elapsed in the assessment of severity (Chu & Guo, 2014).

Consistent with major burn severity mapping efforts (Eidenshink et al., 2007), burn severity can be defined as the degree of fire-induced change to vegetation and soils, as measured with satellite image metrics (Parks, Dillon & Miller, 2014). The two most commonly used satellite image-based metrics of burn severity are the delta normalized burn ratio (dNBR) (Key & Benson, 2006) and its relativized form (RdNBR) (Miller & Thode, 2007), both of which depend on the calculation of normalized burn ratio (NBR). NBR is sensitive to the amount of chlorophyll content in plants, moisture, and char or ash in the soil (Parks, Dillon & Miller, 2014). All equations for dNBR, RdNBR and RBR use NBR derived from pre- and post-fire satellite images to quantify spectral change. All this metrics are sensitive to changes commonly caused by fire (Zhu et al., 2006; Hudak et al., 2007; Miller et al., 2009). However, the dNBR is an absolute difference which can present problems in areas with low pre-fire vegetation cover, where the absolute change between pre-fire and post-fire NBR will be small. In such cases the relativized version of burn severity (RBR) is advantageous and provides more accurate results (Equation 5) (Parks, Dillon & Miller, 2014). Researchers and practitioners commonly classify these continuous metrics into categorical maps representing unchanged, low, moderate and high burn severity.

$$dNDVI = NDVI_{prefire} - NDVI_{postfire}$$

(1)

$$NBR = \left(\frac{NIR - SWIR}{NIR + SWIR}\right) = \left(\frac{Band\ 8 - Band\ 12}{Band\ 8 + Band\ 12}\right)$$

(2)

$$dNBR = NBR_{prefire} - NBR_{postfire}$$

(3)

$$RdNBR = \frac{dNBR}{\left|\left(NBR_{prefire}\right)\right|^{0.5}}$$

(4)

$$RBR = \left(\frac{dNBR}{\left(NBR_{prefire} + 1.001\right)}\right) = \left(\frac{NBR_{prefire} - NBR_{postfire}}{\left(NBR_{prefire} + 1.001\right)}\right)$$

(5)

For all this, the demand and need of managers to provide cartographic information on the fire severity, as a basis for quantifying and assessing damage on the ecosystem and its recovery should incentivize the work of researchers to find the more accurate and reliable method of calculation. The objective of this work is (1) to delimit the area and classify the burn severity in the case of these two Greek fires using the RBR index, (2) to compare the results with the estimates of Copernicus Emergency Management Service; (3) and also to present a new severity index for the study of wildfires, the burned vegetation index (BVI) that is recommended for the study and calssification of burned vegetation.

2. STUDY AREA AND DATA

Two large fires broke out on the central-southern Greece mainland (Attica region) on 23 July 2018, causing significant casualties, village evacuations, damage to property, while burning thousands of hectares of forestry. Regional Greek authorities have declared a state of emergency in the eastern and western parts of greater Athens, and the EU Civil Protection Mechanism has been activated to request for aerial and ground firefighting assests (Copernicus Emergency Management Service, 2018). The two affected localities were Kineta and Mati near by the capital city of Athens **(Fig. 1)**. Kineta is a beach town in West Attica, situated on the northern coast of the Saronic Gulf, south of the Geraneia mountains. Mati is a village located on the east coast of Attica region, lies east of the Penteli mountains, on the Marathonas Avenue north of Rafina and south of Nea Makri. The resident population of these localities was respectively 1,446 and 200 inhabitants in 2011 (Hellenic Statistical Authority, 2011).

The data used for this study are four Sentinel-2 products. Two data sets of pre-fire and post-fire satellite imagery were obtained for the study of the Kineta fire, and other two for the Mati fire. For the Kineta fire two Sentinel-2A Level 2A tiles (Tile ID: T34SFH) were acquired between on July 3, 2018

Fig. 1. Location of the two main fires, 23 July 2018.

(before the main event) and August 19, 2018 (after the main event). In the same way, for the Mati fire one Sentinel-2A Level 2A (Title ID: T34SFH) and another one Sentinel-2B Level 2B tiles (Tile ID: T34SGH) was acquired between on July 3, 2018 (before the main event) and August 4, 2018 (after the main event).

This four Sentinel-2 scenes have been downloaded free from the official Copernicus Open Access Hub website, operated by the European Space Agency (ESA) and the Copernicus Programme (Copernicus Open Access Hub, 2018). The first two scenes shown below are for Kineta pre-fire state and post-fire state, the last two for Mati pre-fire state and post-fire state.

> S2A_MSIL2A_20180703T092031_N0208_R093_T34SFH_20180703T121025
> S2A_MSIL2A_20180819T090551_N0208_R050_T34SFH_20180819T133811
> S2A_MSIL2A_20180703T092031_N0208_R093_T34SFH_20180703T121025
> S2B_MSIL2A_20180804T090549_N0208_R050_T34SGH_20180804T142040

Mathematical calculations and band combinations were processed with the following Sentinel-2 spectral bands: B3 (Green band), B8 (NIR band), B8A (Vegetation Red Edge), B11 and B12 (SWIR bands). In addition, two maps provided by Copernicus Emergency Management Service and two vector packages (available to open in a GIS interface) accompanied by these products have been obtained free **(Fig. 2)** (Copernicus EMS, 2018). With this data it was possible to compare our results related to the size of the burned areas.
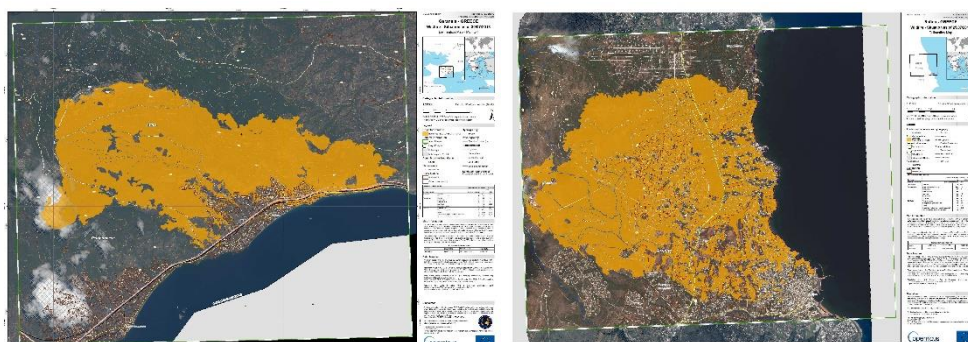
Fig. 2. Copernicus EMS maps of burned areas: Kineta (left), Mati (right) *(Source: Copernicus EMS).*

One of the major problems in Remote Sensing is the ability to have good data, which is, in particular, recorded at favourable time to highlight the objects or phenomena that are sought to be studied (Husson, 1983). In this case it was also essentially important that the areas of interest for this study are not covered by clouds in the satellite images. This is what primarily determines the selection of the time interval between satellite images.

3. METHODOLOGY

3.1. Identification and extraction of burned areas

Processing satellite data requires a GIS (Geographic Information System) environment. For data processing have been used the software SNAP (Sentinel-2 Toolbox), QGIS and Excel for subsequent statistical calculations.

For the Level 2A products that have been used in this study the atmospheric correction has already been applied. Solar radiation reflected by the Earth's surface to satellite sensors is affected by its interaction with the atmosphere. The objective of applying an atmospheric

correction is to determine true surface (Bottom-Of-Atmosphere, BOA) reflectance values from the Top-Of-Atmosphere (TOA) reflectance values, by removing atmospheric effects (Mousivand et al., 2015). Atmospheric correction is especially important in cases where multi-temporal images are compared and analysed as it is in this case (pre-fire and post-fire images). The SNAP software offers the integration of Sen2Cor algorithm for performing atmospheric correction. Sen2Cor is a processor for Sentinel-2 Level 2A product generation and formatting; it performs the atmospheric, terrain and cirrus correction of Top-Of-Atmosphere Level 1C input data. Sen2Cor creates Bottom-Of-Atmosphere, optionally terrain and cirrus corrected reflectance images; additional, Aerosol Optical Thickness, Water Vapour, Scene Classification Maps and Quality Indicators for cloud and snow probabilities (Main-Knorn, 2017).
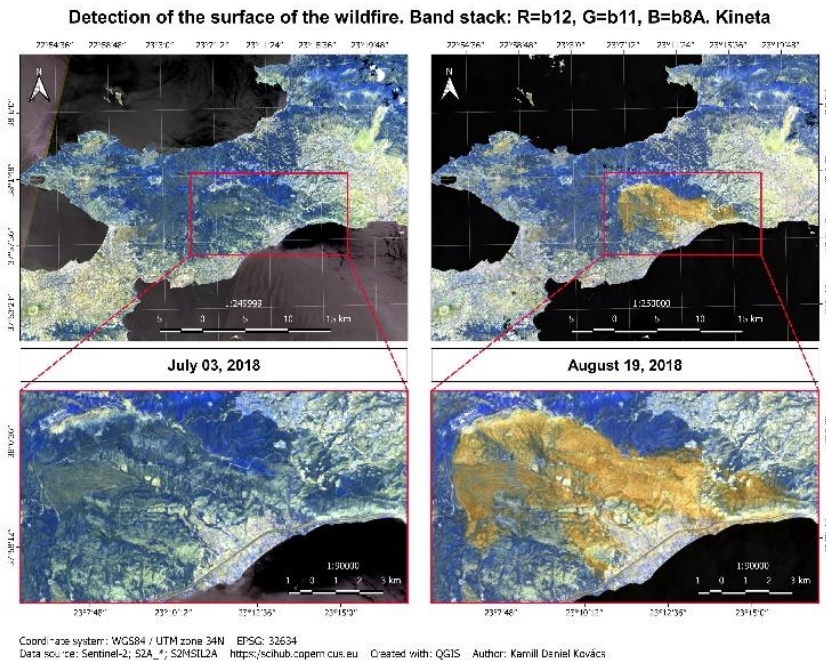
Fig. 3. Band stack, Kineta.

Atmospheric correction using Sen2Cor algorithm is a computationally heavy process and takes several time to be completed depending on the machine. However, since April 2017 the Level-2A products have already been generated and are available to download for acquisitions over Europe (such as this case).

To identify the newly burned areas, the following combination of bands has been established: Red: B12, Green: B11, Blue: B8A. It is possible to identify burned areas in true (natural) colours too but for distinguishing the burned areas it is better to use the Near InfraRed (NIR) and Short Wave InfraRed (SWIR) bands as these provide the best separability **(Fig. 3)**. Likewise, newly burned areas can be well identified with the NDVI index (Equation 6) **(Fig. 4, 5)**.

$$NDVI = \frac{NIR - RED}{NIR + RED} = \frac{Band8 - Band4}{Band8 - Band4} \tag{6}$$
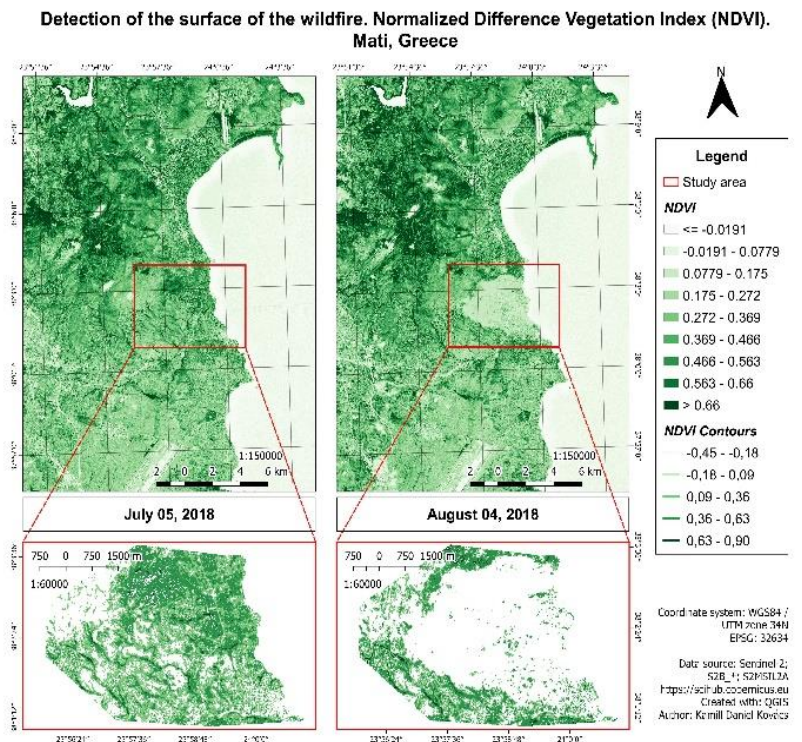
Fig. 4. Pre- and post-fire NDVI, Mati.
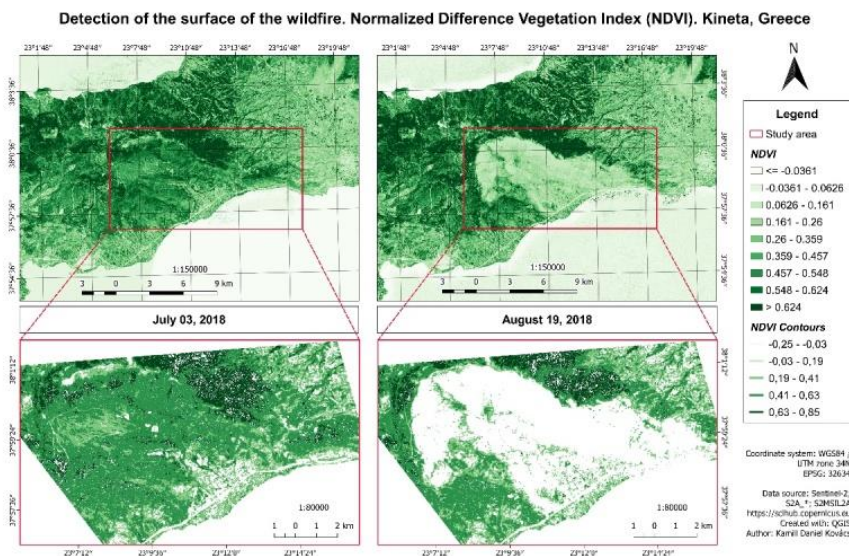
Fig. 5. Pre- and post-fire NDVI, Kineta.

The Sentinel-2 L2-A product conveniently contains vector and cirrus cloud masks, which are created as a product of the atmospheric correction. However, applying the mask on all bands and the entire scene may take some time. A subset could have been done with the product, but the vector products are lost by that operation. So, in this case, to preserve the information a new band was created containing a cloud mask **(Fig. 6)**. Currently, this is not possible to do using the Batch Processing tool in SNAP, so it has been necessary to add the cloud mask band to each product separately.

To identify pixels that contain clouds, the masks
scl_cloud_medium_proba, *scl_cloud_high_proba*, and *scl_thin_cirrus*
have been used with the following expression in Band Maths:
if (scl_cloud_medium_proba + scl_cloud_high_proba + scl_thin_cirrus) <255 then 0 else 1.

The calculation results in a single mask band that contains all clouds.

As mentioned above, the Batch Processing tool available in SNAP allows the user to process all images at the same time, thus saving time with repetitive calculations. To use this tool, it was first necessary to define all the steps of the process that were to be executed. The process steps have been set with the GraphBuilder tool in SNAP. The advantage of the GraphBuilder tool is that no intermediate product will be physically saved, only the final product.

The input products contain 13 spectral bands in 3 different spatial resolutions (10 m, 20 m, 60 m). The SWIR band (B12) that is a component of the NBR index calculation has a spatial resolution of 20 m. Many operators do not support products with bands of different sizes so it was necessary to resample the bands to the equal resolution of 10 m. The reference band for resampling was Band 2 (Blue) which has 10 m resolution **(Fig. 6)**. The resampling method that was used is the bilinear interpolation method (Lyons et al., 2018). In the Subset tab the bands B3 (Green), B8 (NIR), B12 (SWIR) and the cloud mask band were selected. Only these bands are required for the following calculations of NBR and RBR.

The most commonly used metrics for burned area and burn severity mapping, derived from satellite data, is the normalized burn ratio (NBR) (Equation 2). Healthy vegetation has very high near-infrared reflectance and low reflectance in the shortwave infrared portion of the spectrum. Burned areas on the other hand have relatively low reflectance in the near-infrared and high reflectance in the shortwave infrared band. A high NBR value generally indicates healthy vegetation while a low value indicates bare ground and recently burned areas.

After the calculation of NBR pre- and post-fire it was appropriate to merge all the pre- and post-fire bands and products into a single database (Collocation) **(Fig. 6)**. With this merged database of the pre-processed products were calculated the changes in the pre- and post-fire NBR values.

Water bodies may show a similar NBR difference in certain circumstances, therefore they needed to be masked. It was also important to mask the clouds that occur in any of the input images. For this purpose, a single combined mask of water and clouds has been created.
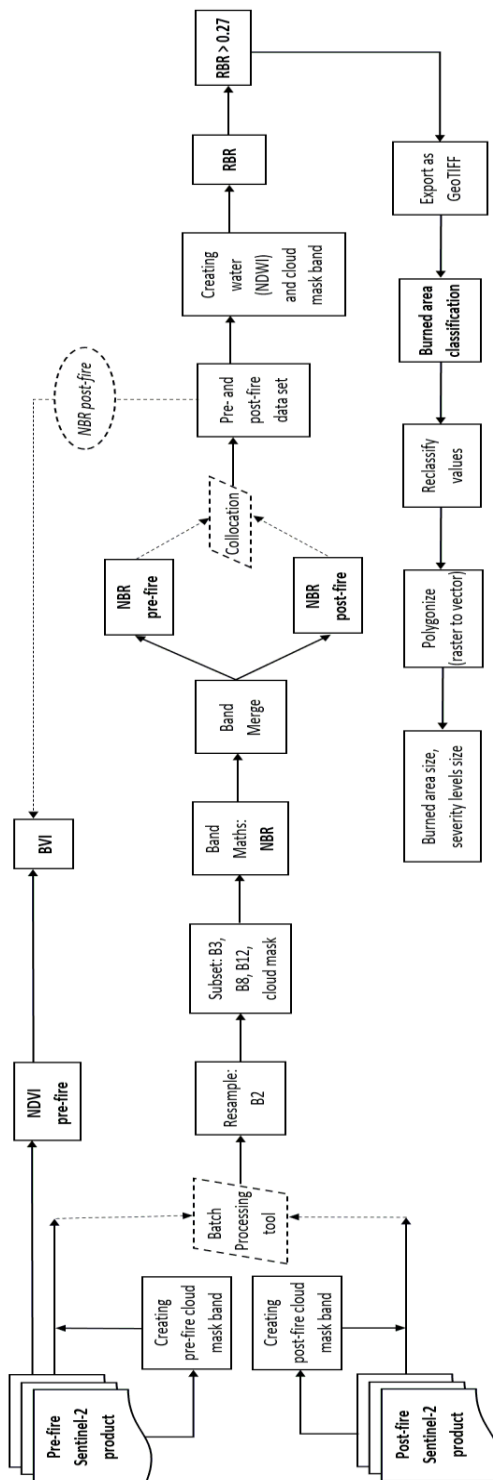
Fig. 6. Flowchart of extracting burned areas by calculating RBR and BVI.

The Normalized Difference Water Index (NDWI) has been used to detect water bodies. The NDWI proposed by McFeeters is designed to maximize the reflectance of the water body in the green band and to minimize the reflectance of water body in the NIR band. McFeeters's NDWI is calculated as (Du et al., 2016):

$$NDWI = \frac{Green - NIR}{Green + NIR} = \frac{B3 - B8}{B3 + B8}$$

(7)

The water and cloud mask was calculated with the following expression in Band Maths:
if (cloud_mask_pre-fire > 0 or cloud_mask_post-fire > 0 or ((B3_pre-fire – B8_pre-fire)/(B3_pre-fire + B8_pre-fire))>= 0.0) then 1 else 0.

To identify recently burned areas and differentiate them from bare soil and other non-vegetated areas we used the Relativized Burn Ratio (RBR) (Equation 5). The RBR is the dNBR divided by a simple adjustment to the pre-fire NBR. Adding 1.001 to the denominator ensures that the denominator will never be zero, thereby preventing the equation from reaching infinity and failing (Parks, Dillon & Miller, 2014). With the calculation of the RBR it has also been applied the cloud and water mask. The RBR was calculated with the following expression in Band Maths: if cloud_water_mask == 0 then ((NBR_pre-fire – NBR_post-fire)/(NBR_pre-fire + 1.001)) else NaN.

To extract only the burned area, another band has been created by establishing a threshold for pixel to be classified as burned to > 0.27 (Keeley, 2009; UN-SPYDER Knowledge Portal). Only those pixels where RBR is larger than 0.27 have been selected. This value of 0.27 corresponds to moderate burn severity areas. Therefore, only areas classified as moderate burn or higher have been selected. To extract this pixels the following expression was introduced in BandMaths: if RBR > 0.27 then RBR else NaN.

After exporting the burned area in GeoTIFF (*.tif, *.tiff) format, burn severity has been interpreted in QGIS according to the following table **(Table 1)**. This values are proposed by The United States Geological Survey (USGS) to interpret the burn severity (dNBR).

Table 1.

Burn severity levels obtained calculating dNBR, proposed by USGS
(Source: Keeley, 2009; UN-SPYDER Knowledge Portal)

Severity Level	dNBR range (scaled by 10^3)		dNBR (not scaled)
Enhanced Regrowth, hight	-500 to -251		-0.500 to -0.251
Enhanced Regrowth, low	-250 to -101		-0.250 to -0.101
Unburned	-100 to +99		-0.100 to 0.099
Low Severity	+100 to +269		0.100 to 0.269
Moderate-low Severity	+270 to +439		0.270 to 0.439
Moderate-high Severity	+440 to +659		0.440 to 0.659
High Severity	+660 to +1300		0.660 to 1.300

In order to calculate the size of the burned area, the obtained raster has been polygonized. The vectorization process was done in QGIS, with the *Reclassify values (simple) (SAGA GIS)* and *Polygonize (raster to vector) (GDAL)* tools. In the process of reclassifying the values, only the values belonging to categories Low Severity, Moderate-low Severity, Moderate-high Severity and High Severity have been reclassified, assigning to these categories the numbers 0, 1, 2, 3, respectively. After the reclassification, these burn severity categories have been polygonized. Obtaining the burned area in a vector format has allowed to calculate the size of the area affected by fire; and also by reclassifying the values

has allowed to calculate the area of the different severity categories, thus obtaining greater detail of the fire. In the QGIS attribute table has calculated the size of the areas of the different severity categories in square meters and hectares. With the help of Excel, the size of the total affected area and the size of the different severity classes were calculated.

3.2. Calculation of the Burned Vegetation Index (BVI)

To present an alternative metric in the study of fire severity, the Burned Vegetation Index (BVI) has been developed which combines the Normalized Difference Vegetation Index (NDVI) and the Normalized Burn Ratio (RBR) for the study of the severity of burned vegetation. The BVI is defined as a difference between NDVI pre-fire and NBR post-fire:

$$\text{BVI} = \left(\frac{\text{NIR}_{\text{prefire}} - \text{Red}_{\text{prefire}}}{\text{NIR}_{\text{prefire}} + \text{Red}_{\text{prefire}}} \right) - \left(\frac{\text{NIR}_{\text{postfire}} - \text{SWIR}_{\text{postfire}}}{\text{NIR}_{\text{postfire}} + \text{SWIR}_{\text{postfire}}} \right)$$

$$\text{BVI} = \text{NDVI}_{\text{prefire}} - \text{NBR}_{\text{postfire}} \tag{8}$$

The BVI first identifies the healthy vegetation reflected in the red and near-infrared bands, and then subtracts from this the pixels identified as burned areas reflected in near-infrared and shortwave infrared bands. Vegetation in good condition has high near-infrared reflectance and low reflectance in the shortwave infrared portion of the spectrum. Otherwise, burned areas have low reflectance in the near-infrared and high reflectance in the shortwave infrared band. Therefore, the pre-fire NDVI gives larger values where vegetation was healthier, while the post-fire NBR gives negative values for surfaces identified as recently burned. As a result of the subtraction, the BVI shows smaller values where vegetation remains healthy and larger values where vegetation suffered fire disturbance. The following classification table is proposed to interpret the BVI **(Table 2)**. The values were classified into five severity categories by equal intervals. The interval values shown in the table were obtained by calculating the mean of the category values in the case of the two fires.

Table 2.

Burned vegetation severity levels obtained calculating BVI *(Source: the author).*

Severity Level	BVI
Highly healthy vegetation	<= 0.124
Healthy vegetation	0.125 to 0.286
Bare soil	0.287 to 0.449
Moderately burned vegetation	0.450 to 0.612
Highly burned vegetation	>= 0.613

3.3. Analysis of the relationship between BVI and RBR, dNDVI, dNBR

For the statistical analysis of the relationship between satellite indices, first has been calculated the number of pixels that exist in each study area (N, population size) with the *Zonal Statistics* tool in QGIS. Having the total number of pixels in the study area, the size of a sample was calculated with a confidence level of 95% and with a margin of error of 5%, using the following formula (Israel, 1992):

$$n = \frac{n_0}{1 + \frac{(n_0 - 1)}{N}} \tag{9}$$

where n is the sample size, N is the population size, and n_0 is calculated as follows:

$$n_0 = \frac{Z^2 pq}{e^2} \tag{10}$$

where n_0 is the sample size, Z^2 is the abscissa of the normal curve that cuts off an area α at the tails (1 - α equals the desired confidence level, e.g., 95%), e^2 is the desired level of precision, p is the estimated proportion of an attribute that is present in the population, and q is 1-p. The value for Z is found in statistical tables which contain the area under the normal curve. With the help of the *Random points in layer bounds* tool in QGIS, the required number of points of the calculated sample has been generated. In QGIS there is another tool that allows to extract the pixel value using a vector layer that contains the sampling points and the raster layers with field/bands to get values from. Thus, with the *Point Sampling* tool, the pixel values that were taken in the sample were extracted for correlation analysis between satellite indices. The intensity of linear relationship between satellite indices was determined using by Pearson correlation coefficient (r). The Pearson correlation coefficient (r) of two variables, xi and yi, was calculated on the basis of the following equation (Lee & Wong, 2001):

$$r = \frac{\frac{\sum_{i=1}^{n} xiyi}{n} - \overline{X} \bullet \overline{Y}}{SxSy} \tag{11}$$

where, $\overline{X}$ and $\overline{Y}$ represent the mean of x and y, and Sx and Sy represent standard deviation of x and y, calculated with the formulas:

$$Sx = \sqrt{\frac{\sum_{n=1}^{n} x^2}{n} - \overline{X}^2} \quad Sy = \sqrt{\frac{\sum_{n=1}^{n} y^2}{n} - \overline{Y}^2}$$

Pearson's correlation coefficient was validated with a t-test. The object of the t-test of a correlation coefficient is to investigate whether the difference between the sample correlation coefficient and zero is statistically significant. It is assumed that the x and y values originate from a bivariate normal distribution, and that the relationship is linear (Kanji, 2006). To test the null hypothesis that the population value of r is zero, the follow test statistic has been calculated:

$$t = \frac{r}{\sqrt{1-r^2}} * \sqrt{n-2} \tag{12}$$

This t-test follows Student's t-distribution with n − 2 degrees of freedom and in this case was two-tailed.

4. RESULTS AND DISCUSSIONS

The delimitation and extraction of the two areas affected by forest fires with the calculation of the RBR index gave different results compared to Copernicus EMS maps. The size of the burned area according to the calculation process of this study in the case of Kineta is 3511 hectares, presenting the following distribution of burn severity: Low Severity: 493 ha (14%), Moderate-low Severity: 1483 ha (42%), Moderate-high Severity: 1370 ha (39%), High Severity: 164 ha (5%) **(Fig. 7)**. On the other hand, the size of the affected area in the case of Mati is 942 hectares, presenting the following distribution of burn severity: Low Severity: 76 ha (8%), Moderate-low Severity: 369 ha (39%), Moderate-high Severity: 271 ha (29%), High Severity: 226 (24%) **(Fig. 8)**. EMS data (emergency maps and vector packages) estimates the size of the burned area in Kineta at 5613 hectares and in Mati at 1275 hectares (Copernicus EMS, 2018).

These differences in the size of the areas affected by the same fire are explained by the different methods used in the delimitation of the burned areas. In the case of Mati the EMS thematic layer has been derived from post-event satellite image, using by means of visual interpretation. The estimated geometric accuracy is 5 m CE 90 or better, from native positional accuracy of the background satellite image. Data sources they used are very high resolution Pléiades pre- and post-fire satellite images. The pre-event image is a Pléiades-1A/B, distributed by Airbus DS, acquired on 07/03/2018, with a ground sampling distance (GSD) of 0.5 m, approximately 0% cloud coverage. The post-event image is a Pléiades-1B acquired on 25/07/2018, with a ground sampling distance (GSD) of 0.5 m, approximately 2.3% cloud coverage. In the case of Kineta the EMS thematic layer has been derived from post-event satellite image using a semi-automatic approach. The pre-event image in this case was a SPOT6/7, distributed by Airbus DS acquired on 06/12/2017, with a ground sampling distance (GSD) of 1.5 m, approximately 0% cloud coverage. The post-event image was also a SPOT6/7, acquired on 30/07/2018, with a ground sampling distance (GSD) of 1.5 m, approximately 5.6% cloud coverage (Copernicus EMS, 2018).

Both visual interpretation and semi-automatic classification of land cover are methods often used in Remote Sensing (Cigna et al, 2011; Cigna et al., 2012; Raspini et al., 2018; Jiang et al., 2012), but in the case of the study and mapping burned areas they give very different results. Firstly, because the methodology for the delimitation and interpretation of the results always depends on the researcher and the purpose of the study for which it is done; and secondly, because the study of the change of land cover in Remote Sensing depends a lot on the date and time when the satellite images were taken, the season of the year in which they were taken, the atmospheric conditions and the time interval between the images.

The Burned Vegetation Index (BVI) in the study and mapping burned areas is focused on represent fire-altered vegetation **(Fig. 9, Fig. 10)**. It captures changes in vegetation using the Red, NIR and SWIR bands of the electromagnetic spectrum. The correlation analysis between BVI and different fire severity metrics (RBR, dNDVI, dNBR) has shown that the BVI corresponds very well with other satellite indices used in the study and mapping burned areas **(Fig. 11)**. In the study area of Kineta there were 1 169 238 pixels, of which a sample of 384 points was taken with the values associated with its pixels. The study area of Mati contained 249 468 pixels, of which a sample of 384 points was taken with the values associated with its pixels. In the case of the relationship between BVI and RBR, the Pearson correlation coefficient (r) gave the value r=0.96 (Kineta) and r=0.94 (Mati). The relationship between BVI and dNDVI was r=0.93 (Kineta) and r=0.90 (Mati). The relationship is also strong in the case of BVI and dNBR giving r=0.96 (Kineta) and r=0.94 (Mati). The coefficient of determination (R^2) using linear regression in the case of BVI and RBR is R^2=0.92 (Kineta) and R^2=0.89 (Mati). In the case of BVI and dNDVI the coefficient of determination is R^2=0.87 (Kineta) and R^2=0.82 (Mati). The coefficient of determination is also high between BVI and dNBR: R^2=0.92 (Kineta) and R^2=0.88 (Mati) **(Table 3)**. The t-test of the correlation coefficient validated that the difference between the correlation coefficient and zero is statistically significant in all cases between BVI and RBR, dNDVI, dNBR. With this it can be affirmed that there is a statistically significant relationship between BVI and RBR, dNDVI, dNBR. The t-test was taken with a confidence level of 95% (CL), margin of error 5% (α) and with the probability of tα/2 = 0.975. Establishing this, the critical value of the T-Student table according to the degree of freedom (df = n-2) in all cases is 1.96 (df= 381 in the case of Kineta and df= 364 in the case of Mati). Between BVI and RBR, dNDVI, dNBR the T-test value (T-stat) is greater than

the critical value (T-critical), stating that there is statistically significant relationship between the variables **(Table 3)**.

In the study of forest fires, it is not sufficient to assess and delimit the affected areas after the event. From a socio-economic perspective it is important to develop vulnerability models to wildfires. Further studies underline the need to find optimal ways of evacuating the population in cases of forest fires (Hasnat et al., 2018; Nicoară & Haidu, 2014). In addition, the study of burned areas with Remote sensing methods in other studies is complemented by meteorological indicators (Furtună & Holobâcă, 2013). Mateescu (2006) in its study on post-fire assessment introduces the dedicated BAS2 tool for wildfires. From a hydrological perspective, Sever's study (2019) reveals the impact of mega-fires on watersheds.

Table 3.

The degree of dependence between BVI and RBR, dNDVI, dNBR.

Relationship/Fire	r	R^2	T-stat	T-critical	df
BVI & RBR (Kineta)	0.96	0.92	67.8	1.96	381
BVI & RBR (Mati)	0.94	0.89	54.2	1.96	364
BVI & dNDVI (Kineta)	0.93	0.87	49.7	1.96	381
BVI & dNDVI (Mati)	0.90	0.82	40.2	1.96	364
BVI & dNBR (Kineta)	0.96	0.92	67.6	1.96	381
BVI & dNBR (Mati)	0.94	0.88	52.4	1.96	364

Colour	Fire Severity	Number of pixels	area (m2)	area (ha)	area (ha) %
	Low Severity	9365	4931005	493	14%
	Moderate-low Severity	2319	14834377	1483	42%
	Moderate-high Severity	1477	13701737	1370	39%
	High Severity	654	1643389	164	5%
	TOTAL	13815	35110508	3511	100%
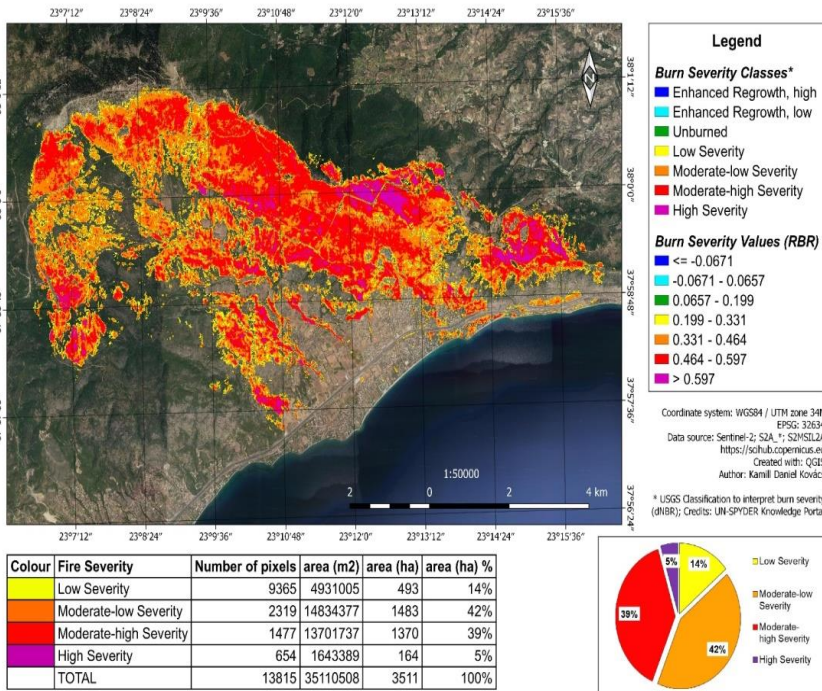
Fig. 7. Burned area size and burn severity levels, Kineta.
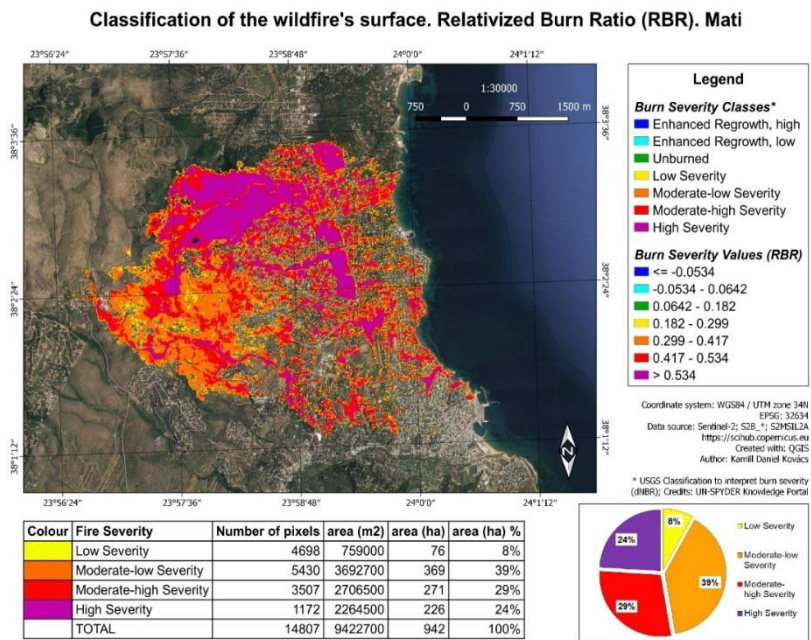
Fig. 8. Burned area size and burn severity levels, Mati.
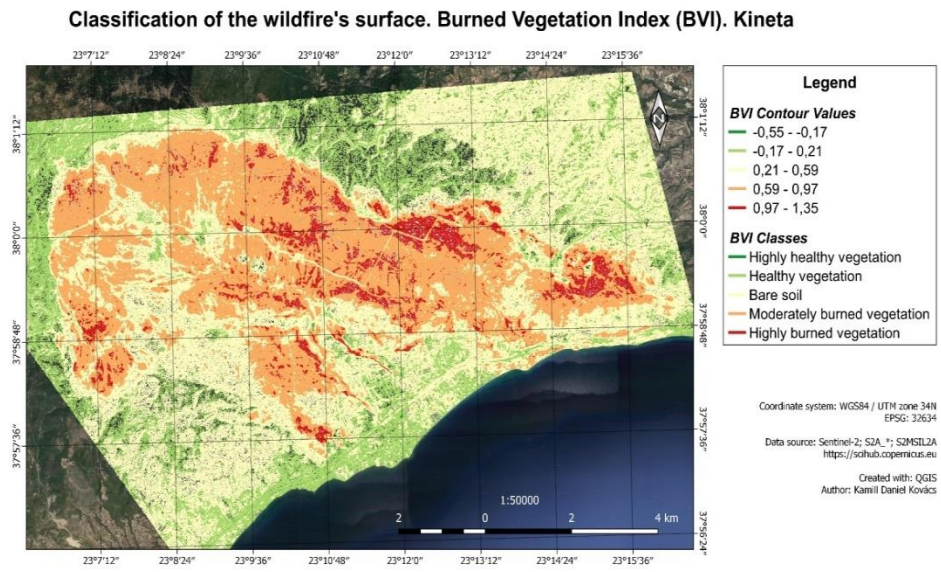
Fig. 9. BVI severity levels, Kineta.
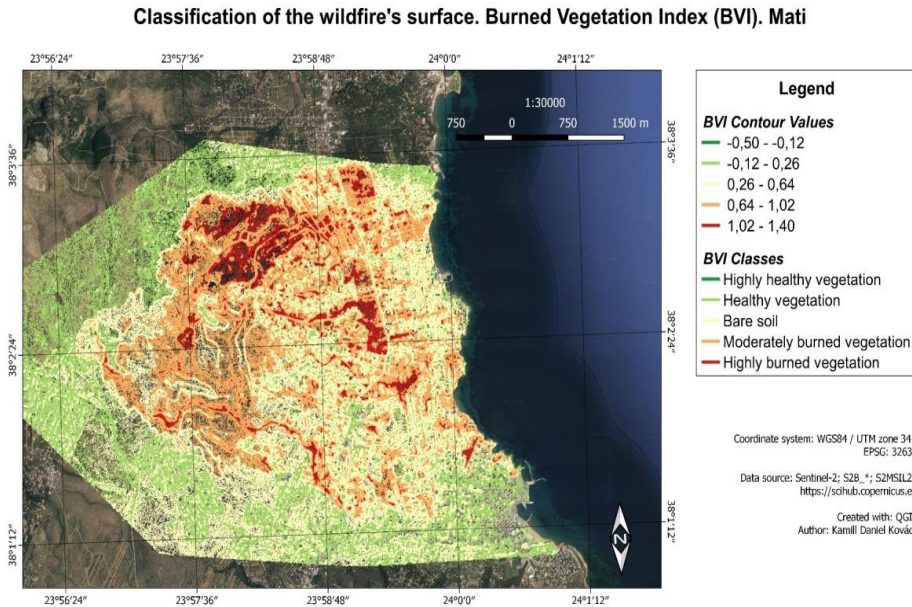
Fig. 10. BVI severity levels, Mati.

5. CONCLUSIONS

Sentinel-2 satellite images available for free are a good source of data for analyzing **and interpreting** burn severity of forest fires because they have a relatively high spatial resolution of 10 m. However, Copernicus EMS data have shown that the delimitation of the area affected by fire is based on criteria defined by the researcher and also depends on the purposes of the investigation. In this study, the affected areas have been delimited with the calculation of the RBR index and according to the USGS proposition to interpret burn severity, setting a threshold of RBR > 0.27 to extract only the areas that were burned. EMS maps are developed to handle emergencies, therefore reflect situations almost immediately after the events (a few days after the event). Moreover, the study of the relationship between BVI and RBR, dNDVI, dNBR demonstrated that BVI is a good alternative for the study of wildfires, specially adapted for fire-altered vegetation research.
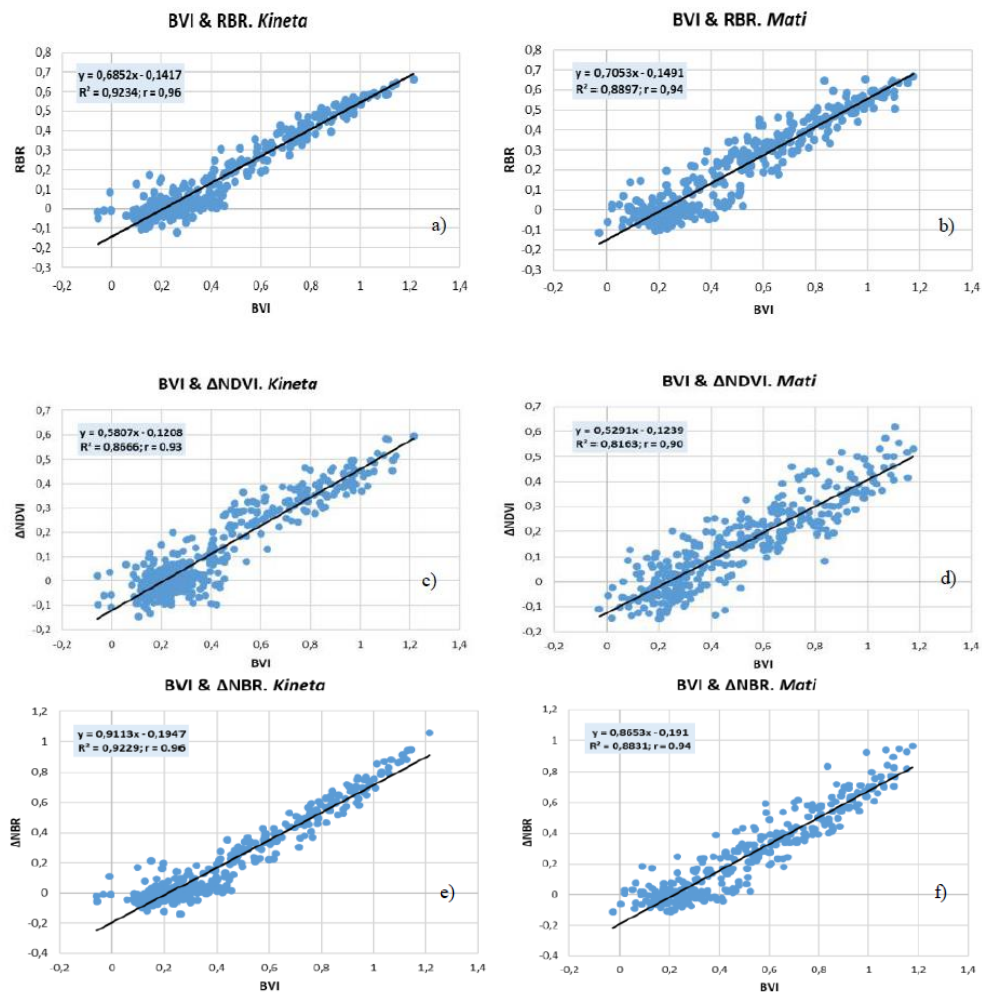
Fig. 11. Graphs correlating BVI and RBR, dNDVI, dNBR.

R E F E R E N C E S

Cantarello, E., Newton, A.C, Martin, P.A, Evans, P.M., Gosal, A., Lucash, M.S (2017) Quantifying resilience of multiple ecosystem services and biodiversity in a temperate forest landscape. *Ecol. Evol,* 7 (22), 9661–9675.

Chu, T., & Guo, X. (2014) Remote Sensing Techniques in Monitoring Post-Fire Effects and Patterns of Forest Recovery in Boreal Forest Regions: A Review. *Remote Sensing*, 6 (1), 470-520.

Cigna, F., Del Ventisette, C., Liguori, V. & Casagli, N. (2011) Advanced radar-interpretation of InSAR time series for mapping and characterization of geological processes. *Natural Hazards and Earth System Sciences*. 11 (3), 865–881.

Cigna, F., Tapete, D. & Casagli, N. (2012) Semi-automated extraction of Deviation Indexes (DI) from satellite Persistent Scatterers time series: tests on sedimentary volcanism and tectonically-induced motions. *Nonlinear processes in geophysics,* 19 (6), 643–655.

Copernicus EMS (2018) – Copernicus Emergency Management Service. EMSR300: Forest Fires in Attika, Greece. Available from: https://emergency.copernicus.eu/mapping/list-of-components/EMSR300 [Accessed October 2019].

Copernicus Open Access Hub (2018) - Available from: https://scihub.copernicus.eu [Accessed October 2018].

Chuvieco, E. (1999). *Remote Sensing of Large Wildfires in the European Mediterranean Basin*, Springer, New York.

Díaz-Delgado, R. & Pons, X. (1999) Empleo de imágenes de teledetección para el análisis de los niveles de severidad causados por el fuego. *Revista de Teledetección*, 12, 63-68.

Doblas-Miranda, E., Martínez-Vilalta, J., Lloret, F., Álvarez, A., Ávila, A., Bonet, F. J., Brotons, L., Castro, J., Curiel Yuste, J., Díaz, M., Ferrandis, P., García-Hurtado, E., Iriondo, J. M., Keenan, T. F., Latron, J., Llusià, J., Loepfe, L., Mayol, M., Moré, G., Moya, D., Peñuelas, J., Pons, X., Poyatos, R., Sardans, J., Sus, O., Vallejo, V. R., Vayreda, J. & Retana, J. (2015) Reassessing global change research priorities in mediterranean terrestrial ecosystems: how far have we come and where do we go from here? *Global Ecology and Biogeography*, 24 (1), 25-43.

Du, Y., Zhang, Y., Ling, F., Wang, Q., Li, W., & Li, X. (2016) Water Bodies' Mapping from Sentinel-2 Imagery with Modified Normalized Difference Water Index at 10-m Spatial Resolution Produced by Sharpening the SWIR Band. *Remote Sens*, 8 (4), 354.

Eidenshink, J., Schwind, B., Brewer, K., Zhu, Z.L., Quayle, B. & Howard, S. (2007) A project for monitoring trends in burn severity. *Fire Ecol*, 3 (1), 3–21.

Escuin, S., Navarro, R. & Fernández, P. (2008) Fire severity assessment by using NBR (Normalized Burn Ratio) and NDVI (Normalized Difference Vegetation Index) derived from LANDSAT TM/ETM images. *International Journal Remote Sensing,* 29 (4), 1053-1073.

Fontúrbel, M. T., Fernández, C. & Vega, J. A. (2015) Cambios en la repelencia al agua del suelo en función de la severidad del fuego en el suelo. *Flamma*, 6 (3), 122-124.

Furtună, P., Holobâcă, I.H. (2013) Forest fires study using Remote sensing and meteorological indicators. Study case. *Geographia Technica*, 8 (2), 23-37.

González De Vega, S., de las Heras, J., Gómez-Sánchez, E. & Moya, D. (2015) Response of plant communities in the short-term after fire: influence of fire severity and resilience. *Flamma,,* 6 (3), 149-153.

González-De Vega, S., de las Heras, J. & Moya, D. (2016) Resilience of Mediterranean terrestrial ecosystems and fire severity in semiarid areas: Responses of Aleppo pine forests in the short, mid and long term. *Science of the Total Environment*, 573, 1171-1177.

Hasnat, Md. Mehedi, Islam, Md. Rakibul, Hadiuzzaman, Md. (2018) Emergency Response During Disastrous Situation in Densely Populated Urban Areas: a GIS Based Approach. *Geographia Technica*, 13 (2), 74-88.

Hedo, J., Rubio, E., Dadi, T., López-Serrano, F. R., Alfaro-Sánchez, R., Moya, D. & De las Heras, J. (2014) Is Remote Sensing a Good Method to Define Forest Fire Resilience? A Particular Case in the South-eastern of the Iberian Peninsula, In: Viegas, D.X. (Ed.) *Advances in forest fire research*, 556-563, Coimbra: Universidade de Coimbra.

Hellenic Statistical Authority (2011) – Available from: http://www.statistics.gr/en/2011-census-pop-hous [Accessed October 2019]

Hudak, A.T., Morgan, P., Bobbitt, M.J., Smith, A.M.S., Lewis, S.A., Lentile, L.B., Robichaud, P.R., Clark, J.S. & McKinley, R.A. (2007) The relationship of multispectral satellite imagery to immediate fire effects. *Fire Ecol*., 3 (1), 64–90.

Husson, A. (1983) Télédétection des incendies de forêt en Corse entre 1973 et 1980. *Méditerranée,* 54 (4), Télédéctection III., 53-59.

Israel, G.D (1992) *Determining Sample Size*. University of Florida Cooperative Extension Service, Institute of Food and Agriculture Sciences, EDIS, Florida. Available from: https://www.tarleton.edu/academicassessment/documents/Samplesize.pdf [Accessed October 2019].

Jiang, D., Huang, Y., Zhuang, D., Zhu, Y., Xu, X. & Ren, H. (2012) A Simple Semi-Automatic Approach for Land Cover Classification from Multispectral Remote Sensing Imagery. *PLoS ONE,* 7 (9). Available from: https://doi.org/10.1371/journal.pone.0045889 [Accessed October 2019].

Keeley. J.E. (2009) Fire intensity, fire severity and burn severity: a brief review and suggested usage. *International Journal of Wildland Fire*, 18 (1), 116–126.

Key, C.H. & Benson, N.C. (2006) Landscape Assessment (LA): Sampling and Analysis Methods. In: Lutes, D., Keane, R.E., Caratti, J.F., Key, C.H., Benson, N.C., Sutherland, S., Gangi, L. (Eds.) *Firemon: Fire Effects Monitoring and Inventory System*, Gen. Tech. Rep. RMRS-GTR-164-CD, Fort Collins, CO: U.S. Department of Agriculture, Forest Service, Rocky Mountain Research Station, LA-1-55.

Lee, J. & Wong, D.W.S.(2001) *Statistical Analysis with ArcView GIS*, John Wiley and Sons, New York.

Lyons, M.B., Keith, D.A., Phinn, S.R., Mason & T.J., Elith, J. (2018) A comparison of resampling methods for remote sensing classification and accuracy assessment. *Remote Sensing of Environment*, 208 (11), 145-153.

Main-Knorn, M., Pflug, B., Louis, J., Debaecker, V., Müller-Wilm, U. & Gascon, F. (2017) 'Sen2Cor for Sentinel-2', *Image and Signal Processing for Remote Sensing XXIII* . Proc. SPIE 10427, 1042704, SPIE REMOTE SENSING. Warsaw, Poland, 11-14 September 2017. Bellingham, Washington: SPIE.

MAPAMA (2016) – Ministerio de Agricultura, Pesca, Alimentación y Medio Ambiente. Available from: https://www.mapa.gob.es/es/desarrollo-rural/estadisticas/Incendios_default.aspx [Accessed October 2019].

Mateescu, M. (2006) Burnt Area Statistics 3D GIS Tool for Post-Fire Assessment. *Geographia Technica*, 1 (2), 56-65.

Miller, J.D., Safford, H.D., Crimmins, M. & Thode, A.E. (2009) Quantitative evidence for increasing forest fire severity in the Sierra Nevada and southern Cascade Mountains, California and Nevada, USA. *Ecosystems*, 12 (1), 16–32.

Miller, J.D. & Thode, A.E. (2007) Quantifying burn severity in a heterogeneous landscape with a relative version of the delta Normalized Burn Ratio (dNBR). *Remote Sens. Environ*., 109 (1), 66–80.

Mousivand, A., Verhoef, W., Menenti, M. & Gorte, B. (2015) Modeling Top of Atmosphere Radiance over Heterogeneous Non-Lambertian Rugged Terrain. *Remote Sens.,* 7 (6), 8019–8044.

Moya, D., Alfaro-Sánchez, R., López-Serrano, F. R., Dadi, T., Hernández-Tecles E., Ferrandis, P. & de las Heras, J. (2014) Post-fire management of mediterranean forests: carbon storage in regenerated areas in eastern Iberian Peninsula. *Cuadernos de Investigación Geográfica*, 40 (2), 371-386.

Moya, D., De las Heras, J., Lopez-Serrano, F. R., Condes, S., Alberdi, I. (2009) Structural patterns and biodiversity in burned and managed Aleppo pine stands. *Plant Ecology*, 200 (2), 217–228.

Nicoară, P.S., Haidu, I. (2014) A GIS based network analysis for the identification of shortest route access to emergency medical facilities. *Geographia Technica*, 9 (2), 60-67.

Parks, S. A., Dillon, G. K. & Miller, C. (2014) A New Metric for Quantifying Burn Severity: The Relativized Burn Ratio. *Remote Sens*., 6 (3), 1827-1844.

Paula, S., Arianoutsou, M., Kazanis, D., Tavsanoglu, Ç., Lloret, F., Buhk, C., Ojeda, F., Luna, B., Moreno, J. M., Rodrigo, A., Espelta, J. M., Palacio, S., Fernández-Santos, B., Fernandes, P. M.

& Pausas, J. G. (2009) Fire-related traits for plant species of the Mediterranean Basin. *Ecology*, 90 (5), 1420.

Pausas, J. G. (1999) Mediterranean vegetation dynamics: modelling problems and functional types. *Plant Ecology*, 140 (1), 27–39.

Raspini, F., Bianchini, S., Ciampalini, A., Del Soldato, M., Solari, L., Novali, F., Del Conte, S., Rucci, A., Ferretti, A. & Casagli, N. (2018) *Continuous, semi-automatic monitoring of ground deformation using Sentinel-1 satellites.* Available at: https://www.nature.com/articles/s41598-018-25369-w.pdf [Accessed October 2019].

Regueira, N., Benito, E., Fontúrbel, M. T., Fernández, C., Jiménez, E. & Vega, J. A. (2015) Efectos de quemas experimentales de diferente severidad en el carbono orgánico y en propiedades físicas del suelo. *Flamma*, 6 (3), 129-133.

Sánchez, J. M., Rubio, E., López-Serrano, F. R., Artigao, M. M., Caselles, V., Moya, D. & Odi, M. M. (2009). Estudio a través de imágenes Landsat 5-TM del efecto de un incendio sobre el balance de energía en superficie en una zona de bosque mediterráneo. *Revista de Teledetección*, 32 (6), 72-85.

San-Miguel-Ayanz, J. & Camia, A. (2009) Forest fires at a glance: facts, figures and trends in the EU. In: Birot, Y. (Ed.) *Living with Wildfires: What Science Can Tell Us. A Contribution to the Sciencepolicy Dialogue*. Joensuu, Finland: European Forest Institute, 11–18.

Sever, M. (2019) Wildfires affect water resources long after the smoke clears. *Eos*, 100. Available at: https://doi.org/10.1029/2019EO134717 [Accessed October 2019].

Spano, D., Camia, A., Bacciu, V., Masala, F., Duguy, B., Trigo, R., Sousa, P., Venäläinen, A., Mouillot, F., Curt, T., Moreno, J. M., Zavala, G., Urbieta, I. R., Koutsias, N. & Xystrakis, F. (2014) Recent trends in forest fires in Mediterranean areas and associated changes in fire regimes, In: Moreno, J. M., Arianoutsou, M., González-Cabán, A., Mouillot, F., Oechel, W. C., Spano, D., Thonicke, K., Vallejo, V. R., Vélez, R. (Eds.), *Forest Fires Under Climate, Social and Economic Changes in Europe, the Mediterranean and other Fire-affected Areas of the World*: *FUME: lesson learned and outlook*, Adelaïde: Calyptra Pty, 6–7.

Tessler, N., Wittenberg, L., Provizor, E. & Greenbaum, N. (2014) The influence of short interval recurrent forest fires on the abundance of Aleppo pine (Pinus halepensis Mill.) on Mount Carmel, Israel. *Forest Ecology Management*, 324, 109–116.

UN-SPIDER Knowledge Portal – United Nations Office for Outer Space Affairs. Available from: http://un-spider.org/advisory-support/recommended-practices/recommended-practice-burn-severity/in-detail/normalized-burn-ratio [Accessed October 2019].

Vallejo, V. R., Arianoutsou, M. & Moreira, F. (2012) Fire ecology and post-fire Restoration approaches in southern European forest types. In: Moreira, F., Arianoutsou, M., Corona,P., De Las Heras, J. (Eds.) *Post-fire Management and Restoration of Southern European Forests*, 93–119. Netherlands: Springer.

Vega, J. A., Fontúrbel, T., Fernández, C., Díaz-Raviña, M., Carballas, T., Martín, A., González-Prieto, S., Merino, A. & Benito, E. (2013) *Acciones urgentes contra la erosión en áreas forestales quemadas. Guía para su planificación en Galicia.* Santiago de Compostela: Centro de Investigación Forestal de Lourizán, Consellería do Medio Rural e do Mar, Xunta de Galícia, Instituto de Investigaciones Agrobiológicas de Galicia del CSIC (IIAGCSIC), Universidad de Santiago de Compostela, Universidad de Vigo, FUEGORED.

Vlassova, L., Pérez-Cabello, F., Mimbrero, M. R., Llovería, R. M. & García-Martín, A. (2014) Analysis of the Relationship between Land Surface Temperature and Wildfire Severity in a Series of Landsat Images. *Remote Sensing*, 6 (7), 6136-6162.

Zhu, Z., Key, C.H., Ohlen, D., Benson, N.C. (2006) *Evaluate Sensitivities of Burn-Severity Mapping Algorithms for Different Ecosystems and Fire Histories in the United States*. Available at: https://www.firescience.gov/projects/01-1-4-12/project/01-1-4-12_final_report.pdf [Accessed October 2019].

GMT BASED COMPARATIVE ANALYSIS AND GEOMORPHOLOGICAL MAPPING OF THE KERMADEC AND TONGA TRENCHES, SOUTHWEST PACIFIC OCEAN

Polina LEMENKOVA[1]

ABSTRACT:
Current study is focused on the GMT based modelling of the two hadal trenches located in southwest Pacific Ocean, eastwards from Australia: Tonga and Kermadec. Due to its inaccessible location, the seafloor of the deep-sea trench can only be visualized using remote sensing tools and advanced algorithms of data analysis. The importance of the developing and technical improving of the innovative methods in cartographic data processing is indisputable. Automatization in data analysis has been significantly increased over the past years. However, using programming and scripting in cartography still remains lower comparing to the use of the traditional GIS. Therefore, developing GMT-based methods for the geomorphological data processing is crucial for better understanding the landforms of the seafloor. Methodology includes application of the GMT scripting toolset for the automated digitizing of the profiles crossing the trenches in perpendicular direction. A sequence of the GMT codes enabled to visualize raster and vector data, perform geomorphological modelling, descriptive statistical data analysis and quantitative comparison of the two trenches. Using GMT, the bathymetric sample data of the Kermadec and Tonga trenches were modeled, analyzed and compared. The results show deeper bathymetry and more seafloor roughness for the Tonga. Comparing to Kermadec, Tonga Trench has steeper gradient of the profiles. The seafloor geomorphology is strongly affected by a variety of factors that shape actual form of both trenches. The experimental methodology is fully based on the GMT scripting with presented and explained codes.

Key-words: GMT, geomorphology, mapping, hadal trench, Tonga, Kermadec

1. INTRODUCTION

The structure of the ocean seafloor has been the subject of the attention in Earth sciences recently (Micallef, 2011; Mitchell, 2015). The rapidly developing GIS methods, machine learning algorithms and automatization in geospatial analysis improves the precision and quality of the mapping. One of these tools, the Generic Mapping Tools (GMT), a geospatial scripting toolset developed by Wessel & Smith (1991) provides advanced cartographic solutions that enable to model, analyze, map, visualize and calculate the phenomena of the submarine geology that can only be studied by the remote sensing methods and complex algorithms of data analysis. A variety of the GMT modules (Wessel *et al*, 2013) specifically adjusted for modelling raster grids, plotting vector maps, computing descriptive statistical graphs and aesthetic cartographic mapping proved to be a perfect tool for modelling oceanological data. Current work is fully based on using GMT for comparative analysis and geomorphic modelling of two hadal trenches.

The presented research is focused on the comparative analysis and geomorphological modelling of the two hadal trenches located in the Pacific Ocean: Kermadec and Tonga

---

[1] *Ocean University of China, College of Marine Geo-sciences, 266100, Qingdao, Shandong Province, China, pauline.lemenkova@gmail.com or lemenkovapolina@stu.ouc.edu.cn;*

(**Fig. 1**). Using GMT modelling, the shapes of their orthogonal transect profiles were compared and analyzed in order to highlight differences and variations in the landforms of the two trenches located close to each other yet different in structure. The majority of research either focus on the biota communities of the deep-sea ecosystems (Leduc, 2015; Nunnally *et al.*, 2016; Leduc *et al*, 2016) or the tectonic movements of the plates in the Pacific Ocean (Duncan et al., 1985; Tappin, 1993; Piller *et al.,* 1999). The presented work aims to contribute to the studies on the geomorphological modelling of the hadal trenches of the Pacific Ocean.
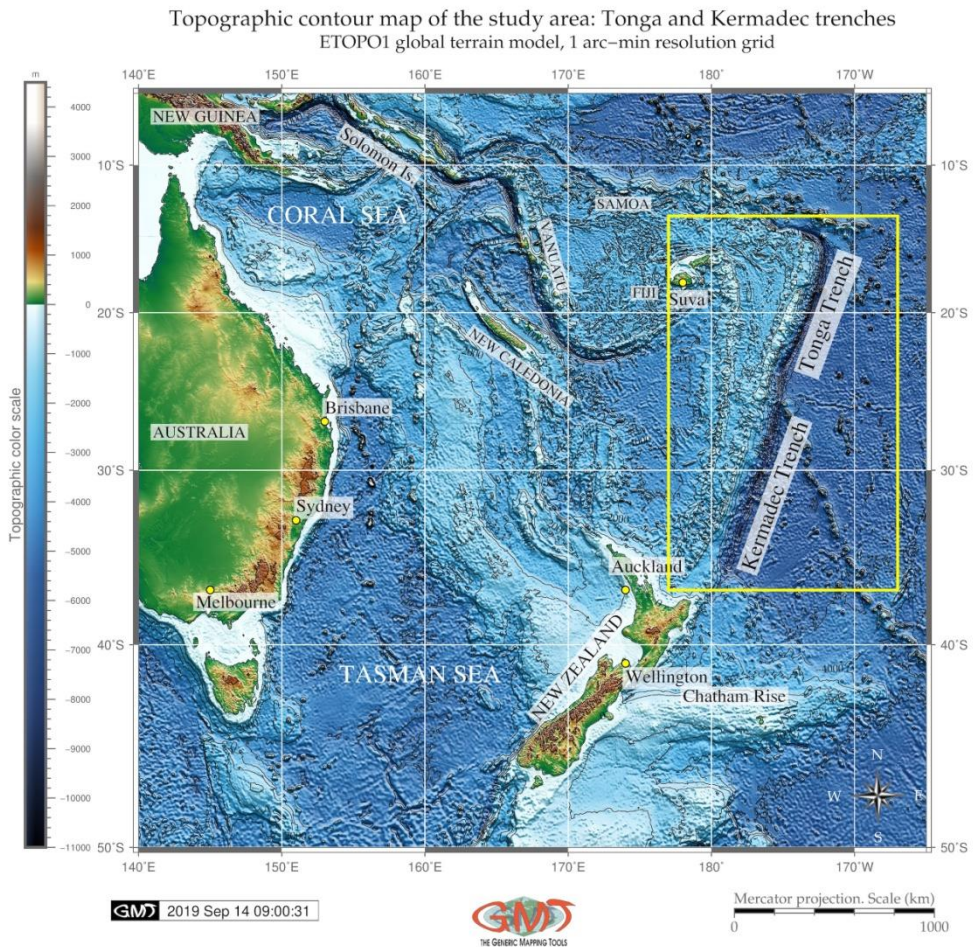
Fig. 1. Map of the study area: Kermadec and Tonga trenches, Pacific Ocean *(Source: author).*

2. STUDY AREA AND DATA

The study area is focused on two hadal trenches located in south-west Pacific Ocean northwards from Australia and New Zealand: Kermadec and Tonga. Their brief geographic description can be characterized as follows. Kermadec Trench is the southern from the two located 120 km off the New Zealand with axis continuing from ca. 26°S to 36°S. It is the 5th deepest trench in the world with a maximum depth of 10,177 m (Jamieson, 2015) m and a

length of 1500 km (Jamieson *et al*, 2011). Its closeness to the Antarctic makes it one of the coldest trenches in the world (Belyaev, 1989).

Kermadec Trench runs parallel to the Kermadec Ridge with geomorphology of V-shape formed by tectonic subduction of the Pacific Plate under the Indo-Australian Plate extending from approximately 26° to 36°S near the northeastern tip of New Zealand's North Island (Leduc & Rowden, 2018).
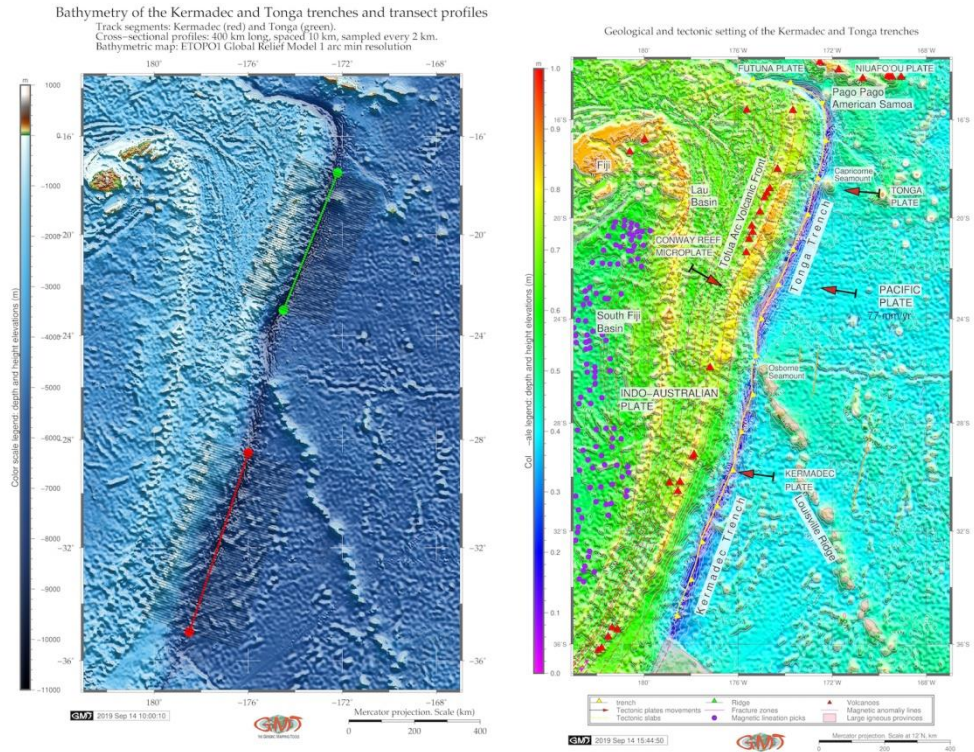
Fig. 2. Transect segments of the cross-secton profiles in Kermadec and Tonga trenches (left). Geologic and tectonic settings of the trenches (right) *(Source: author).*

The specific conditions of the tectonic setting in the study area is the subduction of the Pacific Plate at a rapid rate beneath the Indo-Australian Plate along the Tonga–Kermadec Trench (Castillo *et al.*, 2009), **Fig. 2,** right. Specifically, a convergence at maximal rate ~ 249 mm/yr) along the Tonga–Kermadec arc system makes it one of the most seismically active subduction zones in the world (Bevis *et al*., 1995). Due to the complex interaction of various factors (ocean currents, closeness to the Antarctica) the deep Pacific Ocean seafloor underlying the trenches is notable for variable surface productivity (Linley *et al*, 2017). Detailed description of the environmental, geological and tectonic settings of the Kermadec is in Smith *et al.* (2003); Anderson, 2006; Regelous et al., 1997; Smith & Price, 2006.

Tonga Trench is adjacent, continuing Kermadec Trench northwards with axis stretching from ca. 15°S to 26°S. Located in close proximity to the Kermadec, it is separated by a sill located on the Tonga Platform (Wright *et al.*, 2000) and by the Louisville Seamount Chain

(Jamieson *et al*, 2013) (**Fig. 2**, right). With maximum depths of 10,882 m, the Tonga Trenches is the 2nd deepest trench in the world (Blankenship *et al*, 2006). Similar to the Kermadec, Tonga Trench belongs to the South Pacific Subtropical Gyre (SPSG) biogeochemical province and has the same primary productivity rate rate of 87 g C m-2 y−1 (Xu *et al*, 2018). Both trench axes have roughly 30° slight from the longitude line. Further studies on Tonga Trench, its environment and communities can be found in relevant literature (Tappin, 1993; Ewart *et al.*, 1993; Hergt & Woodhead, 2007).

3. METHODOLOGY

3.1. GMT codes for the topographic and geological mapping

A methodological approach consists in the sequence of the GMT modules. Each module consists of the small code line. Combined together as a script, they are used for mapping. Thus, the following GMT modules were used to map **Fig. 1**:

```
gmt grdcut earth_relief_01m.grd -R140/195/-50/-5 -Gtkt_relief.nc -V
```

Here the necessary part of the image was cut off and the coordinates were given (-R140/195/-50/-5) in WESN way. The raster data used as a basis map is ETOPO1. The coordinates in southern hemisphere are given as negative values. The module 'grdinfo' was used to analyze the output raster (tkt_relief.nc):

```
gmt grdinfo @tkt_relief.nc
```

The color palette was made using 'makecpt' module from the available 'geo' palette adjusted according to the data range (topography from -11000 to 4500):

```
gmt makecpt -Cgeo.cpt -V -T-11000/4500 > myocean.cpt
```

Following that the raster image was visualized:

```
gmt grdimage earth_relief_01m.grd -Cmyocean .cpt \
    -R140/195/-50/-5 -JM6i -P -I+a15+ne0.75 -Xc -K > $ps
```

Here the '-JM6i' means Mercator projection with 6 inches width of the map; '-P' means portrait orientation; '-K' means continue of the script (not finalized).

The legend was added using 'psscale' module using the following code snippet:

```
gmt psscale -Dg131/-50+w14.8c/0.4c+v+o0.3/0i+ml Rtkt_relief.nc -J -Cmyocean.cpt -
-FONT_LABEL=8p,Helvetica,dimgray                                    --
FONT_ANNOT_PRIMARY=5p,Helvetica,dimgray -Baf+l"Topographic color scale" -I0.2
-By+lm -O -K >> $ps
```

3.2. GMT codes for the geological mapping of the study area

The geological layers (lines and points) were added on **Fig. 2** (right) using the following code snippet. As can be seen (the code below), the plotting of the vector elements on the map is done using '-W' command, e.g. '-Wthinnest,red'.

Each code is saved to the initially created file using >>ps command. The first mention of this command goes with single bracket, e.g. '> $ps'. Then all the elements that are added to the map overlay the same. In this sense, there is certain similarity with GIS layers and a sequence of codes in the whole GMT script. The initial files with extension gmt (e.g. ridge.gmt) are tables with attribute data (coordinates and values) in native GMT format.

Hence, the following code was used for geological mapping on **Fig. 2**, right:

```
gmt makecpt -Crainbow -T0/700/50 -Z > rain.cpt
gmt psxy -R -J volcanoes.gmt -St0.4c -Gred -Wthinnest -O -K >> $ps
gmt psxy -R -J ridge.gmt -Sf0.5c/0.2c+l+t -Wthinnest,black -Ggreen -O -K >> $ps
gmt psxy -R -J LIPS.2011.gmt -L -Gpink1@50 -Wthinnest,red -O -K >> $ps
```

Adding slab contours and magnetic lineation picks
gmt psxy -R -J SC_tonga.txt -W0.6p,red,- -O -K >> $ps
gmt psxy -R -J GSFML.global.picks.gmt -Sc0.2c -Wthin,purple -Gpurple -O -K >> $ps
gmt psxy -R -J trench.gmt -Sf1.5c/0.2c+l+t -Wthick,yellow -Gyellow -O -K >> $ps
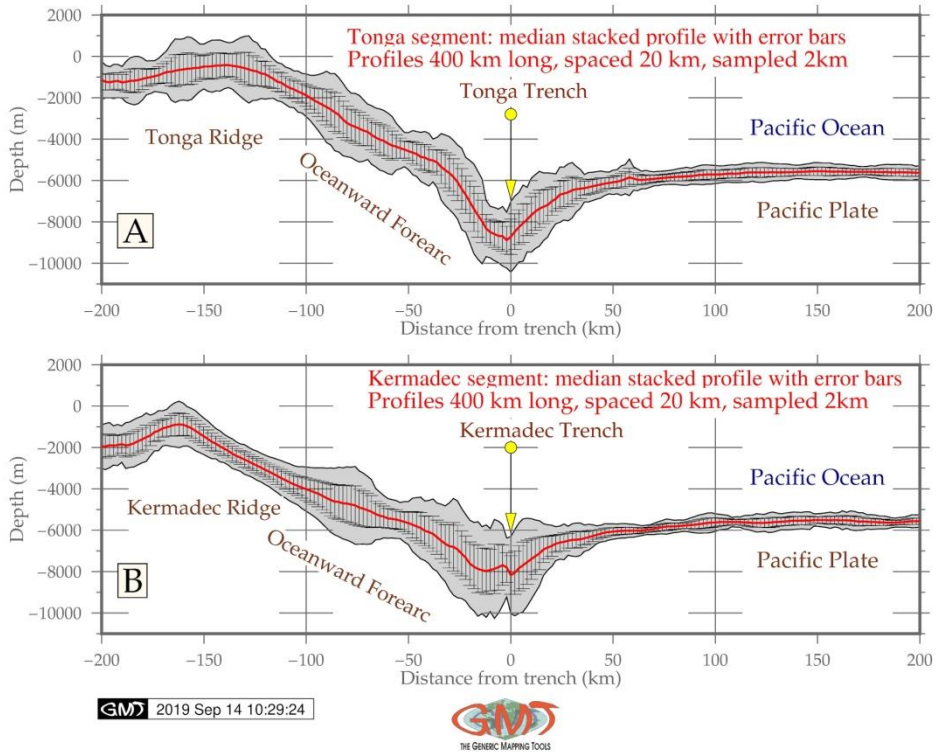
Fig. 3. Geomorphological modelling of the trenches by GMT *(Source: author).*

The GMT module 'psxy' was used for adding annotations on the maps, plotting geologic lineaments and sample points. The 'psbasemap' and 'grdcontour' GMT modules were used to map base map elements: bathymetry contours, net grids, titles and subtitles.

3.3. GMT codes for the geomorphological modelling of the cross-section profiles

The combination of several GMT modules was used for mapping geomorphological profiles (**Fig. 2**, left). The modelling was done using following code (example for the Kermadec Trench). The trench segment and end points were plotted:

gmt psxy -Rtkt_relief.nc -J -W2p,red trenchK.txt -O -K >> $ps # my line

gmt psxy -R -J -Sc0.15i -Gred trenchK.txt -O -K >> $ps # points

Then, the profiles 400 km long, spaced 10 km, sampled every 2km were generated using 'grdtrack' GMT module based on the 'tkt_relief.nc' raster in NetCDF format:

gmt grdtrack trenchK.txt -Gtkt_relief.nc -C400k/2k/10k+v -Sm+sstackK.txt > tableK.txt

The profiles were written into table: gmt psxy -R -J -W0.5p tableK.txt -O -K >> $ps

The modelling of the profiles was performed by the following code snippet:

gmt psxy -R-200/200/-11000/2000 -JX15.2c/5c -Bxag100f50+l"Distance from trench (km)" -Byag2000f1000a2000+l"Depth (m)" -BWeSn \
    -Glightgray -W0.5p envK.txt -UBL/-2p/-45p -K > $ps
gmt psxy -R -J -W1.0p -Ey+p0.2p stackK.txt -O -K >> $ps
gmt psxy -R -J -W1p,red stackK.txt -O -K >> $ps
The annotations were added using Unix utility 'echo', for example:
echo "-70 -100 Profiles 400 km long, spaced 20 km, sampled 2km" | gmt pstext -R -J -Gwhite -F+jBL+f12p,red -O -K >> $ps
Final visualization is presented on **Fig. 3**.
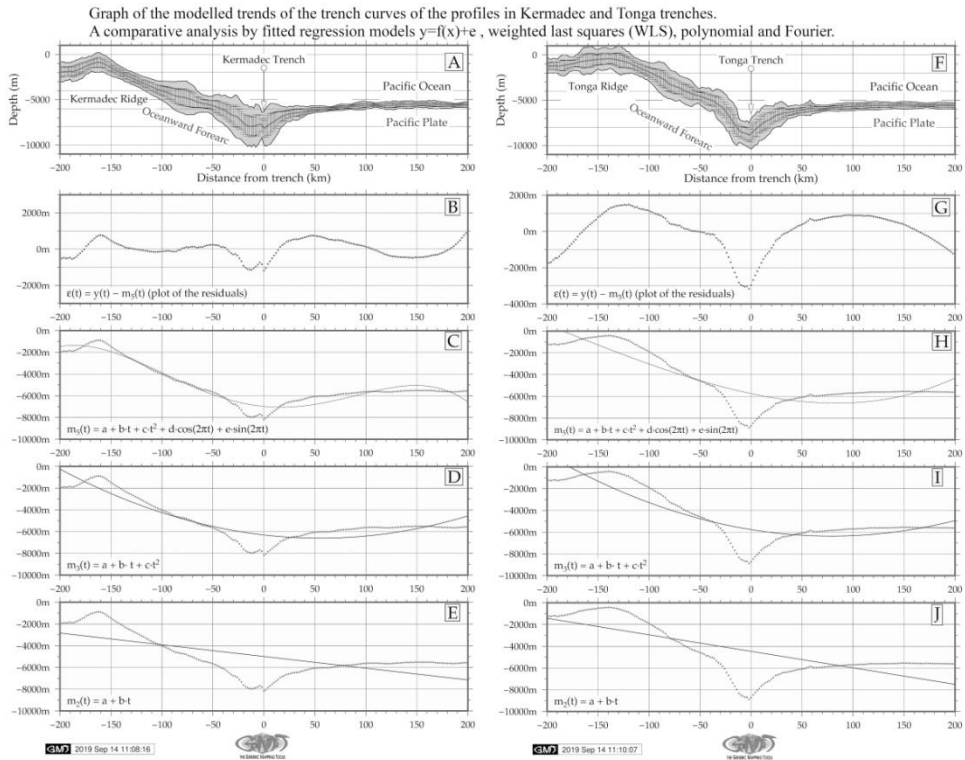
Fig. 4. Mathematical approximation of the trend curves of the profiles *(Source: author)*.

3.4. GMT codes for the mathematical approximation of the trends and histograms

A sequence of the codes was applied to model trends visualized on **Fig. 4** by modules: For example, basic LS line shown on the **Fig. 4**, E (lower left), $y = a + bx + cx^2$ was plotted using following methodology combining GMT and Unix utilities:

gmt trend1d -Fxm stackK.txt -Np2 > model.txt
gmt psxy -R -J -Bpxag100f10 -Bsxg50 -Bpyaf+u"m" -Bsyg2000 \
    -BWSne+gazure1 -Sc0.05c -Gred stackK.txt -Y5.0c -O -K >> $ps
gmt psxy -R -J -W0.5p,blue model.txt -O -K >> $ps
echo "m@-3@-(t) = a + b\267 t + c\267t@+2@+" | gmt pstext -R -J \
    -F+f11p+cBL -Dj0.1i -Glightyellow -O -K >> $ps

echo "180 -1500 D" | gmt pstext -R -J -F+jBL+f18p,black -Gfloralwhite -W0.5p -O -K
>> $ps
    rm -f model.txt
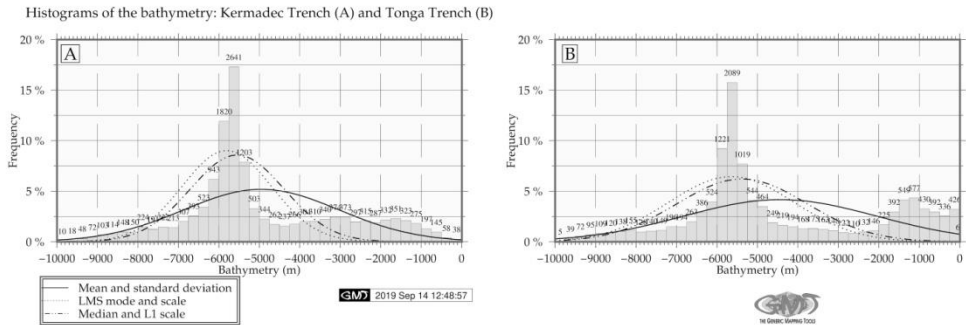
Fig. 5. Histograms of the bathymetry: frequency of the distribution of depths by data for both trenches. Left: Kermadec, right: Tonga *(Source: author).*

The same procedure was repeated for several mathematic approximations of the trend lines showing general profile shapes and gradients for both trenches. The comparison of trenches was computed using module 'pshistogram' (**Fig. 5**) by following code:

```
gmt pshistogram tableK.txt -i4 -R-10000/6/0/20 -JX4.8i/2.4i \
    -Bpxg1000a1000f100+l"Bathymetry (m)" \
    -Bpyg5a5f2.5+l"Frequency"+u" %" -Bsyg2.5 \
    -BWSne+t"Histograms of the bathymetry: Kermadec Trench (A) and Tonga Trench
(B)"+gsnow1 -Glightsteelblue1 \
    -D+f7p,Times-Roman,black -L0.1p,dimgray -Z1 -W250 -N0+pblack -N1+p..- -
N2+p. \
    -UBL/8.5c/-1.8c -K > $ps
```

4. RESULTS AND DISCUSSIONS

The resulting profiles are visualized as two segments (red and green for both trenches) on **Fig. 2**, left. Automatic digitizing of the cross-section profiles for Kermadec and Tonga trenches demonstrated that Tonga trench's geomorphology has steeper gradient slope on the western flank (**Fig. 3, A**). On the contrary, Kermadec trench (**Fig. 3, B**) has more gentle shape form of the western slope off Tonga Ridge. The results of the comparative analysis of the two trenches show that Tonga Trench has shallower depths on the eastern part along but kermadec Trench has more abrupt shape with 2,641 depth records s from -6,600 to -6,800 meters (**Fig. 5**). Comparing the deepest values >9,000 meters for Tonga Trench there are 5, 39, 72, 95, 109 observations, that sums together 320 samples. As for kermadec Trench for the same depth range there are 10, 18, 48, 72 and 103, which gives together 251 observation samples proving that Tonga Trench is deeper than Kermadec Trench.

If we compare the variations of the seafloor depths at range from -6,000 to -5,000, it can be sen (Fig. 5) that Kermadec Trench has more values in this range: 1820, 2641, 1203 and 503 giving together 6167 samples. For the Tonga Trench, the same range gives 4803 (a sum of 1221, 2089, 1019 and 544). That means that Kermadec has more gentle slope and

shallower depths which can also be seen on **Fig. 3**. This illustrates tectonic and geological local variations, as well as different sedimentation of the Kermadec and Tonga trenches causing variations in their geomorphic shape despite their close location to each other.

5. CONCLUSIONS

Various factors affect formation, functioning and sustainability of the marine habitats and hadal trenches as one of the unique places of the oceans, as discussed in previous papers (Lemenkova, 2018a; Pollnac *et al.,* 2001; Pelletier. & Louat, 1989; Lemenkova, 2018b). The complex analysis of the structure of the ocean ecosystem based on the advanced data analysis, software and scripting tools significantly increases the precision and speed of the data processing and reliability of the results. Examples of the application of programming languages and statistical tools specifically for the oceanological data modelling were presented in previous publications: Python (Yu *et al.,* 2019; Lemenkova, 2019c; Lemenkova, 2019d), R (Lemenkova, 2019a; Lemenkova, 2019b), SPSS (Lemenkova, 2019f), Gretl (Lemenkova, 2019e). Using GMT advanced scripting toolset for the cartographic modelling increases automatization of the mapping routine. Therefore, GMT is strongly recommended for the geospatial data analysis and thematic mapping.

There are both theoretical and practical innovations of the presented research that can be applied in the similar works. The theoretical novelty lies in the comparative geomorphological mapping of the two hadal trenches that does not exists in the available literature. The practical novelty consists in the developed methodology of the GMT-based mapping rather than traditional GIS, applied for the geomorphic modelling. Tested, presented and explained functionality of the several GMT modules enables to do automated digitizing of the orthogonal profiles crossing trenches in the perpendicular direction. Through this modelling, the shape of the landforms and steepness gradient of the trenches were visualized, compared and statistically analyzed. The traditional handmade cartographic digitizing is a tedious routine usually prone to minor or major errors. On the contrary, using GMT based machine learning for the automatization of the cartographic techniques significantly improves the quality and precision of the modelling.

6. ACKNOWLEDGEMENTS

R E F E R E N C E S

Anderson, M. E. (2006) Studies on the Zoarcidae (Teleostei: perciformes) of the Southern Hemisphere. XI. A new species of Pyrolycus from the Kermadec Ridge. *Journal of the Royal Society of New Zealand*, 36, 63–68. doi: 10.3853/j.0067-1975.46.1994.9.

Belyaev, G. M. (1989) Deep-Sea Ocean Trenches and Their Fauna. Nauka Publishing House.

Bevis, M., Taylor, F. W., Schutz, B. E., Recy, J., Isacks, B. L., Helu, S., Singh, R., Kendrick, E., Stowell, J., Taylor, B., Calmant, S. (1995) Geodetic observations of very rapid convergence and back-arc extension at the Tonga arc. *Nature* 347, 249–251.

Blankenship, L. E., Yayanos, A. A., Cadien, D. B. & Levin, L. A. (2006) Vertical zonation patterns of scavenging amphipods from the Hadal zone of the Tonga and Kermadec Trenches. *Deep-Sea Research I,* 53, 48–61. doi: 10.1016/j.dsr.2005.09.006

Castillo, P. R., Lonsdale, P. F., Moran, C. L. & Hawkins, J. W. (2009) Geochemistry of mid-Cretaceous Pacific crust being subducted along the Tonga–Kermadec Trench: Implications for the generation of arc lavas. *Lithos*, 112, 87–102. doi:10.1016/j.lithos.2009.03.041

Duncan, R. A., Vallier, T. L. & Falvey, D. A. (1985) Volcanic episodes at 'Eua, Tonga Islands. In: Scholl, D.W., Vallier, T.L. (Eds.), Geology and Offshore Resources of Pacific Island Arcs; Tonga Region. Circum-Pac. Counc. Energy and Miner. Resour., Houston, TX, United States, 281–290.

Ewart, A., Collerson, K. D., Regelous, M., Wendt, J. I. & Niu, Y. (1998) Geochemical evolution within the Tonga–Kermadec Lau arc back- arc systems: the role of varying mantle wedge composition in space and time. *Journal of Petrology,* 39 (3), 331–368. doi: 10.1093/petroj/39.3.331

Hergt, J. M. & Woodhead, J. D. (2007) A critical evaluation of recent models for Lau–Tonga arc–backarc basin magmatic evolution. *Chemical Geology*, 245, 9–44. doi: 10.1016/j.chemgeo.2007.07.022

Jamieson, A. J., Kilgallen, N. M., Rowden, A. A.,Fujii, T., Horton, T., Lörz, A.-N., Kitazawa, K. & Priede, I. G. (2011) Bait-attending fauna of the Kermadec Trench, SW Pacific Ocean: Evidence for an ecotone across the abyssal–hadal transition zone. *Deep-Sea Research I*, 58, 49–62. doi: 10.1016/j.dsr.2010.11.003

Jamieson, A. J., Lacey, N. C., Lörz, A.-N., Rowden, A. A. & Piertney, S. B. (2013) The supergiant amphipod Alicella gigantea (Crustacea: Alicellidae) from hadal depths in the Kermadec Trench. SW Pac. Ocean. *Deep-Sea Research Part II Topical Studies in Oceanography,* 92, 107–113. doi: 10.1016/j.dsr2.2012.12.00

Jamieson, A. J. (2015) The hadal zone: life in the deepest oceans. Cambridge University Press, Cambridge.

Leduc, D. & Rowden, A. A. (2018) Nematode communities in sediments of the Kermadec Trench, Southwest Pacific Ocean. *Deep-Sea Research Part I*, 134, 23–31. doi: 10.1016/j.dsr.2018.03.003

Leduc, D. (2015) New species of Thelonema, Metasphaerolaimus, and Monhystrella (Nematoda, Monhysterida) from Kermadec Trench, Southwest Pacific. *European Journal of Taxonomy*, 158, 1–19. doi: 10.5852/ejt.2015.158

Leduc, D., Rowden, A. A., Glud, R. N., Wenzhöfer, F., Kitazato, H. & Clark, M. R. (2016) Comparison between infaunal communities of the deep floor and edge of the Tonga Trench: possible effects of differences in organic matter supply. *Deep-Sea Research Part I Oceanographic Research Papers,* 116, 264–275. doi: 10.1016/j.dsr.2015.11.003

Lemenkova, P. (2019a) Statistical Analysis of the Mariana Trench Geomorphology Using R Programming Language. *Geodesy and Cartography*, 45 (2), 57–84. ISSN: 2029-6991. doi: 10.3846/gac.2019.3785

Lemenkova, P. (2019b) An Empirical Study of R Applications for Data Analysis in Marine Geology. *Marine Science and Technology Bulletin,* 8(1), 1-9. doi: 10.33714/masteb.486678

Lemenkova, P. (2019c) Processing oceanographic data by Python libraries NumPy, SciPy and Pandas, *Aquatic Research*, 2, 73-91, doi: 10.3153/AR19009

Lemenkova, P. (2019d) Testing Linear Regressions by StatsModel Library of Python for Oceanological Data Interpretation. *Aquatic Sciences and Engineering*, 34, 51–60, doi: 10.26650/ASE2019547010

Lemenkova, P. (2019e) Regression Models by Gretl and R Statistical Packages for Data Analysis in Marine Geology. *International Journal of Environmental Trends,* 3(1), 39–59, doi: 10.6084/m9.figshare.8313362.v1

Lemenkova, P. (2019f) Numerical Data Modelling and Classification in Marine Geology by the SPSS Statistics. *International Journal of Engineering Technologies*, 5(2), 90–99. doi: 10.6084/m9.figshare.8796941

Lemenkova, P. (2018a) R scripting libraries for comparative analysis of the correlation methods to identify factors affecting Mariana Trench formation. *Journal of Marine Technology and Environment*, 2, 35-42, doi: 10.6084/m9.figshare.7434167

Lemenkova, P. (2018b) Factor Analysis by R Programming to Assess Variability Among Environmental Determinants of the Mariana Trench. *Turkish Journal of Maritime and Marine Sciences*, 4, 146–155, doi: 10.6084/m9.figshare.7358207

Linley, T. D., Stewart, A. L., McMillan, P. J., Clark, M. R., Gerringer, M. E., Drazen, J. C., Fujii, T. & Jamieson, A. J. (2017) Bait attending fishes of the abyssal zone and hadal boundary: Community structure, functional groups and species distribution in the Kermadec, New Hebrides and Mariana trenches. *Deep–Sea Research Part I*, 121, 38–53. doi: 10.1016/j.dsr.2016.12.009

Micallef, A. (2011) Developments in Earth Surface Processes. *Developments in Earth Surface Processes. Chapter 13 – Marine Geomorphology: Geomorphological Mapping and the Study of Submarine Landslides,* 15, 377-395. doi: 10.1016/B978-0-444-53446-0.00013-6

Mitchell, N. C. (2015) Submarine Geomorphology. *Reference Module in Earth Systems and Environmental Sciences*. doi: 10.1016/B978-0-12-409548-9.09249-6

Nunnally, C. C., Friedman, J. R. & Drazen, J. C. (2016) In situ respiration measurements of megafauna in the Kermadec trench. *Deep–Sea Research Part I*, 118, 30–36. doi: 10.1016/j.dsr.2016.10.009

Pelletier, B. & Louat, R. (1989) Seismotectonics and present-day relative plate motions in the Tonga– Lau and Kermadec–Havre region. *Tectonophysics*, 165, 237–250. doi: 10.1016/0040-1951(89)90049-8

Pollnac, R. B., Crawford, B. R. & Gorospe, M. L. (2001) Discovering factors that influence the success of community-based marine protected areas in the Visayas, Philippines. Ocean and Coastal Management, 44(11), 683-710. doi: 10.1016/S0964-5691(01)00075-8.

Regelous, M., Collerson, K. D., Ewart, A. & Wendt, J. I. (1997) Trace element transport rates in subduction zones: evidence from Th, Sr and Pb isotope data for Tonga–Kermadec arc lavas. *Earth and Planetary Science Letters,* 150, 291–302. doi: 10.1016/S0012-821X(97)00107-6

Smith, I. E. M. & Price, R. C. (2006) The Tonga–Kermadec arc and Havre–Lau back-arc system: their role in the development of tectonic and magmatic models for the western Pacific. *Journal of Volcanology and Geothermal Research*, 156, 315–331. doi: 10.1016/j.jvolgeores.2006.03.006

Smith, I. E. M., Worthington, T. J., Stewart, R. B., Price, R. C., Richard, C. & Gamble, J. A. (2003) Felsic volcanism in the Kermadec Arc, SW Pacific; crustal recycling in an oceanic setting. *Geological Society Special Publications*, 219, 99–118.

Tappin, D. R. (1993) The Tonga frontal arc basin. In: Ballance, P.F. (Ed.), Sedimentary Basins of the World: South Pacific Sedimentary Basins, 2. Elsevier, Amsterdam.

Wessel, P. & Smith, W. H. F. (1991) Free software helps map and display data. *EOS Transactions of the American Geophysical Union* 72 (41), 441.

Wessel, P., Smith, W. H. F. Scharroo, R., Luis, J. F. & Wobbe, F. (2013) Generic mapping tools: Improved version released, *EOS Transactions of the American Geophysical Union* 94(45), 409– 410, doi:10.1002/2013EO450001

Wright, D. J., Bloomer, S. H., MacLeod, C. J., Taylor, B. & Goodlife, A. M. (2000) Bathymetry of the Tonga Trench and Forearc: a map series. *Marine Geophysical Researches* 21, 489–511.

Xu, Y., Ge, H. & Fang, J. (2018) Biogeochemistry of hadal trenches: Recent developments and future perspectives. *Deep-Sea Research Part II*, 155, 19–26. doi: 10.1016/j.dsr2.2018.10.006

Yu, Q.-Y., Bagas, L., Yang, P.-H. & Zhang, D. (2019) GeoPyTool: A cross-platform software solution for common geological calculations and plots. Geoscience Frontiers, 10(4), 1437-1447.

A COMPARATIVE ANALYSIS THROUGH TIME AND SPACE OF CENTRALITY'S ROLE IN COUNTY CENTERS' SPATIAL POSITION FOR SEVERAL COUNTIES IN ROMANIA

Zsolt MAGYARI-SÁSKA[1]

ABSTRACT :
The aim of the study was to measure the importance of county centers in terms of central positioning and accessibility. The actual county centers have been chosen not only based on their central position but also based on other reasons such as their cultural, traditional and especially historical importance. With all these through time they should enforce their central position also in terms of accessibility – as some administration procedures can be managed just in these cities – and to became truly the centers of their counties. We want to check if the actual county centers fulfill these considerations, how strong is these fulfillments and in case of failure which cities could take their places. We also made some comparisons with former administrative organizations at the beginning of the 20th century before car traffic appeared.

Key-words: *network modeling, weighted network, closeness centrality, eigenvector centrality, ranking*

1. INTRODUCTION

The actual county centers have been chosen not only based on their central position but also based on other reasons such as their cultural, traditional and especially historical importance. With all these through time they should enforce their central position also in terms of accessibility – as some administration procedures can be managed just in these cities – and to became truly the centers of their counties. Through history the border of middle level administrative entities has changed but in many cases the same cities remained as county centers for the newly created or modified administrative entities. Our research is focused on calculating and comparing the centrality of county centers by calculating those centrality indices which can be directly related to accessibility, considering the population movement too. In those cases, where the importance of a county center in terms of accessibility is not eloquent we try to show alternative locations and evaluate the whole county's accessibility if they would be county centers.

The comparison is made not just between different counties in present but also between two different time periods with different administrative borders, being 100 years apart from each other. The selected counties cover the major part of actual Transylvania, including Crișana but excepting the Banat region.

For characterizing the spatial accessibility there are many indicators, mainly connected to different centrality measures (Rodrigue, 2017; Miller, 2018).   The   importance   of accessibility is present in many fields: city planning, emergency evaluation, touristic destination management or agriculture (Bilasco et all., 2018). The present research aim is to study the centrality of different settlements, especially the county centers, trying to prove that centrality was an important factor in tracing administrative borders. Various indices

---

[1] *Babeş-Bolyai University, Gheorgheni Extension, Gheorgheni, Romania, zsmagyari@gmail.com*

characterizing the centrality are defined for network models, considering the nodes' degree, the participation of a node in multiple path, the distance of a node form the other etc. (Bennison, 2010). Although, studies which evaluates the centrality of nodes, representing settlements or inner points of settlements are not new (Kang, 2015) these researches are part of a continuously developing mainstream not just by their results but also with their research methodology (Hellerik et all., 2019).

2. METHODS AND DATA

2.1. Methods

2.1.1. Shape index

The accessibility of polygons' centroid is undoubtedly related to the shape of the polygon. For a regular shape is much easy to have a high accessibility value than for an irregular or elongated shape having the same area. Through its shape every polygon holds a potential to have a higher or lower accessibility value for its centroid and also for its other points. This potential can be expressed by the shape index which is a ratio between the polygon perimeter and area. Through time were used several indices, but some of them were size dependent (Frohn, 1998; Lang & Blaschke, 2007). The variant of the shape index that is scale independent is the ratio between the perimeter and the square root of area multiplied with 4π (equation 1).

$$si = \frac{perimeter}{\sqrt{4\pi area}} \tag{1}$$

Its value is close to 1 in case of circular shapes and more distant for irregular and elongated shapes (Patton, 1975; Schumaker, 1996). In our case lower values will represent a higher centrality potential for a given county.

2.1.2. Centrality

The centrality of a node in a network can be measured in multiple ways. All of these try to determine how important is a node in a given network. Some of the most commonly used are (Bennison, 2010):

1) degree centrality, which considers that the most important node is that which has the most connections;

2) closeness centrality for which the most important node is that, which has the lowest average distance from all other nodes in the network;

3) betweenness centrality, which choses the most important node based on the number of shortest routes which are going through it.

Closeness centrality measures how distant is a given node form all other nodes in a network based on the shortest paths average distance (Sabidussi, 1996), (eq. 2).

$$cc_i = \frac{\sum_{i,x \in G} d_{(i,x)}}{n-1} \tag{2}$$

where cc_i is the closeness centrality value for node i, $d_{(i,x)}$ is the length of shortest path between nodes i and x, n is the number of nodes in the connected graph G. The shortest path can be calculated in weighted and unweighted networks. The closeness centrality can be defined also for node weighted networks. In this case depending on application this

weight can be a combination of node pair values for every shortest path or considering just one nodes' value. In our research as we were interested in studying the incoming population for a county center, we considered as node weight just the population of the incoming node. For shortest path calculation we used Dijkstra's algorithm, determining in one step all shortest routes from a given node (Dijkstra, 1959). A similar procedure was used by Nicoara & Haidu (2014) in order to identify shortest route access to emergency medical facilities. All calculation concerning centrality values were made in an external application written in C++.

Eigenvector centrality is an index which measures the importance of a node in a network (Negre et all., 2018; Hexmoore, 2015). This importance can be expressed as a selected weight assigned to every node of the network. The calculus of the eigenvector centrality starts from an arbitrary vector assigned to every node. In every step new eigenvector values are calculated as a product between their existing (old) values and the node's weight. After that the obtained vector is normalized by the highest value obtained in present step calculus. The number of steps is defined by a threshold value, for the sum of the differences of the previous and current eigenvector values. In our present research we used eigenvector centrality considering as weight both the physical distance (shortest route) and the weighted distance expressed as a product between physical distance and the number of incoming population. By definition higher eigenvector centrality values mean higher influence for a node. In our case, as the weights represent costs and not benefits, smaller cost (distances) are better, the interpretation of eigenvector values is opposite – lower eigenvector values are more desirable.

2.2. Data sources and preprocessing

In our study the data acquisition and preprocessing was made in QGIS, and the accessibility analysis was made on a network model because it is one of the most suitable way to model spatial relations (Bobková, 2017). As we made our research for two different time periods we have to get map date for both of it.

In case of the beginning of the 20th century we used the map sheets of the Austro-Hungarian Empire, which scale varied between 250.000 to 400.000. The map sheets were georeferenced using the Bessel ellipsoid parameters. Two thematic layers were digitized from them: the settlement and the road network layer. The non-spatial data regarding the population number of that time was collected from statistical records of the 1910 census digitally prepared and made publicly available by Varga E. Árpád (1992).

Unfortunately, the version of the database management application used by UNESCO in which the digital census data is freely available, has several inconvenient. It is an application that cannot be run on current 64-bit operating systems, it uses a custom data format and has limited export capabilities. To regain the data recorded in this format was a challenge in itself. It was necessary to install an old, unsupported 32-bit version of Windows XP, and it was necessary to search for a full version of WINISIS because the version downloaded from the website did not have the proper export capability. After resolving the situation, the database was converted to Excel format and based on settlement's name it was joined with the locations on the map.

In case of the nowadays data, the road network was obtained from OpenStreetMaps, the settlement location from geo-spatial.org portal, which made publicly available different vector data including Romania's cities position, while the data source for population data of 2011 census was the National Statistical Institute of Romania.

The main reason for choosing OSM is that raw data can be downloaded, while for proprietary maps (Microsoft Bing Maps, Google Maps, Here Technologies Here WeGo etc.) only the analysis results can be obtained freely (ex. shortest routes). OpenStretMaps data being a Volunteered Geographic Information (VGI) it's normal to check the data accuracy. Fortunately, there are studies about this issue testing the data accuracy from China (Wang et al, 2013) through Turkey (Hacar et al., 2018) and Germany (Helbich et al, 2012) to Great Britain (Haklay, 2010) and Ireland (Ciepłuch et al, 2010). Hacar and collaborators emphasizes how the volunteers experience level determines the accuracy. In case of China the position data accuracy proved to be very poor especially for low level roads. The situation is much better in Europe where position imprecision varies a few meters, mentioning that high accuracy is mainly present in highly populated urban centers.

Both for the beginning of 20th century and for nowadays the points representing the settlements were connected with the road network by direct connections and a graph based network model was created. In that model some of the nodes are representing the crossroads while others the settlements. Each road segment between different node pairs had the length attribute and each node that represents a settlement had the population number, resulting a node and edge weighted network model for further analysis.

3. RESULTS AND DISCUSSION

Calculating the polygon scale index, we defined the theoretical possibility for every county to could have a well (centrally) positioned center, as for circle like forms it's more easy to have a highly accessibile center than for elongated or irregular shapes.
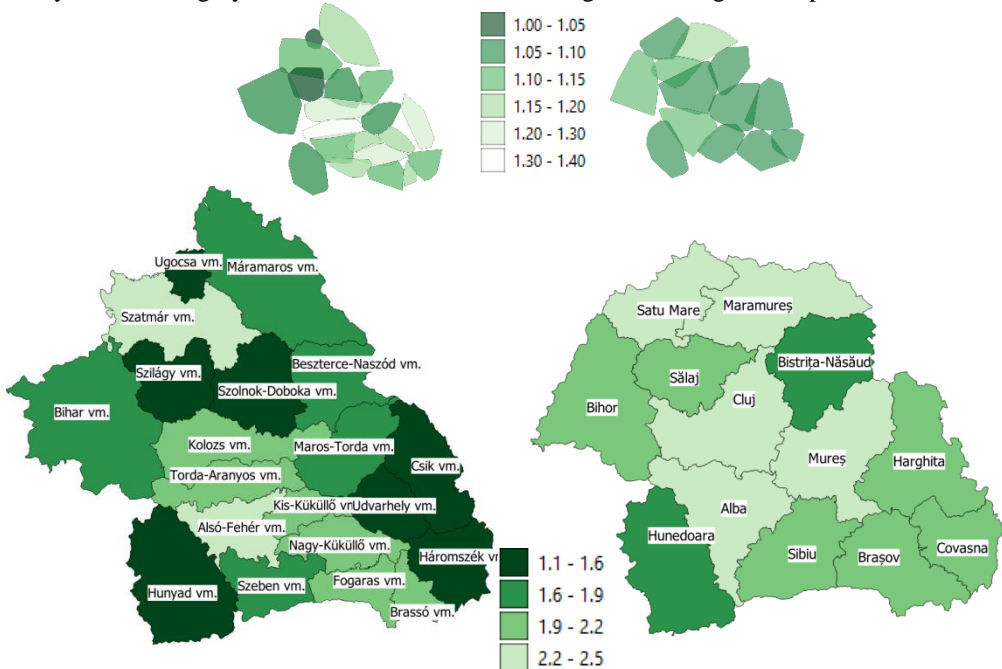
Fig. 1. County shape index at present (right) and past (left) with actual border and settlement defined hull polygons (upper maps).

Using the same legend category, it was unexpected to see, that administrative entities from the beginning of the 20th century are most suitable to create centrally positioned centers then the current administrative units.

We identified that the vectorization scale for the two cases could have influence on the results as the perimeter of shapes depends more on vectorization detail than the area. To overcame this difference, we created convex hull polygons for both time moments for each county based on their settlements (**Fig. 1**). Calculating the scale index for these newly created hull polygons the results seems to model more accurate the situations. For nowadays the distribution of scale index is more balanced, having middle to high values for most of the actual counties. For the beginning of 20th century the scale index distribution has a wider range with two counties in the best scale index range, but also four counties in the two worst value range, using the same legend category for both cases.

In conclusion the current administrative boundaries offer a better theoretical positioning for county centers to have an excellent accessibility. This is proved also by the average values of the shape index for the hull polygons. The relative standard deviation for the counties existing at the beginning of the 20th century is 0.069, while for actual situation is only 0.022.
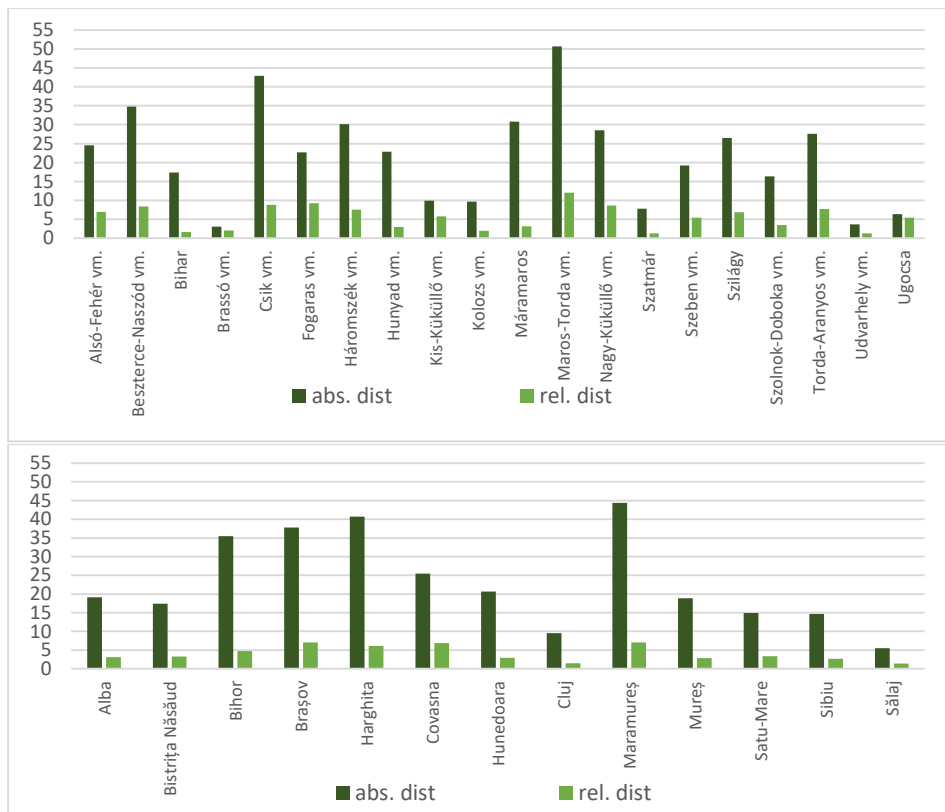
Fig. 2. Distances between polygon centroids and county center.

We continued with measuring the distance between the polygons' centroids and the actual county centers. The raw values are similar for the two time moments with a slightly higher average distance for actual time but also with a lower standard deviation. To have a more precise representation we calculated the relative distance against the area of the polygons, because it's normal to have higher values for larger areas and the actual counties area are much higher than the counties in the beginning of the 20th century (**Fig. 2**). The mentioned relative distance improved both calculated indicators: the average of the relative distance with 20%, the standard deviation with 31% for current time. Even if the current counties have larger areas then those at the beginning of the 20th century, their county centers are relatively closer to the polygon centroids and by this they have a better location potential to fulfill their central role.

Till now the analysis' regarded the counties having a continuous space with free movement inside them, in the following the road network was considered to measure the accessibility. For that we have calculated the closeness centrality for each settlement inside the county that belongs to. This value indicates for every settlement how suitable is to be the county center. We performed this centrality analysis both in not weighted and weighted form. We considered as weight the number of population in the settlements.
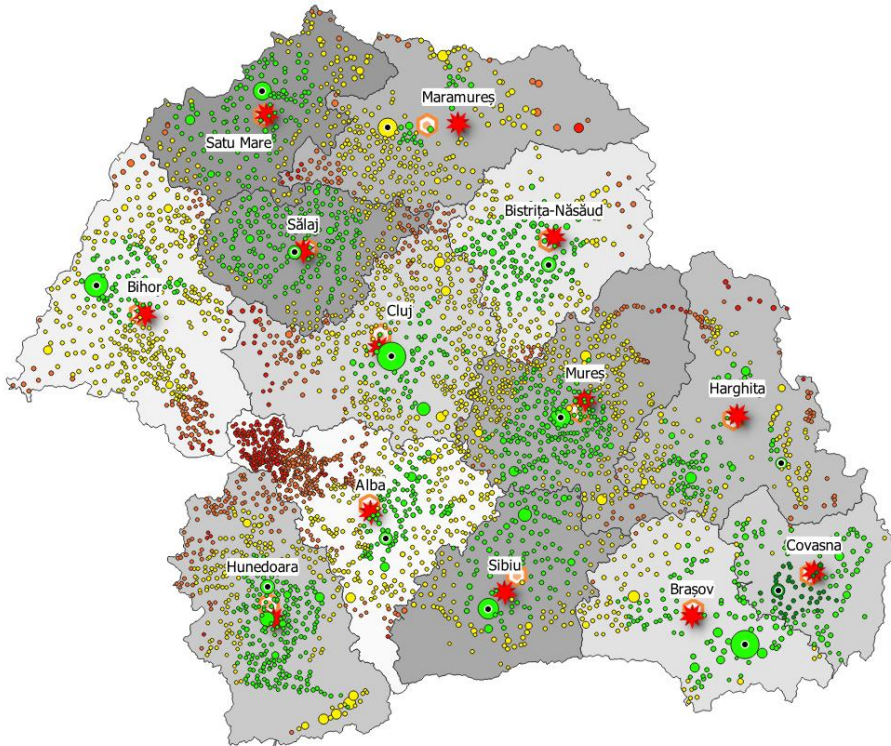
Fig. 3. Settlements' accessibility measured as weighted closeness centrality. County centers are marked with black points, the circles' area is proportional with their population, the red starts mark the county polygon's center and the orange hexagon the hull polygons' center. The colors indicate the suitability category for each settlement to became county center in terms of accessibility (green to red – higher to lower).

To make a proper modeling in every analysis we considered that the currently analyzed settlement (for which we are calculating the closeness centrality) has the population of the current county center's population by temporary swapping their population number. Without this consideration we could not have a realistic modeling, as due to the important population number in county centers just the nearby settlements could candidate to the county center role.

Even if the graphical representation is picturesque (**Fig. 3**) it could not provide all details, we summarized the important results in **Table 1**. The candidate settlements were selected based on their population number. Just those settlements are mentioned which has at least 10.000 inhabitants. There are some very clear situations.

In case of Bihor, Cluj, Mureş and Satu-Mare the county centers are really best positioned, in some other cases the situation maybe doesn't seem ideal but in reality it's very good, with no mentionable alternatives such as Braşov, Covasna, Sălaj. Based on the results we think that for Harghita and Hunedoara neither by structural nor by practical point of view we cannot say that the actual county centers are the best choices, of course just regarding the accessibility.

<div align="right">Table 1.</div>

**Ranking of actual city centers based on closeness centrality
and proposed alternative county centers.**

County name	R_{cc}	R_{wcc}	CS_{cc}	CS_{wcc}
Alba	3	10	-	-
Bihor	1	1	-	-
Bistriţa-Năsăud	7	25	-	Năsăud [18], Beclean [21]
Braşov	2	8	-	-
Covasna	1	8	-	-
Cluj	1	1	-	-
Harghita	13	68	Odorheiu Secuiesc [3]	Odorheiu Secuiesc [23], Gheorgheni [63]
Hunedoara	7	80	Simeria [4]	Călan [3], Haţeg [20], Hunedoara [34], Simeria [49]
Maramureş	1	35	-	Baia Sprie [22]
Mureş	1	1	-	-
Sălaj	2	3	-	-
Satu Mare	2	1	-	-
Sibiu	1	45	-	Mediaş [33]

R_{cc} - actual county center's rank in closeness centrality measure / R_{wcc} - actual county center's rank in weighted closeness centrality measure CS_{cc} - candidate settlements from closeness centrality values CS_{wcc} - candidate settlements from weighted closeness centrality values. Values in brackets indicates settlement ranking for candidate cities.

Calculating the eigenvector centrality both in unweighted and weighted way we got the values indicating the influence of every settlement in the network. The results are presented in **Table 2** which in main part matches with the situation based on closeness centrality: Mureş, Cluj and Satu-Mare are clearly the winners, while Hunedoara and Harghita are laggards.

For those settlements who were marked as candidate for the county center role we have remade the weighted closeness centrality and weighted eigenvector centrality analysis,

considering those settlements as county centers but keeping their population number. We want to see whether in this case their weighted centrality and weighted eigenvector centrality will have better values that the actual county centers.

The obtained result can be summarized as follows: in case of Sălaj county Jibou would not be a viable county center. In case of Sibiu county Mediaș would not be a better choice in terms of weighted closeness centrality, having a worst relative rank, although its ranked higher than Sibiu. The best solution for Bistrița Năsăud county would be to have Beclean as county center if we look just at the weighted closeness centrality. In this case also Năsăud city would have a higher rank than in actual situation. For Hunedoara county the best case would be to have Călan as county center, for Maramureș county with the city of Baia Sprie being county center would have higher accessibility. In case of Brașov county the city of Codlea it could be a viable alternative as county center, and in case of Harghita county Odorheiu Secuiesc could take the place of Miercurea Ciuc.

If we consider the distances between alternative and actual city centers just in two cases the theoretical change of county center would produce significant changes, as in case of Sibiu and Harghita county the distance exceeds 50km.

Table 2.

**Ranking of actual city centers based on eigenvector centrality
and proposed alternative county centers.**

County name	R_{ec}	R_{wec}	CS_{ec}	CS_{wec}
Alba	172	1	-	-
Bihor	6	1	-	-
Bistrița-Năsăud	4	4	-	-
Brașov	82	17	Făgăraș [13], Codlea [42]	-
Covasna	13	19	-	-
Cluj	1	1	-	-
Harghita	25	31	Odorheiu Secuiesc [3]	Gheorgheni [29]
Hunedoara	3	93	-	Călan [6], Hațeg [11], Hunedoara [37], Simeria [57]
Maramureș	13	68	Baia Sprie [9]	Baia Sprie [40]
Mureș	1	1	-	-
Sălaj	9	3	Jibou [4]	-
Satu Mare	1	1	-	-
Sibiu	2	5	-	-

R_{ec} - actual county center's rank in eigenvector centrality measure / R_{wec} - actual county center's rank in weighted eigenvector centrality measure CS_{ec} - candidate settlements from eigenvector centrality values CS_{wec} - candidate settlements from weighted eigenvector centrality values. Values in brackets indicates settlement ranking for candidate cities. Values in brackets indicates settlement ranking for candidate cities.

As mentioned our research want to compare the actual situation with that of 100 years ago. The direct comparison is practically impossible as the county boundaries have changed. We perform the analysis for those cities which were county centers even 100 years ago to see how imposing they were at that time. For this analysis we considered as alternative county centers those cities which had at least 3.000 inhabitants at that time.

Looking at **Table 3** and **Table 4** we can notice that in several cases the situation was the same: Oradea as county center for Bihor/Bihar, Sfântu Gheorghe as county center for Covasna/Háromszék, Cluj-Napoca as county center for Cluj/Kolozsvár and Satu Mare for Satu Mare/Szatmár had the best accessibility and influence inside their (changed) counties. On the other side Miercurea-Ciuc and Deva had a not very clear position even 100 years ago. Târgu Mureș through time enforced a little it's accessibility to nowadays while Bistrița and Brașov had a little bit better accessibility in the past.

Table 3.

Ranking of cities which are historically county centers based on closeness centrality and proposed alternative county centers based on data from the beginning of 20th century.

County center name	R_{cc}	R_{wcc}	CS_{cc}	CS_{wcc}
Bistrița	1	1	-	-
Oradea	1	1	-	-
Brașov	1	2	-	-
Miercurea Ciuc	7	27	-	Sândominic [5]
Sfântu Gheorghe	9	13	-	-
Deva	9	25	-	Hunedoara [9]
Cluj-Napoca	4	4	-	-
Târgu Mureș	1	2	-	-
Satu Mare	1	1	-	-
Sibiu	2	18	-	Selistea [9]
Zalău	19	21	Simleu Silvaniei [16]	Simleu Silvaniei [14]

Table 4.

Ranking of cities which are historically county centers based on eigenvector centrality and proposed alternative county centers based on data from the beginning of 20th century.

County center name	R_{ec}	R_{wec}	CS_{ec}	CS_{wec}
Bistrița	1	2	-	-
Oradea	1	1	-	-
Brașov	1	1	-	-
Miercurea Ciuc	13	25	Frumoasa [12]	Sândominic [5], Joseni [18], Frumoasa [21], Gheorgheni [24]
Sfântu Gheorghe	22	26	-	-
Deva	11	29	Hunedoara [5]	Hunedoara [3]
Cluj-Napoca	1	1	-	-
Târgu Mureș	23	24	Reghin [5]	Reghin [5]
Satu Mare	1	1	-	-
Sibiu	3	13	-	Selistea [9]
Zalău	15	17	-	-

4. CONCLUSIONS

The presented research wanted to characterize how accessible were and are the county centers for several Romania's counties. For evaluation two approaches were used, the shape index and two centrality measures: closeness and eigenvector centralities in unweighted and weighted variants. We have found that the shape index representing the centrality potential for counties has no relation with actual road network based accessibility. The correlation values between shape index and centrality values are far below a considerable value.

The role of county centers inside their counties, measured as accessibility values are not so different through 100 years even if the administrative boundaries has changed, sometimes substantially. Most of county centers has an excellent or good accessibility and influence and even if some's accessibility is just acceptable, the obtained alternatives would not produce important changes. In these cases, using the actual road network a significantly better location could not be found. This appreciation is valid for past and present. In the study we identified two counties where the change of the county centers it would make sense in terms of accessibility.

Through our research we proved that there are cases when historical, cultural or other arguments may prevail over a practical aspect, expressed in this case with centrality.

REFERENCES

Bennison, D.J. (2010), The measurement of settlement centrality, *The Professional Geographer*, 30(4), 371-376

Bilaşco, S., Roşca, S., Păcurar, I., Moldovan , N., Vescan, I., Fodorean, I., Petrea, D. (2018), Roads accessibility to agricultural crops using GIS technology. Methodological approach., *Geographia Technica*, 13(2), 12-30

Bobková, M., Holesinka, A. (2017), Networking in a destination from the perspective of virtual relationships and their spatial dimension, *Geographia Technica*, 12(2), 10-19

Ciepłuch, B., Jacob, R., Mooney, P., Winstanley, A.C. (2010), Comparison of the accuracy of OpenStreetMap for Ireland with Google Maps and Bing Maps, *Proceedings of the Ninth International Symposium on Spatial Accuracy Assessment in Natural Resources and Environmental Sciences 20-23rd July 2010.* p. 337.

Dijkstra, E.W. (1959). A note on two problems in connexion with graphs, *Numerische Mathematik*, 1, 269–271.

Frohn, R.C. (1998) *Remote Sensing of Landscape Ecology: New Metric Indicators of Monitoring, Modeling and Assessing of Ecosystems*. Lewis Publishers, Boca Raton, Florida.

Hacar, M., Kilic, B., Shabaz, K. (2018), Analyzing OpenStreetMap Road Data and Characterizing the Behavior of Contributors in Ankara, Turkey, *International Journal of Geo-Information*, 7, 1–12

Haklay, M. (2010), How good is Volunteered Geographic Information? A comparative study of OpenStreetMap and Ordnance Survey Dataset, *Environment and Planning B: Urban Analytics and City Science*, 37(4), 682–703

Helbich, M., Amelunxen, C., Neis, P., Zipf, A. (2012), Comparative Spatial Analysis of Positional Accuracy of OpenStreetMap and Proprietary Geodata, in Jekel, T., Car, A., Strobl, J. & Griesebner, G. (Eds.): *GI_Forum 2012: Geovizualisation, Society and Learning*, 24–33

Hellervik, A., Nilsson, L., Andersson, C. (2019), Preferencial centrality – A new measure unifying urban activity, attraction and accessibility, *Environment and Planning B Urban Analytics and City Sciences*, 46, 1331-1346

Hexmoor, H. (2015), Network Analysis, in *Computational Network Science*, 15-19

Kang, C-D (2015), The effects of spatial accessibility and centrality to land use on walking in Seoul, Korea, *Cities*, 46, 94-103

Lang, S., Blaschke, T. (2007) *Landschaftsanalyse mit GIS*, Eugen Ulmer Stuttgart

Miller, E.J. (2018), Accessibility: measurement and application in transportation planning, *Transport Reviews*, 38(5), 551-555

Negre, C.F.A, Morzan, U.N., Hendrickson, H.P., Pal, R., Lisi, G.P., Loria, J.P., Rivalta, I., Ho, J., Batista, V.S. (2018). Eigenvector centrality for characterization of protein allosteric pathways, *Proceedings of the National Academy of Sciences,* 115(52), 12201–12208.

Nicoara, P-S. & Haidu, I. (2014) A GIS based network analysis for the identification of shortest route access to emergency medical facilities. *Geographia Technica*, 9(2), 60-67.

Patton, D.R. (1975). A diversity index for quantifying habitat 'edge'. *Wildlife Society Bulletin,* 3, 171-173.

Rodrigue, J-P *et al.* (2017) *The Geography of Transport Systems*, Hofstra University, Department of Global Studies & Geography, https://transportgeography.org

Sabidussi, G (1966). The centrality index of a graph, *Psychometrika,* 31(4), 581-603.

Schumaker, N.H. (1996) Using landscape indices to predict habitat connectivity. *Ecology*, 77, 1210-1225.

Varga E.A. (1992), *Népszámlálások a jelenkori Erdély területén*, Regio-MTA Történettudományi Intézet, Budapest, 214

DEVELOPMENT ASSESSMENT OF THE SINGAPORE LAND: A GIS SPATIAL-TEMPORAL APPROACH BASED ON LAND COVER ANALYSIS

Mărgărit-Mircea NISTOR[1], Harianto RAHARDJO[1], Alfrendo SATYANAGA[1]*

ABSTRACT:
Urban indicators plays an important role in the planning and sustainable development of the cities. This paper presents a methodology to determine the favorability index for development of Singapore based on land cover. The 'City Index' of Singapore was calculated using five indicators – Social, Environmental, Industrialization, Economic, and Naturality. Two indices 'Environmental Capacity of Development' and 'Land Restriction' were used as correction factors in the Singapore favorability index for development determination. The analysis of indicators and final index were carried out based on the land cover of Singapore in 2014 and in 2030 projection. A high favorability index was observed in the central and northwestern sides, in Pulau Tekong and Pulau Ubin 'Environmental Capacity of Development' factor is related to the significant importance in the natural territories and in the reclamation areas. Hence the central, North-West and surrounding islands registered higher values (close to 1) of the "Environmental Capacity of Development". The high values of the 'Land Restriction' factor indicating many infrastructures and special use areas spread over the Singapore Island. On the other hand, the moderate values of the 'Land Restriction' factor are observed in few locations from North, South, central and northeastern islands of Singapore. The 'Favorability index for development of Singapore' depicts the central and northwestern sides together with the Tekong and Pulau Ubin as high favourable areas. The southern part of Singapore, near the coastline and the eastern extremity are predicted to be favourable areas in the future due to new reclamation lands extensions. The approach presented in this paper is indispensable tool for the Singapore urban decisions and future planning. Moreover, the methodology is useful and it can be adapted for large cities or metropolitan areas of capitals.

Key-words: *City development, Development indicators, Land covers analysis, Naturality, Singapore.*

1. INTRODUCTION

Regional development is highly dependent on the Globalization trajectories. In general, the administrative units of the countries are commonly structured in each activity, such that the main sectors of industry, agriculture, and tertiary are very well defined. Christaller (1933, 1966) indicated in his ′Central Place Theory′ that the spatiality of the concentric development is observed at regional scale which is mainly occurred in the cities. This concept illustrates the development of cities and metropolitan areas around of core with

---

[1] *Nanyang Technological University, School of Civil and Environmental Engineering, 50 Nanyang Avenue, Singapore. *Corresponding author email: margarit@ntu.edu.sg*
Co-authors e-mail: chrahardjo@ntu.edu.sg, alfrendo@ntu.edu.sg

main functionality and concentric zones with various functions in the industry, agriculture, and others sectors. Further, his theory was analysed by Beguin (1996) and it was used in the regional geography and urban planning. Based on the natural landscapes, including the relief and geomorphology, rivers, coastal areas, and succession of cities, the anisotropic regions were defined. On the high specialization influence and technologies improvement, the cities of the world have a development that tends to population growth and area extension. The population migration is focussing on viable and functional cities, gross domestic product, and main economic attractions to build-up the careers and society. Many sectors in the big urban areas become fully occupied and they adopt multi-functionality for their prosperity. Thus, the strategic plans and immediate future actions should be analysed for correct decisions on a favourable territory.

The changes at the global scale are firstly induced related to the climate warming (Stocks et al., 1998; Shaver et al., 2000; Haeberli et al., 1999; IPCC, 2001; Stavig et al., 2005; The Canadian Centre for Climate Modelling, 2014) illustrating major changes after the ice mass changes (Kargel et al., 2005; Oerlemans, 2005; Shahgedanova et al., 2005; Dong et al., 2013; Xie et al., 2013; Elfarrak et al., 2014; Nistor & Petcu, 2015), reduction of river flows, depletion in the spring discharge, and poor groundwater quality due to the increases of the groundwater temperature (Taylor and Stefan, 2009; Figura et al., 2011; Kløve et al., 2012; Haldorsen et al., 2012; Kløve et al., 2014). Due to these negative issues, the ecosystems and anthropic areas require a good management for the next future planning. Moreover, the agricultural and industrial activities are continuing to be significant indicators for the cities and regions sustainability.

Up to present, the functionality of the cities and its sustainable development were very well documented (Ayram, 2017). Singh et al. (2012) indicated that the man indicators should be considered in the sustainability assessment. They used four core indicators for sustainable development based on the United Nations Commission for Sustainable Development framework presented by Labuschagnea et al. (2005). These indicators refer to social, economic, environmental, and institutional. Ayram et al. (2017) used the land use intensity, time of human landscape intervention, and biophysical vulnerability to revise a multidimensional spatial human footprint index in Mexico and to analyze the effects of landscape trans-formation on the habitat mammal species. Sands & Podmore (2000) developed an Environmental favorability index for development using 15 sub-indices to analyse the corn and wheat agricultural production systems in southeastern Colorado. Holden (2006) carried out the urban indicators for the sustainability development in the Vancouver area, Canada.

Gardi et al. (2010) found an optimal index for the Emilia-Romagna region from Italy based on the CORINE Land Cover database. They propose four determinant indicators (urbanization, industrialization, agricultural, and agricultural intensity) and two state indicators (naturality and biodiversity). The formula and the indicators calculation for the Land Use favorability index for development were established by Gardi et al. (2010).

In the large city-state as Singapore, some activity sectors are very well defined, but others are inferred between them (i.e. educational institutions and residential areas). To determine the favourable index in Singapore, five main indicators and two correction factors have been set and implemented in a new framework in this study. These indicators were calculated based on the land cover of Singapore in two periods of time (i) current period (2014 master plan) and (ii) near-future period (2030 master plan). The study area includes the main land of Singapore and the surrounding islands.
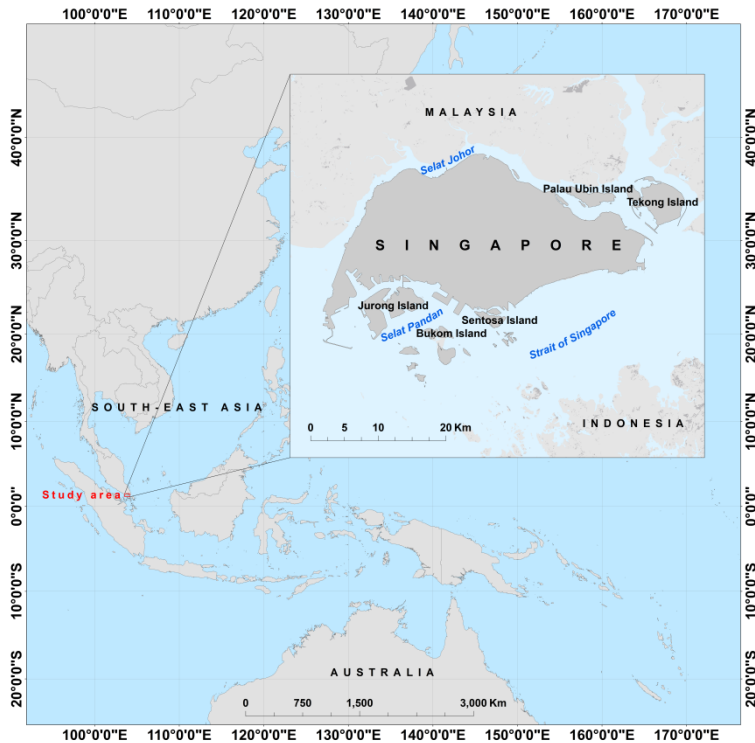
Fig. 1. Location of Singapore city-state on South-East Asia map.

2. MATERIALS AND METHODS

2.1. Study area

Singapore is a city-state located in the South-East Asia, between Indonesia and Malaysia (**Fig. 1**). The main island is around 50 km in length and 25 km in width. Numerous islands could be found around the Singapore, including in principal the Jurong, Sentosa, and Bukom islads in the South and Pulau Ubin and Pulau Tekong in the North-East. Land cover in Singapore register a dynamic growth of the artificial areas (**Tab. 1**).

The development of the Singapore started since 1950s years and currently, more than 60% of the territory is artificial area, mainly with residential and industrial areas (**Fig. 2**). North-West and central areas as well as the Pulau Ubin, Pulau Tekong, and Sentosa islands shows a large area of open and recreational space, while in southern sides and Jurong Island, there are predominantly the industrial area. The infrastructure areas are mainly composed by harbour sectors designated to navy boats and heavy platforms for shipping and the Changi Airport. Sparsely are presented the areas with special use, reserve sites, and lakes. **Table 2** reports the area values (km^2 and %) of each land cover type in Singapore related to 2014 and 2030.

The complex demographic aspects and the actual construction plans signal the necessity of a detailed analysis of the land use sustainability.
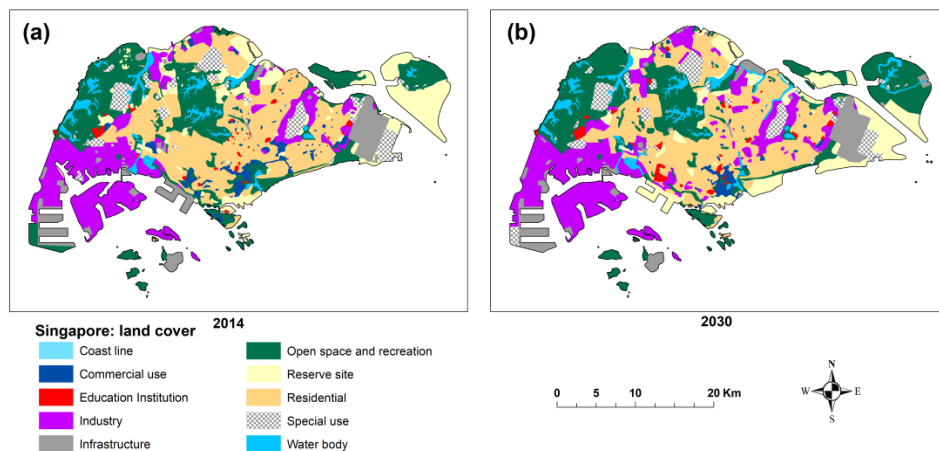
Fig. 2. a) Land cover map of Singapore related to 2014;
b) Land cover map of Singapore related to 2030.
Source: Urban Redevelopment Authority: Master Plan for 2014 and 2030.
(https://www.ura.gov.sg/uol/).

Table 1.

Land use in Singapore: current (2014) and near-term (2030) periods

Land type	2014		2030	
	Area (km²)	Area (%)	Area (km²)	Area (%)
Coast line	13.84	1.73	13.41	1.61
Commercial use	21.64	2.71	12.28	1.48
Education Institution	6.97	0.87	11.21	1.35
Industry	134.02	16.79	152.82	18.41
Infrastructure	57.37	7.19	58.75	7.08
Open space and recreation	180.08	22.56	189.68	22.85
Reserve site	93.14	11.67	92.74	11.17
Residential	216.01	27.06	214.81	25.87
Special use	44.80	5.61	46.33	5.58
Water body	30.30	3.80	38.24	4.61
Total	798.18	100.00	830.28	100.00

2.2. Overview of the methodology and data

The favorability index for development is a product of the 'City Index′calculated using five indicators and the 'Environmental Capacity of Development', further divided to 'Land Restriction'. The appropriate indicators for 'City Index' determination are selected based on common factors used for the cities development and Singapore Island. These indicators are: 'Social', 'Environmental', 'Industrialization', 'Economic', and 'Naturality'. Each one

reflects the capacity of the development in various sectors and it is easy to be extracted from the land cover or master plan of the city. Thus, the Social Indicator was defined in this study based on residential, educational institution, infrastructure, and special use areas. The 'Environmental Indicator' is composed from reserve sites, open space and recreational areas, water bodies, and coastline areas. Industrialization, Economic, and Naturality (i.e. coastline, water bodies, and open space) indicators are defined as industrial areas, commercial units, and open space respectively. The Economic Indicator could also include other variables (i.e. gross domestic product) which have direct impact for the economy.

In the favorability index for development determination, we applied two correction factors specifically for Singapore. The 'Environmental Capacity of Development' represents a strong development factor and it is composed by reserve sites, coastline, and open space areas. These areas are most available territory for the new built-up and reclamation lands (i.e. coastal zone). The 'Land Restriction for Development' is a weak factor for development and it is composed mainly of areas with very low capacity for development and society wellness. The areas considered for the correction factor were normalized from 0.5 (low impact) to 1 (high impact) following the Gardi et al. (2010) approach. The nil values in this type of normalization were avoided due to the mathematical operations, but also because some land cover designation could be changed into another. Figure 3 shows the general framework of the favorability index determination methodology into the urban areas.

Table 2.
Normalized values of land cover for determination of favorability index for development of Singapore

Land type	Environmental Capacity for Development	Land Restriction for Development
Coast line	0.90	0.50
Commercial use	0.50	0.75
Education Institution	0.50	0.75
Industry	0.50	0.75
Infrastructure	0.50	1.00
Open space and recreation	0.80	0.75
Reserve site	1.00	0.50
Residential	0.50	0.75
Special use	0.50	1.00
Water body	0.50	1.00

The main data used in the paper refers to the master plan of Singapore, published in 2014 and the masterplan projection for year of 2030. The raster maps of master plan, for both periods were collected from the Urban Redevelopment Authority site (https://www.ura.gov.sg/uol/master-plan) and were georeferenced in ArcGIS 10.5 environment. The vector data of the land cover pattern was extracted from the raster grid data and they were divided into 10 classes, as it was proposed in the Master Plan of Singapore. Then, the vector data of land cover for 2014 and 2030 were used to calculate the indicators values, i.e. the 'City Index', the correction factors of 'Environmental Capacity of Development' and 'Land Restriction for Development', and the 'favorability index for development of Singapore'.
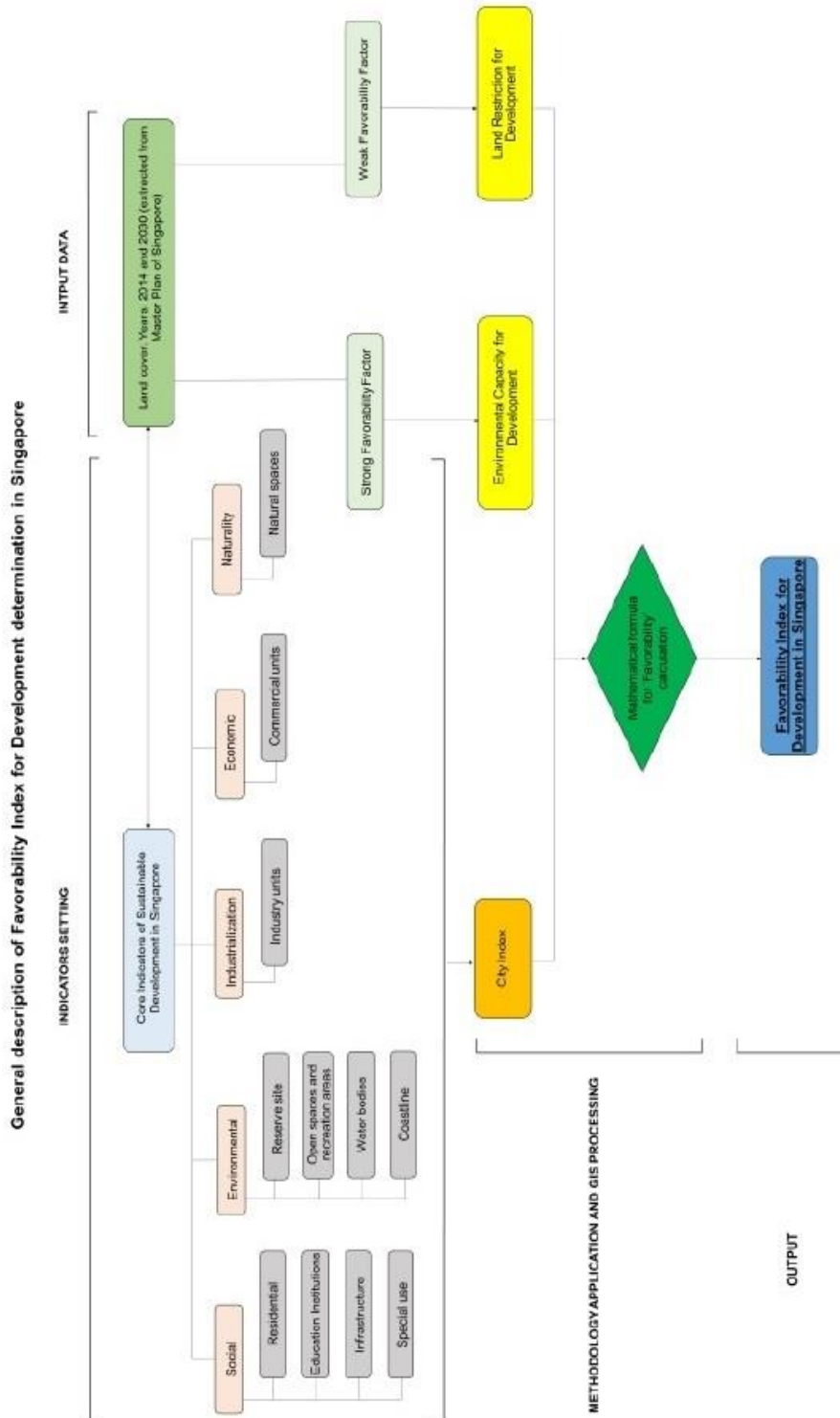
Fig. 3. Schematic diagram showing the methodology.

2.3. Indicators setting and calculation

The five indicators: 'Social', 'Environmental', 'Industrialization', 'Economic', and 'Naturality', were incorporated in Eq. (1) to calculate the 'City Index' of Singapore. The network 1Х1 km was used to create the equal units (cells) over the Singapore territory. The indicators were incorporated in each cell adopting the Gardi et al. (2010) method. They divided the areas of the indicators in every unit to the area of the unit. To incorporate the variation of land use in each province and the complexity of these provinces, the biodiversity index was used in their study. Using the mathematical formula, Gardi et al. (2010) determined the Land Use favorability index for development at regional scale in Emilia-Romagna from Italy. In this study, the formula used by Gardi et al. (2010) was adopted by replacing biodiversity with two correction factors which are more representative for the city development. These two factors are 'Environmental Capacity of Development' and 'Land Restriction for Development' and they were used in the determination of favorability index for development of Singapore (Eq. (2)). The correction factors used in this paper contains normalized values in range from 0.5 (minimum value) to 1 (maximum value) as proposed by Gardi et al. (2010). The minimum and maximum values are determined for types of land cover which represent strong and weak capacity for development in Singapore. Other land cover types were classified accordingly between 0.5 and 1 (**Tab. 2**). Note that the minimum values of 0.5 is not representing the nil influence, but the most unlikely for the index. The moderate influence was set between 0.5 and 1.

$$\text{City Index} = (\text{SocInd} \times 20) + (\text{IndusInd} \times 10 + \text{EcInd} \times 2) + (\text{EnviInd} \times 20) + (\text{NatInd} \times 20) \quad (1)$$

where:
SocInd = Social Indicator
IndusInd = Industrialization Indicator
EcInd = Economic Indicator
EnviInd = Environmental Indicator
NatInd = Naturality Indicator

$$\text{Favorability index for development of Singapore} = \frac{\text{City Index} \times \text{Environmental Capacity of Development}}{\text{Land Restriction for Development}} \quad (2)$$

4. RESULTS

4.1. Core indicators and ʹCity Indexʹ in Singapore

The indicators, ʹCity Indexʹ, correction factors, and favorability index for development of Singaporeʹ were calculated based on the proposed methodology in this study, for years of 2014 and 2030. **Figure 4** illustrates the variations of different indicators over Singapore island. In 2014, the Social indicator indicates high values (above 0.8) in the southern, central, northern and eastern parts of Singapore (**Fig. 4a**), while in 2030, the Social indicator increases slightly in the South and West parts (**Fig. 4b**). In 2014, the results of the Environmental indicator shows maximum values (1) in the West, West-central, and East of Singapore, in Pulau Ubin and Pulau Tekong. In addition, high values could also be identified in the South and South-West near the coastline of Singapore. **Figures 4c** and **4d** depict the Environmental indicator for both periods. Industrialization indicator is more developed in the western and southwestern sides of Singapore including Jurong Island (**Fig. 4e** and **4f**).
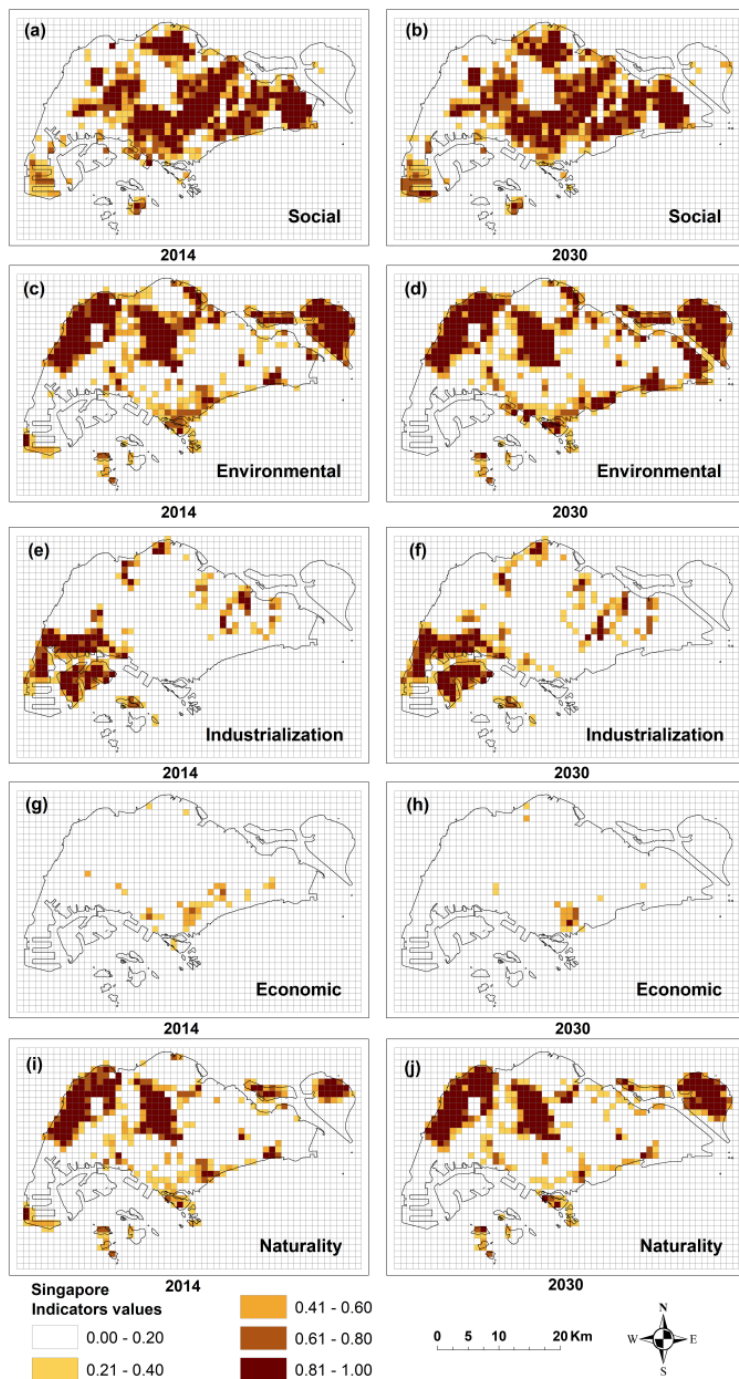
Fig. 4. Spatiality of indicators used into City Index calculation for Singapore.

Few territories with industry activities are present in the East, East-central and North. Between years 2014 and 2030, the increase in the industrialization indicator is observed in the central, northern, western and Jurong Island parts. The Economic indicator is identified in the South of Singapore, while it is very sparsely over South-West, South-East, and North of Singapore. **Figures 4g** and **4h** bring forward the spatial distribution of the Economic indicator in Singapore. Interestingly for the future period, this indicator will increase up to 1 and will be more concentrated in the South of Singapore. An extended territory is defined by 'Naturality' indicator, mainly in the northwestern, central, and southern parts of Singapore. Sentosa, Pulau Ubin and Pulau Tekong register high values (over 0.8) of this indicator in 2014 (**Fig. 4i**) while Tekong Island is expected to be more natural land in 2030 (**Fig. 4j**).

Five indicators are required to calculate the 'City Index'in Singapore. For both periods, the 'City Index' shows a large territory with medium values especially in the residential areas and infrastructure places (**Fig. 5a** and **5b**). The high values were depicted mainly in the natural areas and open spaces, Pulau Ubin and Tekong islands. The low values overlap with the industrial areas and spread more in the West, East, and North of Singapore. In the future period, the highest values of 'City Index' are expected to decrease in the central and southern sides, while in the northwestern and Tekong Island 'City Index' is expected to occupy larger territory.

4.2. Correction factors

Many successful built-up projects can be found in the open space and in the reclamation areas. **Figures 6a** and **6b** show the'Environmental Capacity of Development' correction factor in 2014 and 2030. The lands with low restriction values extend to the North, South, and East on the coastline as well as to the north-eastern islands. Future projection in 2030 indicates major changes in the map with favourable lands are expected to be found on the South and East coastline. The low values of 'Environmental Capacity of Development'can be observed especially in the residential and industrial areas and cover the West, East, East-central and North territory of Singapore for both periods. The maximum values of 'Land Restriction for Development'are sparsely distributed in territory, but mainly occupy few land of North, East and West sides. These territories overlap with the infrastructure, body water, and special use lands. Major part of the Singapore Island has values between 0.5 and 0.75 and only few lands with low restriction are present in the North, South, sparsely in central, and in the Palau Ubin and Tekong islands. **Figures 7a** and **7b** depict the spatial distribution of 'Land Restriction for Development' factor over Singapore.

4.3. Favorability index for development of Singapore

Utilizing'City Index'and two correction factors, the'favorability index for development of Singapore' were calculated for years 2014 and 2030. In 2014, the low and very low favorability was depicted in the southwestern side of Singapore including Jurong Island, in the eastern side, and some parts of South and North of Singapore. These areas corresponded to the field with the industrial lands, residential areas, and infrastructure. The medium favorability index for development of Singapore'is observed sparsely within Singapore island in 2014 (i.e. some territories cab found in the South, central, North-West, and in the North of Pulau Ubin) which overlaps with commercial and open space areas.
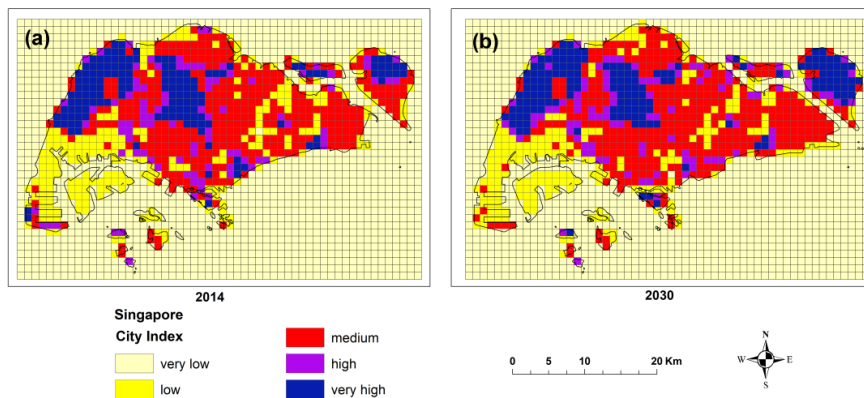
Fig. 5. City Index distribution over Singapore. a. City Index in 2014. b. City Index in 2030.
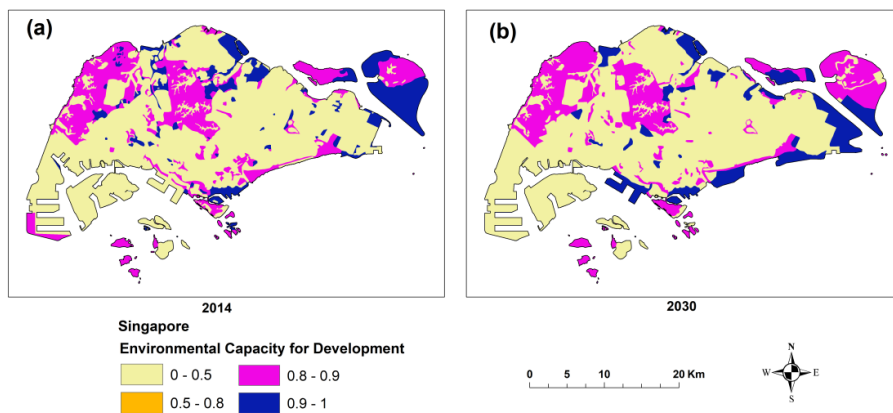
Fig. 6. Environmental Capacity of Development factor over Singapore. a. in 2014. b. in 2030.
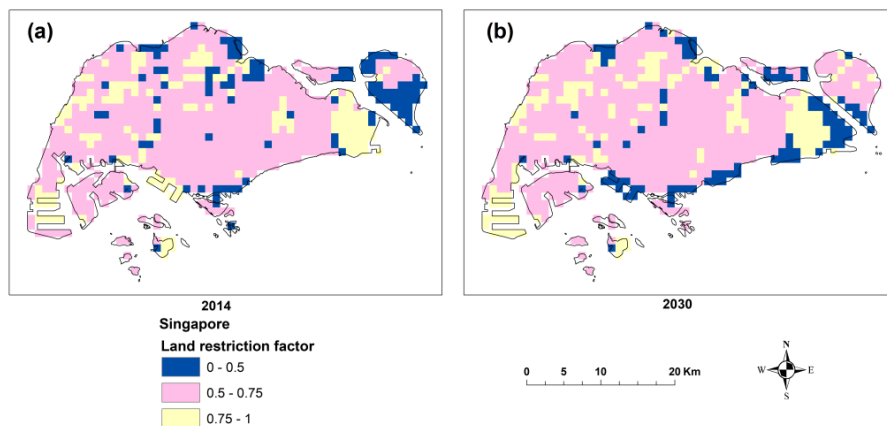
Fig. 7. Land Restriction for Development factor over Singapore. a. in 2014. b. in 2030.

The high and very high ´favorability index for development of Singapore´ were indicated in the West and central sides of the main island with few territories in South, East, and South-West of Singapore. Pulau Ubin and Pulau Tekong are classified under high and very high favourable areas, while the southern islands has land that is classified under very low, low, medium and high favourable areas. **Figures 8a** and **8b** show the favorability index for development of Singapore for the years 2014 and 2030.

In 2030, the favorability index for development Index of Singapore is very low and low in the South-West, East, and few sides in South and North of Singapore. This pattern follows the spatial distribution of favorability index for development of Singapore in 2014. The numbers of areas in medium class decrease whereas the numbers of areas in high and very high classes increase. The medium favourable areas can be observed in the South, West, West-central, and North sides, while the high and very high favourable areas are indicated in the central, West and North-West, and in the South of Singapore. Interestingly, the favourable indexes of Pulau Ubin, Pulau Tekong and the eastern extremity of the Singapore main island are expected to increase due to the reclamation land in 2030. In both periods, the high and very high favourable have direct relationship with the reserve sites, open space and recreation areas.
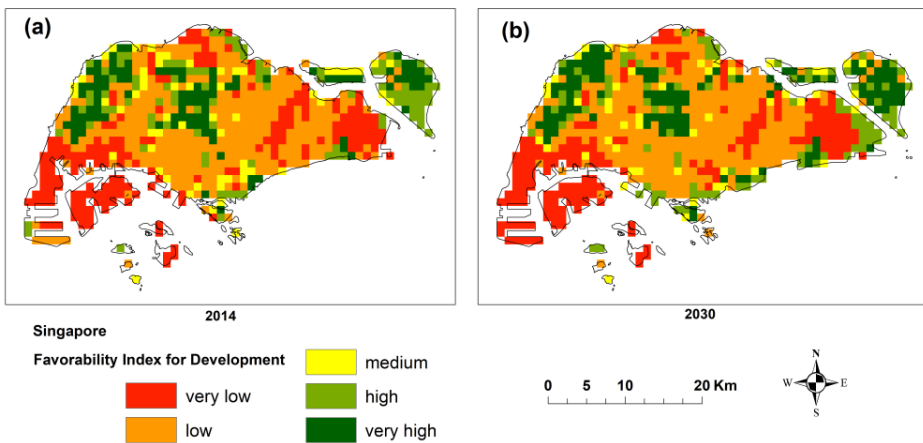
Fig. 8. Favorability index map for development in Singapore. a. in 2014. b. in 2030.

5. DISCUSSION

The main goal of this paper was to propose a methodology to assess the favourable index in the urban areas using the terrain data of land cover and land use. A new method was proposed for the city-state of Singapore considering 'City Index' and two correction factors such as 'Environmental Capacity of Development' and 'Land Restriction for Development'. The methodology was applied for two GIS database for years of 2014 and 2030 to assess the development of Singapore in 2014 and 2030. The spatial distribution of five indicators was served to calculate the 'City Index' over Singapore. The high and very high values of the index overlap to areas which can support the new constructions and development, showing that the open space and reserve sites are the land with high favorability for development in the urban area. In opposite, the industrial zones of the

Singapore have low 'City Index', because these lands cannot support the development of the city from society point of view (i.e. educational and institutions units). In the same time, the airport and harbours areas have low favourable index.

As expected, Pulau Ubin and Pulau Tekong represent the lands with high 'City Index' due to the green spaces and environmental spaces. As Singapore has limited spaces, the non-constructed areas and reserve sites play very important roles in the development of of Singapore. Nistor & Petcu (2014) observed that the ecosystems plays an important role, not only in the natural areas, but also inside the cities. Thus, the harmony of the built-up and parks areas could be inferred to manage the development of the city. The coastline represent in Singapore a strong opportunity and a big challenge for the extension of the city. New reclamation lands are proposed for Singapore to 2030 fact for that the coastal areas constitute a high favorability of development.

The new method has been applied on Singapore territory to assess the favorability for development of the city in two different periods. The proposed procedure combined several comprehensive indicators extracted from land cover in two different times. The analysis included the 'City Index' and two correction factors which refer to the Singapore territory. The selection of indicators and correction factors could be slightly modified from place to place. Based on these analyses, the land with high favorability were identified on the North, West, Pulau Ubin and Pulau Tekong. The approach is a new spatio-temporal method that contributes to specific literature of cities development. Our results represent a useful tool for the urban planning and future strategy at spatial level of Singapore. This study is limited by the weights setting and the combination of layer although this doesn't affect too much in the final analysis.

6. CONCLUSIONS

Based on the land cover data for 2014 and 2030, the 'favorability index for development of Singapore' was calculated. Five indicators mostly used for the cities development assessment have been analysed in the present study at spatial scale of Singapore to carry out the 'City Index'. This index combined with two correction factors contributed to the final calculation of the favorability index for development of Singapore. In 2014, it was observed that the central, North-West, Pulau Ubin and Pulau Tekong Island sides of Singapore shows a high and very high favorability. In 2030, the eastern side and the southeastern coastline parts show an important switch in the favorability for development increase due to the new reclamation lands.

Even if the procedure is complex and requires several calculations, the method presented here reflects an appropriate way in which the cities development should be calculated. Moreover, with slightly modifications, the method that we proposed here could be easily adapted to other study cases.

The results of the present paper bring forward the relationship of the land cover of the Singapore city-state and various indicators used in the favorability for development. Normally, in the large cities the open areas and non-constructed land may constitute an advantage for the urban area development while the infrastructure and industrial areas are more rigid and supply only the internal connections, workforce. In case of Singapore, the reserve sites and coastal areas represent two strong development factors due to the terrain availability for development capacity, new reclamation land and maybe for new residences. The Pulau Ubin and Pulau Tekong, which are closer to the main island and also the largest

of Singapore territory, may be connected to the main land and could represent a significant pole for future development: new traditional neighbourhoods, research centres.

This study contributes to the scientific methodology, which evaluate the favourable indicators at spatial scale and proposes a procedure to integrate the strong and weak factor and calculate the favorability index for development of Singapore. Moreover, the maps and provided details represent a tool for urban planning and management strategy for Singapore. Future investigations could be drawn on particular sites of Singapore and an interactive favorability model could be proposed in ArcGIS as a new tool.

REFERENCES

Ayrama, C.A.C., Mendoza, M.E., Etter, A. & Salicrup, D.R.P. (2017) Anthropogenic impact on habitat connectivity: A multidimensionalhuman footprint index evaluated in a highly biodiverse landscape of Mexico. *Ecological Indicators,* 72, 895–909.

Beguin, H. (1992) Christaller's central place postulates. *A Comentary. Ann. Reg. Sci.*, 26, 209-229.

Christaller, W. (1933) *Die zentralen Orte in Süddeutschland*. Fischer, Jena.

Christaller, W. (1966) *Central places in Southern Germany*. Prentice-Hall, Englewood Cliffs.

Dong, P., Wang, C. & Ding, J. (2013) Estimating glacier volume loss used remotely sensed images, digital elevation data, and GIS modelling. *International Journal of Remote Sensing,* 34(24), 8881–8892.

Elfarrak, H., Hakdaoui, M. & Fikri, A. (2014) Development of Vulnerability through the DRASTIC Method and Geographic Information System (GIS) (Case Groundwater of Berrchid), Morocco. *Journal of Geographic Information System,* 6, 45–58.

Figura, S., Livingstone, D.M., Hoehn, E. & Kipfer, R. (2011) Regime shift in groundwater temperature triggered by the Arctic Oscillation. *Geophysical Research Letters,* 38(L23401), 1–5.

Gardi, C., Bosco, C., Rusco, E. & Montanerella, L. (2010) An analysis of the Land Use Sustainability Index (LUSI) at territorial scale based on Corine Land Cover. *Management of Environmental Quality: An International Journal,* 21(5), 680-694.

Haldorsen, S., Heim, M. & van der Ploeg, M. (2012) *Impacts of Climate Change on Groundwater in Permafrost Areas - Case Study from Svalbard, Norway*. pp. 323–340. In: Treidel, H., Martin-Bordes, J.J., Gurdak, J.J. (Eds.), Climate Change Effects on Groundwater Resources: A Global Synthesis of Findings and Recommendations. International Association of Hydrogeologists (IAH). International Contributions to Hydrogeology. Taylor & Francis Publishing, pp. 414.

Haeberli, W.R., Frauenfelder, R., Hoelzle, M. & Maisch, M. (1999) On rates and acceleration trends of global glacier mass changes. *Geografiska Annaler, Series A, Physical Geography,* 81A, 585–595.

Holden, M. (2006) Urban indicators and the integrative ideals of cities. *Cities,* 23(3), 170–183.

IPCC. (2001) *Climate change 2001: the scientific basis.* In: Houghton, J.T., Ding, Y., Griggs, D.J., Noguer, M., van der Linden, P.J., Dai, X. (Eds), Contribution of Working Group I to the Third Assessment Report of the Intergovernmental Panel on Climate Change. Cambridge University Press: Cambridge and New York, New York, pp. 881.

Kargel, J.S., Abrams, M.J., Bishop, M.P., Bush, A., Hamilton, G., Jiskoot, H., Kääb, A., Kieffer, H.H., Lee, E.M., Paul, F., Rau, F., Raup, B., Shroder, J.F., Soltesz, D., Stainforth, S., Stearns, L. & Wessels, R. (2005) Multispectral imaging contributions to global land ice measurements from space. *Remote Sensing of Environment,* 99(1), 187–219.

Kløve, B., Ala-Aho, P., Okkonen, J. & Rossi, P. (2012) *Possible Effects of Climate Change on Hydrogeological Systems: Results From Research on Esker Aquifers in Northern Finland*, pp. 305–322. In: Treidel, H., Martin-Bordes, J.J., Gurdak, J.J. (Eds.), Climate Change Effects on Groundwater Resources: A Global Synthesis of Findings and Recommendations. International

Association of Hydrogeologists (IAH). International Contributions to Hydrogeology. Taylor & Francis Publishing, pp. 414.

Kløve, B., Ala-Aho, P., Bertrand, G., Gurdak, J.J., Kupfersberger, H., Kværner, J., Muotka, T., Mykrä, H., Preda, E., Rossi, P., Bertacchi Uvo, C., Velasco, C. & Pulido-Velazquez, M. (2014) Climate change impacts on groundwater and dependent ecosystems. *Journal of Hydrology,* 518, 250–266.

Labuschagnea, C., Brenta, A.C., Ron, P.G. & Van Ercka, P.G. (2005) Assessing the sustainability performances of industries. *Journal of Cleaner Production*, 13, 373–385.

Nistor, M.M. & Petcu, I.M. (2014) The role of glaciers in the evolution of Prince William Sound landscape ecosystems, Alaska. *STUDIA UBB AMBIENTUM*, LIX(1-2), 97-109.

Nistor, M.M. & Petcu, M.I. (2015) Quantitative analysis of glaciers changes from Passage Canal based on GIS and satellite images, South Alaska. *Applied Ecology and Environmental Research,* 13(2), 535–549.

Oerlemans, J. (2005) Extracting a Climate Signal from 169 Glacier Records. *Science,* 308, 675–677.

Sands, G.R. & Podmorea, T.H. (2000) A generalized environmental sustainability index for agricultural systems. *Agriculture, Ecosystems and Environment,* 79, 29–41.

Shahgedanova, M., Stokes, C.R., Gurney, S.D. & Popovnin, V. (2005) Interactions between mass balance, atmospheric circulation, and recent climate change on the Djankuat Glacier, Caucasus Mountains, Russia. *Journal of Geophysical Research,* 110(D16107), 1–12.

Shaver, G.R., Canadell, J., Chapin III, F.S., Gurevitch, J., Harte, J., Henry, G. et al. (2000) Global warming and terrestrial ecosystems: a conceptual framework for analysis. *BioScience,* 50(10), 871–882.

Singh, R.K., Murty, H.R., Gupta, S.K. & Dikshit, A.K. (2012) An overview of sustainability assessment methodologies. *Ecological Indicators,* 15, 81–299.

Stavig, L., Collins, L., Hager, C., Herring, M., Brown, E. & Locklar, E. (2005) The effects of climate change on Cordova, Alaska on the Prince William Sound. Alaska Tsunami Papers, The National Ocean Sciences Bowl. https://seagrant.uaf.edu/nosb/papers/2005/cordova-nurds.html (accessed 23 April 2014).

Stocks, B.J., Fosberg, M.A., Lynham, T.J., Mearns, L., Wotton, B.M., Yang, Q., et al. (1998) Climate change and forest fire potential in Russian and Canadian boreal forests. *Clim. Change,* 38, 1–13.

Taylor, C.A. & Stefan, H.G. (2009) Shallow groundwater temperature response to climate change and urbanization. *Journal of Hydrology,* 375(3–4), 601–612.

The Canadian Centre for Climate Modelling and Analysis. (2014) The first generation coupled global climate model publishing web. URL: http://www.ec.gc.ca/ccmac-cccma/default.asp?lang=En&n=540909E4-1 (accessed 20 March 2015).

Urban Redevelopment Authority. (2017) Plans and Maps. URL: https://www.ura.gov.sg/uol/master-plan. (accessed on June 10, 2017)

Xie, X., Li, Y.X., Li, R., Zhang, Y., Huo, Y., Bao, Y., & Shen, S. (2013) Hyperspectral characteristics and growth monitoring of rice (Oryza sativa) under asymmetric warming. *International Journal of Remote Sensing*, 34(23), 8449–8462.

AN INVESTIGATION OF DROUGHT AROUND CHI WATERSHED DURING TEN-YEAR PERIOD USING TERRA/MODIS DATA

Tanutdech ROTJANAKUSOL[1], Teerawong LAOSUWAN[2] *

ABSTRACT:
To examine the drought affected area is highly challenging because the drought is a natural disaster that starts and expands slowly. The severity of the drought is different when the rainfall is imbalance in the area. The objective of this study was to analyze the drought around Chi watershed with total area of 49,131.920 km^2 by using data from Terra/MODIS satellite during 10 years (2007-2016). On part of method operation, the NDVI data was obtained from Terra/MODIS satellite, and VCI (Vegetation Condition Index) analysis was performed to examine the condition of plants which could identify the condition of drought in the area. According to the study, it was found that in 2015, it was the time when the drought affected area was at most which was equal to 91.54 percent, or 44975.23 km^2. When the analysis results of these ten years were brought to find relationship with rainfall, it was found that the decision coefficient was $R^2 = 0.913$. It can be concluded from the results of this study that VCI could be used as indicator and could identify the drought in Chi watershed in terms of area and time reasonably.

Key-words: *Drought, Remote Sensing, Chi Watershed, NDVI, VCI*

1. INTRODUCTION

Drought is one of the top disasters of Thailand that cause considerable damage especially against the agriculture and cultivation due to the geography and weather that are risk factors of drought (Gomasathit rt al., 2015; Laosuwan et al., 2016). The Chi watershed, located at the northeastern region of Thailand, has been affected by drought for a very long period of time; this is considered as one major problem which is mainly caused by rainfall and other related factors including the absorption of soil, the water source on the ground, the water source under the ground, and the use of land (Uttaruk & Laosuwan, 2017). The drought is caused by an absence of rain during rainy season during June to July. According to the analysis into the pattern of rain in terms of area and time, it was found that an absence of rain also happens after September as well, especially in Chi watershed which is highly affected by drought since it is the area where the southwestern monsoon could not reach to; also, if there is no tropical hurricane moving through in a certain year, there would be more severe drought (Rotjanakusol & Laosuwan, 2018). The consequence from drought was a lack of consumable water to be used in various activities, especially in agriculture which is the main career of the people living around Chi watershed; also, it would have an impact on people's consumption. Therefore, a lack of water would severely affect the

---

[1,2] Department of Physics, Faculty of Science, Mahasarakham University, Khamriang Sub-District, Kantarawichai District, Maha Sarakham, 44150,Thailand, tanutdech.r@msu.ac.th, teerawong@msu.ac.th, *Corresponding author

cultivation – it decreases the agricultural plants thus leading to economic, social, and environmental problems (Bordi & Fraedrich, 2009; Wang et al.,2014).

The study to try to understand the characteristics of drought therefore becomes vital, and must be done for the benefit in providing advance precaution to those concerned, and there would be a plan to solve the problems (Fensham & Holman, 1999; Gebrehiwot et al., 2011). In analyzing the drought, a wide variety of data are used including rainfall, moisture of the soil, the evaporation of water. Often, there is no comprehensive data for the whole area that would affect the quality of the analysis result in a particular area (Lines et al., 2017). The data obtained from satellite thus is used to analyze the drought since it is the source of data that can store data continuously, covering the vast area and could be used to identify the location also (Furtuna & Holobaca, 2013; Chang et al., 2018; Nistor et al., 2018; Son et al., 2018; Canedo-Rosso et al., 2019). The word "drought" has no universal clear definition; it is just the period of time when the climate is dried and affects the change of plants and moisture in soil. The growth of plants is the direct key indicator for the analysis of drought (Tucke, 1979; Wang et al., 2003; Dutta et al., 2015; Jiao et al., 2016; Rimkus et al., 2017). With such reasons, the objective of this study, consequently, focuses on the analysis of drought and the assessment for drought in Chi watershed by using data from Terra/MODIS satellite during 10 years (2007-2016).

2. AREAS AND DATA

2.1 Study area

The Chi watershed is located at the northeastern region of Thailand (**Fig.1**); it is located between the 15° 30' north latitude to 17° 30' north latitude, and is between the 101°30' east longitude to 104° 30' longitude, with total area of 49,131.920 km^2, with average temperature in the whole year of 26.9 °C, with maximum temperature in April of 35.9 °C, and minimum temperature in December of 16.9 °C, with annual average rainfall of 1,231 mm.
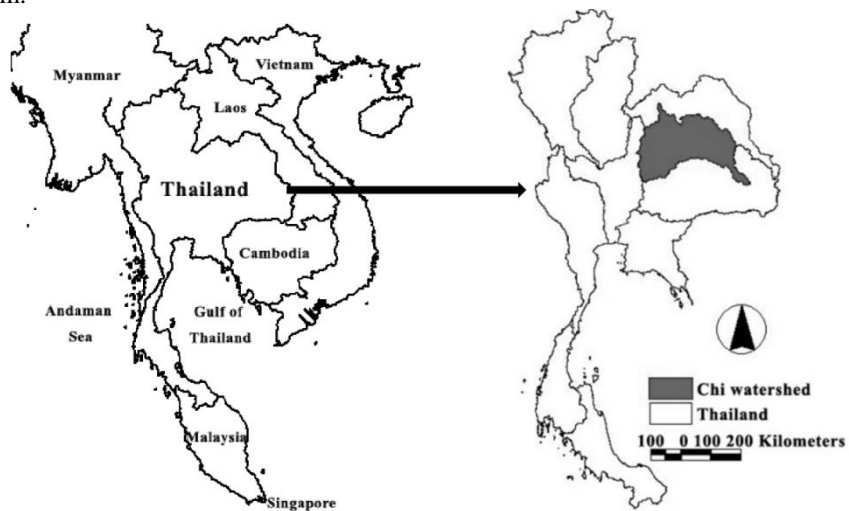
Fig. 1. Study area.

2.2 Data

2.2.1 Satellite data

Terra/MODIS satellite was designed to be used in exploring and monitoring natural resources data on earth, with the width of swath of about 2,330 km^2, with spatial resolution ranging from 250 m to 1000 m, with data recording system of 36 wavelengths (Xiong et al., 2009). Therefore, data from Terra/ MODIS satellite are appropriate in monitoring change in vast area like Chi watershed. In this study, MOD13Q1 product dataset (**Tab. 1**) was collected in vegetation indices from Terra/MODIS satellite during Augusts of 2007 to 2016 (10 years); subsequently, the geometric correction was done by adjusting the reference coordinates to be in WGS84-UTM zone 48 N system; the pixels were assessed by nearest neighbor method, and data from Terra/MODIS satellite were subset by using boundary line of Chi watershed.

Table 1.

Characteristics of MOD13Q1.

Characteristic	Description
Temporal Granularity	16-Day
Temporal Extent	February 2000 - Present
Spatial Extent	Global
Coordinate System	Sinusoidal
Geographic Dimensions	1200 km x 1200 km
Pixel Size	250 m
SDS Name	NDVI

2.2.2 Rainfall data

In this study, monthly rainfall data measured from ground rainfall measuring stations located in Chi watershed of Thai Meteorological Department (TMD) were collected. These monthly rainfall data would be used in finding the statistical relationship with analysis results from Terra/MODIS satellite data further.

3. METHODOLOGY

In this study, the procedures in analyzing data were determined as shown in **Fig. 2**, with details of operation as follows:
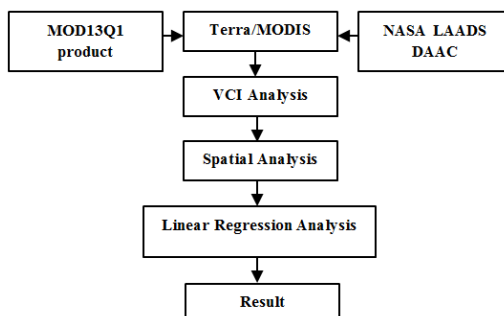
Fig.2. Implementation procedures.

3.1 Vegetation Condition Index (VCI) Analysis

Since VCI is the value developed from NDVI, in the study the data from Terra/MODIS of 16 days and MOD13Q1 product set were used. Data used from this product was NDVI indices which are beneficial indicators and are widely used in the inspection of plant changes. NDVI is the calculation from ratio between difference and sum total of reflection of Red wavelength and NIR wavelength of objects on earth. NDVI of between -1 to +1 would be obtained from the calculation. In the area covered by plants, the reflective value in NIR wavelength would be higher than that in Red wavelength, thus making the NDVI value to be positive, whereas the soil surface, the open area, and the construction area would have similar reflective value between these two wavelengths thus making NDVI value to approach near zero (Park et al., 2008; Rotjanakusol & Laosuwan, 2019). In the case of water surface, the reflective value in NIR wavelength would be lower than Red wavelength thus making NDVI value to be negative (Thavorntam et al., 2015). The method in calculating NDVI is shown in Equation 1. For VCI, it would be the adjustment of NDVI to be brighter by using maximum and minimum values of NDVI to be used in the calculation where the VCI value would vary between 0 to 100; this would be related to the change of plant condition from the least to the most value. VCI can be shown as in Equation 2.

$$NDVI = \frac{NIR - RED}{NIR + RED} \tag{1}$$

Where;
NIR = Near Infrared Band
RED = Red band

$$VCI = \frac{NDVI - NDVI_{min}}{NDVI_{max} - NDVI_{min}} \times 100 \tag{2}$$

Where;
$NDVI_{max}$ = Maximum NDVI at study time of each pixel
$NDVI_{min}$ = Minimum NDVI at study time of each pixel.

3.2 Spatial analysis

The spatial analysis of drought is the classification of levels of plants conditions during Augusts of each year (2007-2016). In this study, the VCI drought levels were divided into 5 levels (**Tab. 2**) with 0-20 score meaning the worst condition of plants (very high drought) to 80-100 score meaning best condition of plants (very low drought).

Table 2.

VCI drought levels.

Level	VCI
00.00-20.00	very high drought
21.00-40.00	high drought
41.00-60.00	moderate drought
61.00-80.00	low drought
81.00-100.00	very low drought

3.3 Analysis of relationship between VCI and rainfall

The analysis of relationship between VCI and rainfall is divided into 2 forms including 1) the analysis into statistical relationship – the VCI analysis result from Item 3.2 and rainfall data collected from TMD would be used to find statistical relationship in form of Linear Regression Analysis, 2) the analysis of change in terms of time by comparing data between VCI and rainfall during Augusts of each year (2007-1016).

4. RESULTS AND DISCUSSIONS

4.1 VCI analysis result

As mentioned above, VCI value is the value developed from NDVI. The result of NDVI analysis obtained from Terra/MODIS satellite (MOD13Q1) can be shown in **Fig.3**. For the NDVI analysis, it can be concluded that the maximum, the minimum, the means, and the standard deviation of NDVI during Augusts of each year (2007-2016) in each period of time reveal the different conditions of plants; the NDVI means could identify the condition of plants or drought in each year. According to the NDVI analysis result, it was found that the minimum means was 0.196 in 2015 and the maximum means was 0.314 in 2013.
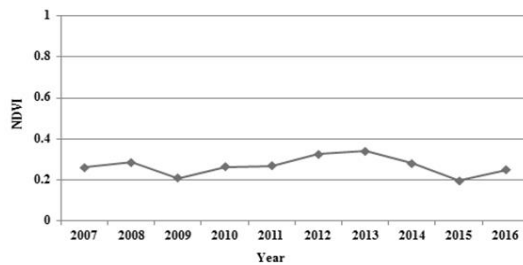
Fig.3. NDVI result.

For the VCI analysis result, it was found that the means could identify the condition of plants or drought during Augusts of each year with minimum means of 24.015 in 2015 and maximum means of 91.635 in 2013. The VCI means data in 10 years can be concluded in **Fig. 4**, with graph showing the variance of VCI in each year, depending on the condition of plants and rainfall.
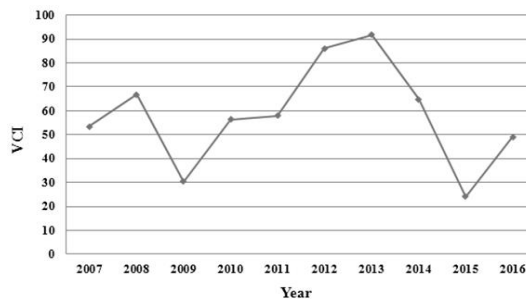
Fig.4. VCI result.

4.2 Spatial analysis result

The spatial analysis result during Augusts of each year reveal the different conditions of plants of 0 – 100 scores; such scores is consistent with the theory, where the means can identify the condition of plants or drought in each year. The spatial analysis result in this study can be shown in **Fig. 5**.
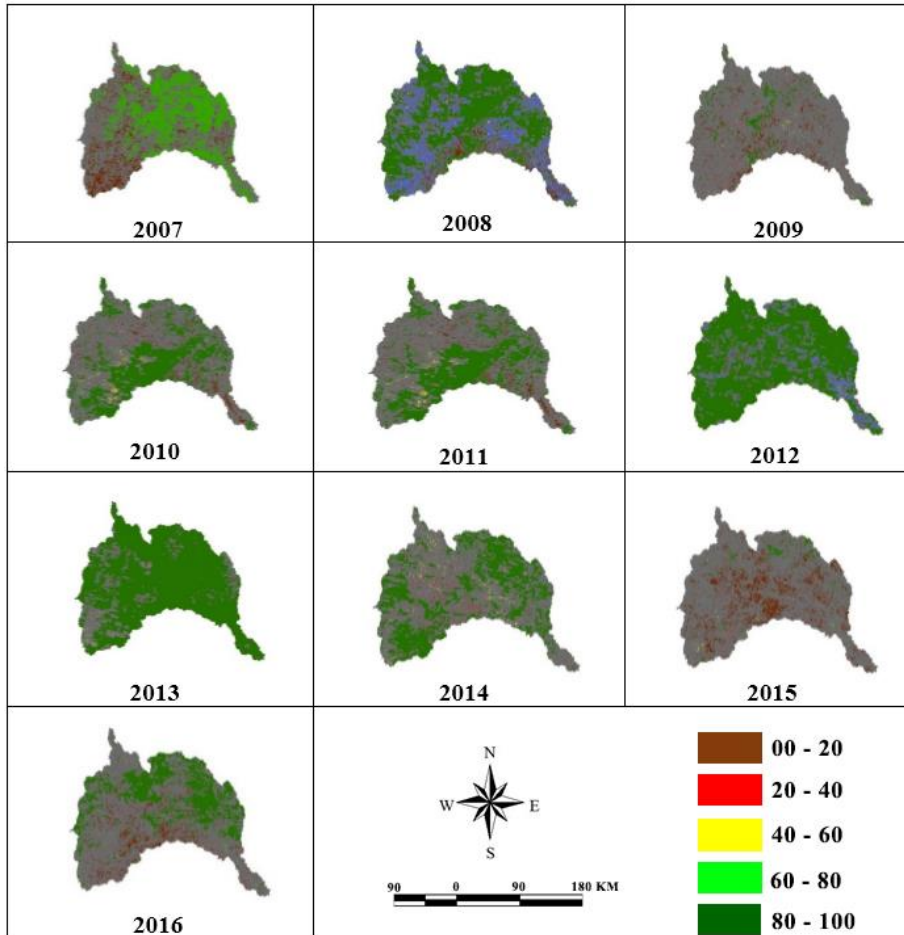
Fig.5. Spatial analysis.

According to **Fig. 5**, it was found that in the area in Chi watershed in northeastern region of Thailand in 2007, 2008, 2010, 2011, 2014, and 2016, the condition of plants was at moderate level, signifying that during such period, the Chi watershed was moderately affected by drought. In 2009 the condition of plants was low and was lowest in 2015, signifying that the drought was at much and most level, respectively. And in 2012, there condition of plants was high and highest in 2013, pointing out that the drought was little and least respectively. Besides, the researcher had brought the VCI spatial analysis result to perform analysis in percentage of drought as shown in **Fig. 6**.
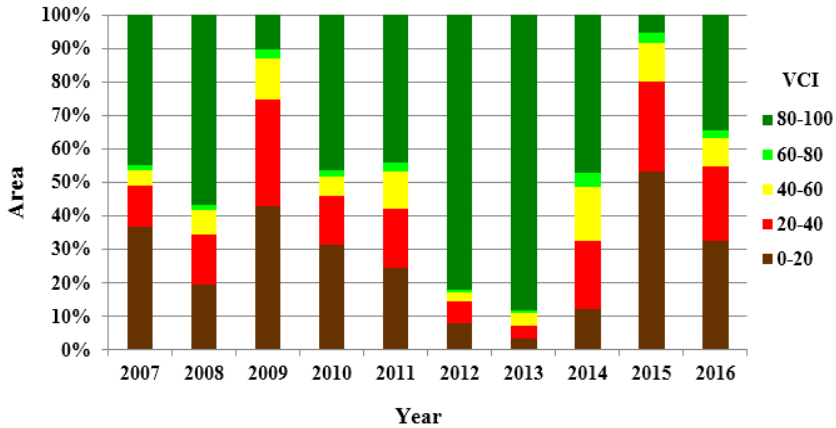
Fig.6. Percentage of drought.

According to **Fig.6**, it was found that in 2015 the drought was most level, with the level of very low drought of 53.303 percent or equal to 26,188.794 km², and the drought of low level equal to 26.983 percent or the area of 13,257.251 km², and the moderate drought equal to 11.254 percent or the area of 5529.187 km², reflecting the clear condition of drought of Chi watershed.

4.3 Result of analysis of relationship between VCI and rainfall Spatial analysis result

4.3.1. Analysis result of statistical relationship

The analysis result of relationship between VCI (independent variable) and rainfall (dependent variable) during Augusts of each year (2007-2016) was found that the change of VCI is consistent with the rainfall; the analysis result of relationship is shown in **Fig. 7**. From the **Fig. 7**, the result of analysis into the relationship between VCI and the rainfall lead to the equation of y = 0.1839x+186.64, and with decision of coefficient of R^2 = 0.913; the coefficient is near 1, showing that the relationship is of high level. It can be explained that if in August of any year, the VCI is of high level, then the rainfall measured would be of high level accordingly; on the contrary, if VCI is little, the rainfall measured would be little accordingly as well.
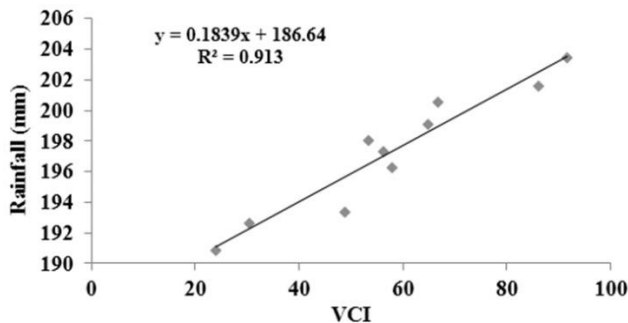
Fig.7. Relationship between VCI and the rainfall.

4.3.2 Analysis results of change in terms of time

The result of analysis into change in yearly term of VCI and rainfall in this study was that the change in terms of time of VCI means was consistent with the rainfall; however, the change of VCI may be changed more slowly than that of the rainfall since the plants were developed after there was sufficient amount of water for the growth. The change of VCI and the rainfall in 2015 would be lowest, and in was found that in 2013, the VCI and the rainfall was highest; the result of analysis of change on yearly basis of VCI and the rainfall is shown in **Fig. 8**.
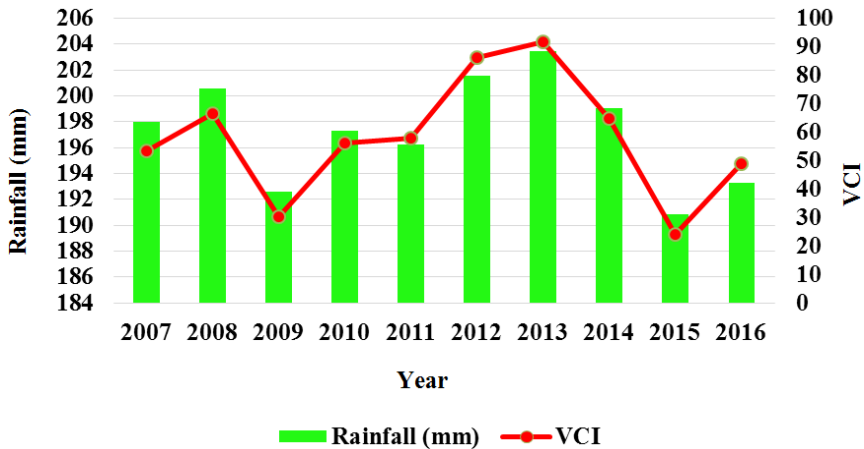
Fig. 8. The result of analysis into change in yearly term of VCI and rainfall.

5. CONCLUSIONS

The drought in Thailand directly affects the agriculture and water source since Thailand is the country where the people do farming especially growing rice; also, Thailand is considered as one of the largest field of rice production in the world. Mostly, the drought in Chi watershed that directly affects agriculture occurs in rainy season where the rainfall is absent for an extended period of time. In this study, the focus was on drought and the assessment for drought in Chi watershed by using data from Terra/MODIS satellite during Augusts in 10 years (2007-2016). The reason why it is such period of time is that under the calendar, the main agricultural cultivation of Thailand such as rice (wet season rice), oily plant (soybean, green bean and peanut), field plant (corn for feeding animals), would grow with fully green leave (The Department of Agricultural Extension, 2017); if in such month of any year, the agricultural plants grow with many green leaves compared with all area, it would mean that the drought is little, on the contrary, if the agricultural plants grow with just a few green leaves compared with all area, it would mean that the drought is of much level. In this study, it was found from the study that in 2015, it was the time when drought was at most level equal to 91.54 or equal to 44975.23 km^2. When the results of the study were used to compare with other similar researches such as research on "Application of remote sensing technology for drought monitoring in Mahasarakham Province, Thailand" by Laosuwan et al., (2016), research on "Drought Detection by Application of Remote Sensing Technology and Vegetation Phenology" by Uttaruk & Laosuwan, (2017), research

on "Remote Sensing Based Drought Monitoring In The Middle-Part of Northeast Region of Thailand" by Rotjanakusol & Laosuwan, (2018), research on "Surface Moisture and Vegetation Cover Analysis for Drought Monitoring in the Southern Kruger National Park Using Sentinel-1, Sentinel-2, and Landsat-8" by Urban et al., (2018), it was found that 4 researches had the analysis results in the same direction with that of this study. The result of this study can be used as criteria in making reasonable decision on the Chi watershed area affected by drought, and also can be used to assess the drought area rapidly and reliably. The concerned agencies can apply this method in analyzing the drought area and can apply the result to prepare for plan in preventing and alleviating the drought sustainably in other areas of Thailand further.

R E F E R E N C E S

Bordi, I., Fraedrich, K., & Sutera, A. (2009). Observed drought and wetness trends in Europe: An update. *Hydrology and Earth System Sciences,* 6(3), 3891-3915. Doi:10.5194/hessd-6-3891-2009

Canedo-Rosso, C., Hochrainer-Stigler, S., Pflug, G., Condori, B., & Berndtsson, R. (2019). Drought risk in the Bolivian Altiplano associated with El NiñoSouthern Oscillation using satellite imagery data. *Natural Hazards and Earth System Sciences*, 1-21. Doi:10.5194/nhess-2018-403

Chang, S., Wu, B., Yan, N., Zhu, J., Wen, Q., & Xu, F. (2018). A Refined Crop Drought Monitoring Method Based on the Chinese GF-1 Wide Field View Data. *Sensors*, 18(4), 1297. Doi:10.3390/s18041297

Dutta, D., Kundu, A., Patel, N., Saha, S., & Siddiqui, A. (2015). Assessment of agricultural drought in Rajasthan (India) using remote sensing derived Vegetation Condition Index (VCI) and Standardized Precipitation Index (SPI). *The Egyptian Journal of Remote Sensing and Space Science,* 18(1), 53-63. Doi: 10.1016/j.ejrs.2015.03.006

Fensham, R., & Holman, J. (1999). Temporal and spatial patterns in drought-related tree dieback in Australian savanna. *Journal of Applied Ecology*, 36(6), 1035-1050. Doi:10.1046/j.1365-2664.1999.00460.x

Furtuna, P. & Holobaca, I. (2013). Forest fires study using remote sensing and meteorological indicators. Case study. *Geographia Technica*, 8(2), 23-37.

Gebrehiwot, T., Veen, A. V., & Maathuis, B. (2011). Spatial and temporal assessment of drought in the Northern highlands of Ethiopia. *International Journal of Applied Earth Observation and Geoinformation*, 13(3), 309-321. Doi: 10.1016/j.jag.2010.12.002

Gomasathit T., Laosuwan T., Sangpradit S., & Rotjanakusol T. (2015). Assessment of Drought Risk Area in Thung Kula Rong Hai using Geographic Information Systems and Analytical Hierarchy Process. *International Journal of Geoinformatics*, 11(2), 21-27.

Jiao, W., Zhang, L., Chang, Q., Fu, D., Cen, Y., & Tong, Q. (2016). Evaluating an Enhanced Vegetation Condition Index (VCI) Based on VIUPD for Drought Monitoring in the Continental United States. *Remote Sensing*, 8(3), 224. Doi:10.3390/rs8030224

Laosuwan, T., Sangpradid, S., Gomasathit, T., & Rotjanakusol, T. (2016). Application of Remote Sensing Technology for Drought Monitoring in Mahasarakham Province, Thailand. *International Journal of Geoinformatics*, 12(3), 17-25.

Lines, D., Werner, M., & Bastiaanssen, W. (2017). The predictability of reported drought events and impacts in the Ebro Basin using six different remote sensing data sets. *Hydrol. Earth Syst. Sci.*, 21, 4747-4765. Doi: 10.5194/hess-21-4747-2017

Nistor, M.M., Man, T.C, Benzaghta, M.A., Nedumpallile Vasu, N., DezsiI, Ş. & Kizza, R. (2018). Land Cover and Temperature Implications for the Seasonal Evapotranspiration in Europe. *Geographia Technica*, 13(1), 85-108. DOI: 10.21163/GT_2018.131.09

Park, J., Kim, K., & Choi, Y. (2008). Application of Vegetation Condition Index and Standardized Vegetation Index for Assessment of Spring Drought in South Korea. *IGARSS 2008 - 2008 IEEE International Geoscience and Remote Sensing Symposium*. Doi:10.1109/igarss.2008.4779463

Rimkus, E., Stonevicius, E., Kilpys, J., Maciulytė, V., & Valiukas, D. (2017). Drought identification in the Eastern Baltic region using NDVI. *Earth System Dynamics*, 8, 627-637. Doi: 10.5194/esd-8-627-2017

Rotjanakusol, T. & Laosuwan, T. (2018). Remote Sensing Based Drought Monitoring In The Middle-Part of Northeast Region of Thailand. *Studia Universitatis Vasile Goldis Arad, Seria Stiintele Vietii*, 28(1), 14-21.

Rotjanakusol, T., & Laosuwan, T. (2019). Drought Evaluation with NDVI-Based Standardized Vegetation Index in Lower Northeastern Region of Thailand. *Geographia Technica*, 14(1), 118-130. Doi:10.21163/GT_2019.141.09

Son, N. T., Chen, C. F., Chen, C. R., Masferrer, M. G., & Recinos, L. E. (2018). Multitemporal Landsat-MODIS fusion for cropland drought monitoring in El Salvador. *Geocarto International*, 1-21. Doi:10.1080/10106049.2018.1489421

Thavorntam, W., Tantemsapya, N., & Armstrong, L. (2015). A combination of meteorological and satellite-based drought indices in a better drought assessment and forecasting in Northeast Thailand. *Natural Hazards*, 77(3), 1453-1474. Doi:10.1007/s1106 9-014-1501-0

The Department of Agricultural Extension. (2017). *Crop Calendar Thailand*. Available at http://www.servicelink.doae.go.th/webpage/book%20PDF/rice/tmie_ rice.pdf. (Accessed on 2 October 2017).

Tucker, C. J. (1979). Red and photographic infrared linear combinations for monitoring vegetation. *Remote Sensing of Environment*, 8(2), 127-150. Doi:10.1016/0034-4257(79)900 13-0

Urban, M., Berger, C., Mudau, T., Heckel, K., Truckenbrodt, J., Odipo, V. O., Smit, I., Schmullius, C. (2018). Surface Moisture and Vegetation Cover Analysis for Drought Monitoring in the Southern Kruger National Park Using Sentinel-1, Sentinel-2, and Landsat-8. *Remote Sensing*, 10(9), 1482. Doi:10.3390/rs10091482

Uttaruk, Y., & Laosuwan, T. (2017). Drought Detection by Application of Remote Sensing Technology and Vegetation Phenology. *Journal of Ecological Engineering*, 18(6), 115-121. Doi:10.12911/22998993/76326

Wang, J., Rich, P. M., & Price, K. P. (2003). Temporal responses of NDVI to precipitation and temperature in the central Great Plains, USA. *International Journal of Remote Sensing*, 24(11), 2345-2364. Doi:10.1080/014311602101 54812

Wang, H., Lin, H., & Liu, D. (2014). Remotely sensed drought index and its responses to meteorological drought in Southwest China. *Remote Sensing Letters*, 5(5), 413-422. Doi:10.10 80/2150704x.2014.912768

Xiong, X., Wenny, B., & Barnes, W. (2009). Overview of NASA Earth Observing Systems Terra and Aqua moderate resolution imaging spectroradiometer instrument calibration algorithms and on-orbit performance. *J. of Applied Remote Sensing*, 3(1), 032501. Doi: 10.1117/1.3180864

DEVELOPMENT OF THE RURAL LANDSCAPE: THE DAČICE REGION CASE STUDY, CZECHIA

Jiří SCHNEIDER[1], Aleš RUDA[1], Michaela VENZLŮ[2]

ABSTRACT:
The traditional agricultural landscape of the Czech Republic, with the advent of the Industrial Revolution, began to change slowly into an urban and industrial landscape. However, the biggest changes in the landscape character occurred in the period of world wars, in the post-war period and finally in the transformation of the economy after 1990. The importance of agricultural production in the Czech Republic is decreasing. However, in some rural areas, its position is still a tradition. The aim of the paper is to evaluate changes in the development of land use in the cadastral areas of the Dačice region in 1845, 1948, 2001 and 2014. Land use records were provided by the Czech Office for Surveying, Mapping and Cadastre and Cadastral Office in Dačice. Previous land use categories were regrouped into seven specific categories according to classification in 2014 - arable land, gardens, permanent grassland, forests, water bodies, built-up areas, and other areas and for each category, the proportional changes were computed, explained and visualized. During the monitored period, a loss of arable land in the area was found, which is gradually grassed. The area of coniferous forests is further expanding during. From the urban point of view, there is no intensive development but some evidence of new built-up areas mainly located on the open area was identified. Based on our findings we can state that results practically copy the national development of cultivated land.

Key-words: Landscape management, CORINE, Land use, Land cover, Rural region.

1. INTRODUCTION

Land use represents a specific demonstration of human activity in time and space (Olah et al., 2006) and it is clear that the landscape is a faithful reflection of the state and the development of a society (Lipský, 2011). The changes taking place just in the society can be distinguished according to their technological, demographic, economic, political or social character. They also reflect the way of using an arrangement of the landscape, both cultural and natural. The reasons for variable landscape researches are primarily given by serious problems in the environment, e.g. land's degradation and erosion (Bürgi, Hersperger & Schneeberger, 2004). Different driving forces (economic factors, social factors, and general public) cause changes in the landscape and influence processes in an evolutional trajectory of the landscape itself (Bürgi, Hersperger & Schneeberger, 2004; Bičík et al., 2001). These factors create a coherent system in relation to their mutual interaction and feedback on various levels of time and space. In the last century, land use has been especially influenced by continuing differences between cores and peripheries.

[1]*Department of Environmentalistics and Natural Resources, Faculty of Regional Development and International Studies, Mendel University in Brno, tř. Generála Píky 2005/7, 613 00, Brno, Czech Republic; jiri.schneider@mendelu.cz; ales.ruda@mendelu.cz*

[2] *Department of Landscape Management, Faculty of Forestry and Wood Technology, Mendel University in Brno, Zemědělská 3, 613 00, Brno, Czech Republic; venzlu.m@seznam.cz*

The spatial structure of land use develops not only towards more and more spatial differentiation but also towards different dynamics of structural changes in territories, which are given by society in a certain stage of its development. The land use in Czechia has been clearly changing in the last two centuries, both vertically and horizontally. Hereby the regional heterogeneity of single territories hereby evolves towards more significant territorial differentiation and also different dynamics of land use functions.

Any kind of change in the context of land use and land cover has a significant role in the climatic system (Loveland & Mahmood, 2014; Melillo et al., 2014). Except for heat production from industrial and other activities, the consequences of changes in land use (e.g. tree harvesting, rising food consumption, etc.) have had also an important influence on climatic changes (Nistor et al., 2018). Monitoring and analysis of historical changes in land use with the aim of capturing significant changes in manners in the landscape to various aspects of the environment, as well as monitoring the current state of the landscape and the development of landscape structures is currently a frequent topic. Since 1990, the number of papers on land use changes has increased significantly both at European and world level (Lipský, 2011). Among scholars, there are many approaches to landscape development assessment, e.g. Skaloš et al., 2011; Irwin & Geoghegan, 2001; Bürgi & Russell, 2001. Most of the papers concerning changes in the development or land use in Czechia are based on analysis of historical maps of the Stable Cadastre, e.g. Eremiášová & Skokanová, 2009; Brůna & Křováková, 2005a; Brůna & Křováková 2005b; Lipský, 1994; Bičík, 2012; Šťastná et al., 2015. Plánka (2013) dealt with an overview of historical cartographical works for landscape development. Furthermore, the changes in the frame of land use in Czechia were solved by Tlapáková et al. (2013) or Štych (2010), who displayed the changes in landscape structure using GIS tools. The assessment of changes in land use development in historical contexts and the subsequent understanding of landscape management is based on Land Use / Land Cover Changes, and on CORINE Land Cover Database (CLC) (Kolejka, 2011). Himiyama (1999) describes the LUCC program that recommends surveying the development of land use structures in the period of the last 300 years. Due to the increasing spatial and temporal resolution of data sources, the recommendation of monitoring land use changes has been reduced to the last 100 years respectively 50 years. Feng and Flewelling (2004) point out that although land use/land cover categories are commonly used in environmental modeling or landscape development, they might be taken as subjective information and thus their interpretation depends on the original purpose of the study and the quality of data sources.

The aim of the widely used CLC database is to display land cover across Europe based on a consistent methodology and regular update of this database. Overall, the database contains 44 categories, with 29 in Czechia and 11 in the study area. Generally, the information on land use through the CLC is taken as supplementary information because of its focus and uniform methodology (Feranec et al., 2000). Land cover categories were also by Rodríguez et al. (1999) for assessing the core of cities of similar size. Ahlqvist (2005) deals more closely with the issue in land cover categories. The study by Feranec et al. (2014) focuses on comparing CORINE Land Cover, National Land Cover Data Set (NLCD) and FAO Land Cover Classification System (LCC). Authors argue that these three typologies together with their similarity (compatibility and interchangeability) are needed to address environmental issues.

The aim of the paper is to document the development of the rural landscape and highlight important causes of land use changes on the example of the Dačice region in Czechia.

2. STUDY AREA

The study area is defined by the administrative boundary of the district of the municipality with extended powers Dačice (hereinafter referred to as MEP). The Dačice rural region lies in the southeast corner of the South Bohemian Region of the Czech Republic (**Fig. 1**).

Fig. 1. Cadastral areas within the Dačice region *(Source: own processing, geodatabase ArcČR 500).*

In the north and east it borders the South Moravian Region and the Vysočina Region, the southern border is formed by the state border of the Czech Republic with the federal state Lower Austria, specifically the tourist area Waldviertel.

The border position of the area greatly affects the political, economic and socio-economic development of the region's landscape. MEP Dačice includes together a total of 23 municipalities situated in 85 cadastral areas with a total area of 472 km^2 with a population exceeding 20.000 inhabitants. The population density is 43 inhabitants/km^2, which is a low value compared to other self-governing units in the South Bohemian Region. It reaches only two-thirds of the South Bohemian region's value and less than a third of the Czech Republic's average.

The study area is characterized as an intensively cultivated agricultural area with a smaller proportion of forests. Currently, a total of 27.656 ha of agricultural land is farmed, which represents almost 59% of the total area of the region. The secondary economic sector occupies the largest number of registered entities in terms of the sector structure of the national economy in the Dačice region. This is followed by the tertiary sector. Although there is the lowest number of registered economical entities in the primary sector, the region has very favorable agricultural conditions in its eastern part.

From the geomorphological point of view, the study area belongs to the extensive sub-composition of the Bohemian-Moravian unit which is a part of the Czech Uplands. The landscape of the Dačice region has a harmonic character that is given especially by its small-sized terrain segmentation created by valleys, small-sized streams and minor forested complexes on the tops of hills with rurally utilized arable lands.

The settlement structure is characterized by the fragmentation of smaller municipalities throughout the study area. Mostly there are municipalities with up to 500 inhabitants (almost 87%). Most people (64%) are concentrated in the area of the largest cities - Dačice (39%) and in the villages Studená and Slavonice (25%).

3. DATA AND METHODOLOGY

The methodology for assessing changes in landscape development in the study area used available data from the Stable Cadastre imperial prints, historical maps and aerial photographs, and the CORINE Land Cover database. GIS software was used to illustrate changes in land cover categories.

The monitored period in 1845, 1948, 2001 and 2014 was determined on the basis of available data, where necessary land use categories (in percentage representation within each cadaster in study area) were provided by records from Czech Office for Surveying, Mapping and Cadastre (years 1845 and 1948) and Cadastral Office in Dačice (years 2001 and 2014). Finally, land use categories were regrouped into seven specific categories according to classification in 2014 - arable land, gardens, permanent grassland, forests, water bodies, built-up areas, and other areas. This reclassification was accepted because the original classification and names of categories in the years 1845 and 1948 were different from those in the years 2001 and 2014. Specifically, reclassification concerned gardens (including orchards and vineyards), permanent grassland (including grassland and pastures), water bodies (including swamps, ponds, lakes, rivers, and streams) and other areas (including infertile land, roads, and tracks).

4. RESULTS

Development of land use categories in the period 1845 – 2014

In the years 1845 - 2014 the area of arable lands decreased by 6% (**Fig. 2**). This decline is mainly due to a change in the economic and political situation after World War II, the onset of socialism and the subsequent transformation of the Czech economy during which arable land was gradually grassed. The gradual abandonment of livestock was significantly affected by the loss of permanent grassland by 8%. These areas have been replaced by arable land or have been reforested. The area of forests increased by 8%. Furthermore, the acreage of coniferous forest areas increased in connection with the replacement of mixed forests and afforestation of low stands in their surroundings. A noticeable increase is also observed in the category of other areas by 4% as a consequence of industrialization and urbanization (construction of new roads, etc.). Although the area of water bodies has increased only by 1% point, its area (in absolute values) has almost doubled. In the study area, the inhabitants are concentrated mainly in towns or larger municipalities, and therefore there are also elements of suburbanization. As a result, the area was mainly concerned with the afforestation of uncultivated agricultural land, in some places also with slight grassing.
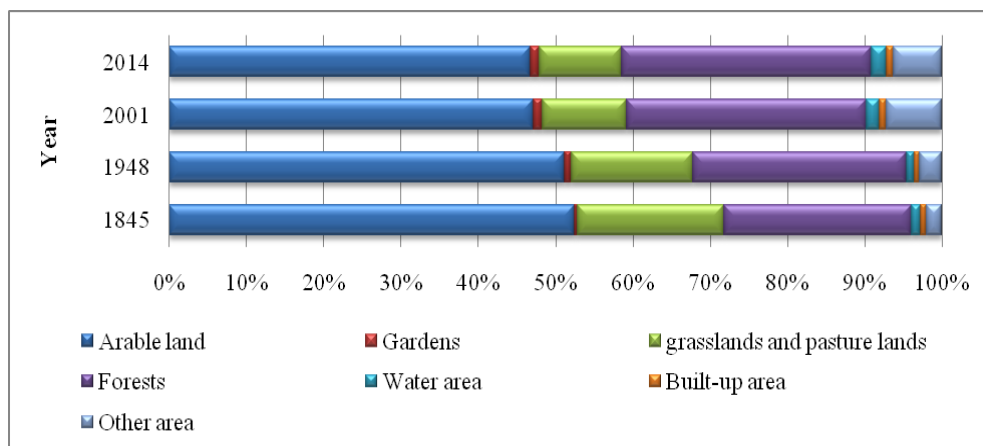
Fig. 2. Proportional representation of individual land use categories between 1845 – 2014 *(Source: own processing, data source: Czech Office for Surveying, Mapping, and Cadastre).*

4.1 Arable land

Arable land reached in Dačice region the highest area (24 602.61 ha) at the beginning of in 1845 (**Fig. 3**). In the upcoming 100 years, the area of this category decreased minimally. Between 1948 and 2001, arable land decreased to 22 411.35 ha. The first decline in this category was due to the economic and political situation that occurred in our country after the end of the Second World War when Czech Germans were transferred from the border region and it remained unsettled. The second decline was caused by the socialization of agriculture and extensive industrialization, through the violent collectivization of the peasants.

Fig. 3. Changes in arable land area between 1845 and 2014 *(Source: own processing, data source: Czech Office for Surveying, Mapping, and Cadastre).*

The merging of discontinuous and scattered agricultural areas due to their better accessibility and more efficient use in economic and technical adjustments has led to significant changes in landscape structure. Orthophotos (**Fig. 4**) illustrate two different situations in 1953 and 2010 which document the area merging process.
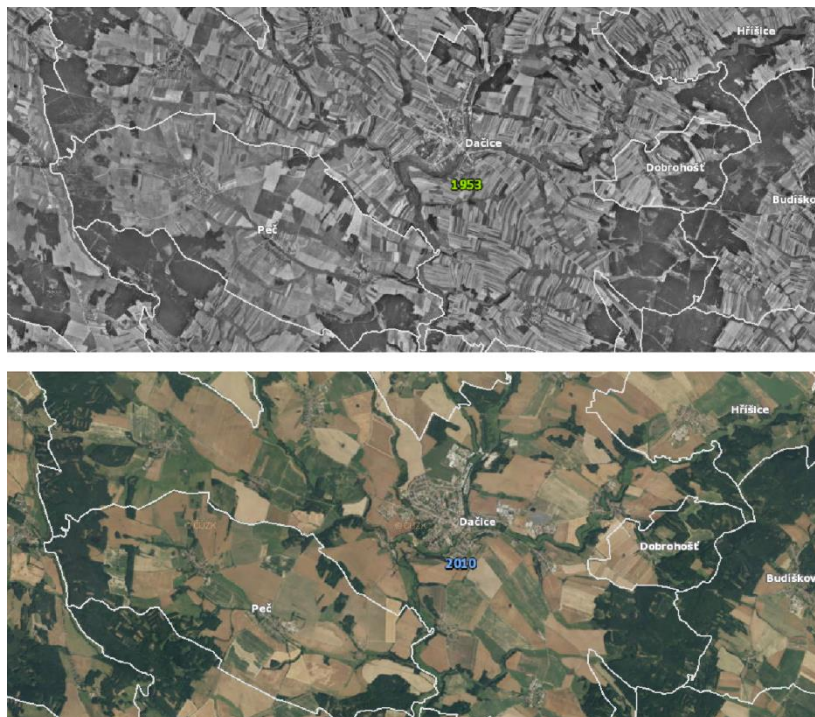
Fig. 4. Landscape structure before and after land consolidation *(Source: Czech Office for Surveying, Mapping, and Cadastre).*

4.2 Gardens

Gardens represent the largest increase of acreage in the study area. The lowest acreage was reached in 1845 with following gradual growth until today (**Fig. 5**). Dačice and Slavonice municipalities dominated. Usually, town houses were connected with barns and other farm buildings followed by agricultural areas, which were converted into gardens. Nature protection is very significant in these areas. During the last century, various beautifying associations, alley in the streets and greening the squares were created in the town and the villages, and also fruit gardens were planted near the urban area (built-up areas of municipalities). The aforementioned expansion of tree greenery in streets, especially in villages, was also associated with the change from the economic zone to the rest zone.

	1845	1948	2001	2014
Gardens	189,51	381,29	516,65	525,72

Fig. 5. Changes in gardens area between 1845 and 2014 *(Source: own processing, data source: Czech Office for Surveying, Mapping, and Cadastre).*

4.3 Permanent grasslands

The development of permanent grasslands including meadows and pastures have a typical decreasing character in the long-term period (**Fig. 6**).

	1845	1948	2001	2014
Grasslands and pasture lands	8 867,17	7 417,06	5 171,01	5 048,44

Fig. 6. Changes in permanent grasslands area between 1845 and 2014 *(Source: own processing, data source: Czech Office for Surveying, Mapping, and Cadastre).*

The main causes of this decline in 1845-1948 are associated with a decline in livestock farming and the transition from pasture to intensively cultivated agricultural land. In the following years, the decrease in the area of permanent grasslands is connected with the growth of forest influenced by organized planting or spontaneous afforestation.

4.4. Forests

Since the beginning of the monitored period, the area of forests has increased (**Fig. 7**) as a counterpart to the development of agricultural land. In the years 1948 - 2001, the increase of acreage is associated with an afforestation of abandoned, uncultivated agricultural land in higher altitudes and permanent grasslands. Most of forests is located in the western part of the region at the border with Lower Austria, respectively in the villages of Slavonice, Stálkov, Matějovec, and Stoječín, which belong to the natural park Česká Kanada.

Fig. 7. Changes in forest area between 1845 and 2014 *(Source: own processing, data source: Czech Office for Surveying, Mapping, and Cadastre).*

At present, a higher proportion of forests can be found in the northern part. Although the village of Staré Hobzí is rather an agriculturally cultivated area, the pro-portion of forests is relatively high, despite the fact that we can see practically the lowest proportion of forests in other areas with the dominanting arable lands and vice versa. Comparing the current orthophotomap with maps from the 3rd Military Mapping Survey illustrates no significant changes in forest areas (**Fig. 8**). There is a clear increase only in forests in the western part of the Dačice region. Using CLC database terminology, we are talking about the increasing proportion of coniferous trees in already existing mixed forests.

4.5 Water bodies

The study area once belonged to one of the largest pond areas in Moravia. The transition from a three-field management system to an alternating (rotary) farming and the cultivation of new fodder crops resulted in a decrease in the area of water bodies in the years 1845 - 1948. In our country, mainly in lowland fertile areas, as well as in highlands and hills, ponds were discharged and sugar beet and potatoes began to grow (**Fig. 9**). The Dačice region is referred to potato production sub-area B1, including the cultivation of ware, industrial and seed potatoes, feed grains, rape, and flax. The largest proportion of water bodies is located in the northwestern and western parts of the region (Studená, Horní Meziříčko, Volfířov, Lipnice, Markvarec, etc.). A relatively large part of larger water

bodies is situated in the center of the Dačice region, on the western edge (there is a cascade of ponds) and around the town of Slavonice and in the village of Český Rudolec. Czech fish farming has a long tradition and together with the European Union funds not only large fishing companies but also private family fishing companies are supported.
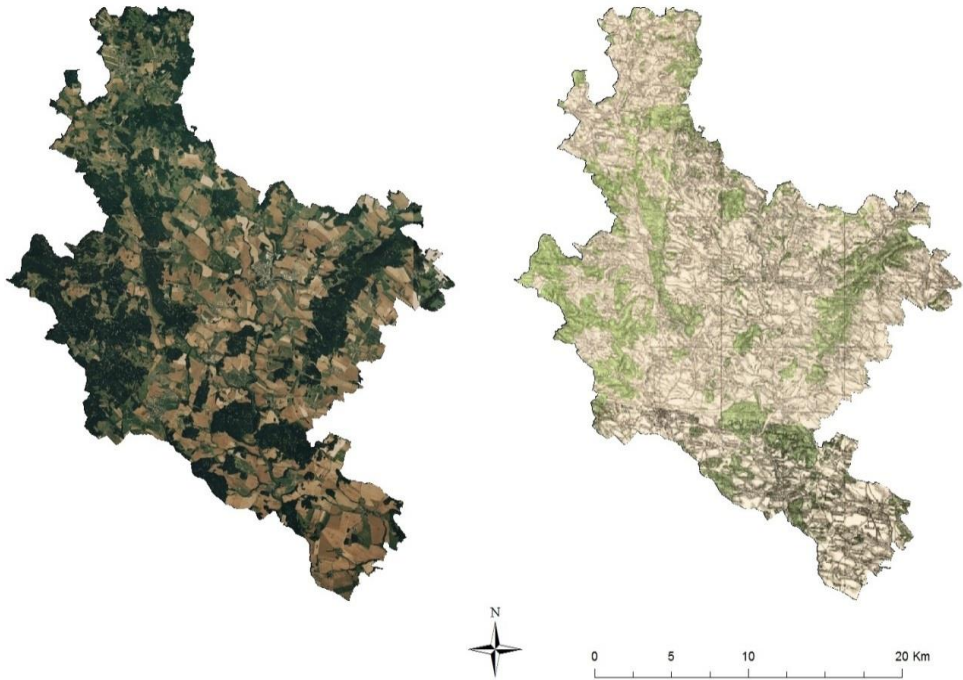
Fig. 8. Comparing the area of forests between orthophoto (dark green color) in 2014 (left) and map (green color) from the 3rd Military Mapping Survey (right) *(Source: Czech Office for Surveying, Mapping, and Cadastre).*

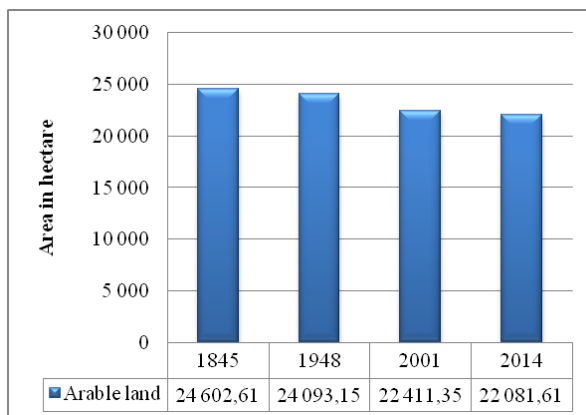|	1845	1948	2001	2014
Water area	584,87	465,06	837,85	919,87
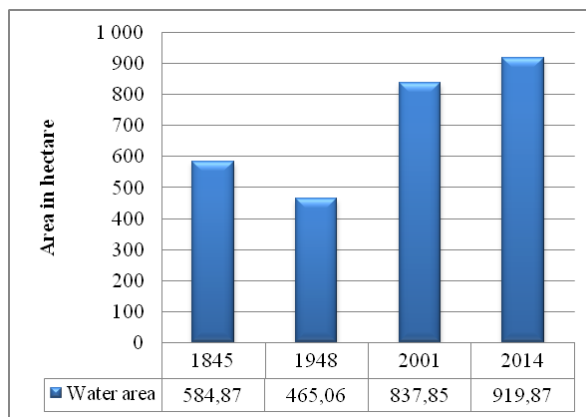
Fig. 9. Changes in water bodies area between 1845 and 2014 *(Source: own processing, data source: Czech Office for Surveying, Mapping, and Cadastre).*

4.6 Built-up areas

Between 1845 and 1948, the size of the built-up areas was reduced (**Fig. 10**). This phenomenon is linked to both World Wars and the transfer of the German population from the border. On the basis of the Munich Dictation, the Dačice region had to withdraw its borderland, namely 26 municipalities, in favor of Nazi Germany.
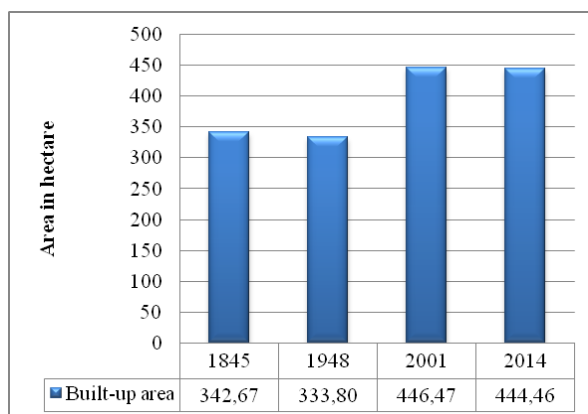
Fig. 10. Changes in built-up area between 1845 and 2014 *(Source: own processing, data source: Czech Office for Surveying, Mapping, and Cadastre).*

This territorial change lasted until 1945. Between 1948 and 2001, the increase of built-up areas was influenced by the concentration of the population in cities and rural settlements. Especially with the rise of socialism and the importance of industrialization, the character of populated areas, such as housing development, expansion of industrial zones outside the city and suburbanization, has changed (**Fig. 11**). In the villages, family houses and cottages including agricultural buildings were built.

The original character of these villages is distorted by the current construction of family houses. In smaller cadastral areas, the original character of the settlement is still preserved. Between the years 2000 – 2006, changes recorded in the CLC database concerned the built-up areas and the separated residential development areas in Dačice. Within these years, family and residential buildings were built on the western edge of the city. In addition, two separate residential development areas have been added, but they are not recorded as changes in the CLC database. The original character of these villages is distorted by the current construction of family houses. In smaller cadastral areas, the original character of the settlement is still preserved. Within these years, family and residential buildings were built on the western edge of the city.

4.7 Other areas

Concerning this category we observe a significant change after 1948 when there was intensive construction of paved roads, production and storage areas, construction of industrial and municipal waste dumps, etc. (**Fig. 12**). Other areas include not only man-made landscape elements (roads, handling areas, quarries, landfills, etc.) but also unused or infertile land (protected areas, nature parks). The increase of the area of this category was also strongly influenced by the process of industrialization and urbanization, but moreover, there is a significant influence of nature and landscape protection. A significant part of the area of other areas is located in the northern part of the region around the villages of Studená, Horní Bolík, Sumrakov, Horní Pole and Světlá pod Javořicí.
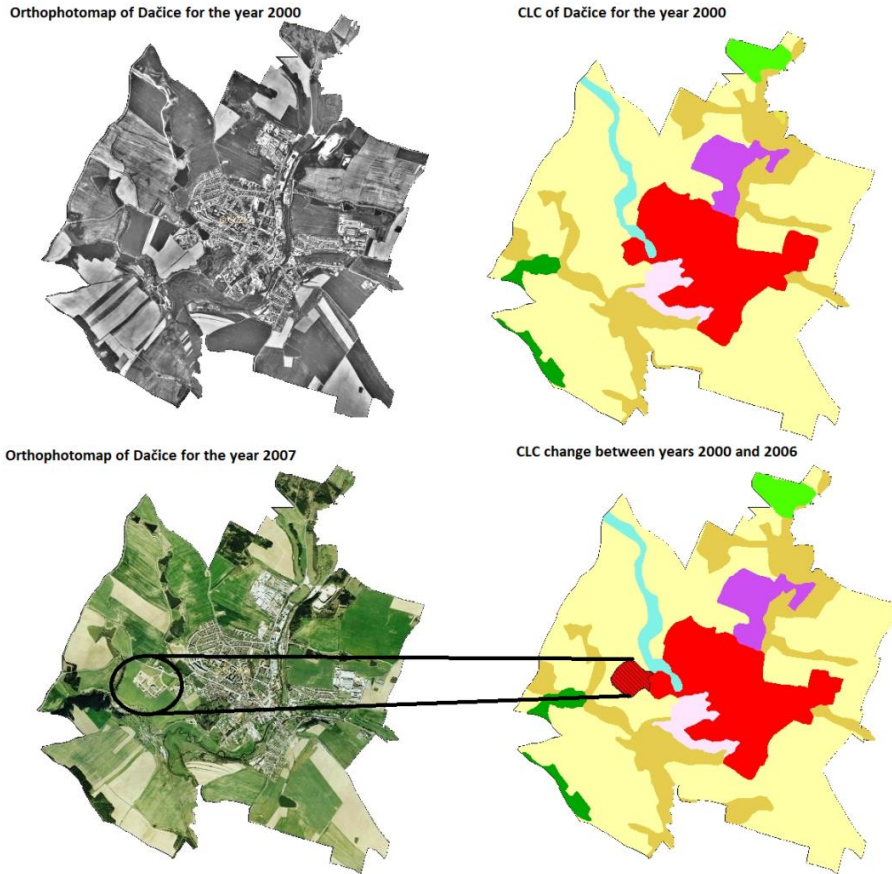
Fig. 11. Increase of built-up areas in the Dačice region during the suburbanization between 2000 – 2006 *(Source: own processing according to CLC and geoportal.gov).*
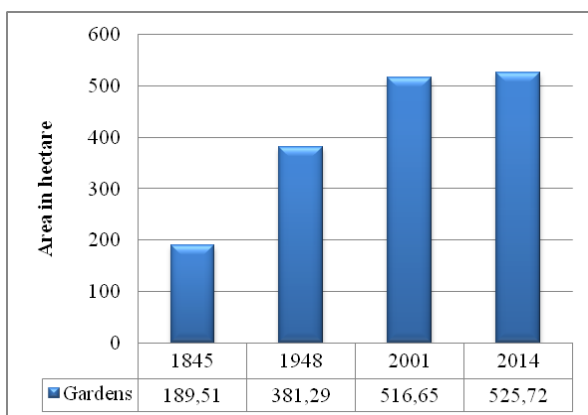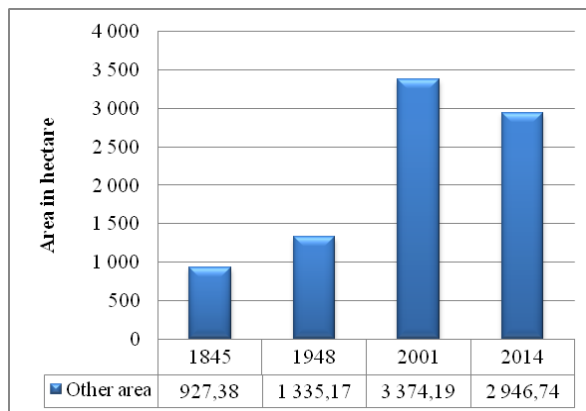

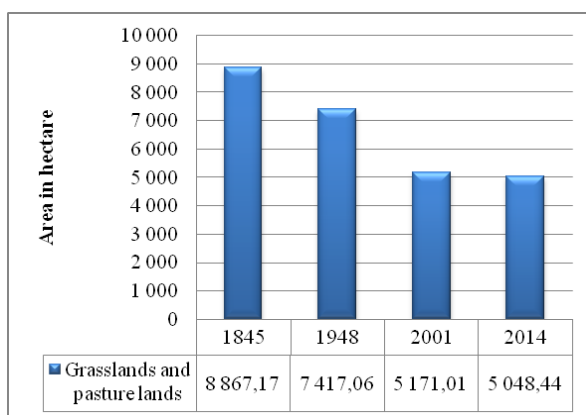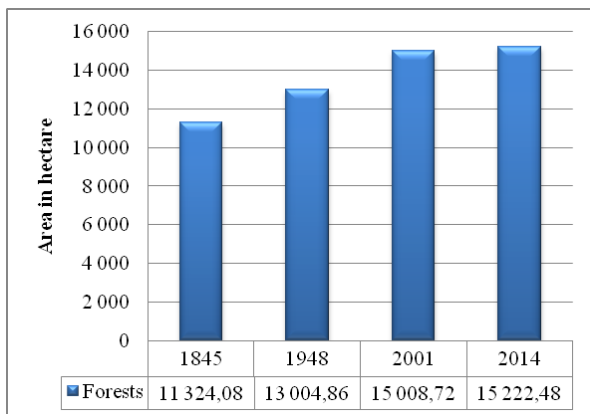**Fig. 12.** Changes in other areas between 1845 and 2014 *(Source: own processing, data source: Czech Office for Surveying, Mapping, and Cadastre).*

5. CONCLUSION

The Dačice Region is appreciated especially for its distinctive character of the landscape and preserved architectural and cultural wealth. Generally, it is a rural area with a high proportion of agricultural land. The onset of socialism was the period of the strongest impacts on the landscape. The landscape character was heavily affected due to the technical and economic changes in land consolidation. The transition from the centrally planned economy to the market economy, a period of transformation and restructuralisation in the 1990s, had a significant impact on the countryside and its land cover. In spite of larger or smaller interventions, the territory is characterized by a historically preserved urban structure of settlements. Here, it is appropriate to further protect the territory development as well.

R E F E R E N C E S

Ahlqvist, O. (2005) Using uncertain conceptual space to translate between land cover categories. *International Journal of Geographical Information Science,* 19 (7), 831–857.

Bičík, I., Jeleček, L. & Štěpánek, V. (2001) Land use changes and their social driving forces in Czechia in the 19th and 20th centuries. *Land Use Policy*, 18 (3), 65-73.

Bičík, I. (2012) *Vývoj využití ploch v Česku*. Česká geografická společnost, Praha.

Bičík, I. & Kupková, L. (2006) Vývoj využití ploch v Pražském městském regionu. In: Ouředníček, M. (ed.) *Sociální geografie Pražského městského regionu*. Univerzita Karlova v Praze, Praha. pp. 41-61.

Brůna, V. & Křováková, K. (2005a) Staré mapy jako cenný zdroj informací o stavu a vývoji krajiny: Mostecko na starých mapách. *Zahrada-Park-Krajina*, 4, 25-29.

Brůna, V., Křováková, K. (2005b) Analýza změn krajinné struktury s využitím map stabilního katastru. Historické mapy. *Zborník referátov z vedeckej konferencie Bratislava*: Kartografická spoločnosť Slovenskej republiky. pp. 1-8.

Bürgi, M., Hersperger, A. M. & Schneeberger, N. (2004) Driving forces of landscape change – current and new directions. *Landscape Ecology*, 19 (8), 857–868.

Bürgi, M. & Russell, E. (2001) Integrative methods to study landscape changes. *Land use policy*, 18 (1), 9-16.

Melillo, Jerry M., Terese (T. C.) Richmond & Gary W. Yohe (2014) *Climate Change Impacts in the United States. The Third National Climate Assessment*. U.S. Global Change Research Program, Washington.

Eremiášová, R. & Skokanová, H. (2009) Land use changes (recorded in old maps) and delimitation of the most stable areas from the perspective of land use in the Kašperské hory region. *Journal of Landscape Ecology*, 2 (1), 20-34.

Feranec, J., Bossard, M. & Otahel, J. (2000) *CORINE land cover technical guide – Addendum 2000*. European Environment Agency, Copenhagen.

Feranec, J., Solin, L., Kopecká, M., Otahel, J., Kupková, L., Štych, P., Bičík, I., Kolar, J., Čerba, O., Soukup, T. & Brodský, L. (2014) Analysis and expert assessment of the semantic similarity between land cover classes. *Progress in Physical Geography*, 38 (3), 301-327.

Feng, C. C. & Flewelling, M. D. (2004) Assessment of semantic similarity between land use/land cover classification systems. *Computers, Environment and Urban Systems*, 28 (3), 229–246.

Himiyama, Y. (1999) Historical information bases for land use planning in Japan. *Land Use Policy*, 16 (3), 145 - 151.

Irwin, E. G. & Geoghegan, J. (2001) Theory, data, methods: developing spatially explicit economic models of land use change. *Agriculture, Ecosystems and Environment*, 85 (1-3), 7–24.

Kolejka, J. (2011) *Krajina Česka a Slovenska v současném výzkumu*. Masarykova univerzita, Brno.

Lipský, Z. (2011) Protichůdné tendence současného vývoje české venkovské krajiny a jejich důsledky: opuštěná půda a vznik nové divočiny v kulturní krajině. In: Kolejka, J. (ed.) *Krajina Česka a Slovenska v současném výzkumu*. Masarykova univerzita, Brno. pp. 196-222.

Lipský, Z. (1994) Změna struktury české venkovské krajiny. *Sborník České geografické společnosti*, 99 (4), 248-260.

Loveland, T. & Mahmood, R. (2014) A Design for a Sustained Assessment of Climate Forcing and Feedbacks Related to Land Use and Land Cover Change. *Bulletin of the American Meteorological Society*, 95 (10), 1563-1572.

Nistor, M-M., Man, T. C., Benzaghate, M. A., Nedumpallile Vasu, N., Dezsi, S., Kizza, R. (2018) Land Cover temperature implications fro the seasonal evapotranspiration in Europe. *Geographia Technica*, 13 (1), 85-108.

Olah, B., Boltižiar, M., Petrovič, F. & Gallay, I. (2006) *Vývoj využitia krajiny slovenských biosférických rezervácií UNESCO*. Technická univerzita Zvolen, Zvolen.

Plánka, L. (2013) Historická kartografická díla České republiky pro studium vývoje krajiny. *Životní prostředí*, 47 (1), 3-7.

Rodrígues, A. M., Egenhofer J. M. & Rug, D. R. (1999) Assessing semantic similarities among geospatial feature class definitions. In: Vckovski, K. E., Brassel, E. K. and Schek, J-H. (eds.) INTEROP'99, Berlin, Springer. pp. 189–202.

Rounsevell, Mark D. A., Pedroli, B., Erb, K. H., Gramberger, M., Gravsholt Busck, A., Haberl, H., Kristensen, S., Kuemmerle, T., Lavorel, S., Lindner, M., Lotze-Campen, H., Metzge, M. J., Murray-Rust, D., Popp, A., Pérez-Soba, M., Reenberg, A., Vadineanu, A., Verburg, P. H. & Wolfslehner, B. (2012) Challenges for land system science. *Land Use Policy*, 29 (4), 899-910.

Skaloš, J., Weber, M., Lipský, Z., Trpáková, I., Šantrůčková, M., Uhlířová, L. & Kukla, P. (2011) Using old military survey maps and orthophotograph maps to analyze long-term land cover changes – Case study (Czech Republic). *Applied Geography*, 31 (2), 426-438.

Šťastná, M., Vaishar, A., Vavrouchová, H., Ševelová, M., Kozlovská, S., Doskočilová, V. & Lincová, H. (2015). Changes Of A Rural Landscape In Czech Areas Of Different Types. *European Countryside*, 7 (2), 111-133.

Štych, P. (2010). Evaluation of long-term land-use changes in case studies in Central Bohemia. *Bohemi centralit*. Praha, 30, 121-137.

Tlapáková, L., Stejskalová, D., Karásek, P. & Podhrázská, J. (2013) Landscape Metrics as a Tool for Evaluation Landscape Structure – Case Study Hustopeče. *European Countryside*, 5 (1), 52-70.

CALCULATION OF THE VERTICAL DISTRIBUTION OF WATER TEMPERATURE IN THE BLACK SEA BY SATELLITE DATA

Andrii SRYBERKO[1]

ABSTRACT:
The studies on calculation of vertical distribution of water temperature in the Black Sea by satellite data are described. The research was carried out in the active layer of the deep part of the Black Sea at depths of 0 – 50 meters. The initial data of the actual water temperature values were station data or measurement from the ship data (OSD – Ocean Station data), data measured with the help of floats (PFL – Profiling float data) and satellite data of the sea surface temperature. Calculations were based on the definition of statistical dependencies between the values of water temperature at the neighboring levels of vertical temperature distribution in the Black Sea by OSD & PFL data of water temperature and the development of regression equations. Calculations showed statistically significant results in spring-autumn period. Correlation coefficients between the values of the water temperature on the neighboring levels in the Black Sea amounted to 0.88 – 0.99. To increase the accuracy of results the equations for the calculation of adjustments for the temperature of the water at depths: 10, 20, 25 and 50 meters were developed. Standard calculation errors of the vertical distribution of water temperature amounted to 2 °C in the Black Sea in 2017 year.

Key-words: *Black Sea, water temperature calculation, correlation coefficient, statistical dependence, regression equation, satellite data.*

1. INTRODUCTION

Water temperature is the most regularly measured parameter by comparison with other hydrological characteristics and can be used as an indicator for hydrophysical, hydrochemical, hydrobiological processes of the World Ocean.

Implementations of various contemporary ocean research programs in the last decade have generated considerable progress toward understanding the Black Sea's basic physical and biogeochemical processes. Physical and biogeochemical data accumulated from these studies were able to resolve many features of the Black Sea circulation and ecosystem structure. The description and understanding of basin scale dynamical features have reached maturity. Modelling and data assimilation tools have been developed and implemented but they still require further calibration and validation exercises by availability of new data sets (Oguz et al., 2004).

Primarily study on verification and calibration data are based on the set of satellite measurements and data from the stations or it can be based on the sea surface temperature data measured from the ship (Andrianova et al., 2004; Kara et al., 2008; Dufois et al., 2012).

---

[1] *Hydroacoustics Branch of Institute of Geophysics of National Academy of Sciences of Ukraine, 3 Preobrazhenska st., Odesa, 65082, Ukraine, sriberko@gmail.com*

Research of water temperature based on satellite information in the Black Sea aims to study sea surface temperature variability (Manev et al., 2005; Shapiro, Aleynik & Mee, 2010). Despite many researches the identification and analysis of trends and temperature anomalies in the long-term variability of the thermohaline characteristics are under the major focus. But the possibility of creating they're of vertical distribution based on satellite data is practically unexplored.

Indirect definitions of the vertical distribution of water temperature, i.e. through the development of various methods for the calculation of the distribution of water temperature on the vertical are used to date (Andrianova et al., 2015).

Study of vertical distribution of water temperature in the Black Sea was carried out in the deep-water part sea at standard levels (0, 10, 20, 25, 30, 50 meters) in spring – autumn period. This area of research is represented by the highest number of measurements and is included in the Main Black Sea current zone.

2. MATERIAL AND METHODS

Calculations of the vertical distribution of water temperature in the Black Sea are founded on the "Method of calculation of the vertical distribution of water temperature in the Black Sea based on satellite information" (hereinafter referred to as the Method) created by us in 2015 year (Andrianova et al., 2015).

In undertaking this work the developed Method (Andrianova et al., 2015) was significantly completed with new equations, criteria for calculations, corrections for the temperature of the water, which significantly improve the accuracy of the calculations of the vertical distribution of water temperature. Complex calculations of linear and exponential regression equations were included in the last Method version compare to Method of the 2015 year where the calculations were performed only on the equations of exponential regression.

2.1. Initial data

Initial data were used to determine the statistical dependencies between values of water temperature on the neighboring levels 10, 20, 25, 30, 50 meters in the Black Sea and to create the regression equations. Those initial data were the actual water temperature data from the stations or measured data from the ship (OSD – Ocean Station data) from 1890 to 2005 years and data measured using floats (PFL – Profiling float data) from 2005 to 2017 years (NOAA, 2019).

Due to the small number of OSD and PFL water temperature data on the level 0 meters a climatic data of satellite measurements of the Black Sea surface temperature (T_{clim}) with step 4 km to latitude and longitude measured companion NASA (Terra MODIS) (NASA's OceanColor Web, 2019) from 2000 on the 2017 years were used as initial data.

The initial satellite data were the daily data on satellite measurements of the Black Sea water surface temperature with 4 km step on latitude and longitude, measured companion NASA (Terra MODIS) (NASA's OceanColor Web, 2019) were used to calculate the vertical distribution of water temperature in the Black Sea.

Analysis and comparative estimation of calculations of vertical distribution of water temperature by satellite data was carried out between the values calculated on the regression equations and PFL data (Profiling float data) of water temperature on standard levels in 2017 year (NOAA, 2019).

2.2. Method of calculation

Calculations of vertical distribution of water temperature in the Black Sea were carried out in three main stages.

The first stage – the finding of statistical dependences between the values of water temperature at the neighboring levels in the Black Sea according to the data of water temperature and the creation of regression equations.

The second stage – setting the criterion for calculating the vertical distribution of water temperature ($\pm \Delta T$).

The third stage – calculation of water temperature corrections at depths of 10, 20, 25, 50 meters.

The first stage of the calculation. To development the regression equations the average by 72 squares (**Fig. 1**) in the size of 40' to 60', months and standard levels perennial (for the period from 1890 to 2017) OSD and PFL data of the water temperature in the Black Sea were used.

The data were selected for spring – autumn period because there are small amount of data available during the cold period of the year.
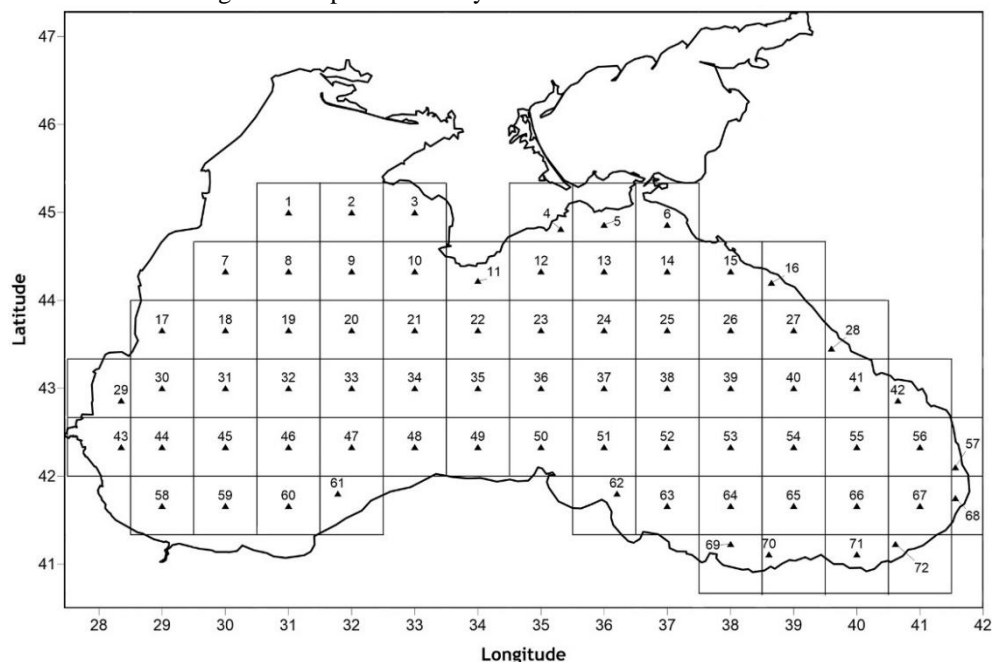
Fig. 1. Location of squares (square size 40' to 60') for calculating regression equations in the Black Sea.

Equation of exponential and linear regression was calculated in each square (**Fig. 1**) (Kobzar, 2006; Eliseeva, 2007; Andrianova et al., 2015; Hogg, Tanis & Zimmerman, 2015; Ahn, 2018) for a particular month of the year

$$y = ae^{bx} ,\qquad\qquad (1)$$

and

$$y = ax + b, \tag{2}$$

where a and b are regression coefficients; y – water temperature at the studied level; x - water temperature on the overlying level.

The second stage of the calculation. In (Glagoleva & Skriptunova, 1979) states that the change of the vertical profile of water temperature is obey the exponential distribution law. Our researches show that at large deviations of values of sea surface temperature from climatic values (T_{clim}) of water temperature the linear dependence between values of water temperature on neighboring levels prevails.

The criterion ($\pm \Delta T$) serves as a factor determining the method of calculating the vertical distribution of water temperature by the equations of exponential or linear regression. The role of the criterion ($\pm \Delta T$) is to set the boundary conditions for calculating the water temperature according to the exponential regression equations or linear regression equations.

If the value of the sea surface temperature (T_0) is in the interval $[T_{clim} - \Delta T < T_0 < T_{clim} + \Delta T]$, the vertical distribution of water temperature is calculated by exponential regression equations. If T_0 is not included in that interval, the linear regression equation is used.

The criterion value ($\pm \Delta T$) for the calculation of the vertical distribution of water temperature is determined experimentally and individually for specific water areas of the World Ocean depending on its hydrological conditions.

The third stage of the calculation. Calculation of water temperature corrections (hereinafter referred to as the correction) at depths of 20, 25, 50 meters were conducted by finding statistical dependencies between values of water temperature on the neighboring levels and building linear equations of regression

$$\delta y_z = ax_k + b, \tag{3}$$

where δy_z – the water temperature at depth z meters; x_k – the water temperature at a depth k meters; *a* and *b* coefficients of the regression equation.

For a correction on 20 meters the dependence between the values of water temperature on the levels 25 – 20 meters, for corrections on 25 and 50 meters – on the levels of 30 – 25 meters and 30 – 50 meters respectively was determined.

The calculation of the correction at a depth of 10 meters is more complex than for 20, 25, 50 meters. The calculations have been carried out by the method of the analytical presentation of the distribution of surface water temperature as functions of the coordinates. Satellite data of sea surface temperature were decomposed into the ranks on algebraic polynomials - the Chebyshev polynomials (Kobzar, 2006; Gil, Segura & Temme, 2007). In marine forecasts this method was used for the first time by N. A. Belinsky, M. G. Glagoleva (Kudryavaya, Seryakov & Skriptunova, 1974).

Using decomposition by Chebyshev polynomials the water temperature field is represented as a sum of elementary fields each of which describes the individual traits of the real distribution. Decomposition of a function of two variables in a series on Chebyshev polynomials is

$$T(x, y) = A_{00}\varphi_0(x)\psi_0(y) + A_{10}\varphi_1(x)\psi_0(y) + \cdots + A_{ij}\varphi_i(x)\psi_j(y), \tag{4}$$

where φ_i, ψ_j – Chebyshev polynomials representing the parabola *i, j* - order (*i* = 1, 2, ..., *M*; *j* = 1, 2, ..., *N*), A_{ij} – coefficients of decomposition.

The values of the coefficients of the decomposition are calculated according to the equation:

$$A_{ij} = \frac{\sum\limits_{m=1}^{k}\sum\limits_{n=1}^{l}T(x_m, y_n)\varphi_i(x_m)\psi_j(y_n)}{\sum\limits_{m=1}^{k}\varphi_i^2(x_m)\sum\limits_{n=1}^{l}\psi_j^2(y_n)} \tag{5}$$

where *k* – number of nodes, which is set to feature in the direction of axis *x*, *l* – in the direction of axis y.

The function field $T(x_m, y_n)$ is represented as a matrix

$$T(x_m, y_n) = \begin{vmatrix} T(x_1, y_1) & T(x_1, y_2) & \cdots & T(x_1, y_l) \\ T(x_2, y_1) & T(x_2, y_2) & \cdots & T(x_2, y_l) \\ \cdots\cdots\cdots\cdots\cdots\cdots\cdots\cdots\cdots\cdots \\ T(x_k, y_1) & T(x_k, y_2) & \cdots & T(x_k, y_l) \end{vmatrix}, \tag{6}$$

The absolute values of the decomposition coefficients A_{ij} show the specific weight of this elementary field in the source field, which is represented as a series.

To simplify calculations it is convenient to use the method proposed by B.H. Rybak (Kudryavaya, Seryakov & Skriptunova, 1974).

If

$$Z = F(T), \tag{7}$$

and the distribution of *T* is represented analytically Chebyshev polynomials, i.e.

$$T = f(A_{00}A_{10}\cdots A_{ij}), \tag{8}$$

the regression equation for *Z* will be written as

$$Z = a_0 + a_1 A_{00} + a_2 A_{10} + a_3 A_{01} + \cdots + a_r A_{ij}, \tag{9}$$

where a_0, a_1, a_r – numeric coefficients of the regression equation; A_{00}, A_{10}, A_{01},..., A_{ij} – coefficients of decomposition in a series on Chebyshev polynomials element T from which distribution the function *Z* depends.

Therefore, to calculate the Z function the coefficients A_{ij} must be calculated first by the equation (5) and then substituted in equation (9).

The sequence of calculation of temperature corrections as follows: calculate the correction at 25 meters first, then to 20 and 10 meters, and at 50 meters in the autumn.

2.3. Statistical characteristics for estimating calculations

The measure of statistical dependence between the values of the water temperature was: when linear dependence – linear coefficient of correlation r $(-1 \le r \le 1)$, the coefficient of multiple correlation R $(0 \le R \le 1)$, with nonlinear dependence – correlation index I $(0 \le I \le 1)$ (Draper and Smith, 1998; Kobzar, 2006; Eliseeva et al., 2007; Hogg, Tanis & Zimmerman, 2015).

To assess the significance of the correlation index (I), linearization was applied to the exponential equations (1). If we take the (natural) logarithm of both sides of equation (1), we get

$$Ln(y) = Ln(a) + bx$$

if we define $y' = Ln(y)$ and $a' = Ln(a)$. We get: $y' = a' + bx$. This is the equation of a straight line (linear). Then, the measure of statistical dependence will be described by the correlation coefficient r'. In our case, the value of the correlation index (I) is equal to the value of the correlation coefficient r' $(I = r')$.

Checking the significance of r, R, r' was carried out by comparing the correlation coefficients with the critical value of the correlation coefficients r (α) (for pair correlation) and R (α) (for multiple correlation) at a significance level α = 0.05 (or confidence coefficient $(1 - \alpha)$ = 0.95).

The critical value of the correlation coefficients r (α) can be calculated by the equation:

$$r(0.05) = \sqrt{\frac{t_{0.025}^2}{n - 2 + t_{0.025}^2}} , \qquad (10)$$

where $t_{0.025}$ – the critical values of Student's t distribution at significance level α = 0.025 (or confidence coefficient $(1 - \alpha)$ = 0.975), n – the number of members of the series.

For multiple correlation:

$$R(0.05) = \sqrt{\frac{(k-1)F_{0.05}(f_1, f_2)}{n - k + (k-1)F_{0.05}(f_1, f_2)}} , \qquad (11)$$

where $F_{0.05}$ – the critical value for an F distribution with f_1 and f_2 degrees of freedom at significance level α = 0.05 (or confidence coefficient $(1 - \alpha)$ = 0.95), n – the number of members of the series, k is the number of variables in the regression equation (Kobzar, 2006).

Also, r (α) and R (α) can be determined from the tables (Kobzar, 2006; Hogg, Tanis & Zimmerman, 2015; Ahn, 2018).

If r (or R) $\ge$ r (α) (or R (α), respectively), then the corresponding correlation is considered significant (Kobzar, 2006).

Another criterion of significance r, R, r' was the ratio r/E_r. To assess the correlation values the values of probability errors E_r, E_R, $E_{r'}$ of correlation coefficients were calculated (Kudryavaya, Seryakov & Skriptunova, 1974), according to the type of dependency:

$$E_k = 0.67 \frac{1 - r^2}{\sqrt{n}} , \qquad\qquad (12)$$

where k – the index of the correlation's values (r, r', R), r – the correlation coefficient (r, r', R), n – the number of members of the series.

At reliable dependencies the correlation coefficient (r) in 6 to 10 times greater than its the probable error E_r (Kudryavaya, Seryakov & Skriptunova, 1974).

The assessment of the significance and reliability of linear regression equations was carried out by the critical value for an F distribution with f_1 and f_2 degrees of freedom $F_\alpha(f_1, f_1)$ at significance level $\alpha = 0.05$ (or confidence coefficient (1 - α) = 0.95). If the calculated value of $F > F_\alpha(f_1, f_1)$ (critical), then the statistical regression equation reliability is recognized as significant and reliable (Kobzar, 2006; Eliseeva et al., 2007).

Also, the estimation of the accuracy of the calculations is determined by the efficiency of the method. The ratio S/σ_T allows determining the reliability and efficiency of the calculation method simultaneously. S is a mean square error of the correlation (standard error) and σ_T is the standard deviation of the actual values (standard deviation) (Kudryavaya, Seryakov & Skriptunova, 1974; Abuzyarov et al., 1988). The values of S and σ_T can be calculated by known formulas (Kudryavaya, Seryakov & Skriptunova, 1974; Abuzyarov et al., 1988; Deep, 2006; Kobzar, 2006; Hogg, Tanis & Zimmerman, 2015; Ahn, 2018).

The ratio S/σ_T is smaller, the method is more reliable. For a functional dependency of ratio $S/\sigma_T = 0$, and at $S/\sigma_T = 1$ variation of the function does not depend on variations of the argument. Consequently the relationship between variables is absent (Kudryavaya, Seryakov & Skriptunova, 1974; Abuzyarov et al., 1988). For our calculations of the vertical distribution of water temperature the permissible error is: $S/\sigma_T \leq 0.57$ at $n \leq 15$ and $S/\sigma_T \leq 0.67$ at $n > 25$.

3. RESULTS

3.1. Development of regression equations and determination of criteria's for calculation

In each square (**Fig. 1**) the equations exponential and linear regression (1) and (2) were built for each month in the period May – October. The total number of equations exponential regressions amounted to 432 and linear regression equations – 432 respectively.

Correlation coefficients r and r' (*I*) were within 0.88 – 0.99 at the developing regression equations stage. They did not exceed the critical value r (0.05) = 0.878 (Kobzar, 2006; Hogg, Tanis & Zimmerman, 2015).

Probabilistic errors E_r and $E_{r'}$ of the correlation coefficients r, r' were calculated according to the equation (12). Errors do not exceed 0.07 during the period May – October. The minimum values of the relations r/E_r and $r/E_{r'}$ is 13. That means a correlation is reliable between the averaged values of water temperature in all squares of the Black Sea (**Fig. 1**) in the period May – October.

The calculated values of F were within $10.36 - 1136.43$ and greater than the critical value $F_{0.05} = 10.13$. The values of the criterion (S/σ_T) were $0.06 - 0.55$, which is less than the critical value 0.57. This means that all the developed regression equations are effective, reliable and significant.

To visualize we shall give an example of calculation of vertical temperature distribution by satellite data at three stations and compare the obtained results with PFL data measured on 30.05.2017, 27.06.2017 and on 10.09.2017 respectively. Coordinates of the first station –Longitude: 29,038°, Latitude: 42,138°, the second station – Longitude: 36,294°, Latitude: 42,172° and the third – Longitude: 37,990°, Latitude: 43,480°.

Considering the **Fig. 1** we define that the stations fall into the squares 44, 51 and 26 respectively.

The criterion ($\pm\Delta T$) was used as determining factor in the calculations of the vertical distribution of water temperature on equations, exponential or linear regression.

Studies have shown (> 1000 numerical experiments) that when the deviation of the sea surface temperatures from climatic values of water temperature (T_{clim}) in the Black Sea is $\pm2°C$ a linear relationship between water temperature values is dominated on the neighbouring levels.

Thus, if the value of the sea surface temperature (T_0) is in the interval $[T_{clim} - \Delta T < T_0 < T_{clim} + \Delta T]$, the vertical distribution of water temperature is calculated by, exponential regression equations (1). If they are not included in this interval, the equations of linear regression (2) are used.

For our example the calculation intervals and the predominant type of statistical dependency are shown in **Table 1**.

Table 1.

Intervals for the determination of the predominant types of statistical dependence.

Number station	Number square	Month	T_0 [°C]	T_{clim} [°C]	Interval [°C]	Statistical dependence
1	44	5	17.770	15.63	[13.63-17.63]	Linear
2	51	6	22.145	20.98	[18.98-22.98]	Exponential
3	26	9	24.500	23.37	[21.37-25.37]	Exponential

Table 1 shows that at the station 1 the calculation of the vertical distribution of water temperature needs to be carried out on a linear regression equation and at stations 2 and 3 by the equations of exponential regression.

Considering the values of the criterion ($\pm\Delta T$) and intervals (**Table 1**) the vertical distribution of water temperature at station 1 is calculated by linear regression equation, and at stations 2 and 3 – on exponential regression equations.

The built regression equations by formulas (1) and (2) for our example, and the corresponding of the standard errors (S) of calculation are presented in **Table 2**.

Table 2.

The regression equation, standard errors (S) of calculations of the vertical temperature distribution.

Number station	Number square	Month	The regression equation	S
1	44	5	$y = 0.9207x - 0.6741$	1.41
2	51	6	$y = 4.6081e^{0.0628x}$	2.27
3	26	9	$y = 5.1155e^{0.0531x}$	2.37

The vertical distribution of water temperature is calculated by the regression equations (**Table 2**) from the surface to a depth of 50 meters. The water temperature values on the surface are satellite data of sea surface temperature.

The results of calculations on regression equations (**Table 2**) are presented in **Fig. 2**.

Fig. 2. The graphs of the vertical distribution of water temperature at stations 1 (a), 2 (b) and 3 (c) built on the PFL data (*T*) and calculated values by the equations of exponential (T_{exp}) and linear (T_{line}) regressions (**Table 2**).

Fig. 2 shows that PFL data and the calculated value of water temperature on standard levels well consistent. Weak match between PFL data and calculated values is observed only in the thermocline zone at a large gradient of temperatures. It is confirmed by the results of research conducted by us previously (Andrianova et al., 2015).

3.2. Calculation of water temperature corrections at depths of 10, 20, 25, 50 meters

To improve the results of calculation of the vertical distribution of water temperature based on the satellite data, regression equations were developed to calculate the water temperature corrections at depths of 10, 20, 25 and 50 meters.

Research has shown that water temperature corrections must be entered depending on the time of the year. So, for the spring – summer period the correction at depths of 10, 20, 25 meters should be introduced. For autumn correction should be introduced at depths of 10, 20, 25 and 50 meters.

The built linear regression equations by equation (3) for corrections at a depth of 20, 25, 50 meters and the relevant criteria for accuracy and effectiveness of the regression equations are presented in **Table 3**.

Table 3.

The regression equations for corrections at a depth of 20, 25, 50 meters, statistical characteristics.

Season of the year	Depth (m)	The regression equation	*r*	*r*(0.05)	*r/E$_r$*	*F*	*F$_{0.05}$*	*S/σ$_T$*
Spring	20	$y_{20} = 1.08x_{25} + 0.323$	0.93	0.03	620	25187	3.84	0.44
	25	$y_{25} = 0.98x_{30} + 0.999$	0.91	0.03	506	19301	3.84	0.46
Summer	20	$y_{20} = 1.02x_{25} + 1.756$	0.97	0.02	2425	142229	3.84	0.27
	25	$y_{25} = 1.08x_{30} + 0.714$	0.98	0.02	3267	208227	3.84	0.24
Autumn	20	$y_{20} = 0.85x_{25} + 3.933$	0.91	0.03	535	21691	3.84	0.38
	25	$y_{25} = 0.90x_{30} + 2.945$	0.94	0.03	783	33459	3.84	0.32
	50	$y_{50} = 0.33x_{30} + 4.385$	0.57	0.08	75	293	3.85	0.43

As can be seen from **Table 3**, that all calculated statistical characteristics do not exceed critical values. This means a correlation between values of water temperature throughout the Black Sea in spring – autumn period is reliable and indicates the effectiveness of the developed regression equations.

The calculation of the corrections at a depth of 10 meters was carried out by method of the statistical dependencies between satellite values of sea surface temperature and values of PFL data of water temperature at a depth of 10 and 20 meters. Further equations of multiple regression were built.

Satellite data of water temperature on the surface were presented in the form of water temperature fields and formed a matrix (5 on 5) with step 5 to the latitude at 5 in longitude. Water temperature fields were set by 25 points through 4 km in latitude and 4 km in longitude. **Fig. 3** shows an example of the location of the satellite data values of the water temperature to calculate the correction at a depth of 10 meters.
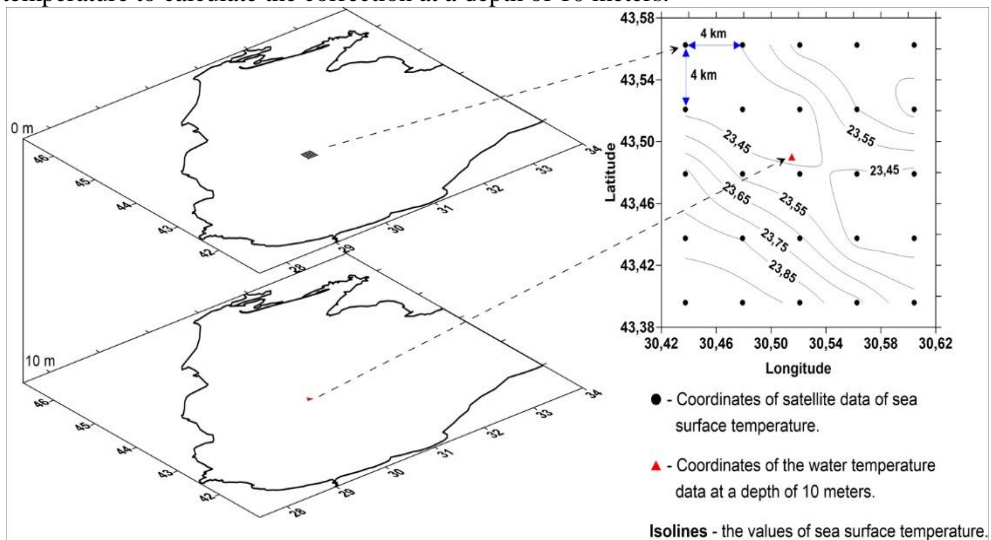
Fig. 3. Diagram of the location of satellite data of sea surface temperature to calculate the correction at a depth of 10 meters.

The fields of water temperature have been decomposed into the ranks on the Chebyshev polynomials and the decomposition coefficients

($A_{00}, A_{10}, A_{20}, A_{30}, A_{01}, A_{02}, A_{11}, A_{12}, A_{13}$) were calculated according to the equation (5).

Depending on the task the number of coefficients in the multiple regression equation may be different. In our case for a more accurate assessment of the relationship between the sea surface temperature and the temperature at a depth of 10 meters 5 coefficients of decomposition ($A_{00}, A_{20}, A_{01}, A_{02}, A_{12}$) have been applied. Also, in the multiple regression equation another coefficient was added. That coefficient was the value of the water temperature at a depth of 20 meters.

Using a simplified method of calculation, the equation (9) will be written as

$$\delta y_{10} = 0.378x_{20} + 0.755A_{00} + 2.822A_{20} + 0.513A_{01} - 1.913A_{02} + 1.911A_{12} - 1.875, \quad (13)$$

where δy_{10} – the water temperature at depth 10 meters; x_{20} – the water temperature at a depth of 20 meters; $A_{00}, A_{20}, A_{01}, A_{02}, A_{12}$ – coefficients of decomposition of the sea surface temperature field.

The results of the studies show a high correlation between values of water temperature at a depth of 10 meters, the water temperature at a depth of 20 meters and coefficients of decomposition $A_{00}, A_{20}, A_{01}, A_{02}, A_{12}$ in spring – autumn period. The multiple correlation coefficient (R) was 0.90 and greater than the critical value R (0.05) = 0.14. Probabilistic error multiple correlation coefficient (E_R) was 0.005 the ratio (R/E_R) was 180. This indicates the significance of R and a reliable correlation. Standard error (S) of correlation was 1.7°C.

The calculated value F = 404 and greater than the critical value $F_{0.05}$ = 2.11. The criterion (S/σ_T) equal to 0.18 at n = 605 that does not exceed the tolerable error 0.67 $(S/\sigma_T \leq 0.67)$. This indicates about the significance of the regression equation, reliability and effectiveness of the method of calculation of correction by the equation (13).

Described above example of calculation of the vertical distribution of water temperature at three stations was used for the visualization.

The results taking into account the water temperature corrections calculated on the regression equations (**Table 3**) and equation (13) are presented in **Fig. 4**.
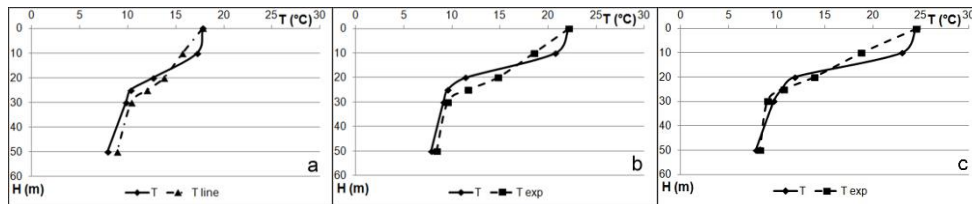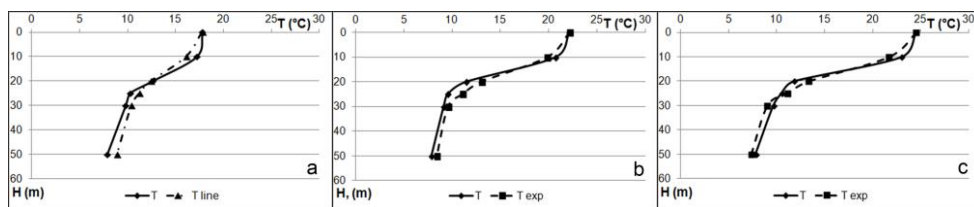

Fig. 4. The graphs of the vertical distribution of water temperature at stations 1 (a), 2 (b) and 3 (c) built on the PFL data (T) and calculated values by the equations of exponential (T_{exp}) and linear (T_{line}) regressions (**Table 2**), taking into account the corrections to the water temperature.

Fig. 4 shows a significant increase in the accuracy of calculated water temperature values on standard levels compare to **Fig. 2**. Improvement of accuracy of calculations of vertical distribution of temperature of water is confirmed by values of standard errors (S) presented in **Table 4**.

Table 4.

Standard errors (S) of calculating the vertical distribution of water temperature considering the corrections in water temperature.

Number station	Number square	Month	The regression equation	S
1	44	5	$y = 0.9207x - 0.6741$	0.93
2	51	6	$y = 4.6081e^{0.0628x}$	1.23
3	26	9	$y = 5.1155e^{0.0531x}$	1.12

The results of calculations of the vertical distribution of water temperature by satellite data on 160 stations in the Black Sea in period of spring-autumn in 2017 year showed that the standard error (S) amounted to 2°C, at n = 960 (σ_T = 6.4).

3.3. Calculation of the vertical distribution of water temperature in the Black Sea by satellite data

The local calculation of the vertical distribution of water temperature in the Black Sea by satellite data in the layer 0 – 50 meters at several stations can be easily carried out by applying the above equations. But if the whole water area of the Black Sea should be counted, this process is very time consuming.

Therefore, we designed a prototype of a computer program (hereinafter referred to as the Program) for the calculating of the vertical distribution of water temperature in the Black Sea by satellite data. The Program includes 864 exponential and linear regressions equations to calculate the vertical distribution of water temperature on all squares (**Fig. 1**) in the Black Sea and the months between May – October; linear regression equations to calculate corrections for temperature at standard levels (10, 20, 25, 50 meters); intervals to determine the calculation by exponential or linear regression equations.

Thus, the Program automatically determines where and by what equations the vertical distribution of water temperature in the Black Sea and the corrections to the water temperature can be calculated.

The initial data for the calculations are only daily satellite data of the sea surface temperature and the month of the year.

To visualize the results of the calculations by the Program the maps of the spatial distribution of water temperature at standard levels, zonal (latitude 44° N) and meridional (longitude 36° E) cuts for 30.05.2017, 27.06.2017 and 10.09.2017 were built.

The spatial distribution of sea surface temperature on satellite data shown in **Fig. 5**.
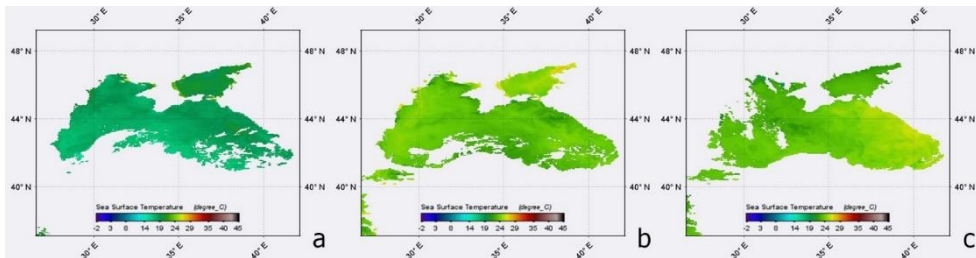
Fig. 5. The spatial distribution of Black Sea surface temperature on satellite data for 30.05.2017 (a), 27.06.2017 (b) and 10.09.2017 (c).

Maps of spatial distribution of the surface temperature of the Black Sea on satellite data (**Fig. 5**) were built with the help of specialized software NASA – SeaDAS (NASA's SeaDAS, 2019).

The missing satellite data can be seen in **Fig. 5** as a white area. The reason of this might be a high cloud cover at the time of measurement. Temperature scale corresponds to the original scale for these measurements (NASA's OceanColor Web, 2019).

The results of calculations of the vertical distribution of water temperature on satellite data at the standard levels in the Black Sea for 30.05.2017 are shown in **Fig. 6**.

The results of calculations of zonal (latitude 44° N) and meridional (longitude 36° E) cuts in the Black Sea for 27.06.2017 and 10.09.2017 are presented in **Fig. 7** respectively.

Figs. 6 and **7** are built using computer program Ocean Data View (ODV) that is intended for the interactive exploration and graphical display of oceanographic and other geo-referenced profile, trajectory or time – series data (Schlitzer, 2019).
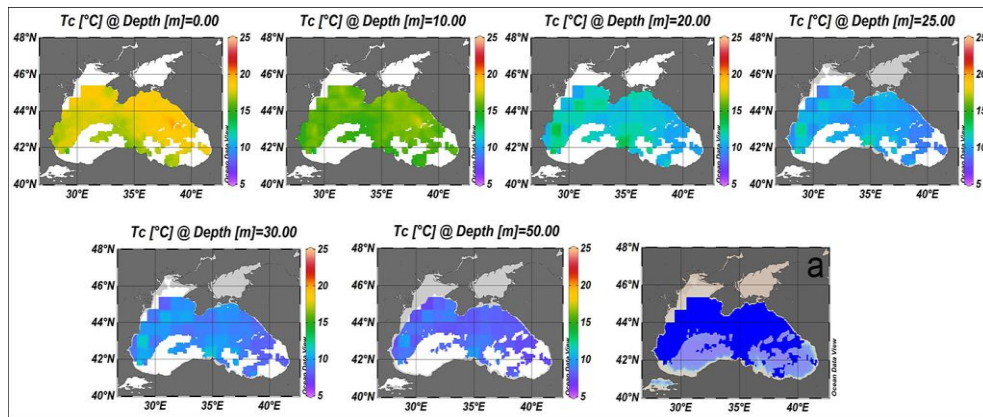
Fig. 6. Maps of spatial distribution of calculated water temperature (T_c) at the standard levels in the Black Sea for 30.05.2017. Map (**a**) is map of the distribution of data for calculation.
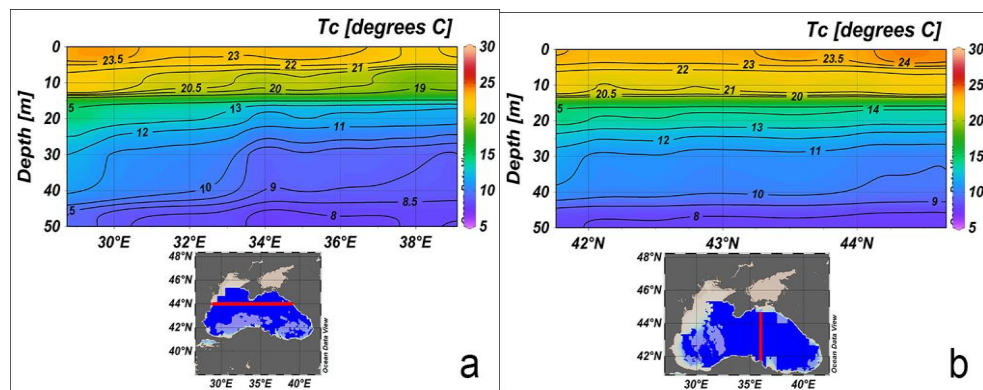
Fig. 7. Distribution of calculated of water temperature (T_c) on zonal at latitude 44° N (**a**) and meridional at longitude 36° E (**b**) cuts in the Black Sea for 27.06.2017 and 10.09.2017, respectively. The maps show the location of cuts in the Black Sea.

4. CONCLUSIONS

Research results from the calculations of the vertical distribution of water temperature in the Black Sea by satellite data at standard levels (0, 10, 20, 25, 30, 50 meters) in spring – autumn period showed that the change in the vertical profile of water temperature obeys the exponential law of distribution.

The linear law of distribution is dominated when the deviation of sea surface temperatures (T_0) from climatic water temperature values (T_{clim}) is more than ± 2°C.

Water temperature corrections are introduced on the levels of 10, 20, 25 meters during spring – summer, and in autumn – on the levels 10, 20, 25, 50 meters.

Standard error (S) of calculations of the vertical distribution of water temperature in the Black Sea by satellite data in 2017 year is amounted to 2°C.

Designed by us, the prototype of a computer program to calculate the vertical distribution water temperature in the Black Sea by satellite data could serve as a basis for the establishment of a "Monitoring system of water temperature in the Black Sea". With the help of which the dynamics of water temperature and water temperature change effects on hydrobiological, hydrochemical, hydrophysical processes in the Black Sea and the ecosystem of the sea in general can be evaluated.

In our view the described algorithm of calculation of the vertical distribution of water temperature by satellite data can be applied to others water area of the World Ocean taking into account their hydrological conditions.

R E F E R E N C E S

Abuzyarov, Z. K., Kudryavaya, K. I., Seryakov, J. I., & Skriptunova, L. I. (1988). *Marine Forecasts*. Leningrad, Gidrometeoizdat. (in Russian)

Ahn, H. (2018). *Probability and Statistics for Science and Engineering with Examples in R*, Second Editon. California, Cognella Inc. & University Readers.

Andrianova, O.R., Batyrev, A.A., Skipa, M.I. & Sriberko, A.V. (2004) *Undersatellite authentication and interpretation of the data of space surveys of a sea surface*. Kosmìčna Nauk. ì Tehnol. 10, 92–95. (in Russian; Abstract in English)

Andrianova, O.R., Skipa, M.I., Sryberko, A. V. & Stepanova, Y. V. (2015) *Estimation of ability of vertical temperature distribution's calculation for the Black sea's water by satellite data*. Her. ONU 20, 9–21. (in Russian; Abstract in English)

Deep, R. (2006) *Probability and Statistics: with Integrated Software Routines*. Elsevier Academic Press Publications, USA.

Draper, N.R. & Smith, H. (1998) *Applied Regression Analysis*. John Wiley & Sons, Inc., Hoboken, NJ, USA.

Dufois, F., Penven, P., Peter Whittle, C. & Veitch, J. (2012). *On the warm nearshore bias in Pathfinder monthly SST products over Eastern Boundary Upwelling Systems*. Ocean Model. 47, 113–118.

Eliseeva, I. I. (ed), Kurysheva, S. V., Kosteeva, T. V., Pantina, I. V., Mikhailov, B. A., Neradovskaya J.V., Shtroe, G. G., Bartels, K . & Rybkina, L. R. (2007) *Econometrics*. Moscow, Finance and Statistics. (in Russian)

Gil, A., Segura, J. & Temme, N.M. (2007) *Numerical Methods for Special Functions*. Philadelphia, Society for Industrial and Applied Mathematics.

Glagoleva, M.G. & Skriptunova, L.I. (1979) *Prediction of Water Temperature in Oceans*. Leningrad, Gidrometeoizdat. (in Russian)

Hogg, Robert V., Tanis, Elliot A. & Zimmerman, D. (2015) *Probability and Statistical Inference*. – 9th ed., Pearson Education, Inc., USA.

Kara, A.B., Barron, C.N., Wallcraft, A.J., Oguz, T. & Casey, K.S., (2008) *Advantages of fine resolution SSTs for small ocean basins: Evaluation in the Black Sea*. J. Geophys. Res. 113, C08013.

Kobzar, A.I. (2006) *Applied Mathematical Statistics. For Engineers and Scientists*. Moscow, Fizmatlit. (in Russian)

Kudryavaya, K.I., Seryakov, E.I. & Skriptunova, L.I., (1974) *Marine hydrological forecasts*. Leningrad, Gidrometeoizdat. (in Russian)

Manev, A., Palazov, K., Stoianov, St. & Raykov, St. (2005) *Satellite researches of temperature anomalies on the Black sea surface*. Trakia J. Sci. 3, 24–27.

NASA's OceanColor Web (2019). - National Aeronautics and Space Administration, OceanColor Web. Available from: https://oceancolor.gsfc.nasa.gov/cgi/l3 [Accessed May 2019].

NASA's SeaDAS (2019). - National Aeronautics and Space Administration, SeaDAS. Available from: https://seadas.gsfc.nasa.gov/about/ [Accessed July 2019].

NOAA (2019). - National Oceanic and Atmospheric Administration, National Oceanographic Data Center, World Ocean Database. Available from: https://www.nodc.noaa.gov [Accessed May 2019].

Oguz, T., Tugrul, S., Kideys, A.E., Ediger, V. & Kubilay, N. (2004) *Physical and biogeochemical characteristics of the Black Sea (28, S)*. sea 14, 1331–1369.

Schlitzer, R., 2019. Ocean Data View. https://odv.awi.de

Shapiro, G.I., Aleynik, D.L. & Mee, L.D. (2010) *Long term trends in the sea surface temperature of the Black Sea*. Ocean Sci. 6, 491–501.

THE ANALYSIS OF THE LANDSLIDE VULNERABILITY SUB WATERSHEDS ARUS IN BANYUMAS REGENCY

SUWARNO [1]*, SUTOMO [1], Maulana Rizki ADITAMA [2]

ABSTRACT:
Landslide vulnerability is affected by several factors including the condition of the geology, geomorphology, soils, and land use. The purpose of this research is to examine landslide Vulnerability class by using synthetic geomorphological approach in the research area. Survey research method was use which includes field work and laboratory work. Field work intended for the mapping landslide of area, measurement and observation of the land characteristics. Laboratory work is aimed at analyzing the soil texture. The data of the field work and the laboratory are used to determine the landslide vulnerability class by using geographical information system technology. Landslide vulnerability class is analyzed by using 11 parameters. Data processing parameters of each land forms is done by giving values between the prone and not cartilage. The determination of the class prone determined how many parameters of value-prone. The results of the study show that the landslide vulnerability class research area is divided into two classes, namely medium and high vulnerability class. High vulnerability is dominating class with broad reaching 89.58% of the total area. A class of high vulnerability dominates due to various reasons including geological conditions i.e. all areas with sloping rocks of structure bedded with a slope of more than 10°, and arranged Halang and Tapak rock formations.

Key-words: *Vulnerability, Landslides, Geomorphological approach.*

1. INTRODUCTION

Disaster-prone is a condition or characteristics of the geological, hydrological, biological, climatological, geographical, social, cultural, political, economic, and technology in an area for a specific period which reduces the ability to prevent, attenuate, reaching preparedness, and reduced ability to respond to the impact of bad certain danger (law No.24/2007 RI about disaster management Chapter 1). The area of the landslide-prone is the protected area or the area of cultivation covering potential avalanche zones (PMPU No. 22/PRT/M/2007 on guidelines for Spatial Areas prone to Landslide). Landslide-prone areas can be interpreted as an area that is easy to landslide. The abundance of landslide and the density of incident occurrence is affected by several factors, they are the shape of the land surface morphology, geological conditions, the distance between the river flows, earthquakes (Havenith, et al., 2015).

*[1] Geography Education Department of Universitas Muhammadiyah Purwokerto, Jl. Raya Dukuh Waluh Kembaran, Purwokerto, Jawa Tengah, Indonesia, *Corresponding author suwarnohadimulyono@gmail.com; sutomo@ump.ac.id*
[2] Universitas Jenderal Soedirman, Indonesia, maulana.rizki.a@mail.ugm.ac.id

The area characteristics that are used to determine the landslide vulnerability consist of slope, topography, vegetation cover, the framer of rocks, rainfall and the incidence of landslide. The effect of topographic factors on the landslide morphology is a form of vulnerability and a big slope, landslide will happen on a large hill with a slope morphology 10-15 º (Edoardo, et al., 2014). The geological structure area of faulting and tilting of rocks bedded composed of sedimentary rocks which have already experienced the weathering and vegetation cover change occurs, then the region will be much going of landslide (Kevin, et al., 2017; Luigi, et al., 2014). Rainfall is a factor triggering landslide events, landslide events more occur in regions with annual rainfall in wet years (Susana, et al., 2014).

Sub Watersheds Arus include into landslide vulnerability area. Landslide area is influenced by the physical condition of the land and due to human activities. When the management of land is not suitable, then it will trigger landslide. Landslides are very detrimental to the surrounding community because it may cause casualties, either loss of life or property. The things that need to be avoided in landslide management are related to human activities include cutting slopes for construction of roads, houses, farms and mining the rock and sand (Sartohadi, 2008).

The landslide incidence caused by human activities such as the use of land for agriculture, housing, roads, homes, farms and mining the rock and sand (Sartohadi, 2008). Cardinali, et al. (2002) explained the factors that cause landslide are physical factor such as the local geology and morphology. Geological factors consist of the type of materials/rocks, fracturing of rock mass structure of the mayor, while other factors consists of morphology, elevation, slope angle, slope aspect, type of avalanches, land use, soil type and rainfall (Glenn, et al., 2006; Nadim, et al., 2006; Thapa and Esaki, 2007; LAN, et al., 2004). Forest land use is less susceptible to landslides, because on forest land use less damage than wooded slopes, then on the land use of the forest with the same topographic factor will be less landslide events (Elmar, et al., 2017).

Landslide is a down movement the slopes of rocks and/or soil slipping along the plane of the surface. Landslide is always associated with a disruption of the balance of the relationship that exists between pressure and strength in the material above the slopes. The relationship between the pressure and the power is determined by factors such as altitude and the steepness of the slope and density, strength of cohesion and the shift of the material (Smith, 1996). Huabin, et al. (2005) distinguishing factor is the cause of landslide into two categories namely intrinsic variables such as the geological conditions and the structure of the slopes, and extrinsic variables such as rainfall and human activities. Human activity influence on landslide such as the manufacture of the roads and the railway construction, mining, development of the town in mountainous areas (Sassa, et al., 2007).

2. METHODOLOGY

Analysis of landslide vulnerability classes using parameters for landslide-prone areas issued by the Department of Public Works namely PMPU No. 22 / PRT / M / 2007. In the PMPU, the criteria of landslide-prone land classification are based on climatology, geomorphology, geology, soil and land use factors. These factors consist of 11 variables: 1) thick rainfall, 2) landslide events, 3) slope, 4) relief, 5) thick weathering, 6) texture, 7) permeability, 8) rock type, 9) layer structure rocks, 10) earthquakes, and 11) land use. The causal variable is considered to be vulnerable or not vulnerable based on **Table 1** below.

The Criteria of vulnerability causes to Determine the Landslide Vulnerability

No	Causes	Variable	Vulnerable Landslide	Value	
				Yes	No
1	Rain fall	Yearly rain fall (mm)	≥2,500 mm/year	1	0
2	Landslide Occurrence	Frequency	Landslide occurrence	1	0
3	Topography	Slope	≥15%	1	0
		Relief	Hilly to mountainous	1	0
4	Soil	Thickness of weathering	≥90 cm	1	0
		Texture	Clay and its variant	1	0
		Permeability	Medium to slow	1	0
5	Geology	Rock	Sedimentary rock: clay, marl, tuff, limestone, sand at tertiary-age, and pyroclastic	1	0
		Structure	Layer of rock parallel with the slope	1	0
		Earthquake	Earthquake influence	1	0
6	Land Use	Type of land use	Settlement, one-seasoned farming with terrace, and fish ponds	1	0

Source: Suwarno, et al., 2013.

Based on the assessment in **Table 1**, each variable is given a value that is vulnerable and not vulnerable. The parameters used for the assessment of landslide vulnerability classes are 11 variables that cause vulnerability. Eleven of these variables are categorized into two, which are vulnerable and not vulnerable. Variables categorized as not vulnerable are given a value of 0 (zero), while the variables categorized as vulnerable are given a value of 1 (one), because it is considered that each of these variables has the same degree of influence on the causes of landslide vulnerability, then given the same weight. Based on the many values causing landslide vulnerability, the lowest 0 and the highest value were obtained. Landslide vulnerability class was divided into 4 classes, namely very low, low, medium and high classes. The class interval width is calculated using Formula 1, then the width of the class interval (11 - 0): 4 = 2.77 is rounded to 3. The landslide vulnerability class division is presented in **Table 2** below.

The width of vulnerability class and landslide occurrence

No	The numbers of landslide causes	Vulnerability class
1	≤ 2	Very low
2	3 – 5	Low
3	6 – 8	Medium
4	9 – 11	High

3. RESULTS AND DISCUSSIONS

The results of each variables are based on **Table 1** and classified to determine the landslide susceptibility class based on **Table 2**. Landslide vulnerability classes in the research area consist of two classes of vulnerability namely medium and high class. The research area did not have landforms that entered the very low and low vulnerability classes. Landslide susceptibility classes are currently available in three landform units, namely landform units of Slope II Structural Hills, Valley of Slope I Structural Hills, Slope

III Structural Hills. High landslide susceptibility classes are scattered in 5 landform units, namely landform units of Slope Synchronous Hills III, IV Slope Settlements, Slope V Slope Hills, IV Slope Structural Hills, and Slope V Structural Hills. Landslide vulnerability class distribution is presented in **Figure 1** below.
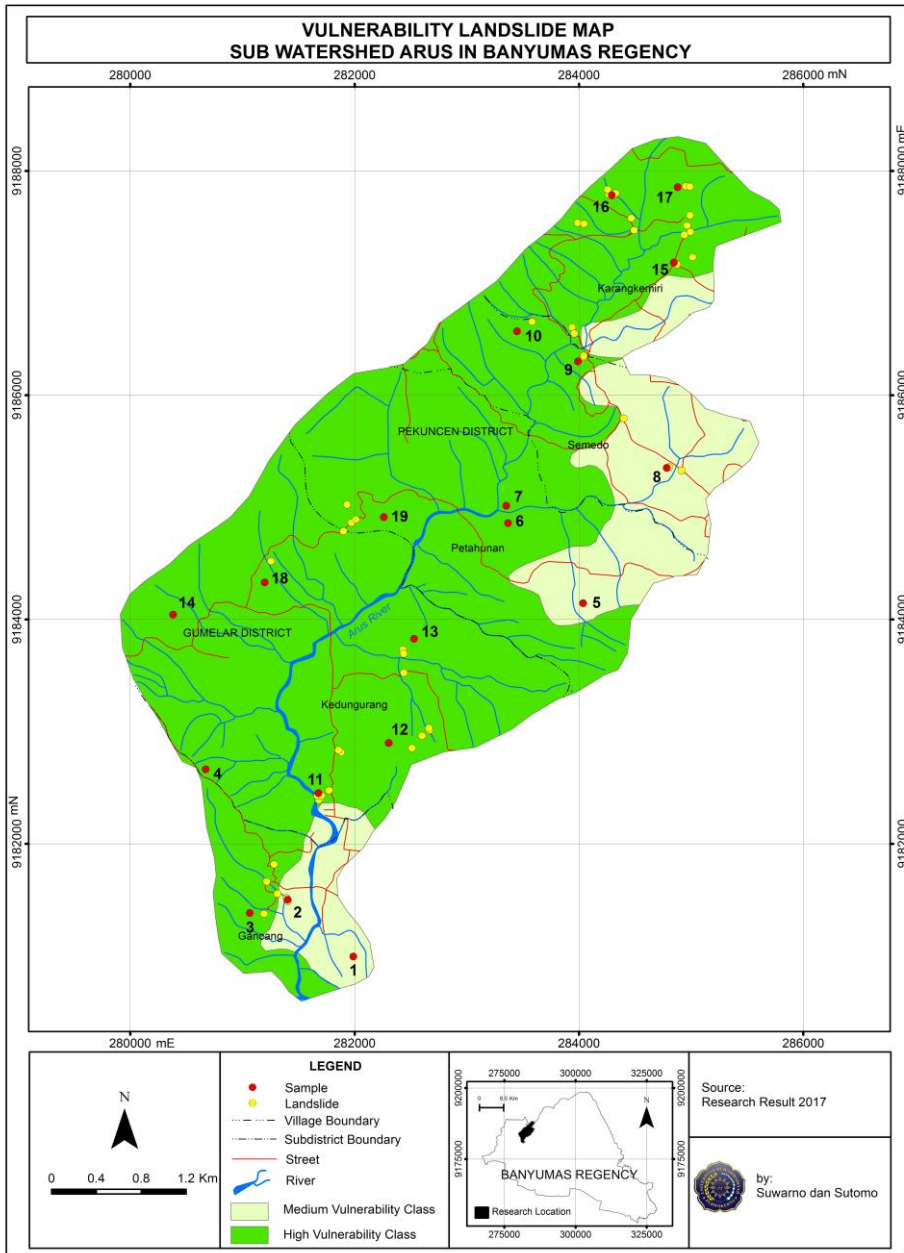
Fig.1. Landslide Vulnerability Map Sub Watersheds Arus in Banyumas Regency.

Based on **Figure 1** it can be seen that the distribution of landslide landscaping classes is being found in landform units with slope classes I to III. The high vulnerability class dominates due to various reasons including geological conditions, namely all regions with sloping rock layering structures with slopes of more than 10º, and composed of Halang and Tapak rock formations. These rock formations are composed of water-resistant rocks which are good slip fields for landslides. The area of each landslide class is presented in **Table 3** below.

Table 3.

The width of each landslide vulnerability class

No	Vulnerability class	Width		Landslide Occurrence	
		(ha)	(%)	Sum	(%)
1	Medium	380.92	18,77	5	10.42
2	High	1648.86	81,23	43	89.58
	Sum	2029.78	100.00	48	100.00

Source: Fig. 1

Based on **Table 3** above, the study area of 819.23% entered a high vulnerability class, with a total landslide incidence of 89.58% of the total landslide events. The vulnerability class is currently occupying 18.77% of the total area, with landslide events 10.42% of the total incidence. The study area does not have very low and low landslide susceptibility classes, this can be caused by various factors. These factors include geomorphic conditions which are composed of structural landform units with various slope classes. Geological structure in the form of sloping and sloping layers. High annual rainfall of more than 2500 mm per year.

High vulnerability occupies the widest class III to V slopes. Landform unit that entered on the vulnerable high class is the sinklinal slopes of hills III, sinklinal hills, sinklinal hills IV slopes slope of V, structural slope hills IV, and structural slope Hills V. Landslide occurrence is found in the high vulnerability class. On a high vulnerability class with steep slopes, rock-lined sloping structure, morphology, the hills to the mountains, land use with the intensive management activities. Landslide in many research areas occur on the steep slopes of the suitable with the opinion of the (Chien-Yuan dan Wen-Lin, 2013; Mutasem,et al., 2013; Edoardo, et al., 2014; Ching-Ying, et al., 2015). Morphological factors that form the structural hills are also factors that led to the research area of the incoming high vulnerability class. According to (Reichenbach, *et al.,* 2014) landslide distribution influenced by topography, morphology, hydrology, litologi, and land use.

The geological condition in the research area consist of structures sinkinal and bedded rocks are tilted, as well as Formation composed of *Halang* (Tmph), and the formation of *Tapak* (Tpt). *Halang* formation (Tmph) Tertiary age (Middle Miocene – end), composed of andesite, Tuff sandstones, marls and sandstones, breksi, sandstones. The formation of *Tapak* (Tpt) age of tertiary (Pliocene), consisting of rough colored greenish sandstones, marls, sandstones Temple looks greenish, the temple looks Tuff, and greenish marls (Suwarno and Sutomo, 2017). The geological condition of determining the high vulnerability class especially geologic structure and types of rocks.

Sandstones and clays are one of the causes of the landslide high vulnerability class (Barančoková, et al., 2014). Age of rocks on the formation of *Halang* (Tmph) Tertiary age (Middle Miocene – end), at the age of these rocks occur landslide of 54.17% (Suwarno and Sutomo, 2017). Landslide in Maierato most occur in the Miocene rocks from to Plio-Pleistocene (Luigi, et al., 2014). Landslide in Central Europe a lot happens on the border between sedimentary rocks and volcanic rocks or (Piotr, et al., 2016).

Rainfall in the area of study is tall, an annual average of over 2000 mm, on most of the average annual precipitation above 3000 mm. Rainfall is the cause of high incidence of landslide. Rainfall is landslide trigger factors (Gao, et al., 2017), meaning that the incidence of landslide will quickly occur if supported by high rainfall.

4. CONCLUSIONS

Night-time Landslide vulnerability in research areas lies in the middle to high class. A high class vulnerability of its widest and covers in five units of land forms. A high class vulnerability is caused by various factors including high rainfall, condition of geomorphology, geology, and soil properties. Rainfall is spread evenly throughout the region. The research on area of geomorphology units is controlled by structural context, as the morphology of the area situated in the form of rolling hills and valleys with steep to rugged slope.

The geological conditions in the form of geological structure of synclinal folds and oblique layers, composed of sedimentary rocks of tertiary age. Solum is thick soil, soil texture dominated by clay and loam. The earthquake did not affect the vulnerability caused due to the research locations were not positioned near to the centers of earthquakes.

R E F E R E N C E S

Barančoková M., Kenderessy P. (2014) Assessment of landslide risk using GIS and statistical methods in Kysuce region. Ekológia (Bratislava), **33** (1) 26–35.

Cardinali, M., Reichenbach, P., Guzzetti, F., Ardizzone, F., Antonini, G., Galli, M., Cacciano, M., Castellani, M., and Salvati, P. (2002) A geomorphological Approach to The Estimation of Landslide Hazards and Risks in Umbria, Central Italy, *Natural Hazards and Earth System Sciences;* **2**, 57 – 72.

Chien-Yuan Chen &Wen-Lin Huang (2013) Land use change and landslide characteristics analysis for community-based disaster mitigation, *Environ Monit Assess,* **185**, 4125–4139

Ching-Ying Tsou, Masahiro Chigira, Daisuke Higaki, Go Sato, Hiroshi Yagi, Hiroshi P. Sato, Akihiko Wakai, Vishnu Dangol, Shanmukhesh C. Amatya, Akiyo Yatagai, 2015. Topographic and geologic controls on landslides induced by the 2015 Gorkha earthquake and its aftershocks: an example from the Trishuli Valley, central Nepal, *Landslides juornal. DOI: 10.1007/s10346-017-0913-9*

Edoardo Borgomeo, Katy V. Hebditch, Alexander C. Whittaker, Lidia Lonergan (2014) Characterising the spatial distribution, frequency and geomorphic controls on landslide occurrence, Molise, Italy, *Geomorphology,* **226***,* 148–161

Gao L., Zhang L.M., Cheung R.W.M. (2017) Relationships between natural terrain landslide magnitudes and triggering rainfall based on a large landslide inventory in Hong Kong, *Landslides journal, DOI 10.1007/s10346-017-0904-x*

Glenn,F.N., David, R.S., John, C.D., Glenn, D.T., and Stephen, J.D. (2006) Analysis of LiDAR-derived Topographic Information for Characterizing Landslide Morphology and Activity, *Geomorphology,* **73**, 131 – 148.

Havenith, H.B., Torgoev, A., Schlögel, R., Braunc, A., Torgoev, I., Ischuk, A. , Shan, T. (2015) Geohazards Database: Landslide susceptibility analysis, *Geomorphology, http:// dx.doi.org/10.1016/j.geomorph.2015.03.019*

Huabin, W., Gangjun, L., Weiya, X., and Gonghui, W. (2005) GIS-based Landslide Hazard Asscesment: an overview, *Progress in Physical Geography*, **29** (4), 548-567.

Kevin Roback, Marin K. Clark, A. JoshuaWest, Dimitrios Zekko, Gen Li, Sean F. Gallen, Deepak Chamlagain, JonathanW. Godt (2017) The size, distribution, and mobility of landslides caused by the 2015 Mai 7-8 Gorkha earthquake, Nepal, *Geomorphology journal homepage: www.elsevier.com/locate/geomorph*

Lan, H.X., Zhou, C.H., Wang, L.J., Zang, H.Y., and Li, R.H. (2004) Landslide Hazard Spatial Analysis and Prediction Using GIS in The Xiaojiang Watershed, Yunnan, China, *Engineering Geology,* **76**, 109 – 128.

Luigi Borrelli, Loredana Antronico, Giovanni Gullà, Giovanni Marino Sorriso-Valvo, (2014) Geology, geomorphology and dynamics of the 15 February 2010 Maierato landslide (Calabria, Italy), *Geomorphology*, **208**, 50–73.

Mutasem Sh. Alkhasawneh, Umi Kalthum Ngah, Lea Tien Tay, Nor Ashidi Mat Isa, and Mohammad Subhi Al-batah (2013) Determination of Important Topographic Factors for Landslide Mapping Analysis Using MLP Network, *The ScientificWorld Journal Volume Article ID 415023, 12 pages, http://dx.doi.org/10.1155/2013/415023*

Muhammad Mukhlisin, Ilyias Idris, Al Sharif Salazar, Khairul Nizam & Mohd Raihan Taha (2010) GIS Based Landslide Hazard Mapping Prediction in Ulu Klang, Malaysia, *ITB J. Sci.,* **42 A**, (2), 163-178

Nadim,F., Rodolf, P., Herbert, E., Herbert, K., and Steven, K. (2006) An Introduced Methodology for Estimating Landslide Hazard for Seismic and Rainfall Induced Landslides in a Geographical Information System Environment, *ECI Conference on Geohazards, Lillehammer,* Norway.

Piotr Migoń, Kacper Jancewicz ,Milena Różycka, Filip Duszyński, Marek Kasprzak (2016) Large-scale slope remodelling by landslides – Geomorphic diversity and geological controls, Kamienne Mts., Central Europe, *Geomorphology, journal homepage: www.elsevier.com/locate/geomorph*

Reichenbach, P., Busca, C., Mondini, A. C., Rossi, M. (2014) The Influence of Land Use Change on Landslide Susceptibility Zonation: The Briga Catchment Test Site (Messina, Italy), *Environmental Management*, **54**, 1372–1384, DOI: 10.1007/s00267-014-0357-0

Peraturan Menteri Pekerjaan Umum Nomor 22/PRT/M/2007, tentang Pedoman Penataan Ruang Kawasan Rawan Bencana Longsor.

Sartohadi, J., 2008. The Landslide Distribution in Loano Sub-District, Purworejo District Central Java Province, Indonesia*, Forum Geografi, 22* (2)*, 129-144.*

Sassa, K., Fukuoka, H., Wang, F., dan Wang, G. (2007) *Progress in Landslide Science*, Springer Berlin Heidelberg, New York.

Schmaltz E.M., Steger S., Glade T. (2017) The influence of forest cover on landslide occurrence explored with spatio-temporal information, *Geomorphology* **290**, 250–264

Smith, K. (1996) *Environmental Hazards*, London and New York.

Susana Pereira, José Luís Zêzere, Ivânia Daniela Quaresma, Carlos Bateira, (2014) Landslide incidence in the North of Portugal: Analysis of a historical landslide database based on press releases and technical reports, *Geomorphology, journal homepage: www.elsevier.com/locate/geomorph.*

Suwarno (2018) An Analysis of Landslide Occurrence Distribution and Geomorphological Conditions of Arus River Sub-Watershed in Banyumas Regency, *5th International Conference on Community Development (AMCA 2018), Advances in Social Science, Education and Humanities Research, volume 231.*

Suwarno and Sutomo (2017) Model Analog Potensi Bencana Alam Longsorlahan Dengan Pendekatan Geomorfologikal Di Sub Das Kali Arus Kabupaten Banyumas, *Laporan Penelitian, LPPM Universitas Muhammadiyah Purwokerto*

Thapa, B.P., and Esaki,T. (2007) GIS-based Quantitative Landslide Hazard Prediction Modelling in Natural Hillslope, Agra Khola Watershed, Central Nepal, *Bulletin of the Department of Geology, Tribhuvan University, Kathmandu, Nepal,* **10**, 63 – 70.

Tareq H. Mezughi, Juhari Mat Akhir, Abdul Ghani Rafek and Ibrahim Abdullah (2010) Landslide Susceptibility Assessment using Frequency Ratio Model Applied to an Area along the E-W Highway (Gerik-Jeli), *American Journal of Environmental Sciences.* **7** (1), 43-50.

CATEGORIZATION OF IMPACT OF THE SELECTED VARIABLES FOR POTENTIAL BROWNFIELD REGENERATION IN THE CZECH REPUBLIC BY MEANS OF CORRESPONDENCE ANALYSIS

Kamila TURECKOVA[1] , Jan NEVIMA[1], Jaroslav SKRABAL[1], Pavel TULEJA[1]

ABSTRACT:

Brownfields are undesirable urbanistic heritage and their occurrence is associated with a number of negative effects, which our society tries to minimize repeatedly, both successfully and unsuccessfully. Especially in the context of the multi-perspective concept of sustainable development, the issue of brownfields is accentuated with the intention to reuse abandoned areas that have lost their original use and regenerate them in a way that enriches not only individual stakeholders but generally the whole society. Although each brownfield is unique within its set of partial characteristics, it is possible to determine by means of mathematical-statistical methods the key patterns that are important for brownfields in terms of their overall nature. The identification of these common patterns across a selected set of brownfields is important for establishing of general recommendations for their potential regeneration. In our paper, we proceeded from the analysis of 460 non-regenerated brownfields located in the Czech Republic, and by means of correspondence analysis we determined which categories most influence the potential brownfield regeneration from the perspective of a two-dimensional (stage) approach. Information on brownfields was taken from the publicly available database of the state-funded company the CzechInvest for 2018 and supplemented by authors with other relevant variables. The analysis of the data revealed factors that may have a major impact in the initial phase of the decision on potential brownfield regeneration, and at the same time factors that do not seem to be substantial for regeneration. The applicability of the results of our analyses creates space for better-targeted brownfield regeneration policies, especially in the area of specifications for calls for brownfield regeneration projects, their financial support, implementation of process innovations, etc.

Key-words: *Brownfield, Multiple Correspondence, Czech Republic, Factor, Regeneration.*

1. INTRODUCTION

Remote sensing offers a wide range of satellite imagery which is widely used in Brownfields represent abandoned and unused areas and buildings that are an integral part of urban consequences of human activities that can be transformed into a source of untapped development potential in both regional and national scope. Especially nowadays, when environmental problems are massively emphasized and many activities are assessed from the viewpoint of their acceptability for sustainable development, the urgency to deal with brownfields is repeatedly accentuated. The topic of brownfields thus becomes a relevant transdisciplinary topic for both professional and lay discussions across public and private sectors. Brownfields are currently perceived as a significant, albeit specific, ele-

[1] *School of Business Administration in Karvina, Silesian University in Opava, Univerzitni Nam. 1934/3, 733 40 Karvina, Czech Republic, tureckova@opf.slu.cz, nevima@opf.slu.cz, skrabal@opf.slu.cz, tuleja@opf.slu.cz*

ment of spatial development and spatial arrangements of their cultural-natural environments are easily connected to the economic development of regions and simultaneously to the dynamic improvement of quality of life of the population. (Turečková & Nevima, 2018).

The regeneration of these unused areas requires a systemic approach within the overall development of both national and regional economies and also individual local municipalities. Although each brownfield is specific, it is certainly possible to determine within this set of specific patterns such features that are more similar than others. The aim of our presented research is to find within the selected data of brownfields the influence of individual categories (internal patterns) that are dominant in the process of their potential regeneration. The mathematical-statistical method of correspondence analysis was used for data analysis and a total of five characteristics of 460 brownfields detected in the Czech Republic were examined. From this perspective, we realize that the results of the survey cannot be generalized but are relevant to a similar type of territory in East-Central Europe that has undergone the same major structural and economic changes over the last decade. In general, the methodology of research and interpretations of conclusions can be also used in the analysis of other data.

Identification of regeneration-relevant patterns of brownfields is primarily important for public sector bodies that are dealing with regional development, environmental protection and cohesion policy within the European Union. If we are aware of common patterns for non-regenerated brownfields, we will be able to target both financial and non-financial support and thus move closer to the possibility of their future regeneration.

According to estimations, there are around twelve thousands of sites and areas in the Czech Republic with a total acreage of almost 38 thousand hectares with various level of contamination (CzechInvest, 2008). These sites are relicts of consequences of artificially impeded development of economic restructuring before 1989 and in particular effects of structural changes in Czech economic space that occurred in the following years. Numerous reasons exist why we should be more engaged in the reuse of brownfields. One of the key reasons is the fact that brownfield regeneration contributes to sustainable urban development (Vráblík, 2009; Pakšiová, 2016), prevents land degradation (Turečková et al., 2018), reduces negative effects of suburbanization and urban sprawl (Jackson, 2002) and preserves local, temporal and urbanistic continuity of settlement, societal and environmental structures of given landscape (Turečková & Chmielová, 2019; Stober et al., 2018).

In the first part of the paper, the issue of brownfields was generally defined together with the relation of brownfields to their neighbourhoods. At the same time, brownfields in the Czech Republic were shortly introduced with a focus on the national brownfield database and its management. More theoretical focus on the research of brownfields can be found in the second chapter of the paper. In the next part, the object of the research was presented and a research proposal together with used methodology was described. The conclusion of the paper summarizes the results of the primary research. In this part, our findings are also discussed and several recommendations are formulated. We also added parts devoted to the practical usage of the results.

2. THE THEORETICAL FRAMEWORK OF THE STUDY

No matter what type of research is conducted, the very first item that has to be necessarily done is to embrace the nature of the researched problem. The topic of brownfields has been in general relatively well introduced by plenty of studies and scientific papers.

Despite all that it was necessary to familiarize ourselves with researches connected to the issue of factors of brownfield regeneration.

Brownfields in regional development might be considered twofold ways. Either as a barrier for regional development or as its source. A fundamental issue is that brownfields are typically bounded with a range of undesirable externalities that tend to even more strengthen the negative perception of brownfields. Brownfields cause minor or major problems, are a limitation for further development of built-up areas and reduce economic development, have a negative impact on the environment, are tied with social and economic impacts on population living in their proximity and have an unfavourable impact on the wider region where they are located (Dennison, 1998). These are the reasons why brownfields should be regenerated. As the authors of plenty of previous studies agree, brownfield regeneration is a site-specific process that is mirrored in the local socio-cultural context and it is a hard task to predict which sites have better chance to be regenerated. It is even more complicated to ensure that particular brownfield regeneration will be successful (Turečková et al., 2018).

A basic requirement of active approach towards brownfields when supporting regional development is to find a new use for abandoned sites and buildings that are instrumental for reduction of pressures on building of new developments on urban greenfields and keeping compactness of present built-up areas. Another supportive argument for reuse of abandoned areas might be found in undesirable effects connected to suburbanization processes and specifically to the problem of urban sprawl. Both mentioned phenomena lead to long term changes of the use of landscape, in other words, they primarily lead to the development of newly built-up areas as well as new technical infrastructure. Within inner parts of cities then remain brownfields, while in the suburban areas, development on greenfields is taking place. Sparse metropolitan development contributes to the increase of commuting distances, to increase of overall time spent by commuting and to the escalation of unjustified requirements for civic amenities and technical infrastructure. We must also mention connections to growing individualisation, loss of social cohesion, weakening of social capital and lack of interest of population on the governance of public matters as we are already aware in cases of socially and culturally homogenous suburban communities (Putman, 2000; Oliver 2001; Jackson, 2002 or Sýkora, 2003).

From the point of view of urbanism, unused sites might be understood as a restriction of disposable sources in community with a direct bond to the public budget. Reuse of such abandoned sites improves the quality of life of local population by means of reduction of criminality and occurrence of socially pathological phenomena, improves local environment, increases prices of the land, increases perceived value of properties in neighbourhoods and attracts entrepreneurs (Hollander et al., 2010 or Turečková et al., 2017). Interventions towards brownfield regeneration have to also respect different location of brownfields in different parts of communities, in so call concentric zones (Park & Burgess, 1925). There is an agreement in the literature that brownfields represent barriers in the contemporary structure of cities that limit urban development (Raco & Henderson, 2006). Based on the zonal model of cities, it can be assumed that in central – the most attractive parts of cities brownfield regeneration will be directed towards support of small entrepreneurship and housing. This hypothesis is in line with contemporary reurbanization tendencies (Buzar et al., 2007 or Kebza 2018).

Brownfields located in the proximity of the city centres that were during the dynamic development of cities incorporated into them, haven considerably variable use, for example for medium-sized entrepreneurs or as buildings where civic amenities are located (Krzyszt-

ofik et al., 2012). Brownfields in the margins of cities are suitable for large industrial sites and warehouses. In cases when preserving of brownfields in relatively original form is not desirable or possible (and no other suitable, effective alternative exists), a demolition of brownfield is necessary which is followed by decontamination of the site. New empty greenfield without particular use as the final product of brownfield regeneration is also possible (Johnson, Glover & Stewart, 2009 or De Sousa, 2000).

Regarding the potential for successful brownfield regeneration, several studies on this topic can be identified trying to explore the general characteristics that determine abandoned areas to be suitable for regeneration. For example, Frantal et al. (2015) in their study claims that a higher rate of brownfields regenerations positively correlates with their occurrence in densely populated and built-up areas, i.e. we assume that a more successful and faster brownfields regeneration process should take place within more populated municipalities. Lange & McNeil (2004) found that the regeneration of brownfields that are located near airports, near the city centres or rail stations is developing faster.

Martinat et al. (2018) warn that brownfield regeneration is closely interconnected with their perception by future users of particular sites and found out that the perception of regeneration significantly differs according to gender. Navratil et al. (2018) in their study documented that heritage preservation of sites is one of the factors of key importance when planning the regeneration project. In the study of Longo and Campbell (2007), successful regeneration is correlated with the prosperous region, i.e. those regions that are successfully developing and it is assumed that this includes positive impact on brownfield regeneration. Similar logic has been utilized also by other authors who argue that in regions where a higher potential of local development is measured, a higher probability exists that local brownfields will be more successfully regenerated. (Pizzol et at., 2016; Bartke et al., 2016 and Limasset et al., 2018). The specifics of brownfield regeneration in the post-communist space are widely discussed by Osman et al. (2015). Among other key aspects of brownfield regeneration belong existence of strong potential markets, long-term vision, strong branding, strong partnerships, integrated development, and getting infrastructure into place (Dixon et al., 2011).

The aforementioned brownfield regeneration factors can also be easily linked to the existence of short-term and long-term business cycles. There is no doubt that in times of economic expansion there is a significant recovery of abandoned and neglected areas, while in times of recession, economic restructuring and disruptions, the number of brownfields is increasing (Rink et al., 2012 or Dixon, 2006). The process of successful brownfield regeneration can also benefit from the effects of the concentration of sectoral economic activities in the given area (Turečková, 2015). On the contrary, contamination and environmental burden of brownfields is a major problem for brownfield regeneration (Hartley et al., 2012 or Doick, 2009).

The process of brownfield regeneration can be positively influenced through both active and passive activities of public institutions. Within the framework of undesirable burdens and barriers to brownfield regeneration, subsidy programs for financial support (McCarthy, 2002 or Bartke & Scharze, 2015) can be offered as part of economic policy at central and local levels, and some of them can be used in the public sector (Schädler et al., 2011). Raising awareness about the issue of brownfields by main of their inclusion in public databases might be also mentioned (Otsukaan, Timothy & Hirokazu, 2013).

3. METHODOLOGY AND DATA

The methods of data analysis accommodated reflect the aim of our research and the availability of data. The starting point of our considerations about this research was publicly available data on brownfields in the Czech Republic that were included in the public database of the state-funded company the CzechInvest in 2018 (the company subordinated to the Ministry of Industry and Trade of the Czech Republic). Our set of non-regenerated brownfields included 460 abandoned sites with which 5 characteristics were analysed due to the characteristics of the data. These were assumed to be key characteristics for brownfield regeneration: (1) the size of particular brownfield (in hectares), (2) ownership of brownfield, (3) contamination of the site, (4) previous use. These four characteristics were supplemented by (5) the distance of individual brownfield to the municipality of extended powers (so-called small district) where the given area administratively belongs (in km). This characteristic was measured manually. It needs to be mentioned that for the brownfields to be listed in the CzechInvest database, the owners need to give their consent. Thus, our set contains approximately 5% of known brownfields in the Czech Republic. However, there is no doubt that the generally used number of 12,000 abandoned sites is underestimated. General information on the analysed set of non-regenerated brownfields is provided in **Table 1**.

Correspondence analysis of data was employed to analyse the brownfield data (460 entries in total). This analysis represents a popular graphic technique used to analyse relationships between categories of one or more variables in contingency tables. By using correspondence analysis, it is possible to describe associations of nominal or ordinal variables and to obtain a graphical representation of connections in multidimensional environ.

Rencher (2002) emphasizes that the basis for the creation of the subjective (correspondent) map are so-called latent variables. The positions of the points in the subjective map directly express the associations, the distances between the points (or, in other words, the distance of the row and column profiles) can be transferred to a two-dimensional Euclidean space in which the points correspond to the individual categories. Hebak et al. (2007) report that correspondence analysis depicts correspondence categories of individual variables and provides a common picture of row and column categories in the same dimensions. Unlike most other multivariate methods, correspondence analysis allows processing of categorized non-metric data as well as non-linear relationships. It represents an analogy of factor analysis, but instead of factors, the influence of individual categories, their mutual similarity or associations with categories of other variables are monitored (Rencher, 2002). Correspondence analysis and factor analysis are therefore rightly perceived as related methods that can identify at first glance hidden structures in data. According to Hebak et al. (2007), correspondence analysis aims to reduce multidimensional vector space of row and column profiles while preserving the maximum information contained in the original data. In the case of our primary research, we have used the so-called multiple correspondence analysis.

In subjective mapping, two-dimensional (plane) or maximum three-dimensional mapping of distances in Euclidean space is most often used. Pearson's chi-square statistics are used more often than the Euclidean distance. This approach was also selected in this case. Near row points indicate rows that have similar profiles across the row, nearby column points indicate columns with similar profiles down over all rows. Row points that are in proximity to column points represent combinations that appear to be expected more fre-

quently than in an independent model in which row categories are not related to column categories (Meloun et al., 2005).

The scattering of points can be assessed according to the inertia indicator, which corresponds to the weighted average chi-square by the distance of the row (or column) profiles from its diameter (Meloun et al., 2005).

Table 1.

Characteristics of selected brownfields in the Czech Republic

NUTS 3 Region	Number of brownfields	Size (hectares)		Owner-ship (public)	Contami-nation (yes)	Previous use	Distance (km)	
		mean	median				mean	median
Karlovy Vary	32	6.74	1.34	25%	16%	4(11); 2(7); 3(5);6(5); 1(4); 5(0)	2.02	1.25
Plzeň	24	4.30	1.87	29.2%	25%	4(11); 1(7); 3(4); 2(1); 6(1); 5(0)	1.78	0.68
Ustí	62	3.36	1.13	32.3%	44%	4(25); 2(10); 1(9); 3(9); 6(6); 5(3)	1.90	1.2
South Bohemian	33	3.23	0.84	15.2%	9%	1(12); 4(10); 2(7); 3(3); 6(1); 5(0)	1.77	0.9
Vysočina	24	1.22	0.21	25%	17%	1(8); 4(7); 2(6); 3(3); 6(0); 5(0)	4.68	0.78
Central Bohemian	30	25.8	1.49	16.7%	10%	4(16); 2(7); 1(4); 3(2); 5(1); 6(0)	4.31	1.55
Pardubice	28	2.36	0.62	46.4%	32%	4(10); 1(9); 2(5); 3(4); 6(0); 5(0)	2.27	0.95
Hradec Králové	24	4.59	1.56	20.8%	29%	4(11); 2(7); 1(2); 4(2); 5(1); 6(1)	1.34	1.55
Liberec	59	3.08	1.46	29.5%	46%	4(29); 2(15); 1(9); 3(5); 6(1); 5(0)	1.83	1.30
Moravian-Silesian	40	5.06	1.89	27.5%	17.5%	4(16); 3(8); 1(7); 2(7); 6(2); 5(0)	3.10	2.05
Olomouc	36	4.56	0.55	5.7%	3%	4(14); 2(10); 1(5); 3(3); 6(3); 5(0);	3.34	1.7
Zlin	15	1.17	0.66	6.7%	0%	4(8); 1(4); 2(2); 3(1); 6(0); 5(0)	1.46	1.1
South Moravian	52	3.57	1.35	26.9%	12%	4(17); 1(13); 2(11); 3(6); 6(4); 5(1)	1.88	1.01
Prague	1	0.98	0.98	0%	0%	4(1)	11.6	11.6
Total	**460**	*mean*	*span*	*share in %*	*share on all*	*most often*	*mean*	*span*
		5.06	**0.0234 - 646**	**25%**	**23%**	*industrial brownfields (188)*	**2.40**	**0.04 – 86.5**

Source: CzechInvest, 2018; own survey.
Note: in previous use: (1) agricultural brownfields, (2) brownfields after civic amenities, (3) military brownfields, (4) industrial brownfields, (5) post-mining brownfields and (6) other brownfields.

The singular value and the inertia correspond to the eigenvalue in the principal component analysis. It represents the measure of variability between profiles explained by a given dimension of solution or a given category. According to this step, we determined the number of dimensions required. Profile differences, measured by chi-square statistics, are reflected in the graph as the distance between items of the same variable. The spacing between items of different variables are images of standardized residues at the intersection of items. Meloun et al. (2005) measure besides the object comparability also the completeness

of data matrix. The solution is based on a matrix of standardized residues, which can be created using one of the standardization methods.

The selection of normalization method depends on the preferences of the researcher as well as the assessment of the degree of variability achieved. When preferring relationships between row categories, the analysis of row profiles is used, while the preference of column categories is based on the analysis of column profiles.

The SPSS Statistics 15.0.1 for Windows software was used to process the data, which represents a modern system for describing and visualizing data relationships. The advantage of the software in data processing is the existence of so-called codebook, which contains information about the data matrix (names and descriptions of variables, descriptions of values, missing values) and which makes the subsequent statistical analyses easier for the user.

4. RESULTS

The data file was divided into two dimensions (areas) using correspondence analysis (see **Figure 1**). The picture itself shows how the resulting data was dimensionally arranged in the cross-section. How do we read the findings? The first dimension in our case consists of three categories of influence of selected variables for potential brownfield regeneration. These are size, ownership and contamination. This is illustrated in **Table 2**, where Eigenvalues are greater than 1 and thus have a significant impact on the data. In the second dimension and from the regeneration point of view, the category of influence of selected variables is less significant (it is the previous use of brownfields and distance from the centre of the municipality).

Table 2.

Categorization of influence of selected variables for potential regeneration (Correlations Transformed Variables).

Variable	Size	Ownership	Contamination	Previous use	Distance
Area	1.000	0.068	0.168	0.162	0.133
Ownership	0.068	1.000	0.092	0.483	0.054
Contamination	0.168	0.092	1.000	0.020	-0.020
Previously	0.162	0.483	0.020	1.000	0.161
Distance	0.133	0.054	-0.020	0.161	1.000
Dimension	1	2	3	4	5
Eigenvalue	1.616	1.096	1.017	0.781	0.491

Source: own survey, 2019 (SPSS 15.0.1).

The rate of variability in both dimensions reached an average of 30%, which can be considered a satisfactory result. In this sense, it should be noted that we tried to identify the hidden structures of the data which would not be possible to conduct employing other methods. In terms of the quality of interpretations, it needs to be mentioned that we are dealing with data when each region (administrative unit) in the Czech Republic has a different number of brownfields, and therefore the categories of impact on possible brownfield regeneration may vary from our findings.
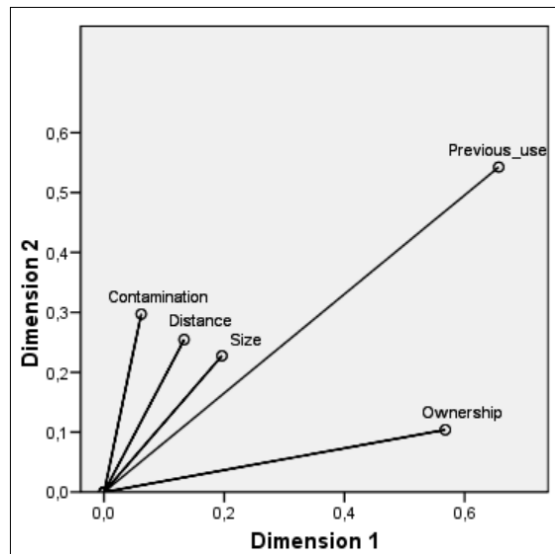
Fig. 1. Principal normalization of variables (discrimination measures).
(Source: own survey, 2019 (SPSS 15.0.1)).

5. DISCUSSION AND CONCLUSIONS

Our knowledge of the characteristics and features of brownfields is a basic prerequisite for their possible and appropriate regeneration. When we reveal the factors, features or categories of influence that are common to a given set of abandoned sites, the accommodation of public policy instruments can be more targeted in this direction. In our case, three categories of influence of selected variables in terms of size, ownership and contamination of brownfields were analysed by means of the technique of correspondence analysis. The factors of previous utilization and distance from the municipality centre are not so crucial in the first phase of the decision on potential brownfield regeneration.

If the results of correspondence analysis to partial characteristics of the surveyed brownfields are correlated, then in terms of the size of the abandoned areas an area around 1.14 hectares (average of the median of all regions) may be considered as optimal, while in terms of the ownership it should be privately owned brownfield (70%)[2] that is free of contamination (77%). The public sector, which decides to reflect these findings in order to minimize the number of brownfields in its territory, might consider the creation of financial and non-financial instruments that will be more likely targeted on small-sized brownfields owned by private entities, offering them support for remediation of contaminations to support their regeneration. These conclusions and recommendations, based on the analysed brownfield data, are following specifics of brownfields located in the Czech Republic. On the other hand, the methodological and interpretative transferability of the above-described research procedure to other relevant sets of brownfields is generally possible.

---

[2] *There are other 5% of brownfields in public private ownership.*

To sum up, in the context of the existence of brownfields it seems a priority to find their new, beneficial use. If we accept this logic, individual brownfields must be considered to have the potential for further development. Together with their regeneration, the growth of economic and social activities and the increase of the attractiveness of the territory for all stakeholders is expected. On the other hand, leaving abandoned sites without trying to find alternative uses prevents further development of built-up areas, adversely affects the environment and society, impedes economic growth and has an overall adverse impact on the entire wider administrative region.

ACKNOWLEDGEMENT

R E F E R E N C E S

Bartke, B. & Schwarze, R. (2015) No perfect tools: Trade-offs of sustainability principles and user requirements in designing support tools for land-use decisions between greenfields and brownfields. *Journal of Environmental Management*, 153, 11-24.

Bartke, S., Martinat, S., Klusacek, P., Pizzol, L., Alexandrescu, F., Frantál, B., Critto, A. & Zabeo, A. (2016) Targeted selection of brownfields from portfolios for sustainable regeneration: User experiences from five cases testing the Timbre Brownfield Prioritization Tool. *Journal of Environmental Management*, 184, 94-107.

Buzar, S., Ogden, P., Hall, R., Haase, A., Kabisch, S. & Steinfiihrer, A. (2007) Splintering urban populations: emergent landscapes of reurbanisation in four European cities. *Urban Studies*, 44 (4), 651-677.

CZECHINVEST (2008). Národní strategie regenerace brownfieldů. Available from: http://www.cityinvestczech.cz/data/files/strategie-regenerace-vlada-1079.pdf [Accessed February 2018].

De Sousa, C. A. (2000) Brownfield redevelopment versus greenfield development: A private sector perspective on the costs a risks associated with brownfield redevelopment in the Greater Toronto Area. *Journal of Environmental Planning a Management*, 43 (6), 831-853.

Dennison, S. M. (1998) *Brownfields Redevelopment*, Rockville: Government Institutes.

Dixon, T. (2006) Integrating sustainability into brownfield regeneration: Rhetoric or reality?–An analysis of the UK development industry. *Journal of Property Research*, 23 (3), 237-267.

Dixon, T., Otsuka, N. & Abe, H. (2011) Critical success factors in urban brownfield regeneration: an analysis of 'hardcore'sites in Manchester and Osaka during the economic recession (2009–10). *Environment and Planning A,* 43 (4), 961-980.

Doick, K. J. (2009) Understanding success in the context of brownfield greening projects: The requirement for outcome evaluation in urban greenspace success assessment. *Urban Forestry & Urban Greening*, 8 (3), 163-178.

Frantal, B., Greer-Wootten, B., Klusacek, P., Krejci, T., Kunc, J. & Martinat, S. (2015) Exploring spatial patterns of urban brownfields regeneration: The case of Brno, Czech Republic. *Cities*, 44, 9-18.

Hartley, W., Dickinson, N. M., Riby, P. & Shutes, B. (2012) Sustainable ecological restoration of brownfield sites through engineering or managed natural attenuation? A case study from Northwest England. *Ecological Engineering*, 40, 70-79.

Hebák, P., Hustopecký, J., Pecáková, I., Průša, M., Řezanková, H., Svobodová, A. & Vlach, P. (2007) *Vícerozměrné statistické metody (3)*. Praha: Informatorium.

Hollander, J. B., Kirkwood, N. & Gold, J. L. (2010) *Principles of brownfield regeneration: clean-up, design, a reuse of derelict land*, Washington: Isla Press.

Jackson, J. (2002) Urban Sprawl. *Urbanismus a území rozvoj*, 5 (6), 21-28.

Johnson, A. J., Glover, T. D. & Steward, W. (2009) One person´s trash in another person´s treasure: The public place-making of "Mount Trashmore". *Journal of Park a Recreation Administration*, 27 (1), 85-103.

Kebza, M. (2018). The development of peripheral areas: The case of West Pomeranian Voivodeship, Poland. *Moravian Geographical Reports*, 26(1), 69-81.

Krysztofik, R., Runge, J. & Kantor-Pietraga, I. (2012) Paths of environmental a economic reclamation: the case of post-mining brownfields. *Polish Journal of Environmental Studies*, 21 (1), 219-223.

Lange, D. A., & McNeil, S. (2004) Brownfield development: Tools for stewardship. *Journal of Urban Planning and development*, 130 (2), 109-116.

Limasset, E., Pizzol, L., Merly, C., Gatchett, A. M., Le Guern, C., Martinat, S., Klusacek, P. & Bartke, S. (2018) Points of attention in designing tools for regional brownfield prioritization. *Science of The Total Environment*, 622, 997-1008.

Longo, A. & Campbell, D. (2007) What are the determinants of brownfields regeneration? An analysis of brownfields in England. *In Proceedings of the conference on the science and education of land use: A transatlantic, multidisciplinary and comparative approach*, Washington DC.

Martinat, S., Navratil, J., Hollander, J. B., Trojan, J., Klapka, P., Klusacek, P. & Kalok, D. (2018) Re-reuse of regenerated brownfields: Lessons from an Eastern European post-industrial city. *Journal of Cleaner Production 2018*, 188, 536-545.

McCarthy, L. (2002) The brownfield dual land-use policy challenge: reducing barriers to private redevelopment while connecting reuse to broader community goals. *Land and Use Policy*, 19 (4), 287-296.

Meloun, M., Militký, J. & Hill, M. (2005) *Počítačová analýza vícerozměrných dat v příkladech*. Praha: Academia.

Navratil, J., Krejci, T., Martinat, S., Pasqualetti, M. J., Klusacek, P., Frantal, B. & Tochackova, K. (2018). Brownfields do not "only live twice": The possibilities for heritage preservation and the enlargement of leisure time activities in Brno, the Czech Republic. *Cities*, 74, 52-63.

Oliver, J. E. (2001) *Democracy in Suburbia*, Princenton: Princenton Uversity Press.

Osman, R., Frantal, B., Klusacek, P., Kunc, J. & Martinat, S. (2015) Factors affecting brownfield regeneration in post-socialist space: The case of the Czech Republic. *Land Use Policy*, 48, 309-316.

Pakšiová, R. (2016) Reporting of non-financial information on companies in the context of sustainable development in Slovakia. *In: Účetnictví a auditing v procesu světové harmonizace. Mezinárodní vědecká konference.* Praha: Vysoká škola ekonomická v Praze, Nakladatelství Oeconomica, 153-160.

Park, R. E. & Burgess, E. W. (1925) *The City*. Chicago: University of Chicago.

Pizzol, L., Zabeo, A., Klusacek, P., Giubilato, E., Critto, A., Frantal, B., Martinat, S, Kunc, J., Osman, R. & Bartke, S. (2016) Timbre Brownfield Prioritization Tool to support effective brownfield regeneration. *Journal of Environmental Management*, 166, 178-192.

Putman, R. (2001) *Bowling Alone*. The Collapse and Revival of American Community. New York: Simon and Schuster.

Raco, M. & Henderson, S. (2006) Sustainable urban planning and the brownfield development process in the United Kingdom: Lessons from the Thames Gateway. *Local Environment*, 11 (5), 499-513.

Rencher, A. (2002) *Methods of Multivariate Analysis*. New York: Wiley.

Rink, D., Haase, A., Grossmann, K., Couch, C. & Cocks, M. (2012) From long-term shrinkage to re-growth? The urban development trajectories of Liverpool and Leipzig. *Built Environment*, 38 (2), 162-178.

Schädler, S. et al. (2011) Designing sustainable and economically attractive brownfield revitalization options using an integrated assessment model. *Journal of Environmental Management*, 92 (3), 827-837.

Stober, D., Brkanić, I., & Lončar, L. (2018). The preferences of residents and tourists for culturaland architectural heritage in a rural landscape: The case of Zlatna Greda, Croatia. *Moravian Geographical Reports*, 26(4), 285-297.

Sýkora, L. (2003) *Suburbanizace a její společenské důsledky*. Praha, Sociologický ústav AV ČR.

Turečková, K. & Chmielová, P. (2019) Regenerace brownfieldů v odvětví kultury v České republice. *In: XXII. mezinárodní kolokvium o regionálních vědách.* Brno: MU ESF Brno, s. 657-664. ISBN 978-80-210-9268-6

Turečková, K. & Nevima, J. (2018) Perceiving the impact of brownfields on the real estate prices: a case study from four locations in the Czech Republic. *Geographia Technica*, 13 (2), 138-151.

Turečková, K. (2015) Sectoral industrial agglomeration and network externalities: concept of ICT sector. *In: Proceedings of 5th International Conference on Applied Social Science.* USA: IERI, 50-55.

Turečková, K., Martinát, S., Škrabal, J., Chmielová, P. & Nevima, J. (2017) How local population perceive impact of brownfields on the residential property values: some remarks from post-industrial areas in the Czech Republic. *Geographia Technica*, 12(2), 150-164.

Turečková, K., Nevima, J., Škrabal, J. & Martinát, S. (2018) Uncovering patterns of location of brownfields to facilitate their regeneration: Some remarks from the Czech Republic. *Sustainability*, 10 (6), 224-234.

Vráblík, P. et al. (2009) Metodika revitalizace území pro hospodářský, sociální a environmentální rozvoj v postižených regionech. Available from: http://fzp.ujep.cz/projekty/wd-44-07-1/dokumenty/dc03/DC003_Metodika_revitalizace_uzemi.pdf [Accessed February].

THE LAND SURFACE TEMPERATURE EVOLUTION (LST) USING LANDSAT SCENES. CASE STUDY: THE INDUSTRIAL PLATFORM SĂVINEŞTI

Cosmina-Daniela URSU[1]

ABSTRACT:

During the communism, the accent of development was put mainly on industry. This is also the case of The Industrial Platform Săvineşti, from Neamţ county, which assured two major productions: textile fibers and chemical fertilizers. After the fall of the regime, the platform was divised and some of the new owners have sold all the equipments, have demolished the buildings, leaving the place barren. In the present, only a few of the old factories still work, and new stakeholders started their businesses. The study aims to show how the land surface temperature (LST) evolved in association with the events that followed from the flowering period of the factory. Three summer months from different years (1991, 2008 and 2018) where taken into consideration and LST was calculated based on Landsat scenes from missions 5-TM and 8-OLI. In order to make the whole process faster, two models were constructed using ArcMap extesion Model Builder. Besides the land surface temperature, there were calculated another two indices: Normalized Difference Vegetation Index (NDVI) and Normalized Difference Moisture Index (NDMI), which offer additional arguments to the changes that took place on the platform. The purpose of the study is to show how land surface temperature changes depending on the use of the territory, thus the importance of remote sensing being emphasised.

Key-words: *Land cover changes, Romanian industry, Model Builder*

1. INTRODUCTION

In the communism era, the industry was the economic field which was predominantly developped. The industrial Platform from Săvineşti began to function in 1959, being described in literature of that time as "the first and most important yarn factory from the country which produced technical yarns for various uses (textile fibers, special yarns, mechanical sieves, industrial fishing gear, belts and tapes). Only the textile fibers production equals the annual wool production of over 4 million sheep" (Maria Mihail, 1977, p. 201-202). The Platform covered an area of approximately 185 ha and it was composed of: Synthetic yarn and fiber plant, Azochim Chemical Fertilizer Plant and a research institute. After the fall of the communist regime, in 1990, the platform was divised in independent structures. Some of them (Yarn Factory) were taken by foreign companies, others like Azochim was bought by Romanian business men. Numerous machines were sold, the old halls were demolished and massive layoffs were made. According to some interviews taken by the press from former workers, in 2004, there were only 350 employees, as opposed to 1990, when 8000 people worked in the yarn factory[1]. **Figures** number **1** and **2** show the differences before the fall of the communism and after.

---

[1] *Babeş Bolyai University, Faculty of Geography, 400006, Cluj-Napoca, Romania,*
 ursucosmina@yahoo.com
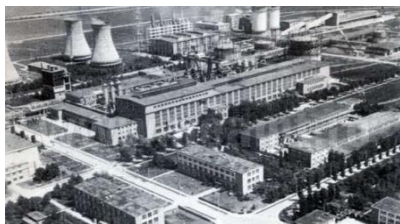
Fig. 1. The Factory of synthetic fibers Săvineşti-1959²

Fig. 2. The Industrial Platform - 2015 (image taken with the drone³)

Remote sensing has prooved its usefullness ever since the beginnings. Landsat is one of the oldest missions which has the advantage of releasing many images free of charge for any type of users. Landsat scenes are often used for various types of analysis: tracking forest changes (Furtuna et al., 2016, Furtuna, 2017), detection of areas affected by storms (Furtuna et al., 2018;), detection of the old scattered windthrows (Haidu et al., 2019).

For the climate domain, the thermal sensor from Landsat allow the calculation of Land Surface Temperature (LST) which is an index that shows the ground temperature recorded by the satellite thermal sensor (Rajeshwari and Mani, 2014). This should not be confused with the air temperature, the two having different values, but being well correlated. In most scientific articles (Zhang & Sun, 2008; Kim, 2009; Choudhury & Das Arijit Das, 2019) LST is used in the determination of urban heat islands (Urban Heat Islands-UHI). The studies mainly analyze urban spaces, less industrial areas, although "the presence of impervious surfaces such as buildings, roads, industrial farms increase the absorption of short radiations and diminish the loss of energy due to the emission of long wave radiation" (Oke, 1976, quoted by Choudhury & Das Arijit Das, 2019). In a case study conducted for a Chinese mining city (Rao et al., 2018) LST correlated with the type of industrial activity from each mining area. The results show that LST differs according to the industrial activity practiced. Other authors have described the link between land use and LST (Voogt & Oke, 2003; Gage & Cooper, 2017), especially analyzing the consequences of the urbanization process in increasing LST (Owen et al., 1998; Small, 2006; Guo et al., 2012).

The study aims to analyze the evolution of land surface temperature on the Platform, using Landsat scenes. The hypothese is the following: the temperature is influenced by the cessation of industrial activity in certain areas of the platform. Moreover, in order to sustain the results of LST, Normalized Difference Vegetation Index (NDVI) and Normalized Difference Moisture Index (NDMI) were added. The analys is performed using ArcMap 10.6. For making the process faster, two models were constructed using Model Builder. After every calculation, the results were compared between years, in order to emphasize the differences.

2. STUDY AREA AND DATA

The Industrial Platform is located in the central area of the Săvineşti Commune, which is part of Neamţ County (**Fig. 3**). For modeling land surface temperature, Landsat scenes from Landsat Collection 1-Level 1 were used, downloaded from USGS Earth Explorer. For each image additional criteria (the cloud cover under 10% and the time of the day) were specified. The three images were chosen in the summer in order to avoid great cloud cover, mist, snow and other natural phenomena.Details about each image could be found in **Tab.1**
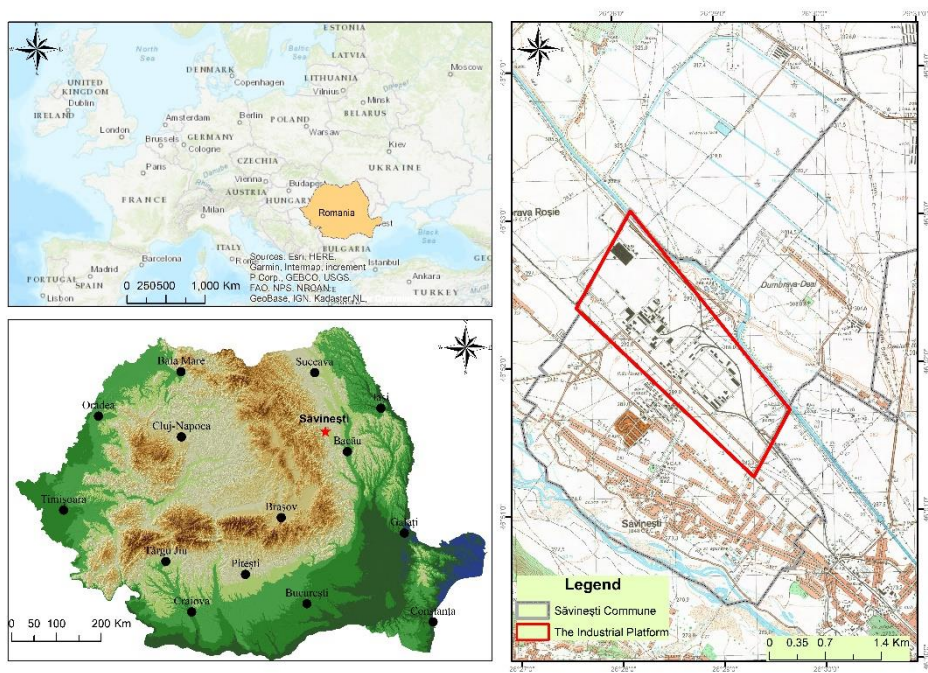
Fig. 3. The localization in the territory of Săvineşti commune.

Details about data.

No.	Path	Row	Date	Satellite
1	183	27	8.08.1991	5
2	183	27	22.08.2008	5
3	183	27	18.08.2018	8

3. METHODOLOGY

Before use, the images were preprocessed using ERDAS version 2014. Operation like Histogram equalization, Haze and noise reduction were performed in order to improve the quality of the image.

Arc Map 10.6.1 was used for land surface temperature estimation. From Landsat 5-TM, the band 6 (10.40-12.50 micrometers) was used, and from Landsat 8-OLI, band 10 Thermal Infrared (10.60 - 11.19 micrometers).

The first step was to reproject the bands of each image from their default projection system (WGS 1984) to Stereo 1970, the projection system used in the country level. The next step was cutting the images after the limit of the case study.

The area includes not only the territory of the platform, but also the surroundings in order to see the temperature differences.

3.1 LST using Landsat 5-TM

The methodology is different based on Landsat mission. Thus, for Landsat 5 the first parameter calculated was the spectral radiance, when the pixells are converted from digital numbers (DN) to units of absolute radiance, using the following formula:

$$L_\lambda = (\frac{LMAX_\lambda - LMIN_\lambda}{QCALMAX - QCALMIN}) \cdot (\text{QCAL-QCALMIN}) + LMIN_\lambda \qquad (1)$$

where:
Lλ = Spectral Radiance at the sensor's aperture in watts/(meter squared * ster * μm)
QCAL = the quantized calibrated pixel value in DN
LMINλ = the spectral radiance that is scaled to QCALMIN in watts/(meter squared * ster * μm)
LMAXλ = the spectral radiance that is scaled to QCALMAX in watts/(meter squared * ster * μm)
QCALMIN = the minimum quantized calibrated pixel value (corresponding to LMINλ) in DN
QCALMAX = the maximum quantized calibrated pixel value (corresponding to LMAXλ) in DN = 255

The next step is calculating the effective satellite visualized temperature of the Earth-atmosphere visual system, which in the case of Landsat 5-7 images corresponds to the land surface temperature (LST) (Chander and Markham, 2003). By adding -273.15, the conversion from Kelvin to Celsius degrees is made. The formula is:

$$T = \frac{K2}{\ln(\frac{K1}{L_\lambda}+1)} - 273.15 \qquad (2)$$

Where:
T = Effective at-satellite temperature in Kelvin
K2 = Calibration constant 2 from metadata fille
K1 = Calibration constant 1 from metadata fille
L = Spectral radiance in watts/(meter squared *ster*μm)

3.2 LST using Landsat 8

In the case of Landsat 8 scenes, the methodology has a higher degree of complexity. The first step is the conversion of the digital numbers into radiance units, using the next ecuation (LANDSAT 8 (L8) data users handbook, 2019):

$$L\lambda = ML*Qcal + AL \qquad (3)$$

Where:
Lλ = Spectral radiance (W/(m2 * sr * μm))
ML= the band-specific multiplicative rescaling factor (RADIANCE_MULT_BAND_n from metadata fille).

AL = the band-specific additive rescaling factor (RADIANCE_ADD_BAND_n din metadate). Qcal = the Band 10 image.

The second step supposes the conversion of spectral radiance to the the actual temperature visualized by the satellite (LANDSAT 8 (L8) data users handbook, 2019):

$$T = \frac{K2}{\ln(\frac{K1}{L_\lambda}+1)} \qquad (4)$$

Where:
T = Effective at-satellite temperature in Kelvin
K2 = Calibration constant 2 (K2_CONSTANT_BAND_n from metadata fille)
K1 = Calibration constant 1 (K1_CONSTANT_BAND_n from metadata fille)
L_λ = Spectral radiance in watts/ (Watts/(m² * sr * μm))

Next, NDVI has to be calculated in order to find out the proportion of vegetation (Pv):

$$NDVI = NIR - R/NIR + R \qquad (5)$$

Where:
NDVI= Normalized Difference Vegetation Index
NIR= Near infrared band
R= Red band

The proportion of vegetation (Pv) could be calculated using the following formula (Sobrino et al., 2004):

$$Pv = (NDVI - NDVImin/NDVImax - NDVImin)^2 \qquad (6)$$

After this, the surface emissivity can be derived (Sobrino et al., 2004):

e=0.004*Pv + 0.986

All this steps have as a result the final formula which gives the Land Surface Temperature (Avdan and Jovanovska, 2016):

$$LST = BT/1 + w * (BT/p) * Ln(e)) \qquad (7)$$

Where:
BT – Effective at-satellite temperature
W - radiation wavelength emitted (band 10)
e – surface emissivity
p= 14380

3.3 Model Builder

All this calculations were implemented using Raster Calculator from Arc Toolbox (**Fig.** 5).
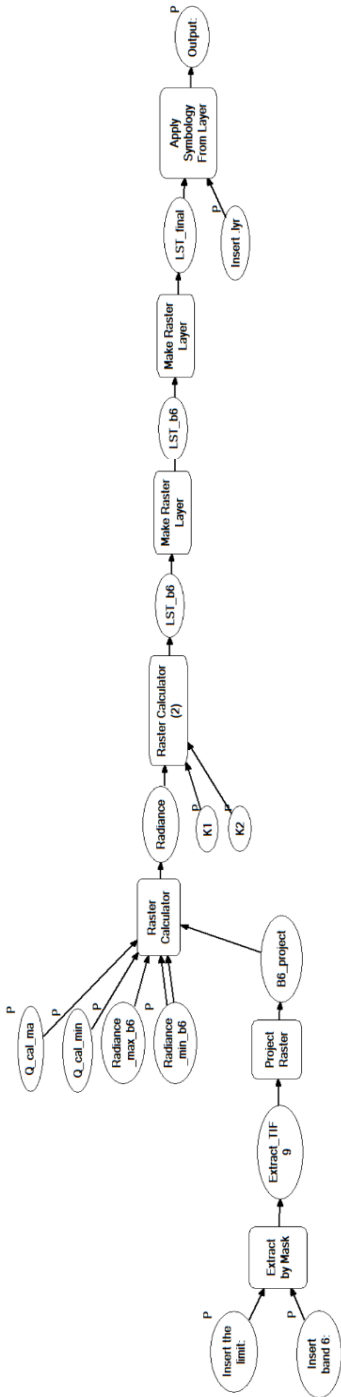
Fig. 4 Model Builder for Landsat 5 (*Source: author*)
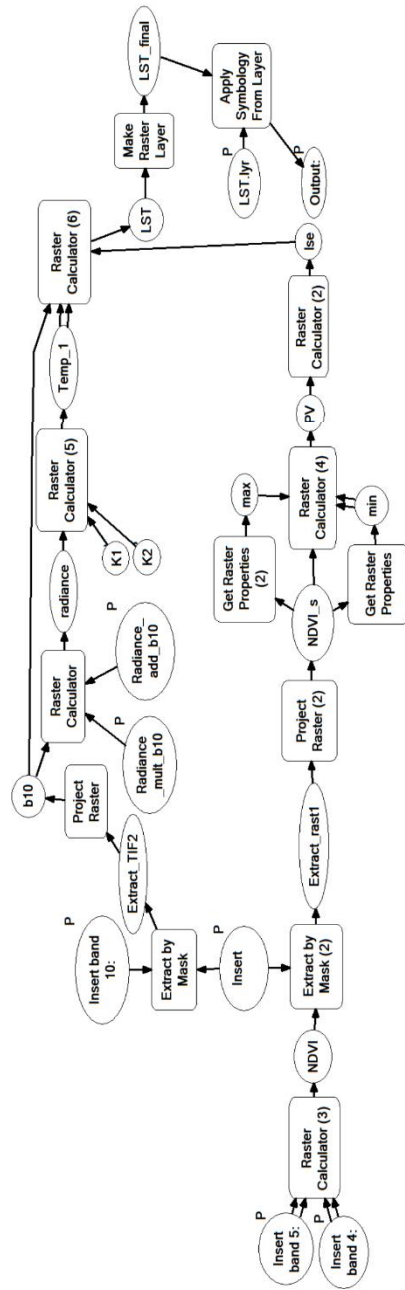
Fig. 5 Model Builder for Landsat 8 (*Source: author*)

(ArcMap 10.6). But due to the fact that there might be mistakes in writing the formulas (like misplacing a space or forgetting a digit) if the process must be repeated for many Landsat scenes, automatic models were constructed with Model Builder from ArcMap 10.6 soft.

For Landsat 5, the model (**Fig. 4**) was constructed of six functions: *Extract by mask* (which cuts the study area from the larger scene), *Project Raster* (converts the scene into the national projection system), *Raster Calculator* (where the user has to introduce the parameters written in the metadata fille for the first formula (1), and then for the second one (2), *Make Raster Layer* and *Apply Symbology from Layer* are used to assign a specific legend for the result. The model calculates LST in just seconds and represent it with the colour ramp choosen by the user.

Given the fact that LST using Landsat 8 requires more operations than Landsat 5, an automatic model is more than needed. For this one (**Fig. 5**), its complexity reside in larger number of functions which have to be applied: *Extract by Mask* and *Project Raster* (have the same function as for Landsat 5 model), *Raster Calculator* (is used to calculate NDVI and other formulas as well- 3-7), *Get Properties* (is used to select the minimum and maximum value of NDVI), *Make Raster Layer* and *Apply Symbology from Layer* (are used to establish the colour ramp for the result).

3.4 NDVI and NDMI calculation

For NDVI retrieval, bands 3 and 4 were used for Landsat 5 and bands 4 and 5 for Landsat 8 scenes (see the formula above).

Normalized Difference Moisture Index (NDMI) was calculated using bands 4 and 5 for Landsat 5 and bands 5 and 6 for Landsat 8 scenes. The formula is:

$$NDMI = NIR - IR/NIR + IR$$

Where: NIR- Near infrared band; IR- infrared band.

4. RESULTS AND DISCUSSIONS

After applying the formulas, the Land Surface Temperature was retrieved for the three moments taken into account (**Fig. 6**).

a. 8.08.1989   b. 22.08.2008   c. 18.08.2018
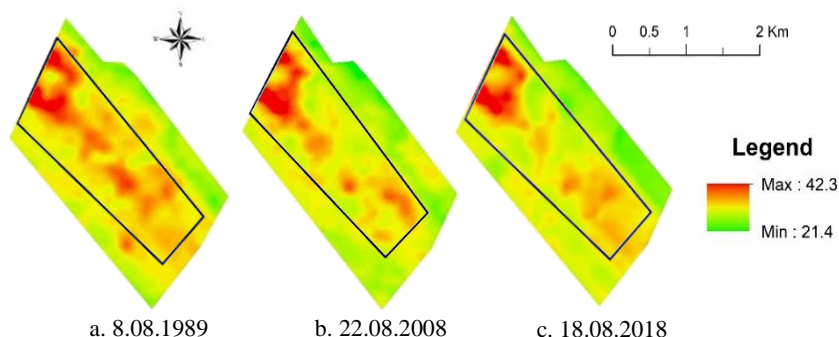
Fig. 6. Land Surface Temperature.

At the first look, the west area had high temperatures, no matter the year of the image. This can be explained by the fact that in that area were located the factories that lasted until today and in that area, other companies have installed after the buildings were left. The central area of the platform suffered severe changes. The temperature went down from 1989 till 2018 as a result of changing the land use. After the existing buildings were destroyed, the soil recovered in time and vegetation started to reclaim its territory. This statement can be sustained by the Google Earth images (**Fig. 7**) which show the evolution of the area.

| 8.06.2011 | 14.09.2014 | 14.09.2017 |
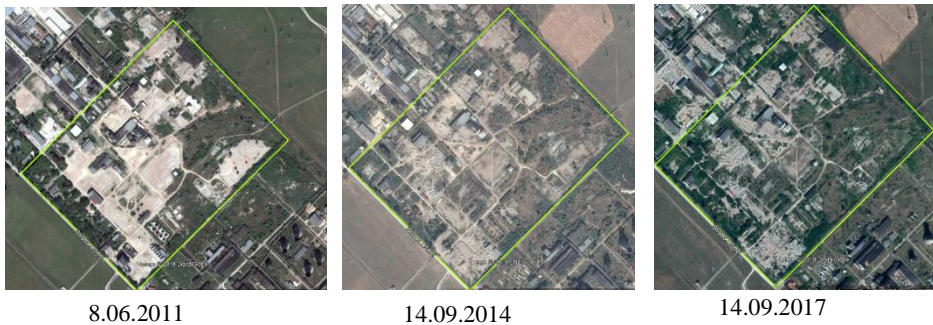
Fig. 7. Evolution of the central area (Source: GoogleEarth).

The east area had fluctuations over the time because there is located Azochim Chemical Fertilizer Plant, which functioned with interruptions. Another observation is focussing on the peripheral areas of the Platform. As it can be remarked, the temperatures on the industrial site are higher that the ones from the surrounding area, like a heat island in the middle of agricultural land. In order to notice better the differences between the three moments, the results have been transformed by lowering opperations. Thus, the results show that the differences between the 2018-2008 are higher than the ones from 2018-1991 because most changes had happened after 2008, as we can see in **Fig. 8**. In both cases, in the south-east and west of the platform were the major changes, due to the interruption of industrial activity in some periods.
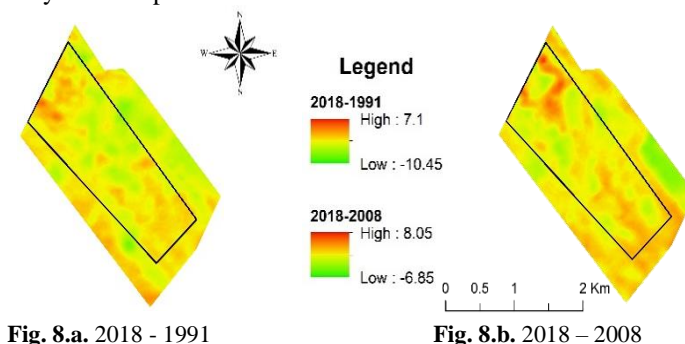
Fig. 8.a. 2018 - 1991   **Fig. 8.b.** 2018 – 2008

Further, NDVI (**Fig. 9**) shows the reduction of the built spaces, followed by the appearance of the spontaneous vegetation on the place of the former halls, especially in the central area. The lack of vegetation in the western part is equivalent to the preservation of buildings where industrial activities are still practiced.

a. 8.08.1991 b. 22.08.2008 c. 18.08.2018
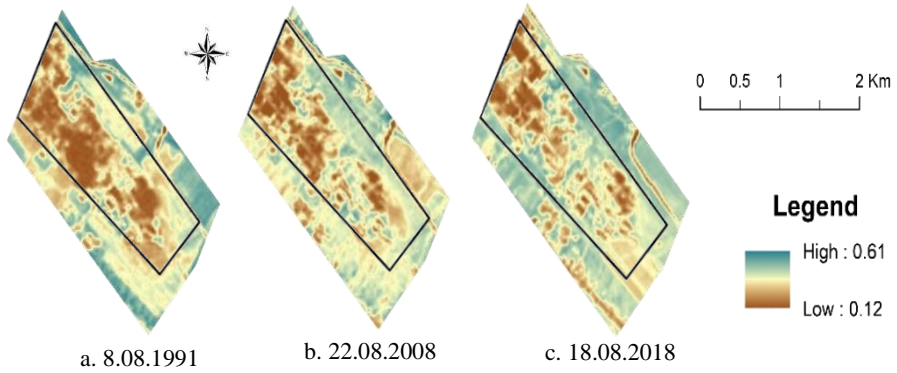
Fig. 9. (a,b,c) NDVI.
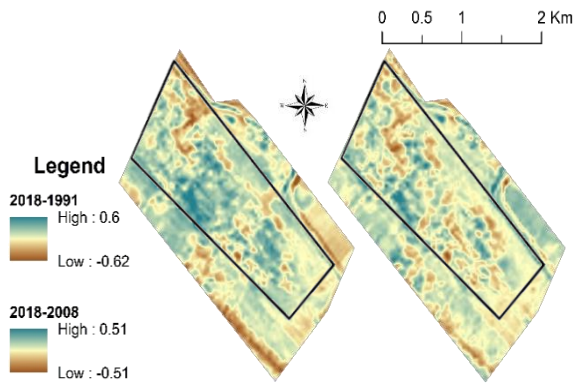
Fig. 10a. 2018 - 1991 **Fig. 10b.** 2018 - 2008

a. 8.08.1991 b. 22.08.2008 c. 18.08.2018
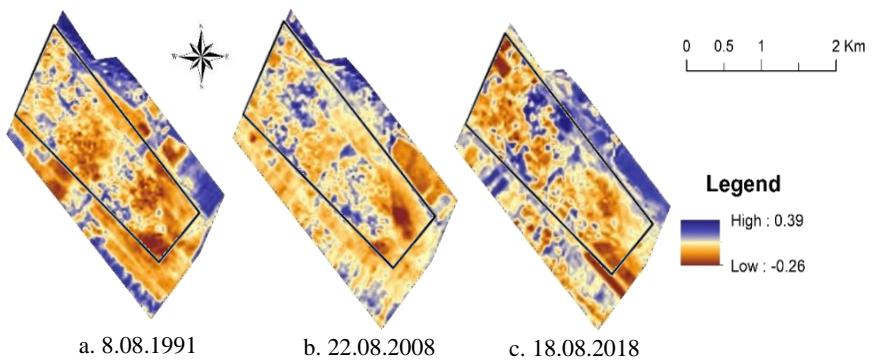
Fig. 11 (a,b,c) NDMI
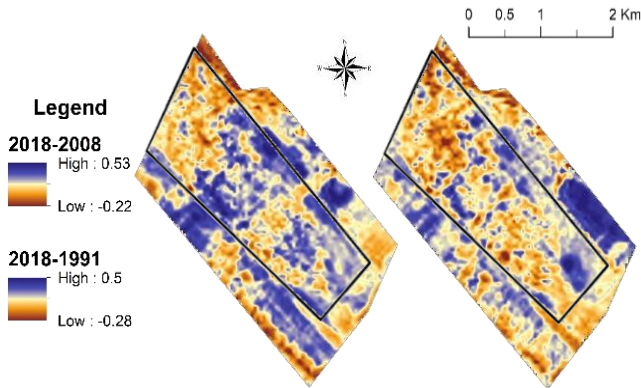
Fig. 12a. 2018-1991   **Fig. 12b.** 2018-2008

The legends of the two periods (**Fig. 10**) show that the differences were bigger for 2018-1991 than for 2018-2008. This is the result of the land use changes that occured after the demolition of some buildings. As it is represented in fig. 8a., changes took place in the center of the industrial platform.

Another index correlated with NDVI is NDMI (**Fig. 11**) which is used to capture the differences between humidity for the study area. In 1989 it is observed that the humidity is lowered especially in the central and eastern part of the platform, and that in 2018 it will increase, those surfaces being fragmented with positive values of humidity, which indicates the lands that have been left bare after the demolition of the industrial halls.

The differences between 2018-1991 and 2018-2008 are represented in **Fig. 12 a,b**. In this case, the values from the interval 2018-2008 are greater that the other interval. This can be correlated with the differences of NDVI: a thicker vegetation retains moisture better and longer than a bare ground.

5. CONCLUSIONS

For Săvinești Industrial Platform, the LST index proves to be a useful tool in observing the involution of the industrial activity. The similar study conducted for a Chinese mining town (Rao et al., 2018) shows that LST is influenced by the type of industrial activity practiced in various areas. And in the case of the platform too, LST shows how the industrial site have evolved, based on owners decisions.

In the three moments (1991, 2008 and 2018) we notice major differences in LST, especially during the summer. It can be deduced that the soil temperature decreases with the decrease of the industrial activity. The area in the western part of the area that remains constant with the highest temperatures is the area where industrial activities are still taking place. The central area is the one which suffered most changes, passing from built land to demolition of the constructions, bare ground and then spontaneous vegetation. The south-east area has various temperatures that coincide with the moments of activity and inactivity.

In conclusion, the evolution of an industrial platform can be demonstrated through satellite imagery. Demolition of buildings, restriction of industrial activity can be observed both visually and by calculating satellite indices such as LST, NDVI, NDMI.

They provide information on how to use the land, on the ground temperature, which can be indicators of the evolution or involution of some industrial areas. Of course, this information obtained from the processing of satellite images must be correlated with the events that have occurred over time, so knowing the history of the study area is a way to confirm or deny the results of the satellite indices.

R E F E R E N C E S

Avdan, U. & Jovanovska, G., (2016), Algorithm for Automated Mapping of Land Surface Temperature Using LANDSAT 8 Satellite Data, *Journal of Sensors,* 2016 (2), 1-8

Chander, G. & Markham, B., (2003), Revised Landsat-5 TM Radiometric Calibration Procedures and Postcalibration Dynamic Ranges, *IEEE Transactions on Geoscience and Remote Sensing,* 41(11), 2764-2677

Choudhury D. & Das Arijit Das, K., (2019), Assessment of land use land cover changes and its impact on variations of land surface temperature in Asansol-Durgapur Development Region, *The Egyptian Journal of Remote Sensing and Space Science,* 22, (2), 203-218

Department of the Interior U.S. Geological Survey, (2019), LANDSAT 8 (L8) Data Users Handbook, *EROS Sioux Falls, South Dakota*, https://prd-wret.s3-us-west-2.amazonaws.com/assets/palladium/production/atoms/files/LSDS1574_L8_Data_Users_Handbook_v4.pdf

Fils, S. C. N., Mimba, M. E., Dzana, J.G., Etouna, J., Mounoumeck, P. V., Hakdaoui, M. (2018), TM/ETM+/LDCM Images for Studying Land Surface Temperature (LST) Interplay with Impervious Surfaces Changes over Time Within the Douala Metropolis, Cameroon, *Journal of the Indian Society of Remote Sensing*, 46(1), 131-143

Furtuna, P., Haidu, I., Alexe, M. & Holobaca, I. (2016) Change Detection in the Cluj forest district, using remote sensing and GIS application, *Environmental Engineering and Management Journal*, 15(6), 1361–1368.

Furtuna, P. (2017) Temporal and spatial variation of forest coverage in Apuseni Natural Park, 2000-2014 period, *Geographia Technica*, 12(1), 46-56. DOI: 10.21163/GT_2017.121.05

Furtuna P., Haidu, I., Maier N. (2018) Synoptic Processes Generating Windthrow. A Case Study for Apuseni Mountains (Romania). *Geographia Technica*, 13(2), 52–61, DOI:10.21163/GT_2018.132.04

Gage, E., Cooper, D.J., (2017), Urban forest structure and land cover composition effects on land surface temperature in a semi-arid suburban area, *Urban forestry and urban Greening* 28, 28-35

Guo, Z., Wanga, S.D., Chengc, M.M., Shub, Y. (2012), Assess the effect of different degrees of urbanization on land surface temperature using remote sensing images, *Procedia Environmental Sciences* 13, 935 – 942

Haidu, I., Furtuna, P., Lebaut, S. (2019) Detection of old scattered windthrow using low cost resources. The case of Storm Xynthia in the Vosges Mountains, 28 February 2010, *Open Geosciences*, 11(1), 492–504, https://doi.org/10.1515/geo-2019-0040

Maria Mihail, (1977), Romania Economic Geography, Part 1, Cluj-Napoca

Owen, T.W., Carlson, T.N., Gillies, R.R. (1998), An assessment of satellite remotely-sensed land cover parameters in quantitatively describing the climatic effect of urbanization, *International Journal of Remote Sensing,* 19(9), 1663-1681

Rajeshwari A. & Mani, N. (2014) Estimation of Land Surface Temperature of Dindigul district using Landsat 8 data, *International Journal of Research in Engineering and Technology*, 3(5), 122–126

Rao, Y., Xua, Y., Zhanga, J., Guob, Y., Fua, M., (2018) Does subclassified industrial land have a characteristic impact on land surface temperatures? Evidence for and implications of coal and steel processing industries in a Chinese mining city, *Ecological Indicators, 89, 22-34*

Small, C., (2006), Comparative analysis of urban reflectance and surface temperature, Remote Sensing of Environment, 104(2), 168-189

Sobrino, J.A., Jiménez-Muñoz, J.C., Paolini L. (2004) Land surface temperature retrieval from Landsat TM 5, *Remote Sensing of Environment*, 90(4), 434-440

Voogt, J.A., Oke T.R. (2003), Thermal remote sensing of urban climate, *Remote Sensing of Environment,* 86 (2003), 370-384

Zhang, Y., Sun, L., (2019), Spatial-temporal impacts of urban land use land cover on land surface temperature: Case studies of two Canadian urban areas, *International Journal of Applied Earth Observations and Geoinformation, 75,171-181*

[1]https://stirileprotv.ro/stiri/actualitate/un-combinat-unic-in-europa-distrus-de-investitorii-straini-pana-acum-2-zile-era-rentabil-si-acum-nu-mai-e.html- online article [Accessed Mars 2019]

[2]https://adevarul.ro/locale/piatra-neamt/cum-s-a-prabusit-platforma-chimica-savinesti-colosul-industrial-lucrau-10000-nemteni-1_535f3b930d133766a82f7760/index.html [Accessed Mars 2019]

[3]https://www.youtube.com/watch?v=byHh-JIMZiU [Accessed Mars 2019].

GEOMEDIA`S ROLE IN THE GEOSYSTEM DEVELOPMENT: DRACULA`S SPATIAL IMAGINARIES IN ROMANIA

Mihai VODA[1], Steven GRAVES[2], Cristina Elena BERARIU[3]

ABSTRACT:

Geomedia techniques are easily acquired, freely available and easy to learn. Most of the modern mobile phones possess digital camera and have incorporated Global Positioning System. Various smartphone applications can be downloaded and used to find, create and control the virtual representations of places, emphasizing humans' central position in the Geosystem. The focus of this research is an assessment of the power of Geomedia techniques as a tool in the identification, construction and development of functional Geosystems. Methodologically, our research in Romania used the grounded theory with data collection based on smartphone apps, web GIS and geospatial datasets from Google Earth, combined with the Geomedia analytic hierarchy (GAH) and the multicriteria decision making (MDM) processor for the geosystems` effectiveness evaluation. We demonstrate how the growing popularity of Geomedia tools can be used to efficiently sustain development in an organized way, at both the national and community levels.

Key-words: *Romania, Geomedia, Dracula, Geosystem, Smartphone apps, Development.*

1. INTRODUCTION

Geomedia`s imagined place experience illustrates the human`s created virtual Geosystems with the complexity of functional interrelated components. Geomedia synthetize all the information that connects different places illustration with coordinates and Geosystem`s characteristic data. All environmental elements are contributing to a geographical place's unique personality, which is spatially developed as a Geosystem, defined by common and unique attributes (Voda & Montes, 2018).

The Geomedia techniques are used by everyone that takes photos with the smartphone`s GPS activated and shares the images on social media, Google Maps, Pinterest, Google Earth or Aibnb. Cherifi et al. (2014) argued that conventional crowd shared images are used for the creation of a destination virtual imagery and Relph (1976) claimed that its qualities influence people`s imagined experience of that place. Croitoru et al. (2013) explained the importance of collective geolocated media generated through web services due to smartphones advancements.

From a Geomedia perspective, the geographical place, once properly surveyed (scanned, measured, photographed) and transformed in a virtual reality model, can become a scientific illustration of an entire Geosystem characterized by `*interconnected physical and social relations*`(Lapenta, 2011, p.16), with active energy, information and matter fluxes between humans and their living environments.

---

[1]*Dimitrie Cantemir University, 540546 Targu Mures, Romania, mihaivoda@cantemir.ro;*

[2]*California State University, Northridge, CA 91330-8249, U.S.A., steve.graves@csun.edu;*

[3]*Dimitrie Cantemir University, 540546 Targu Mures, Romania, cristina.berariu@cantemir.ro.*

This article analyzes the effectiveness of Geomedia techniques in the Geosystems` sustainable development processes by exploring how communities contribute to the identification and promotion of places unique attributes through an analysis of Dracula phenomenon in Romania. This innovative approach focuses on geo-locational issues in a variety of Vlad Țepeș related places; their contradictions, and the role of Geomedia in the evolving Dracula-based Geosystems.

At first glance Geomedia and Geosystems may seem unrelated, albeit both of major concern. However, accumulated knowledge on virtual reality representation of places indicates that Geomedia techniques are more efficient in specific Geosystems, leading to our research question: how do Geomedia stimulate Geosystems development? This question is highly important for finding the best way to manage the Geosystem`s virtual inception, presentation and contextual perception in different cultures.

The Geosystem is like a living organism which thrives under dynamic equilibrium conditions, generating welfare for its inhabitants if they are capable to control the matter, energy and information fluxes. It`s extension varies in accordance to the human collectivity *egregore* that defines the geographical space and stimulates components interaction with the new technologies help: Geomedia (Voda et al., 2019). This research shows that Geomedia is much more than just a reliable source of information. Geomedia is also a unique type of crowd-sourced knowledge created by individuals using a variety of applications that convey their collective values and beliefs.

Modern researchers argue that a message stems from the social context in which it was produced, equally influencing and being influenced by it (Fairclough, 1995; Johnstone, 2002). As in any type of discourse, Geomedia is invested with powers that go beyond the apparently simple message it provides by means of maps, photos and texts, it conveys the cultural identity of the people living in the Geosystem. Any place with a story to tell, with feelings to generate or thoughts to trigger, can, leverage Geomedia to stimulate the valuable sense of place among locals. Once well done Geomedia becomes widely shared, it has the power to bond the community members, connecting them to the local *egregore* and creating a self-sustaining Geosystem. The activated flows of matter, energy and information will increase the local Geosystems` functionality, initiating its development.

The new high-tech solutions and software apps availability that Lapenta (2011) refers to as Geomedia, are represented today as internet platforms where location-based and augmented reality technologies merge in a new form of digital visualization system activated and maintained by social media data exchange power. The humans are the principal piece of their Geosystem, whose empirical scientific illustration evolved from paper maps to virtual computer and smartphone geo-apps (Voda, 2013; Zheng et al., 2010).

This article contributes to the understanding why Geomedia controls Geosystems by synchronizing social etiquette, reshaping spatial imaginaries and harmonizing media interactions. As Lapenta (2011, p.15) observed `*Geomedia are to space what the watch is to time*`. The future of location aware geospatial technologies is created with web-based Geographical Information Science (GIS), smart apps and interactive digital mapping (Wilson, 2012; 2014). Inal et al. (2017) pointed to the value of location-aware smartphones for archaeological field work. Baiocchi et al. (2017), showed the importance of the new Global Navigation Satellite Systems (GNSS) techniques introduced for smartphones in the virtual maps creation process.

Various researchers have examined this issue, notably Wilson (2014, p.298), who outlined the variety of geospatial data interfaces, pointing to Google's "check in" function (also found in Facebook, and other social media) and how the geo-aware social media have

become important to the comprehension of local cultures. Dickinson et al. (2014), Sidali et al. (2017), Meng et al. (2014), demonstrate how Geomedia, through a diversity of smart applications provide directions and information, adding value to the historical and geographical resources of a place. Geomedia techniques offer various visualization opportunities for the chosen Geosystem, considerably influencing development decisions (Voda & Negru, 2015). Echtner and Ritchie (2003), noted that unique functional attributes were of great importance for a geographical location's image.

Recent research suggests that Geomedia users are producing and sharing photos, symbols and text in a way that has significantly reconfigured the interaction of social media and the slightly older world of digital mapping (Lapenta, 2011, p 17; Zheng et al., 2010).

The considerable achievement of the Airbnb's locations for example, is largely a product of new business models afforded by a better visualized Geosystem (Voda & Montes, 2018). Once validated by excellent ratings, the Geosystem's virtual image might attract more visitors, transforming the locals into superhosts, thereby increasing their revenue (Wang & Nicolau, 2017; Liang et al., 2017; Gunter, 2018). Furthermore, the Airbnb phenomenon proved the functionality of local Geosystems virtual imagery, sustained and validated, if genuine, by visitors` reviews (Guttentag & Smith, 2017; Cheng & Jin, 2019).

Airbnb experience of a place will definitely contribute to the local Geosystems` presentation and outer contextual perception because today, Airbnb represents the world leader in peer-to-peer accommodation provision (Sigala, 2017). Anyone can become a host using identification documents and a property's photos as a part of their envisioned Geosystem image. Guttentag (2015) explained the considerable influence of the Airbnb system through the disruptive innovation theory, while Ert et al. (2016) emphasized the critical value of personal images to the platform's construction of credibility among would-be customers. Tussyadiah & Pesonen (2016) observed that the host's incorporation in local community encourages social relationships, enhancing the Airbnb system's efficiency and reliability. From this research Geosystems perspective, the community is comparable to organic entities, with functional common and unique attributes operating in dynamic balance to satisfy its social needs. This article will explore how the use of Geomedia techniques contributes to the place-making efforts of any Geosystem, possibly creating real value as it develops. Geomedia can also become the ultimate type of advertising, with world-wide impact, without the costs typically incurred via expensive, professional and/or governmental marketing efforts (Gupta et al., 2018; Voda & Montes, 2018).

As technological innovation increasingly becomes critical to sustainable development in many locations around the globe, it is worthwhile to examine its impact in Romania, a country easily accessed by both European and North American visitors, with excellent digital infrastructure, and a large number of locals using smartphone applications (Statista, 2018), but with a relatively poorly organized government-based infrastructure.

Romania is today somewhat reliant on the mythology of Dracula, which attracts considerably more visitors to the region than any other touristic attraction. Centered on the Transylvania region of Romania, the Dracula phenomenon is unique and with the support of Geomedia tools could become even more important to Romania's overall development goals (Voda & Negru, 2015; Ernawati et al., 2018).

Specific myths and legends can create powerful brands for the sustainable tourism development (Robinson & Wiltshier, 2011; Ernawati, 2015). As such, Dracula related Geosystems generate broader understanding of the Geomedia techniques role in the construction, content and outer perception of our social worlds.

2. RESEARCH METHODOLOGY

The research methodology is based on the grounded theory using Geomedia techniques for models creation and data analysis. Using the Geomedia techniques in every location, a group of seven criterions were identified as representative for the proper assessment of the Geosystem`s effectiveness: unique attributes, innovation diffusion, geo-referenced illustrations, geomedia competence and the access to geomedia (Voda et al., 2019).

Data collection procedures were based on the specific geographical information systems visual imagery connected to the Dracula phenomenon. The datasets analysis and attributes particular assessment was done using INIS Viewer, Google Maps and Google Earth internet platforms. Comparative analysis revealed Geosystem`s components properties, significantly contributing to the unique attributes identification (Croitoru et al., 2013; Lapenta, 2011; Ernawati et al., 2018; Voda et al., 2017; Zheng et al., 2010). Based on the Romanian Dracula phenomena, this research attempts to emphasize the importance of the local Geosystems` unique attributes and predict future wider applicability of the Geomedia techniques.

Selective coding was applied for Geosystems` access to Geomedia (60-0.150), Geomedia competence (70-0.175), unique attributes score (100-0.250), innovation diffusion (90-0.225) and geo-referenced illustrations (80-0.200) in order to understand the context of Geosystem`s imagery creation, reception and display. Each criterion weight was attained by the geomedia analytic hierarchy (GAH) (Voda et al., 2019). Geomedia technique is integrating all the environmental features in virtual Geosystems with functional interrelated components and fluxes of matter, energy and information. The process returned the selected Geosystems in an array, implying their synthesis and processing into new structures, according to people`s energy inputs and personal experience of the geographical place (Park & Santos, 2017; Voda et al., 2019). It also requires various fluxes identification, attributes interpretation and structure-components property correlations. Finally, the specific behavioral computation was possible and each Geosystem`s effectiveness obtained (Mac, 1996). Our goal was to elaborate Geomedia techniques capable to extend functional Geosystem`s performance and extrapolate its virtual representations qualities.

The *unique attributes* criterion was considered the most important, receiving the maximum relative weight (rw) of 100-0.250. It reflects the geosystem`s authenticity generated by special geographical features, intriguing historical facts, myths or legends. The next value of 90 rw was given to the *innovation diffusion* criterion because it shows the geosystem`s inclusion probability in transformative networks. The *georeferenced illustration* (80 rw) criterion reflects the geosystem`s virtual presence online. *Geomedia competence* (70 rw) and *geomedia acces* (60 rw) are conected to the people`s ability to use geomedia tools and their acces to online internet information (Voda et al., 2019).

The Geomedia data collection techniques involved geographic information, historical texts and documents analysis combined with field work in the selected Dracula related Geosystems. Data was collected during 2015-2018 research field trips in Bran, Sighișoara, God`s Chair, Devil`s Plateau and Borgo Pass geographical areas where 67 locals were asked to rate (<2-very weak, 3-4 weak, 5-6 moderate, 7-8 strong, 9-10 very strong) their access to Geomedia and Geomedia competence. Zheng et al. (2010) believed that geo-referenced images incorporate substantial data related to their geographical area culture. 691 relevant geo-tagged Facebook posts and Google geo-referenced illustrations were selectively coded.

We observed the inner context of created imagery and assessed the outer perception of their visual presentation. Yanai et al. (2009) claimed that specific geographical locations

cultural differentiation can be identified by the extraction process of the most relevant visual images and the emblematic conceptualization confirmed throughout an assembling procedure. Coding the outer context of visual data was essential to understand the act of inception, the act of representing different Geosystems, their content, their contextual perception and development role in the Romanian context (**Table 1**).

<div align="right">**Table 1.**</div>

The relative weight for each criterion used for Dracula related Geosystems.

Geosystem`s name	Access to Geomedia	Geomedia competence	Unique attributes score	Innovation diffusion	Geo-referenced illustrations
Bran Castle	0.196	0.174	0.217	0.196	0.217
Sighisoara	0.195	0.171	0.22	0.22	0.195
Borgo Pass	0.226	0.129	0.226	0.194	0.226
God`s Chair	0.24	0.12	0.24	0.16	0.24
Devil`s Plateau	0.211	0.105	0.263	0.158	0.263

Smartphone GPS high-tech geo-location capabilities were used for photos geotagging process in the studied geographical areas and invert geo-coding were realized for the semantic connotation of specific locations associated to the given GPS coordinates. Furthermore, according to Liu et al. (2006) methodology, geographical observations have been conducted on every site in order to visualize the semantic position typology of the virtual map.

Exchangeable image file (EXIF) data viewer methodology was used for a significant variety of smartphone photos coordinates identification which were obtained from the interchange information digital files and were geo-located on Google Maps™ (Inal et al., 2017; Ernawati et al., 2018; Torpan & Voda, 2019).

For every Dracula related Geosystem, the Facebook geottaged posts were analyzed to generate the innovation diffusion criterion. Data collected on field with the Garmin GPS and smartphone applications (Google Photos, GTCamera) was used for the geo-referenced illustrations validation. A number of 266 Facebook geo-tagged posts and 425 Google geo-referenced illustrations were analyzed and the interchange information digital data extracted for the virtual Geosystems evaluation (**Table 2**).

The geomedia analytic hierarchy (GAH) generated each criterion weight (Geomedia acces -0.150, Geomedia competence - 0.175, Unique Attributes - 0.250, Innovation diffusion – 0.225, Georeferenced illustration – 0.200). The Geosystem`s effectiveness priority score was obtained using the multicriteria decision making (MDM) processor. Geosystems` geographical features, the local history and traditions are stimulating authenticity and the unique attributes creation (Xi et al, 2015). The innovation diffusion is important for the integration capacity in transformative networks. The effectiveness weighted sum is reflecting every analyzed Geosystem`s functionality and it is positively correlated with the Arrow`s theorem results which validated the application of Geomedia techniques and the GAH process (Arrow, 2011; Voda et al., 2019).

Dracula related Geosystems` effectiveness evaluation.

Geosystem`s name	Interviewed people	Arrow points	Arrow score	Geosystem`s effectivness
Bran Castle	16	5	9	92.75
Sighisoara	19	4	8	83
Borgo Pass	11	2	6	62.5
God`s Chair	12	1	5	50.25
Devil`s Plateau	9	0	4	38.75

3. SIGHIȘOARA AND BRAN GEOSYSTEMS` EFFECTIVENESS.

The two most popular Dracula-themed locations in Romania are Bran Castle and the citadel of Sighișoara. Each of these locations has a balanced and robust virtual Geosystem that contributes to the maintenance of a sustainable local tourism industry.

Both locations have similar Geosystems. Climate characteristics are similar, recommending both Sighișoara and Bran for sightseeing all year round. We analyzed the inner and outer context of the natural landscape features that include mountainous terrain, slightly forested hills and poor road networks, coded as functional attributes of both locations (0.220/9- 0.217/10).

The acts of representing Geosystems` visual images was linked to the context of their creation, generating historical credibility to both places because of their connection to the real character, Vlad Țepeș the Romanian ruler. Their unique attributes score and innovation diffusion values are very strong (0.196/9-Bran). The Sighișoara and Bran Geomedia virtual imagery is combining `geo-location, social data and the wisdom of the crowd` for the credible linkage of geographical reality to the virtual imagery creation (Valentino-DeVries, 2010). By using slices of the visual dimension of Sighișoara and Bran representations (101 geo-tagged posts, 166 geo-referenced illustrations), the first Dracula Geosystem models computation and structure-elements attributes correlations was possible. The analysis finds the highest priority score in Bran (92.75/9) reflecting its Geosystem`s effectiveness, closely followed by Sighișoara (83/8).

Sighișoara's old citadel was one of seven walled fortresses built by Transylvania Saxons, but since it is also where Vlad Țepeș was born, it has become an important destination for Dracula tourism. The description of the multilayered context of visualization was performed here in order to understand the Dracula phenomenon connection processes to the Geosystem`s functionality. There is a slighter higher value for the access to Geomedia in Bran (0.196/9) compared to Sighișoara (0.195/8).

On the main square of the citadel sits the yellow house of his father, Vlad Dracul. Plotting situational maps of visual data, all the analytically pertinent elements were analyzed, including the house that represents the core of the local Geosystem: the locals` Geomedia competence has a strong score of 0.171/7. It has been transformed into a significant tourist attraction featuring a traditional restaurant on one floor, and the "Dracula Rooms" on the second floor where crowds of tourists gather before or after eating the "must have" lunch, recommended by digital travel guides authored by fellow tourists.

Dracul name (meaning Devil in Romanian), derives from the Order of Dragon, a semi-military organization Vlad Dracul was a member of. The *Dracula Resurrection* movie validates Sighișoara's fortress symbolic elements of Dracula`s particular image by choosing it for filming locations. Furthermore, the Romanian Ministry of Tourism started the Dracula Park project initiative, envisioned to develop tourism in the region by taking advantage of *Dracula* as a lucrative myth (Jamal & Tanase, 2005; Voda & Negru, 2017).

Echtner and Ritchie (2003), emphasized the unique functional attributes importance for a destination`s image (0.217/10-Bran). Lai and Li (2016), argued that tourist`s destination image reveals the *mental perceptions* held by visitors about a place (0.196/9-Bran, 0.220/9- Sighișoara). Sighișoara (0.195/8) and Bran (0.217/10) geo-referenced illustrations score demonstrate their central and effective Geosystems, which is in line with Asero et al. (2016) explained how tourist may perceive a tourism area as *central* or *peripheral* within a network. The local communities are actively contributing to the valorization of their place unique attribute, Dracula (**Fig. 1**).
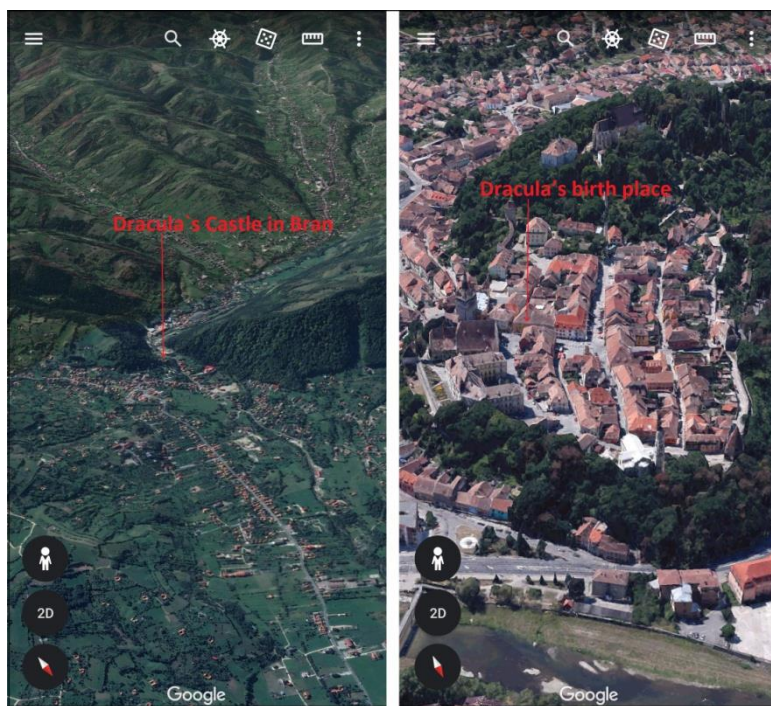
Fig. 1. Bran Castle near Brasov and Vlad Dracul house in Sighișoara (Google Earth, 2017).

The village of Bran has a less historically viable connection to Vlad Țepeș, but thanks to robust Geomedia efforts and perhaps its proximity to Bucharest, is the best developed of the Dracula Geosystems in Romania (92.75/9).

Multiple historians including Anghel (2006) and Curta (2014), agree there is evidence that Vlad Țepeș never actually inhabited Bran Castle. The castle itself was constructed by the inhabitants of Brasov, a city nearly 30 km away as a distant bulwark against invasion

from the South. Perhaps Vlad III bypassed Bran castle during an invasion in the mid-1400s, but never lived there.

The association between the Castle and Vlad Țepeș was invented by Romanian authorities after an International Tourism Trade in 1991. According to Roberts and Simpson (1999), tourism development around Bran was initiated with the help of the international operation *Villages Roumains*, a non-governmental organization under the European Union PHARE funding scheme.

Bran's location is convenient due to its proximity to Brasov, less than three hours from Bucharest (Anghel, 2006; Baca & Rusu, 2017). Bran Dracula Geosystem`s high innovation diffusion (0.196/9) and geo-referenced illustration score (0.217/10) confirm the widely held *expectations* of an imagined place experience. It is located on a spectacular high cliff in Bran village, close to a defensible chokepoint pass (**Fig. 1**).

The architecture and its situation on a cliff, against a rugged backdrop of the Carpathians allow tourists to meet their expectations for a "Scary Castle", worthy of Dracula – the Prince of Darkness to be met in spades (Muresan & Smith, 1998; Voda & Negru, 2017).

For geospatial smart applications development, the Geomedia travel pattern analytic approach can display people`s visiting preferences and thus facilitate traffic patterns observation. Geomedia is linking geography, spatial and visual reality perception offering information, visual examples and apprehension of a specific geographical location (Zheng et al., 2010).

Vlad III was constantly trying to foster and protect his state, being considered cruel, but not mentally ill (Giurescu & Giurescu, 1975). Wallachia`s Prince ferocity was dramatized by his Saxon enemies from Southern Transylvania. Vlad III was known as *Țepeș* (the impaler) only in the `fifteenth to sixteenth century` (Stoicescu, 1976). The collective stereotypical images created about Transylvania are related to Dracula myth. Cherifi et al. (2014) emphasized the importance of people`s naïve images, the virtual representation of a destination, generated by the non-visitors.

Vlad III had two nicknames: *Țepeș (The Impaler)* and *Dracula*. Dracula meant the son of *Dracul*, his father's name after receiving the Order of the Dragon in 1431, from King Sigismund of Hungary (Curta, 2014; Butulescu, 2001). According to Butulescu (2001), Vlad III used to sign as Dracula. Butulescu`s arguments are based on the historical document signed on the 20th of September 1459 by Vlad III his portrait made by Odhsenbach Stambuch from Stuttgart (Butulescu, 2001).

Both Vlad Dracula related Geosystems are properly balanced in a dynamic equilibrium. Energy inputs from locals and tourists drive the Bran and Sighișoara Geosystems. They interact with the human activities around the Castle in Bran village and inside the Old Citadel in Sighișoara. The evidence for this interaction is the tourism development processes that gave rise to the Geosystems main outputs: genuine and functional tourist sites (USGS, 2017; Ernawati et al., 2018). The fictionalized landscapes are given credibility and legitimacy by the frequent retelling of the myth through the Geomedia rich reproduction of the narrative by tourists.

The effectiveness of Geomedia techniques is also reflected in the evolution of peer to peer property rental industry in Bran (0.196/9-AG, 0.174/8-GC) and Sighișoara (0.195/8-AG, 0.171/7-GC), in accordance to Ernawati et al., (2018) who showed the importance of the geo-referenced media for the local community-based tourism development which can use the Airbnb website platform, Facebook geo-tagged posts or Google Earth pinned locations to better valorize their resources. Many inhabitants rent their homes in Airbnb

online accommodation system. In the Bran castle area, for example, there are 43 private houses registered. The number increases to 59 in Sighișoara, where the old citadel has been constantly visited since 2010, when the nearby Biertan village appeared on the Lonely Planet's Romania tourist guide (Voda, 2013; Airbnb, 2018).

4. BORGO PASS, GOD`S CHAIR AND DEVIL`S PLATEAU GEOSYSTEMS

Borgo Pass and God`s Chair are two relatively inaccessible Dracula Geosystems descriebed in Bram Stoker`s book. Like Bran Castle, they also have a tenuous connection to Vlad Tepes, but both locations appeal to true fans of the Bram Stoker's novel. Borgo Pass and God`s Chair are fictional counter parts of Pasul Tihuța and Scaunul Domnului. These locations appeal more to *les connoisseurs* of mythology and leged, those sometimes known as the "Dracula Hunters", than they do to conventional visitors.

Petru and Nastase (2004), suggest that after reading Bram Stoker's *Dracula*, Alexandru Misiuga, the director of the Bistrita County Tourism Authority, claimed that Stoker's "Borgo Pass", exists in the real world in the Northern part of the Calimani Mountains (as Pasul Tihuta). Based on this claim the local authorities decided to build a hotel that they would call "Dracula Castle" in order to boost the regional tourism development. Misiuga managed to obtain the necessary funds (25 million lei) from the central communist authorities in Bucharest. The castle was built at 1227 meters altitude between 1976-1983 (Petru & Nastase, 2004; Mânzat, 2008; Baca & Rusu, 2017).

The Dracula Castle Hotel slightly resembles a medieval castle. The architectural style also clearly suggests Socialist Classicism, common among apartment blocks erected for the working class during the communist era. Dracula Castle's was initially supposed to be built on the way from Piatra Fantanele to Ciosa, on the Paltinului ridge, near Frumuseaua Peak (Mânzat, 2008). That location would have been more credible and successful in terms of a Geomedia imagery development because it has an interesting history, though on a less-travelled road.

Borgo Pass Dracula Geosystem's attractiveness (0.226/7-UAS) can be improved through Dracula themed activities. In line with Barbieri et al. (2016) who suggests that local community involvement represents a prerequisite for the tourist experience success, our results show relatively good Geomedia access (0.226/7-AG) but low competence level (0.129/4-GC).

Attractions that leverage the Dracula theme could include, black horse-drawn carriage rides on dirt roads, vampire-themed paragliding adventures and attractions like jacuzzi tubs fashioned as witches cauldrons. Managed well, it could increase the innovation diffusion (0.194/6-ID) score.

We analysed the Borgo Pass Geosystem's specific functional features, assessing how the Dracula imagery structure correlated to the tourists' experience of the place. The lower 0.226/7-GI score show that energy inputs from visitors slightly drive the unbalanced Dracula Geosystem. As a result, there are no few viable outputs such as, tourist site creation and tourism activities development.

The Geomedia imagery could help generate processes that contribute to the fabrication of a more effective Geosystem (62,5-GE, 6-AS), like we observed in other Vlad Dracula related sites in Bran(92,75-GE, 9-AS) and Sighișoara(83-GE, 8-AS). Their virtual representations qualities can be extrapolated to the Borgo Pass Geosystem and interconnected to God`s Chair's functional attributes.
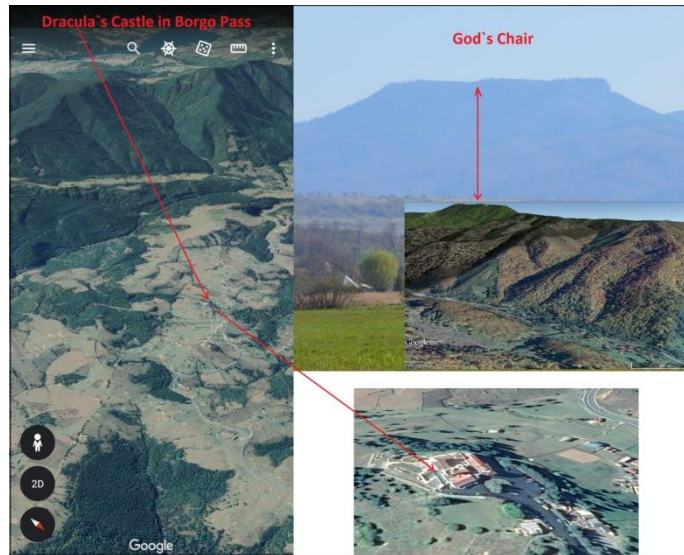
Fig. 2. Dracula Castle from Borgo Pass and God`s Chair (Google Earth, 2017).

The results suggests that the following Borgo Pass (**Fig. 2**) myths can strongly increase its unique attributes score (0.226/7-UAS) and overall Geosystem`s effectiveness (62,5-GE, 6-AS): one is locating an old Vlad citadel on the Frumuseaua Peak; another states that the *Golden Hen* treasure is buried there on the mountain ridge; there is also a legend about Barbu Blacul, Vlad Țepeș`s lieutenant who came on Frumuseaua Mountain in search for the citadel and the hidden treasure; the myth of Ianca and the ghost army is correlated with loud voices, laughs and strange globular lights on Frumuseaua Peak during night times. The cave legend refers to a time travel compression: you enter young and come out old; you die if you tell anyone. There is also a legend about ancient times when the locals suffered of a blood disease, being annoyed by the sunlight, with whitening skin, growing teeth and lips; the remedy was animal blood consumption. The haunted house legend is considered a real story about a group of youngsters who spent a night in a hut situated in the Frumuseaua Peak proximity (Baca & Rusu, 2017).

God's Chair (Scaunul Domnului/ Isten Szeke) is a flat, but sheer-sided mountain top located (1381 meters) in the volcanic Calimani Mountains Range (**Fig. 2**), about 24 km south of the Borgo Pass. The interesting Dracula related Geosystem (0.240/6-UA) is visible from the Reghin-Bistra Muresului road, following the Mures River Valley upstream. Stoker (1897, pp.8) described it in the original Dracula book: '*Look! Isten Szek!*'- 'God`s seat!', as Jonathan Harker travelled Transylvania in search for Dracula's Castle, just before entering the mountains to the Borgo Pass (Voda, 2013; Voda & Negru 2017; Baca & Rusu, 2017). Although the Geomedia competence score is very low (0.120/3-GC), our results show similar values (0.240/6) for the geo-referenced illustrations and unique attributes suggesting that the Dracula themed projects initiated in Bistra Muresului village towards the mountainous gravel roads connecting to Borgo Pass will increase Geosystem`s effectiveness in the future (Voda & Negru 2017; Ernawati et al., 2018). This is in line with Hwang and Stewart (2017) who found that collective actions of the local communities are very important for a sustainable community-based tourist infrastructure development.

Iszten Szeke and Borgo Pass in Romania could very well benefit from capitalizing on the local Dracula's myth to attract more tourists (House, 1997). Other European locations such as La Mancha in Spain, Copenhagen in Denmark or Lapland from Finland successfully valorized Don Quihote, Little Mermaid and Father Christmas themes in tourism development (Muresan & Smith, 1998). Dracula character has fictional mixed origins given by the real historical events and people connections, capable to strengthen the local Geosystem`s unique attributes and increase its effectiveness (50.25-GE, 5-AS). In Bram Stoker`s book, the Romanians are the proud descendants of the Dacians and Dracula is a local born Prince with Szekely blood (Stoker, 1897; Voda, 2013; Baca & Rusu, 2017, Muresan & Smith, 1998). The innovation diffusion lower level (0.160/4-ID) confirms Muresan and Smith (1998) observations that in Romania, Dracula related geographical places should generate `a mix of fiction and realities`, encouraged by literary, film and lately Geomedia references.

Apart from Borgo Pass, Frumuseaua Peak and Iszten Szeke, there is Scholomance (*Solomonărie* in Romanian), the mysterious underground school where Dracul (Devil) was a teacher. The black magic school from Bram Stoker`s book was geo-located in Cindrel Mountains, below the Cindrel Peak (2224 m) on the Iezerul Mare lake shores (Stoker, 1897; Baca and Rusu, 2017). Currently, the Cindrel's geographical area appears to be deserted, presenting no interest until 2011, when the *Transylvania Calling* spiritual festival was organized, proving the Geomedia techniques potential (**Fig. 3**). The special trance gathering created there the *Wonderland* magic realm. Remotely located in the mountains heights, the Geosystem is famous among the shepherds as the Devil`s Plateau.

Fig. 3. Wonderland and Devil`s Plateau in Cindrel Mountains (Google Earth, 2017).

The Devil`s Plateau Geosystem has the lowest competence (0.115/2-GC) and access to Geomedia (0.211/4-AG) values due to its remote geographical position. But as Ernawati et al. (2018) observed, the local inhabitants are committed to learn how to valorize the new

technological advancements, the use of freely available Geomedia techniques for their own benefits. Suggestive photographs, reliable references, mobile phones and internet coverage, can metamorphose their remote households in exquisite rental homes, increasing their Geosystem`s effectiveness (38.75-GE, 4-AS). In accordance with House (1997) statement on legends importance, the unique attributes score (0.263/5-UA) can be improved on grounds of the local legends who describe the fabled *Solomonărie* school location under the Devil`s lake, where selected kids learned the magic plants and hail producing secrets. The sheep man says: `If you throw a stone into the lake` (Iezerul Mare/Devil`s lake) the angry dragon will fly out and severe weather phenomena occurs (Gerard, 1885; Oișteanu, 2004).

As Negru et al. (2015), hypothesized, Dracula`s horses-drawn carriage might have crossed the Calimani Mountains following Bistra river Cofu tributary from God`s Chair to Borgo Pass to reach the controversial castle. Ernawati et al. (2018) elaborated mountain routes GIS profile graphs for dirty tracks connection over the Calimani Range, validating the two Geosystems connection.

For the proper characterization of the Bram Stoker`s Dracula Geosystems, our study utilized a systems-theoretic formulation. Common and unique functional attributes were identified and characterized in order to generate the Geosystem effectiveness for each geographical location. Their structure-elements property correlations were evaluated using data from Vlad Dracula functional Geosystems. The specific behavioral computation revealed a considerable development potential that can be valorized in the future in a community collaborative approach linking Bram Stoker`s Dracula spatial imaginaries to the local myths and legends. Our results confirm Rinne`s (2018) statement that the sharing economy will considerably improve people livelihoods. Borgo Pass, God`s Chair and Devil`s Plateau, unlike any other remotely located Romanian site, possess the most valuable asset: Dracula, their special unique attribute.

5. RESULTS DISCUSSION

Bram Stoker's fictional character of Dracula launched an impressive array of vampire related media production. Dozens of movies, television shows, cartoons and theatrical productions have spun off the original volume (Miller, 2003). Luckily for Romania, the original text placed the fictional character in the real landscape of Transylvania and the association has remained firm in the imagination of many westerners for over 100 years. The analysis finds that Geomedia visualization techniques enhance locations' broader cultural and historical values, conditioning visitors' comprehension of the Dracula phenomenon. Apart from the specifically connected with Vlad Țepeș or Dracula sites, tourists are enjoying other Romania mythical places as well.

Dracula phenomenon compresses elements from literary, movie, dark, cultural and heritage tourism (Hovi, 2014). The *media tourism* term has been proposed to integrate literary and movie-induced tourism with the modern *Internet*, in an effort to quantify the popular culture Dracula tourism (Reijnders, 2011; Light, 2012; Larson et al., 2013; Hovi, 2014).

The results show that Geomedia imagery tends to increase tourist sites visitation rates by offering visitors more options via images encapsulated on smartphones, tablets and laptops. Hence Dracula related spots can be transformed into more successful tourist sites by these newly available technologies. The Geosystem theory has the capacity to explain and predict the Dracula phenomenon in connection to the Geomedia technology used to create it. Friendly interfaces facilitate the use of smartphone applications, helping the locals

in Bran and Sighisoara to produce new visual concepts (Android Development, 2016). The study finds evidence that the future development of Dracula Geosystems becomes possible with the easily apprehended tools and Geomedia access in Borgo Pass and God`s Chair. Wang and Nicolau (2016) observed that smartphone applications were used for geottaged photos location on Google Maps, Google Earth or various social media sharing options during travel or in everyday life. The freely available Geomedia tools can redefine geographical locations such as Borgo Pass, Devil`s Plateau or God`s Chair, increasing their functionality and encouraging Dracula themed tourism development.

Although most people consider that Dracula phenomenon attracts international tourist almost everywhere in Romania, there is a significant preference for the historically rich geographical locations, such as Bran as Sighișoara which represent the functional Geosystem models. As we evaluated our data, we looked specifically at how efficient Geomedia techniques were in the construction and maintenance of semantic narratives surrounding Dracula phenomenon. Currently, Romania's internet availability and good quality connectivity establishes the tourism provider-consumers relationship. Airbnb phenomenon is opening the world for unique experiences, irrevocably changing today's tourism. A better search engine position on the first page increases any business performances, attracting more customers. The analysis finds that Airbnb search engine optimization locates any accommodation posting almost to the top of the Google search engine first page for free. The identification of specific historical geo-locations represented a challenge that has been solved with the help of old paper maps and different archive documents. The precise position determination and coordinates computation constituted the prerogatives of geospatial tools operations (Luo et al., 2009; Voda, 2018).

The study contributed to a better understanding of the Dracula phenomenon. A question that has generated a range of responses is why tourist visit Bran Castle, although Bram Stoker didn't mention it in his *Dracula* book and Vlad Tepes's presence there has never been historically validated. The answer is related to both social and geographical factors, proving Geomedia`s efficiency for the local Geosystem`s functionality increase. Bran Castle's interesting appearance corresponds well to the tourist expectation of their imagined image of Dracula's Castle. Although the spectacular Rasnov Fortress is located only 14 km from Bran Castle, most tourist prefer Bran because of the Dracula-Vlad Țepeș media association and mountain beautiful views. The Piatra Craiului Mountains jagged limestone crests from the East are shining in the sunrise, while Bucegi Massif conglomerate walls are reflecting the sunset light on sheer cliff faces. The Bran Castle tourist site was created in part with that imagery in mind, and Geomedia helps it attract more visitors each year, increasing the local Geosystem`s effectiveness.

Sighișoara's main tourist attraction is represented by the Vlad Dracul house, connected to Vlad Țepeș father, Vlad II, and promoted vigorously as "Dracula's" birth place. Positioned as it is in the old medieval citadel upon a hill, Vlad Dracul's house is surrounded by historical buildings, still inhabited as it was hundreds of years ago. Geomedia generated these historical links and the local Geosystem started to thrive.

The practical application of our findings may contribute to Borgo Pass, God`s Chair and Devil`s Plateau Geosystems functionality increase through their strong connections to Bram Stoker's *Dracula* book (Stoker, 1897). Accurately described by the Irish writer, both geographical locations exist in the real world but lack in credible historical links to Vlad Țepeș. This is why fewer tourists visit these sites. It can be argued that visitors benefit from a variety of wild landscapes, local legends and traditional Romanian customs. These are the perfect prerequisites for sustainable tourism development, which involves local historical

and natural environments, promoting community values and cultural conservation, increasing local welfare (UNWTO, 2013; Eadington & Smith, 1992; Beeton, 2006; House, 1997; Picard, 2008; Weaver, 2006; Singh, 2012; Wang et al., 2019).

Dracula tourism growth is supposed to produce supplementary earnings for the community members, leading to the best administration of all Bistra Muresului and Piatra Fantanele resources (Lu & Nepal, 2009; Voda & Negru, 2017). Geomedia technology application should positively affect the local history and culture, enhancing people's geographical awareness and ancestor`s pride (Voda, Torpan & Moldovan, 2017).

The analysis finds that in Romania, the myth of Dracula is unique and may become the most important functional attribute with the support of Geomedia tools (Voda & Negru, 2015; Ernawati et al., 2018). Romanian tourism development benefits today of the Dracula fame, which attracts considerably more visitors in the region than any other traditional touristic brand. Dracula related spots identification problem arises when tourists try to decide what to visit before actually going there. The geographical place, mountain top or pass, medieval castle, ruins or any specific construction representations qualities are instantly affecting individual`s imagined experience of that place (Voda, 2013; Relph, 1976).

It is important to notice the Dracula phenomena geo-location confusions and Vlad Țepeș related places contradictions. The Geomedia tools were used to coordinate the conception of Dracula`s imagined experience through smartphone applications recent advancements and local geographical information systems assessment (Voda, 2013; Voda & Negru, 2015). Transylvania is a Romanian historical province, located inside the Carpathian Mountains arch, where Bram Stoker, the Irish writer, placed the mysterious castle of Dracula. The world`s most famous vampire was quite often associated and probably inspired by Vlad Țepeș, the tough Romanian ruler who used to impale his prisoners in times of war, bloodshed and persecution of political opponents (McNally & Florescu, 1994; Voda & Negru, 2017; Baca & Rusu, 2017).

The results show the effectiveness of Geomedia techniques in Sighisoara and Bran geosystems` tourism development. From the individual household to the community scale, the Geomedia`s imagined place experience demonstrates the importance of geographical representations qualities in Borgo Pass, God`s Chair and Devil`s Plateau. Matter, energy and information input can balance a geosystem and increase its functionality. Matter can come in different forms of technological advancements and it is efficient if produces quantifiable outputs. For example, more accommodation facilities were created in Bran and Sighisoara due to Airbnb platform opportunities. Education increases any geosystem`s energy and has to be based on the historical and cultural traditions in order to contribute to a strong collective mind formation. Energy represents the connection with the local *egregore* as it is reflected in Bran and Sighisoara. Due to the internet technical evolution, information is widely available in Borgo Pass, God`s Chair and Devil`s Plateau. But information without education is useless for the geosystem`s functionality.

6. CONCLUSIONS

This article examined the role of Geomedia techniques in developing Romania's Dracula themed tourism aided by a variety of freely available tools that local communities can use to present and promote their Geosystems` cultural and historical resources. Google Maps, Google Earth, Facebook and Airbnb constitute a robust Geomedia toolkit for the local community to use creatively. The analysis reveals that people's geographical space

virtual signature will fundament the conception of the local Geomedia imagery built as an attraction site and a potential representation of a future tourist destination.

In addition to empirical research and practical implications, this study made a theoretical contribution and proposed the concept of a more secure form of development, based on education and access to information. Geomedia approach facilitates the inception and control of entire Geosystems where the contextual perception is validating the unique attributes and the digital revolution is empowering the place-based activities extension for the wellbeing of all inhabitants. If they have unity and responsible intelligence, people can easily define and regulate the energy, matter and information flows. Geosystem`s *egregore* preservation will fundament its adaptability to changes. People have to learn their living place history and actively maintain their ancient traditions for a strong collective mind formation.

This article contributes to the understanding why Geomedia controls Geosystems by synchronizing social etiquette, reshaping spatial imaginaries and harmonizing media interactions. The primary Vlad-Dracula geosystems brings numerous visitors to Bran Castle and the Vlad Dracul House in Sighișoara. International and local media promotion lends credibility in terms of genuine historical links to the Wallachian ruler, Vlad Țepeș. The rising number of Airbnb homes will soon surpass traditional tourist accommodations in Bran and Sighișoara, improving Geomedia's effectiveness and while providing extra income to locals.

Borgo Pass, Devil`s Plateau and God`s Chair are less known geographical locations. The accurate description in Bram Stoker`s book correlated with the real places stimulates `*les connaisseurs*`: Dracula Hunters. The more demanding access routes and the lack of local infrastucture is detering conventional tourists.

Geomedia`s smartphone applications are offering unique exploration insights of the world`s most beautiful and intriguing geographical locations. From spectacular castles, forest trails, amazing waterfalls, winter wonderlands, astonishing mountain tops and underground caves, Google Earth`s smartphone application developed travel itineraries based on popular geo-tagged photos. *Bram Stoker`s Dracula* is encouraging tourist to `explore some of the places connected to Stoker`s Transylvanian vampire in Google Earth` (Google Earth, 2017).

Geomedia is generating unprecedented coverage of previously unknown places, opening new opportunities for researching the most mysterious Romanian geographical locations. Geomedia tools such as Google Pixel2 smartphone`s application Photo Sphere Camera, facilitates the elaboration of 360 images and their accurate geographical placement on Google Earth maps. Dracula based virtual reality might be created then for natural and cultural tourist resources valorization from Borgo Pass, God`s Chair and Devil`s Lake Scholomance geographical areas.

Based on the Romanian Dracula phenomenon, this research novelty resides in the unique attributes importance for each Geosystems` development and the future wider applicability of the Geomedia techniques for any Geosystem`s assessment.

We predict that more Dracula based experiences will develop the local Geosystems` functionality and increase its effectiveness. Further geo-historical research should have a closer examination on the Dracula-Vlad Țepeș concealed interconnections.

The limitations of this research are strictly geographical since the Geomedia techniques can be applied in any world's region. Romania benefits from Dracula brand but the Geomedia approach is not restricted to well-known geographical locations. Geomedia is a means of developing Geosystems and the cultural values attached to them, creating an

authentic experience of place, after digitally raising expectations that are hopefully met. In other words, Geomedia literally puts any remote Geosystem with all its cultural values and beliefs on the map.

Future research should have a closer examination on today's technological advances linkage with local communities' social responsibility. Everything is placed on a virtual map, emphasizing the importance of our presence, as humans, in the central part of our environment, the Geosystem. We have the power, as individuals, to create and control our own virtual reality, embedded in the geographical dynamic system. Bram Stoker's book related geographical locations will be widely spread by Geomedia tools, challenging the Romanian mountains wilderness exploration in search for Dracula's shadows.

R E F E R E N C E S

Airbnb (2018). *Airbnb platform*. [Online]. Available from:http://www.airbnb.com. [Accessed January 2018].

Anghel, C. (2006). *Vlad Ţepeş, înger şi demon*. Jurnalul National, [Online]. Available from: http://m.jurnalul.ro/vechiul-site/mitul-si-banii-25490.html. [Accessed October 2017].

Android Development (2016). Basic Android. [Online]. http://www.udacity.com. [Accessed January 2018].

ArcGIS Server, (2017). *Website of ArcGIS Server*. Environmental Systems Research Institute, [Online]. Available from: www.esri.com/software/arcgis/arcgisserver/.[Accessed December 2017].

Asero, V., Gozzo, Simona, and Venera Tomaselli (2016). Building Tourism Networks through Tourist Mobility, *Journal of Travel Research*, 55(6) 751–763.

Baca, I., Rusu, C. (2017). *Borgo Pass: semnificatii geografice, istorice si culturale*. Cluj Napoca: Argonaut.

Barbieri, C., Xu, S., Gil-Arroyo, C., and Rozier Rich, S. (2016). Agritourism, Farm Visit, or . . . ? A Branding Assessment for Recreation on Farms, *Journal of Travel Research*, 55(8), 1094–1108.

Beeton, S. (2006). Community development through tourism. Collingwood, Australia: Landlinks Press.

Butulescu, V. (2001). *Dracula- Carnavalul durerii*. I.D. Bucharest: Sarbu Cultural Foundation Publishing House.

Cheng, M., & Jin, X. (2019). What do Airbnb users care about? An analysis of online review comments, *International Journal of Hospitality Management*, 76 (A), 58-70.

Cherifi, B., Smith, A., Maitland, R., and Stevenson, N. (2014). Destination images of non-visitors. *Annals of Tourism Research*, *49*, 190-202.

Croitoru, A., Crooks, A., Radzikowski, J., & Stefanidis, A. (2013). Geosocial gauge: a system prototype for knowledge discovery from social media, *International Journal of Geographical Information Science*, 27:12, 2483-2508, DOI:10.1080/13658816.2013.825724.

Curta, F. (2014). Florin Curta on the real Dracula. [Online]. Available from: https://history.ufl.edu/2014/10/30/florin-curta-on-the-real-dracula/. [Accessed September 2015.

Dickinson, J.E., Ghali, K., Cherrett, T., Speed, C., Davies, N., Norgate, S. (2014). Tourism and the smartphone app: capabilities, emerging practice and scope in the travel domain. *Current Issues in Tourism*. 17(1), 84-101.

Echtner, C. M., & Brent Ritchie, J. R. (2003). The meaning and measurement of destination image. *The Journal of Tourism Studies*, 14(1), 37–48.

Eadington, W. R., & Smith, V. L. (1992). Introduction: The emergence of alternative form of tourism. In V. L. Smith and W. R. Eadington (Eds.), Tourism alternatives: Potential and problem in the development of tourism (pp.1-12). Phyladelphia, US: University of Pennsylvania Press.

Ernawati, N.M., Torpan, A., & Voda, M. (2018). Geomedia role for mountain routes tourism development. Mesehe and Pisoiu Waterfall comparative study. *Geographia Technica*, 13 (1).

Ernawati, N.M. (2015). Producer–market orientation of community-based tourism (CBT) products: A case study in Bali, Indonesia. Unpublished thesis. Perth: Edith Cowan University.

Ert, E., Fleischer, A., Magen, N. (2016). Trust and reputation in the sharing economy: The role of personal photos in Airbnb, *Tourism Management*, 55, 62-73.

Fairclough, N. (1995) *Critical Discourse Analysis*, Boston: Addison Wesley.

Gerard, E. (1885). *Transylvanian Superstitions*. The Nineteenth Century, v. 18, p. 128-144.

Giurescu, C.C., & Giurescu, D.C. (1975). *Istoria Românilor din cele mai vechi timpuri pînă astăzi* (2nd edition). Bucureşti: Editura Albatros.

Google Earth (2017) *Google Earth Smartphone App*. [Online]. Available from: www.google.com/earth/. [Accessed December 2017].

Gunter, U. (2018). What makes an Airbnb host a superhost? Empirical evidence from San Francisco and the Bay Area. *Tourism Management*, 66, 26-37.

Gupta, S.K., Negru, R., & Voda, M. (2018). The Indian Himalaya`s unique attributes: Hemkund Sahib and The Valley of Flowers. *Geographia Technica*, 13 (2), 62-73.

Guttentag, D. (2015). Airbnb: disruptive innovation and the rise of an informal tourism accommodation sector, *Current Issues in Tourism*, 18:12, 1192-1217.

Guttentag, D.A., & Smith, S.L.J. (2017). Assessing Airbnb as a disruptive innovation relative to hotels: Substitution and comparative performance expectations, *International Journal of Hospitality Management*, 64, 1-10.

House, J. (1997). Redefining sustainability: A structural approach to sustainable tourism. In M. J. Stabler (Ed.), Tourism and sustainability principle to practice (pp. 89-104). Oxon, UK: Biddles ltd.

Hovi, T. (2014). *The Use of History in Dracula Tourism*, Folklore: Electronic Journal of Folklore, pp. 55–78, [Online]. Available from: http://www.folklore.ee/folklore/vol57/hovi.pdf. [Accessed November 2017].

Hwang, D., and Stewart, W.P. (2017). Social Capital and Collective Action in Rural Tourism. *Journal of Travel Research*, Vol. 56(1), 81–93.

Inal, C., Kocak, O., Esen, O., Bulbul, S. & Kizgut, R. (2017). Surveying and Mapping using Mobile Phone in Archaeological Settlements. *Geographia Technica*, 12 (2), 82-96.

Jamal, T., Tanase, A. (2005). Impacts and Conflicts Surrounding Dracula Park, Romania: The Role of Sustainable Tourism Principles, *Journal of Sustainable Tourism*, 13:5, 440-445.

Jin, X., Gallagher, A., Cao L., Luo J. & Han J. (2010) The wisdom of social multimedia: using Flickr for prediction and forecast. In Proceedings of ACM Multimedia.

Johnstone, B. (2002). *Discourse analysis,* Oxford: Blackwell Publishing.

Lai, K., & Li, X.R. (2016). Tourism Destination Image: Conceptual Problems and Definitional Solutions, *Journal of Travel Research*, 55(8), 1065–1080.

Liang, S., Schuckert, M., Law, R., & Chen, C. C. (2017). Be a "Superhost": The importance of badge systems for peer-to-peer rental accommodations. *Tourism Management*, 60, 454-465.

Lapenta, F. (2011). Geomedia: on location-based media, the changing status of collective image production and the emergence of social navigation systems, *Visual Studies*, 26:1, 14-24, DOI: 10.1080/1472586X.2011.548485.

Larson, M., Lundberg, C., & Lexhagen, M. (2013). Thirsting for Vampire Tourism: Developing Pop Culture Destinations. *Journal of Destination Marketing and Management*, Vol. 2, No. 2, pp. 74–84.

Light, D. (2007). Dracula Tourism in Romania: Cultural Identity and the State, *Annals of Tourism Research*, 34, pp. 746–765.

Light, D. (2012). *The Dracula Dilemma: Tourism, Identity and the State in Romania*. Farnham: Ashgate.

Liu L., Wolfson O. & Yin H. (2006) Extracting semantic location from outdoor positioning systems. In Proceedings of the IEEE International Conference on Mobile Data Management.

Luo Z, Li H, Tang J, Hong R, & Chua T-S (2009) ViewFocus: explore places of interests on Google maps using photos with view direction filtering. In Proceedings of ACM Multimedia.

Mac, I. (1996). *Geomorfosfera şi geomorfosistemele*, Editura Presa Universitară Clujeană: Cluj Napoca.

Mânzat, I. (2008). *Ecouri prin zig-zag-urile vietii*. Bistrita: Mesagerul Publishing House.

McNally, T.R., & Florescu, R. (1994). *In search of Dracula: the History of Dracula and Vampires*. New York: Houghton Mifflin Harcourt.

Meng, B., Min-Hyung, K. and Yeong-Hyeon, H. (2014). Users and Non-users of Smartphones for Travel: Differences in Factors Influencing the Adoption Decision, *A.Pac.Jour.Tour.Res.*, DOI: 10.1080/10941665.2014.958508.

Miller, E. (2000). *Dracula: Sense and Nonsense*. Essex: Desert Island Books Limited.

Muresan, A., & Smith, K.A. (1998). Dracula's castle in Transylvania: conflicting heritage marketing strategies. *International Journal of Heritage Studies*, 4(2), 86-102.

Negru, R., Voda, M. & Dumitrache, N.D. (2015). Geodiversity assessment as a tool for Geotourism in the Istenszeke Natural Park. *Academica Science Journal, Geographica Series*, 1(6), 13-21.

Oișteanu, A. (2004). *Ordine şi haos. Mit şi magie în cultura tradiţională românească*. București: Polirom.

Park, S., & Carla Almeida Santos (2017) Exploring the Tourist Experience: A Sequential Approach, *Journal of Travel Research*, 56(1) 16–27.

Petru, C., & Nastase, A. (2004). Tihuta- Hotelul lui Dracula de la Tihuta. [Online]. Available from: http://jurnalul.ro/campaniile-jurnalul/descoperirea-romaniei/12-iulie-2004-tihuta-hotelul-lui-dracula-de-la-tihuta-65193.html. [Accessed March 2015].

Picard, M. (2008). Balinese identity as tourist attraction from 'cultural tourism' (pariwisata budaya) to 'Bali erect' (ajeg Bali). *Tourist Studies*, 8(2), 155-173. doi: 10.1177/1468797608099246

Relph, E. (1976). *Place and placelessness*. London: Pion Limited, 156 p.

Reijnders, S. (2011). Stalking the Count: Dracula, Fandom and Tourism. *Annals of Tourism Research*, Vol. 38, No. 1, pp. 231–248.

Rinne, A. (2018), *The dark side of the sharing economy*. [Online]. Available from: https://www.weforum.org/agenda/2018/01/the-dark-side-of-the-sharing-economy/.[Accessed January 2018].

Roberts, L., & Simpson, F. (1999), Developing Partnership Approaches to Tourism in Central and Eastern Europe, *Journal of Sustainable Tourism*, Volume 7, 3:4, 331-340.

Robinson, P. & Wiltshier, P. (2011). Community tourism. In P. Robinson, S. Heitmann, and P. Dieke (Eds.), Research themes for tourism (pp. 87-99). Wallingford, UK: Cabi [Online]. Available from: http://www.cabi.org.ezproxy.ecu.edu.au/CABeBooks/ShowPDF.aspx?PAN=20113005506. [Accessed January 2018].

Schwanen, T. & Kwan, M-P. (2008). The Internet, Mobile-phone and Space-time Constraints, *Geoforum*, 39 (3) 1362-1377.

Sidali, K. L., Huber, D., & Schamel, G. (2017). Long-Term Sustainable Development of Tourism in South Tyrol: An Analysis of Tourists' Perception. *Sustainability*, 9(10), 1791.

Sigala, M. (2017). Collaborative commerce in tourism: Implications for research and industry. *Current Issues in Tourism*, 20, 346-355.

Singh, S. (2012). Community participation – in need of a fresh perspective. In T. V. Singh (Ed.), Aspects of tourism: Critical debates in tourism (pp. 113-117). Bristol, UK: Channel View Publications. 52.

Statista (2018). *The statistics portal*. [Online]. Available from: https://www.statista.com/statistics/smartphone-romania. [Accessed May 2018].

Stoker, B. (1897). *Dracula*, Westminister Archibald Constable and Company a Whitehall Gardens, London.

Stoicescu, N. (1976). *Vlad Ţepeş*. București: Editura Academiei Republicii Socialiste România.

Torpan, A. & Voda, M. (2019). Mountain Tracks Development Methodology for Adventure Recreation Activities in Gurghiu Mountains. *Geographia Technica*, 14 (1), 156-165.

Tussyadiah, I.P., Pesonen, J. (2016). Impacts of Peer-to-Peer Accommodation Use on Travel Patterns, *Journal of Travel Research*, 55(8) 1022–1040, DOI: 10.1177/0047287515608505.

UNWTO (2016) *United Nations World Tourism Organisation*. Sustainable development of tourism. [Online]. Available from: http://sdt.unwto.org/en/content/about-us-5. [Accessed September 2016].

Valentino-DeVries, J. (2010). Using flickr photos as a travel guide. Wall Street J July 23. http://blogs.wsj.com/digits/2010/07/23/using-flickr-photos-as-a-travel-guide/. [Accessed November 2016].

Voda, M., Kithiia, S., Jackiewicz, E., Du, Q., & Sarpe C.A. (2019). Geosystems' Pathways to the Future of Sustainability. *Scientific Reports*. DOI: 10.1038/s41598-019-50937-z

Voda, M., & Montes, Y.S. (2018). Descending mountain routes future: the North Yungas and Fagaras Geosystem`s comparative study. *Geographia Technica*, 13 (2), 152-166.

Voda, M., Negru, R. (2017). *Dracula myth role in Isten Szek – Bistra Muresului tourism development*. Volume of UDC 28-29.11.2017 International Conference `Education Performance and Development`, Risoprint Publishing House, Cluj Napoca, 166-171.

Voda, M., Torpan, A. & Moldovan, L. (2017). Wild Carpathia Future Development: From Illegal Deforestation to ORV Sustainable Recreation. *Sustainability*, 9(2254), 1-11.

Voda, M. & Negru, R. (2015). Geomedia role in Mures Valley Castles Tourism Development between Ogra and Brancovenesti. *Academica Science Journal, Geographica Series*, 1(6), 63-70.

Voda, M., Moldovan, L. Torpan, A. & Henning, H. (2014). Using Gis for Mountain Wild Routes Assessment in Order to Qualify Them for Tourism Valorisation. *Geographia Technica*, 09 (1), 101-108.

Voda, M. (2013). The role of Geospatial Technologies, Geographic Information and ICT in promoting rural communities sustainable development in Transylvania. *Academica Science Journal, Geographica Series*, 3, 90-95.

Yanai, K., Yaegashi, K., Qiu, B. (2009). Detecting cultural differences using consumer-generated geotagged photos. In: Proceedings of the 2nd international workshop on location and the web. ACM, New York, pp 1–4.

Zheng, Y-T., Zha, Z-J., Chua, T-S. (2010). Research and applications on georeferenced multimedia: a survey. *Multimedia Tools Applications*, 51, 77–98, DOI 10.1007/s11042-010-0630-z**.**

Wang, D., Park, S., & Fesenmaier, D.R. (2012). The Role of Smartphones in Mediating the Tourism Experience. *Journal of Travel Research*, 51(4), 371-387.

Wang, D., Xiang, Z., & Fesenmaier, D.R. (2016). Smartphone Use in Everyday Life and Travel, *Journal of Travel Research*, 55(1), 52–63.

Wang, D. & Nicolau, J. L. (2017). Price determinants of sharing economy based accommodation rental: A study of listings from 33 cities on. *International Journal of Hospitality Management*, 62, 120-131.

Wang, K., Wang, M., Gan, C., & Voda, M. (2019). Residents`Diachronic Perception of the Impacts of Ecological Resettlement in a World Heritage Site, *International journal of environmental research and public health*, 16 (19), 3556, https://doi.org/10.3390/ijerph16193556.

Weaver, D. (2006). Sustainable tourism theory and practice. Oxford, UK: Elsevier.

Wilson, M.W. (2012). Location-based services, conspicuous mobility, and the location-aware future. Geoforum 43, 1266–1275.

Wilson, M.W. (2014). Geospatial technologies in the location-aware future. *Journal of Transport Geography,* 34, 297–299.

Xiang, Z., Wang, D., & O'Leary, J.T. (2015). Adapting to the Internet: Trends in Travelers' Use of the Web for Trip Planning, *Journal of Travel Research*, 54(4), 511–527.

MAPPING OF ACCESS MODE CHOICE PROBABILITY BASED ON MULTINOMIAL LOGIT MODEL TO GET THE COMPETITION DESCRIPTION OF AIRPORT ACCESS MODES

WIRYANTA[1], Ria Asih Aryani SOEMITRO[1], Ervina AHYUDANARI[1]*

ABSTRACT:
Airport mode choice is an essential facilities requirement for air travelers. The various purpose of the travelers from a vast area of origin needs to be accommodated in order to guarantee the seamless movement of the travelers. This paper proposes a model to provide an alternative of access mode choice for Juanda International Airport (JIA). The model is based on the mapping of air traveler characteristics from 38 Districts in East Java. This paper considered travelers pattern of JIA that was analyzed using a multi-nominal logit model. The obtained model is useful in developing a map for identifying the districts that can be facilitated by public transport. The results also provide variables effect in the mode selection process.

Key-words: *Access mode, Mode choice, Mode choice probability.*

1. INTRODUCTION

Quality of access land transport to or from the airport is greatly determined by the choice of its transportation mode. This mode choice is influenced by socioeconomic and demographic features, trip characteristics, available modal options, and road geographies (Pasha & Hickman, 2016). Quality of access road is also influenced by the development of a city. Quantitatively, it can be stated that the bigger city in which there is an airport will lead to more number of access trip to or from the airport. JIA masterplan state that JIA was designed to serve ultimately 75 million per year.

This large number of passengers will cause high traffic access to JIA. Handling of access traffic must be adjusted to the results of in-depth research so that effective policies can be produced. The policy of regulating transportation access always leads to the use of high occupancy modes such as buses or trains. Therefore, it is important to examine the behavior of the choice of access mode in JIA with the consideration that the choice of modal behavior is unique which differs from one region to another or from one airport to another. The diversity of modal choice behavior is the result of the diversity of characteristics of airport users. Based on literature studies, many researchers have examined the choice of airport access modes. The purpose of research can be classified into two, namely identifying variables that influence the mode selection and making mathematical models of modal choices. Methodologically, the study of access mode choice can be distinguished based on the variables used, the type of model used for analysis and model segmentation. There are many variables that influence access mode choice in an airport. Each airport has unique variables, meaning that it differs from one airport to another. But there are 6 (six) variables that are most often used by researchers in constructing mode choice models at various airports in the world, as in **Table 1**.

---

[1] *Department of Civil Engineering, Faculty of Civil, Environmental and Geo Engineering, Sepuluh Nopember Institute of Technology, Surabaya*, *wiryanta@ugm.ac.id*, *ria@ce.its.ac.id*, *ervina@ce.its.ac.id* (**Corresponding author*)

The most popular variables that influence airport access mode choice

No.	Variables	Reseachers
1	Travel time	Harvey (1986), Furuichi & Koppelman (1994), Psaraki & Abacoumcin (2002), Gupta et al (2008), Jou et al (2011), Tam et al (2011), Alhussein (2011), Keumi and Murakami (2012), Tsamboulas et al (2012), Mamdoohi et al (2012), Choo et al (2013), Chang (2013), Akar (2013), Roh (2013), Bao et al (2015), Lee Kyu et al (2016), Gokasar & Gunay (2017)
2	Travel cost	Harvey (1986), Furuichi & Koppelman (1994), Psaraki & Abacoumcin (2002), Gupta et al (2008), Jou et al (2011), Tam et al (2011), Tsamboulas (2012), Bao et al (2015), Gokasar & Gunay (2017)
3	Trip purpose	Harvey (1986), Psaraki & Abacoumcin (2002), Mamdoohi et al (2012), Choo et al (2013), Chang (2013), Akar (2013), Roh (2013), Bao et al (2015), Arbues et al (2016)
4	Household income	Harvey (1986), Gupta et al (2008), Alhussein (2011), Keumi and Murakami (2012), Mamdoohi et al (2012), Choo et al (2013), Akar (2013)
5	Airport user's age	Chebli & Mahmassani (2003), Gupta et al (2008), Jou et al (2011), Tam et al (2011), Mamdoohi et al (2012), Choo et al (2013), Chang (2013), Akar (2013), Roh (2013)
6	Gender	,Chebli & Mahmassani (2003), Gupta et al (2008), Mamdoohi et al (2012), Chang (2013), Akar (2013), Roh (2013)

There are three models that are often used in formulating airport access mode selection, namely the multinomial logit (MNL) model, nested logit (NL) and the multinomial probit (MNP) model. Among the three models, the MNL model is the most commonly used. Because mathematically the easiest execution. The MNL model must fulfill the axiom of Independent of Irrelevant Alternatives (IIA), that is "if two alternatives have the opportunity to be chosen, the ratio of one opportunity to another opportunity is not affected by the existence of other alternatives in a set of choices". So in MNL, the Pj / Pi ratio is a constant that does not depend on other choices. This can be considered as an advantage of the model because it can control new problems quite well. But this behavior is considered as a deficiency that causes the model to be not good if there are alternatives that are correlated.

The existence of modal hierarchies in one group or the existence of correlated modal choices causes the IIA axiom conditions to be unfulfilled. So in such conditions, the MNL model cannot be used. For this reason, a Nested Logit (NL) selection model is needed. According to Kropko (2008), the advantage of MNP compared to MNL or NL is that MNP is not associated with the axioms of IIA. But MNP is mathematically more complicated in its solution. In general, if there are N choices, then solving MNP uses N-1 tuple integrals. The MNP model will become unstable when executing mathematical equations with quadruple integrals upwards. In that condition, the MNP model will always fail to estimate. Therefore, MNP is more efficient when there are fewer choices. If there are more alternative modal choices (more than four choices), the MNL model is more stable than the MNP model. This research uses the MNL model because it involves 6 (six) modal choices and there is no hierarchy in the selection.

The purpose of creating a mode choice model is to determine the behavior of airport users in selecting access modes. Quantification of this model will produce a modal choice probability. This probability will become a benchmark of acceptance or rejection of the access mode being operated. The identification of this probability value is the same as the identification of the market share of access mode users. To obtain complete identification results, the researchers made modeling classifications based on market segmentation. There are two segmentations most often made by researchers namely business and non-business (pleasure) (Furuichi & Koppelman, 1994; Keumi and Murakami, 2012; Mamdoohi et al, 2012; Choo et al, 2013; Lee Kyu et al, 2016). Other segmentations that are also often made by researchers are residents and non-residents (visitors), as did Harvey (1986), Psaraki & Abacoumcin (2002), Gupta et al (2008), Tam et al (2011). Of the many researchers in modeling the access mode, a segmentation based on the area of origin of the passengers in an airport catchment area has not been discussed. This might be caused by development of the city. For the city that growing not following certain pattern, the transportation facilities will be difficult to be provided. This segmentation is important in order to know the spatial distribution of demand in the airport catchment area. Information about the value of the probability of choice and spatial location of demand will be useful in designing routes for access modes that have certain routes such as buses or trains.

Based on the description above, a model based on the area of origin of the passenger has not been explored more. The origin of the air travelers will provide useful information in designing the type of access mode that is suitable for the certain airport. The origin of air traveler represents the accessibility index of the airport. The higher the index determines that the airport has high accessibility inland as well as air. Land accessibility means the air traveler has easiness in traveling to the airport, though they come from the far area from the airport. Air accessibility means that the airport provides a number of routes and has a high frequency of flight for each route.

This research focuses more on modeling the airport access mode based on the origin of passengers. This model will be a base of planning airport access mode in the populated area and distributed in wider coverage. Therefore, this research is expected to be an additional method in designing the airport access mode.

2. METHODOLOGY

2.1. Factor Analysis

Factor analysis is conducted in order to identify the effects of variables that have been studied previously. The analysis process consists of two processes namely *data summarization* and *data reduction*. *Data summarization* is the inter-variable correlation identification process; while data reduction is a new data set grouping so that there are simpler variable groups. This research involves 19 variables that are considered to have effects on access mode choice in Juanda International Airport. Factor analysis is performed on several groups of data that have been classified according to certain segmentation. In this analysis the data segmentation is based on the area of origin of air passengers. The factor analysis refers to the identification of any factors having effects on the airport access mode choice from passengers from various cities or regencies as the catchment area of Juanda International Airport. There are 29 regencies and 9 cities in East Java Province as the catchment area of Juanda International Airport. But, not all respondents taken from

random survey represent 38 regency or city areas. Statistically, there are only 5 (five) areas meeting the data adequacy aspect, namely Surabaya, Sidoarjo, Malang, Jombang and Gresik.

2.2. Mode Choice Model

There are many studies related to the application of this airport access mode choice model. ACRP (2008) has launched some study results of this mode choice model application. The choice model structure is generic consisting of 3 types of models namely binomial logit/multinomial logit, nested logit and probit models. The binomial logit model is used to compete for two modes while multinomial logit is used to compete for more modes simultaneously. The nested logit is used if there is any mode grouping or mode hierarchy. The researchers have basic difference namely on the type of explanatory variables in the modeling. The explanatory variables for each airport are unique and reflect the behavior of mode users. It involves very various explanatory variables between one airport and others, also between one researcher and others. It is because of the different perception of interest level for each variable in each airport location. Then, the initial step to be done before building a model is exploring any considered important variables by airport users at Juanda International Airport, Surabaya. Contribution of each variable in the model will be the basis for making mode utility analysis and access mode choice probability in Juanda International Airport.

In the context of the choice model using two logistic function alternatives, it can be stated as follow:

$$P(i) = \frac{1}{1 + e^{-(Ui - Uj)}}$$

In which Ui and Uj are the utility of i-alternative and utility of j- alternative and P(i) is the probability of selecting i- alternative, then P(i) can also be stated in the following forms.

$$P(i) = \frac{e^{Ui}}{e^{Ui} + e^{Uj}}$$

This form is known as Logit Model or precisely as Binomial Logit Model. If there are more than two choice alternatives, it can develop the following model:

$$P(i) = \frac{e^{Ui}}{\sum_{j \in J} e^{Uj}}$$

J is the number of alternatives. This function is called as Multinomial Logit (MNL). This function has been used broadly in mode choice modeling in the airport by involving two or more option alternatives. Initially, the mode choice model can be presented conventionally and easily in the form of S-curve. But in a further stage, the logit model function can be derived from utility maximum principles, in which decision-makers will select any alternatives with the highest utility.

2.3. Studied Variables

Based on the literature review there are many variables that influence the choice of airport access modes. In this research, 19 variables will be examined which are expected to have a significant effect on the modal selection process at Juanda International Airport. The 19 variables are presented in **Table 2**.

<div align="right">

Table 2.
</div>

<div align="center">

Studied Variables
</div>

No.	Symbol	Variables	No.	Symbol	Variables
1	Q1	Income	11	Q11	Frequency
2	Q2	Family number	12	Q12	Party size of the traveler
3	Q3	Education	13	Q13	Duration of waiting time
4	Q4	Purpose of trip	14	Q14	Duration of walking time
5	Q5	Trip duration (travel time)	15	Q15	Number of transfer
6	Q6	Number of baggage	16	Q16	Security
7	Q7	Trip cost	17	Q17	Comfort
8	Q8	Trip distance	18	Q18	Baggage capacity
9	Q9	Punctuality	19	Q19	Service satisfaction
10	Q10	Travel time reliability			

3. STUDY AREA AND DATA

3. 1. Data of passenger's reference

In survey questionnaires, there are questions related to the social-economic data and preference data of respondents. Respondent preferences are respondent's response toward some variables that influence their access mode choice. In this survey, the respondents are asked to state their responses on the variables written on the questionnaires. The responses are stated into five category levels, namely, Strongly Agree (SA), Agree (A), Neutral (N), Disagree (D) and strongly disagree (SD). Recapitulation of preference data is presented in **Table 3**. A high percentage of strongly agree shows that the variable is very popular. These variables are service satisfaction, comfort, security, trip cost, punctuality and travel time reliability. On the other hand, the least desirable variables can be identified based on the percentage of strongly disagree. The variables that are least desirable are education, family number, income, duration of walking time, trip cost and party size of traveler.

3. 2. Data of mode choice

There are five operating existing access modes in Juanda, namely Bus, Taxi, Travel Car, Private Car, and Motorcycle. To improve the quality of airport access trips, the Government plans a new mode, Train. This train transportation is designed to be elevated by the Gubeng Station - Waru Station - Juanda International Airport. In the questionnaire, it is asked about what modes will be chosen by the respondents if the airport train is

assumed to have operated according to the route. This survey can obtain data from the mode selection. The selection proportion of Bus is 8,3% and the other modes consecutively are Train 35,0%, Travel Car 5,4%, Taxi 6,9%, Private car 38,4% and motorcycle 5,4%.

Table 3.

Recapitulation of Airport Passenger Preference Data's.

Variables	Symbol	SA(%)	A (%)	N (%)	D(%)	SD (%)
Income	Q1	24,2	34,8	7,6	26,2	7,2
Family number	Q2	15,7	35,4	12,3	26,6	10,0
Education	Q3	7,2	12,3	20,8	45,9	13,8
Purpose of trip	Q4	27,2	33,9	16,9	18,3	3,7
Trip duration (travel time)	Q5	42,4	41,2	8,9	6,2	1,2
Number of baggage	Q6	29,1	35,6	12,3	19,7	3,3
Trip cost	Q7	50,1	27,6	6,3	11,7	4,3
Trip distance	Q8	32,3	50,4	6,7	8,1	2,4
Punctuality	Q9	49,1	37,1	4,9	7,9	1,0
Travel time reliability	Q10	43,1	36,7	8,8	9,6	1,9
Frequency	Q11	31,0	39,9	10,8	16,4	1,9
Party size of traveller	Q12	24,0	29,2	13,4	29,1	4,2
Duration of waiting time	Q13	30,2	37,2	13,3	16,4	2,8
Duration of walking time	Q14	18,8	33,6	15,8	25,4	6,4
Number of transfer	Q15	34,0	29,4	14,8	19,0	2,8
Security	Q16	57,0	33,0	4,3	5,2	0,4
Comfort	Q17	62,0	29,6	4,0	4,2	0,2
Baggage capacity	Q18	34,1	43,7	8,0	13,7	0,6
Service satisfaction	Q19	65,8	26,3	3,2	3,9	0,8

4. RESULTS AND DISCUSSION

4. 1. Results of Factor Analysis

Factor analysis is a set of processes consisting of variable selection, variable grouping and creating simpler new factors. Results of all processes will create new factor formulations that contain a group of variables. From the responses to 19 variables that are processed in factor analysis, a number of new factors can be produced which are fewer than the number of origin variables. The number of new factors and their magnitude survey presented as a whole in **Table 4**.

Each factor in the table above has a number of certain influences ranging from the largest to the smallest. A large amount of influence shows that these factors are very dominant to be considered in the selection of access modes by passengers. The formulation and amount of contribution from the most dominant factors in each region are as shown in **Table 5**.

Table 4.
The number of new factors and the total contribution of all factors.

Districts	Number of New Factors	Name of Factors	Contribution of all Factors (%)
Surabaya	6	Transportation (Su_1), Social (Su_2), Accessibility (Su_3), Satisfaction (Su_4), Baggage (Su_5), Travelling-1 (Su_6)	61,88
Sidoarjo	6	Satisfaction (Si_1), Transportation (Si_2), Social (Si_3), Accessibility (Si_4), Travelling-2 (Si_5), Party size (Si_6)	64,08
Jombang	4	Satisfaction (Jo_1), operational pattern-1 (Jo_2), travelling-3 (Jo_3), total trip cost (Jo_4)	68,07
Gresik	4	Operational pattern-2 (Gr_1), satisfaction (Gr_2), operational pattern-3 (Gr_3), party size of traveler (Gr_4)	70,68
Malang	4	Operation & convenience (Ma_1), satisfaction (Ma_2), social (Ma_3), frequency (Ma_4)	68,62

Table 5.
The formulation of the most dominant factors.

Districts	Most dominant factors	Formulation	Contribution (%)
Surabaya	Transportation (Su_1)	$0,653Q8 + 0,715Q9 + 0,753Q10 + 0,618Q11$	13,423
Sidoarjo	Satisfaction (Si_1)	$0,839Q16 + 0,838Q17 + 0,671Q18 + 0,801Q19$	14,678
Jombang	Satisfaction (Jo_1)	$0,638Q1 + 0,832Q16 + 0,855Q17 + 0,876Q19$	22,400
Gresik	Operation pattern-2 (Gr_1)	$0,548Q5 + 0,673Q8 + 0,883Q9 + 0,852Q10$	22,479
Malang	Operation & convenience (Ma_1)	$0,513Q5 + 0,552Q8 + 0,817Q9 + 0,822Q10 + 0,766Q16 + 0,777Q17 + 0,514Q18$	26,376

Factor analysis in **Table 3** and **Table 4** produces factors that influence modal choice in general, not yet referring to certain types of modes. To see the effect of these factors specifically per mode, it is necessary to make a mathematical model of mode choice to quantitatively determine the probability value of selection.

4. 2.   Logit Model of Mode Choice Probability

The logit model is a comparison of probability function between a certain mode and reference mode. In this analysis, the reference mode is a private vehicle. There is five models in a set of the multinomial model in a studied district. Those are the logit model for Bus, Train, Taxi, Rent Car, and Motor Cycle. As the results, the logit models of mode choice for some regions as the hinterland of JIA are as follow:

Logit models of access modes

Origin Districts	Modes	Logit models ($g(x)$) with private car as reference mode
Surabaya	Bus	$-14{,}49 - 0{,}03Su_1 - 0{,}14Su_3 + 0{,}36Su_4 + 0{,}75Su_5 + 0{,}22Su_6$
	Train	$-6{,}78 + 0{,}18Su_1 - 0{,}10Su_3 + 0{,}16Su_4 - 0{,}11Su_5 + 0{,}36Su_6$
	Taxi	$-8{,}98 + 1{,}17Su_1 + 0{,}06Su_3 + 0{,}09Su_4 - 0{,}06Su_5 + 0{,}30Su_6$
	Travel car	$-72{,}36 - 0{,}41Su_1 + 4{,}93Su_3 - 0{,}76Su_4 - 0{,}49Su_5 - 0{,}75Su_6$
	Motorcycle	$0{,}68 + 0{,}06Su_1 + 0{,}03Su_3 - 0{,}50Su_4 - 0{,}38Su_5 + 0{,}45Su_6$
Sidoarjo	Bus	$-6{,}01 + 0{,}09Si_1 + 0{,}10Si_2 - 0{,}02Si_5 + 0{,}18Si_6$
	Train	$-5{,}89 + 0{,}27Si_1 - 0{,}01Si_2 - 0{,}07Si_5 - 0{,}02Si_6$
	Taxi	$-13{,}87 + 0{,}22Si_1 + 0{,}40Si_2 + 0{,}23Si_5 - 0{,}23Si_6$
	Travel car	$-3648{,}33 + 16{,}29Si_1 - 31{,}83Si_2 - 23{,}97Si_5 + 415{,}62Si_6$
	Motorcycle	$-4{,}33 - 0{,}31Si_1 + 0{,}34Si_2 + 0{,}35Si_5 - 0{,}40Si_6$
Jombang	Bus	$8{,}28 - 1{,}04Jo_3$
	Train	$3{,}80 - 0{,}41Jo_3$
	Taxi	$2{,}27 - 0{,}49Jo_3$
	Travel car	$-3{,}95 + 0{,}24Jo_3$
	Motorcycle	$0{,}70 - 0{,}24Jo_3$
Gresik	Bus	$0{,}55 - 0{,}38Gr_1 + 0{,}15Gr_2 + 0{,}15Gr_3$
	Train	$-14{,}06 - 0{,}21Gr_1 + 0{,}65Gr_2 + 0{,}51Gr_3$
	Taxi	$-21{,}28 + 0{,}61Gr_1 + 0{,}53Gr_2 + 0{,}08Gr_3$
	Travel car	$-26{,}24 - 0{,}73Gr_1 + 0{,}88Gr_2 + 1{,}67Gr_3$
	Motorcycle	$-16{,}16 + 1{,}08Gr_1 - 0{,}28Gr_2 - 0{,}16Gr_3$
Malang	Bus	$0{,}25Ma_2 + 0{,}01Ma_3 - 1{,}46Ma_4$
	Train	$0{,}09Ma_2 - 0{,}21Ma_3 + 0{,}22Ma_4$
	Taxi	$154{,}56Ma_2 + 121{,}39Ma_3 - 1534{,}70Ma_4$
	Travel car	$-0{,}01Ma_2 - 0{,}22Ma_3 + 0{,}19Ma_4$
	Motorcycle	$113{,}25Ma_2 + 94{,}32Ma_3 - 1141{,}19Ma_4$

Based on the Logit Model above, it can formulate the probability model of each mode. Generally, the formulation of each mode choice probability is presented in the following equation:

$$P(Bus) = \frac{e^{g(x)Bus}}{1+g(x)Bus+g(x)Train+g(x)Taxi+g(x)Travel+g(x)Motorcycle},$$

and

$$P(Private\ car) = \frac{1}{1+g(x)Bus+g(x)Train+g(x)Taxi+g(x)Travel+g(x)Motorcycle}.$$

Quantitatively, model choice probability values can be calculated based on the Mode Choice Probability Models above. Q value is the quantification of the respondent's answers. SD response has 1 value; D has 2 value, N has 3 value, A has 4 value and SA has 5 value. Factor value is obtained by substituting the variables (Q) in factor formulation. The factor value is then substituted in logit function and probability equations so that it can obtain the probability value of each mode, as in the following tables.

Table 7.

Average probability values of modes choice

Districts	Average Probability Value of Modes					
	Bus	Train	Taxi	Travel	Private car	Motor cycle
Surabaya	0,00681	0,02285	0,00587	0,00000	0,81020	0,15427
Sidoarjo	0,04166	0,13231	0,00378	0,00000	0,79094	0,03131
Jombang	0,34031	0,32756	0,03974	0,02968	0,20292	0,05980
Gresik	0,30312	0,03694	0,00187	0,00035	0,65617	0,00155
Malang	0,09996	0,36587	0,00000	0,13740	0,39677	0,00000

Based on the choice probability values, private vehicles are still the most interest mode by air passengers in all the studied areas. This is reasonable because private vehicle modes have high flexibility compared to other modes. The priority of transportation arrangement policies in airports in the world is to encourage the use of high-occupancy vehicles such as trains and buses. The policy aims to reduce the traffic load on the highway which is an access road to the airport, minimize the environmental impact due to the density of vehicle traffic and also to save energy. Along with that, the Indonesian Government is working with the airport management company to hold bus and train transportation as an airport access mode. This policy will also be applied at JIA.

Regarding the plan to operate the airport train, passengers from Malang and Jombang areas indicate a great interest in the mode. This is due to two issues, firstly because there is already a train line to Surabaya and the second because there is a quite rapid highway to the airport. In conditions of crowded highway traffic, the use of private vehicles is uncomfortable. For passengers from Surabaya and Sidoarjo, they have low interest in both train and bus modes. It can be assumed that it is caused by a relatively close distance to the airport location. So for passengers from Surabaya and Sidoarjo, the mode of private vehicles and motorcycle become the favorite modes. Especially for passengers from Gresik, it can be seen that there is a low interest in the mode of the train because there is yet available train line. While the existing bus lines are available serving the Gresik - Airport routes. So the interest in using bus modes is relatively high compared to train mode.

Efforts to encourage the use of high-occupancy vehicles must pay attention to the factors that explicitly influence the choice of modes, as in **Table 5**. For example for passengers from Surabaya, the choice of train mode is strongly influenced by the transportation factor (Su1), satisfaction factor (Su4) and traveling-1 (Su6) factors. The magnitude of the influence of each factor is the exponential value of the parameter coefficient.

5. CONCLUSION

Research in mapping the pattern of selection airport access mode brought the results in charateritics of access mode choice by passengers of JIA. Overall JIA currently serves 38 (thirty eight) districts in East Java province, but only 5 (five) districts are the object of analysis in this study because of the reason for the adequacy of the data in statistics. Based on passengers characteristics and origin of passengers, private car dominated for all passenger's district areas except Jombang. This is due to the distance and the availability of access mode. This domination is not applicable for passengers from Jombang that has around 89 km from JIA. This selection due to the mix traffic to the airport that cause longer travel time. The domination of private car for almost all JIA's passengers imply that the distribution of originating passengers cause ineffective planning of public transport to serve the passengers. The public transports, as airport access modes, should be planned in the regional corridor which has a high probability of modal choice. The high probability of mode choice shows the high interest of passengers in the mode. Therefore, spacially mapping the probability of choosing a mode in airport catchment area becomes very important. However, this may can be investigated further by having projecting the raise of the demand from each districts. If the demand from each area of study growing fast, the possibility of having specific bus route or train route, as in Soekarno Hatta Airport, can be proposed.

R E F E R E N C E S

Airport Cooperative Research Program (ACRP), 2008, *Airport ground access mode choice model*, ACRP Synthesis 5, Transportation Research Board, Washington D.C.

Akar, G., 2013, Ground access to airports, case study: Port Columbus International Airport, *Journal of Air Transport Management*, 30, 25 - 31

Alhussein, Saad N, 2011, Analysis of Ground Access Mode Choice King Khaled International Airport, Riyadh, Saudi Arabia, *Journal of Transport Geography*, Vol. 19, page: 1361 – 1367.

Arbues, P., Banos, J.F., Mayor, M., Suarez, P., Determinants of Ground Transport Modal Choice in Long Distance Trips in Spain, *Transportation Research Part A*, Vol. 84, page: 131 - 143

Bao, D, Guo, T, Hua, S, 2015, Analysis of airport passenger's access mode choice based on SP/RP combined data, Journal of Wuhan University of Technology (*Transportation Science and Engineering*), 39, 763-767

Chang, Y.C., 2013, Factors affecting airport mode choice for elderly air passengers, *Transportation Research Part E: Logistics and Transportation Review*, Vol 57, page 105 – 112.

Chebli, H., Mahmassani. H. S., 2003, Air traveler stated preferences toward new airport landside access mode services, Annual Meeting of Transportation Research Board, Washington DC.

Choo, S., You, S., Lee, H., 2013, Exploring characteristics of airport access mode choice: a case study of Korea, *Transportation Planning and Technology*, 36, 335 – 351.

Furuichi, M, and Koppelman, F.S, 1994, An analysis of air traveler departure airport and destination

Gokasar, I., Gunay, G., 2017, Mode Choice Behavior Modelling of Ground Access to Airport: A Case Study in Istanbul, Turkey, *Journal of Air Transport Management*, Vol: 59, page: 1 - 7

Gupta, S., Vovsha, P., Donnelly, R., 2008, Air Passenger Preference for Choice of Airport and Ground Access Mode in The New York City Metropolitan Region, *Transportation Research Record*: Journal of The Transportation Research Board 2042, page: 3-11.

Harvey, G, 1986, Study of Airport Access Mode Choice, *Journal of Transport Engineering*, Vol 112 No.5, page: 525 – 545.

Jou, R.C., Henser, D.A., Hsu, T.L., 2011, Airport Ground Access Mode Choice Behaviour after The Introduction of a New Mode: a Case Study of Taoyuan International Airport in Taiwan, *Transportation Research Part E*: Logistic and Transportation Review 47, page: 371 – 381.

Keumi, C., Murakami, H., 2012, The Role of Schedule Delays on Passengers Choice of Access Modes: A Case Study of Japan's International Hub Airports, *Transportation Research Part E*, Vol. 48, page: 1023 – 1031.

Kropko, J., 2008, Choosing between multinomial logit and multinomial probhit models for analysis of unordered choice data, A Thesis Submitted to the Faculty of The University of North Carolina at Chapel Hill, 1 – 46.

Lee Kyu, J., Eui Yoo, K., Han Song, K., 2016, Studi on Travellers Transport Mode Choice Behavior Using The Mix Logit Model: A Case Study of The Seoul – Jeju Route, Journal of Air Transport Management, Vol. 56, page: 131 - 137

Mamdoohi, A., Saffarzade, M., Taherpour, A., Panah, M. Y., 2012, Modelling air passengers ground access mode choice: a case study of IKIA, *International Journal of Modelling and Optimization*, 2, 147.

Pasha, M. M., & Hickman, M. (2016). Airport ground accessibility: review and assessment. *38th Australasian Transport Research Forum (ATRF 2016)*, (November), 15p. Retrieved from http://atrf.info/papers/2016/index.aspx%0Ahttps://trid.trb.org/view/1457919

Psaraki, V., Abacoumkin, C., 2002, Access mode choice for relocated airport: the new Athens International Airport, *Journal of Air Transport Management 8*, page: 89 – 98.

Roh, H., J., 2013, Mode choice behavior of various airport user groups for ground airport access, *The Open Transportation Journal*, 7.

Tam, M.I, Lam, W.H.K, Lo, H.P., 2011, The impact of travel time reliability and perceived service quality on airport ground access mode choice, *Journal of Choice Modelling 4*, page: 49 – 69.

Tsamboulas, D.A., Evmorfopoulos, A.P., Moraiti, P., 2012, Modelling Airport Employess Commuting Mode Choice, Journal of Air Transport Management, Vol. 18, page: 74-77

Aims and Scope

Geographia Technica is a journal devoted to the publication of all papers on all aspects of the use of technical and quantitative methods in geographical research. It aims at presenting its readers with the latest developments in G.I.S technology, mathematical methods applicable to any field of geography, territorial micro-scalar and laboratory experiments, and the latest developments induced by the measurement techniques to the geographical research.

Geographia Technica is dedicated to all those who understand that nowadays every field of geography can only be described by specific numerical values, variables both oftime and space which require the sort of numerical analysis only possible with the aid of technical and quantitative methods offered by powerful computers and dedicated software.

Our understanding of *Geographia Technica* expands the concept of technical methods applied to geography to its broadest sense and for that, papers of different interests such as: G.I.S, Spatial Analysis, Remote Sensing, Cartography or Geostatistics as well as papers which, by promoting the above mentioned directions bring a technical approach in the fields of hydrology, climatology, geomorphology, human geography territorial planning are more than welcomed provided they are of sufficient wide interest and relevance.

Targeted readers:

The publication intends to serve workers in academia, industry and government.
Students, teachers, researchers and practitioners should benefit from the ideas in the journal.

Guide for Authors

Submission

Articles and proposals for articles are accepted for consideration on the understanding that they are not being submitted elsewhere.

The publication proposals that satisfy the conditions for originality, relevance for the new technical geography domain and editorial requirements, will be sent by email to the address editorial-secretary@technicalgeography.org.

This page can be accessed to see the requirements for editing an article, and also the articles from the journal archive found on www.technicalgeography.org can be used as a guide.

Content

In addition to full-length research contributions, the journal also publishes Short Notes, Book reviews, Software Reviews, Letters of the Editor. However the editors wish to point out that the views expressed in the book reviews are the personal opinion of the reviewer and do not necessarily reflect the views of the publishers.

Each year two volumes are scheduled for publication. Papers in English or French are accepted. The articles are printed in full color. A part of the articles are available as full text on the www.technicalgeography.org website. The link between the author and reviewers is mediated by the Editor.

Peer Review Process

The papers submitted for publication to the Editor undergo an anonymous peer review process, necessary for assessing the quality of scientific information, the relevance to the technical geography field and the publishing requirements of our journal.

The contents are reviewed by two members of the Editorial Board or other reviewers on a simple blind review system. The reviewer's comments for the improvement of the paper will be sent to the corresponding author by the editor. After the author changes the paper according to the comments, the article is published in the next number of the journal.

Eventual paper rejections will have solid arguments, but sending the paper only to receive the comments of the reviewers is discouraged. Authors are notified by e-mail about the status of the submitted articles and the whole process takes about 3-4 months from the date of the article submission.

5 948422 015163

UNIVERSITAS · NAPOCENSIS
ROMANIA
PRESA UNIVERSITARĂ